Hydropower Vulnerability in a Changing Climate: Characterizing Future Risks in the Global South

Submitted in partial fulfillment of the requirements for
the degree of
Doctoral of Philosophy
in
Engineering and Public Policy
and
Civil and Environmental Engineering

Ana Lucía Cáceres Cebrecos
B.S. Civil Engineering, Pontificia Universidad Católica del Perú
M.S. Civil and Environmental Engineering, Carnegie Mellon University

Carnegie Mellon University
Pittsburgh, PA

May, 2022

Para mis papás Augusto y Pilar.

Acknowledgements

This research was possible through the support of Carnegie Mellon's Department on Engineering and Public Policy, Carnegie Mellon's Wilton E. Scott Institute for Energy Innovation (2018 Seed Grant for Energy Research), Carnegie Mellon's Steinbrenner Institute (2018 – 2019 Steinbrenner Fellow), and the Rockefeller Foundation E-Guide Project (sub-contract with the University of Massachusetts at Amherst – sub-award #19-10766 A 00). The work presented in Chapter 4 was possible thanks to the Extreme Science and Engineering Discovery Environment (XSEDE) Bridges and Bridges-2 at the Pittsburgh Supercomputing Center (PSC) through allocation TG-ECS180014. This work used the Extreme Science and Engineering Discovery Environment (XSEDE), which is supported by National Science Foundation grant number ACI-1548562. This dissertation has not been formally reviewed by the sponsors; the views expressed are solely those of the authors and do not necessarily reflect those of the sponsors.

I would like to express my most sincere gratitude towards my advisors Prof. Paulina Jaramillo (committee chair), Dr. H. Scott Matthews (committee member), and Prof. Costa Samaras (committee member). Pauli thank you for always being there for me, reviewing my papers, even if that meant I had to completely change them ten times, having meetings half in Spanish and half in English and then wondering why we were speaking in one language or another; I could not have made it through the Ph.D. without you. Scott thank you for believing in me from the start. I would not be where I am today without you. Costa, thank you for reviewing endless presentations slide by slide with me and for always providing a fresh set of eyes to the work that I did. I am truly grateful to you all.

Next, I would like to thank the other committee members for their comments and input: Prof. Bart Nijssen, Prof. David Rounce, and Prof. Mitch Small. I want to give a special shoutout to Bart, who co-authored all three papers, and whose valuable input and insight enriched my work. Bart, thank you for all your comments, the countless back and forth of emails and Zoom meetings from coast to coast, without you none of my papers would have looked as good as they do (haha).

I would like to thank Rachel Sin, now alumni from the department of Civil and Environmental Engineering, who helped me start the literature review for the fourth

chapter of this dissertation. Your work really kickstarted the last chapter of this dissertation.

Along the same lines, I would like to thank Dr. Destenie Nock who came up with the acronym for RICCH. Without your help I have no idea what the tool would be called because mine and Pauli's ideas were not good (haha).

I also want to thank Anna J. Siefken from the Scott Institute for "lending" both Aiswariya Raja and subsequently Luling Huang to the RICCH project. Aiswariya thank you for kickstarting the dashboard. Luling, thank you for making RICCH a reality. Your help really made the last months of my Ph.D. significantly easier.

Many people in EPP and CEE were there for me and offered me support throughout my journey at CMU. First during the master's and then during the Ph.D. Without any particular order; to Bhakti Dave, Carolyn Vega-Gonzalez, Esteban Zegpi, Isabella Solari, Jaime Parra, Joan Nkiriki, Niles Guo, Peter Tschofen, Priyank Lathwal, Shuchen Cong, Dini Maghfirra, Amanda Quay, among others; to all the members of the Green Design Institute for always showing up to my practice presentation runs and were always so willing to help: Francisco Fonseca-Ralston, Jorge Izar-Tenorio, Katie Jordan, among others; to my wonderful GROW+ (former DWEPP) co-facilitator and scribe: Emily Grayek and Nyla Khan (also part of the GDI); to the always smiling, comforting, and helpful EPP staff: Vicki Finney, Debbie Kuntz, Adam Loucks, and Kim Martin; thank you! To the professors who enriched my CMU experience, thank you.

I am so grateful to the people that kept me moving and semi-sane during the pandemic: the "FitFam" and the Schenley Park bootcamp crew. Without you I would not have made it through the Ph.D. AND the pandemic. Thanks Cassie Eng, Karen Edwards, Dr. Nick Golio, Dr. Josh Gyory, Emma Gurchiek, Dr. Caitlin Tenison, Dr. Liz Carter, Dr. Jasmine Kwasa, Zachary Lee, Lettia, and last but not least Ricky Gupta. Karen, your Group-X classes brought me joy every time! I am forever grateful to all of you and your friendships!

To my dearest friends who always reminded me that there was life outside of CMU. My lifelong friends now scattered around the world: Jorge Luis Ayarza, Camila Cantuarias,

Vanessa Donoyan, Chiara Marchese, Matías Quintana, Gabriela Torres, Gonzalo Triveño, Salvatore Venturelli, among others. To my Pittsburgh friends Christian Jewett and Marissa Appel; Brent Hopkins; Gill Goobie and Sean Smillie (technically EPP affiliated). To everyone who always supported me, pushed me to do great things, and believed in me. I am and will be forever grateful.

To Prof. Ramzy Kahhat from the PUCP. If I hadn't taken your environmental engineering class back in 2012, I wouldn't be here today. Thank you for believing in me, being my mentor, and guiding me through it all.

To the Dennin's: you made Pittsburgh feel like a second home and it will forever hold a piece of my heart and be my home. Thank you, Mr. and Mrs. Dennin, Kelly and Dan Reft, AND Jake (haha), for all your love, support, and endless free meals. I love you all.

Finally, and most important, to my family, without whom I wouldn't be here today. To all my aunts (yes, as a proud Latina I will name all my aunts and uncles in the acknowledgements) Ana, Luly, Marifé, Milena, and Pilar; to all my uncles; to my great-aunt Pilar and my great-uncle Alejandro (la ingeniera ahora tiene un título más). To my grandparents, thank you Abuelito Augusto and Abuelita Milena, I miss you every day; thank you Abuelito Isidoro and Abuelita Luisa for always believing in me. To my cousins, special shoutout to Varsha and Andre. To my sister, Estella, who is always part-sister, part-best-friend, part-therapist. To Christian Dammert who I love to bicker with (haha). To my parents, Augusto and Pilar, who always believed in me, supported me, and gave me the freedom to make my own decisions. Esta tesis va dedicada a ustedes! Last but not least, to my husband, Luke Dennin, who can be double/triple/quadruple counted in multiple other categories. Thank you for supporting me throughout this journey and for always being there for me, through the ups, the downs, the radioactive isolations, the pandemics, and it all! I love you.

Abstract

Global electricity demand is expected to increase over the following decades, with more than half a billion people worldwide still lacking access to modern electricity services. Additionally, the power sector is one of the largest contributors to increasing GHG atmospheric concentrations, and there is a pressing need to decarbonize the sector. Unfortunately, emerging economies in the Global South, where most of the electrification needs to happen, are some of the most vulnerable to the potential impacts of climate change. Therefore, to achieve the UN's Sustainable Development Goal 7 of universal electricity access, emerging economies will need to expand their electricity infrastructure while cutting emissions and adapting to climate change.

Hydropower may be a low-carbon option to increase supply and decarbonize electricity generation. Unfortunately, climate change can affect hydropower operations through changes in the timing and magnitude of precipitation, rising temperatures, and glacier mass. Evaluating climate impacts on hydropower generally requires detailed local input data and hydrological models, which may not be available in many places of the Global South. Nevertheless, there is a pressing need to understand these impacts for future planning decisions. Research that focuses on developing flexible data requirement tools and models able to use climate projections and remotely sensed datasets for data-scarce regions is needed. Furthermore, identifying climate impacts and their potential risks on hydropower plants is just the first step towards the future adaptation of the hydropower sector. Communicating assessment results to relevant decision-makers will be crucial, yet effective communication tools for climate adaptation are still lacking.

The objective of this dissertation was to characterize and understand the impacts of climate change on usable hydropower capacity in the Global South. First, I developed a hydrological model paired with a hydropower operations model to assess usable capacity at the power plant level in data-scarce regions of the world. Then, I used the model to analyze the changes in usable capacity in Brazil, Colombia, and Peru under a multi-model ensemble. Later, I used the same model across five African power pools. I expanded the initial assessment to incorporate changes in variability of hydropower resources in Africa; and generate interconnection scenarios based on the complementarities of these resources. The final piece of this dissertation consisted of creating an interactive analysis tool that includes all previous assessments and incorporated 56 more countries across five regions of the Global South.

List of Figures

List of Tables

Table of Contents

Chapter 1 – Introduction

The power sector accounts for more than a third of worldwide greenhouse gas (GHG) emissions[1], making it one of the largest contributing sectors to atmospheric concentrations. GHG emissions have to dramatically decrease to avoid the most severe impacts of climate change[2,3]. Moreover, electricity demand continues to increase worldwide. In 2018, global demand rose by 4%, increasing the power sector's GHG emissions by 2.5%[4]. Still, more than 800 million people worldwide lack access to these modern electricity services[5]. Emerging economies will need to expand their electricity infrastructure in urban and rural communities to meet the United Nations (UN) Sustainable Development Goal (SDG) of universal sustainable electricity access[6]. These economies are some of the most vulnerable to projected climate change impacts, such as extreme heat and precipitation[7]. Moreover, the expansion of their electricity systems will occur in a sector that requires global emission reductions.

Hydropower is the most abundant renewable source of electricity worldwide, and it is expected to play an essential role in the sector's decarbonization[8]. 16% of worldwide electricity generation in 2019 came from this electricity source[9]. Hydropower can balance intermittent renewables (e.g., solar and wind) and be a low-carbon option (e.g., run-of-river) to meet the growing energy demand in emerging economies[10]. Unfortunately, climate change impacts can threaten the viability of future hydropower development and operations. Climate change can affect hydropower operations through changes in the timing and magnitude of precipitation patterns that directly affect streamflow. Additionally, rising temperatures increase evapotranspiration within the basins, reducing the available water volumes, potentially generating decreases in capacity around the world[11,12]. Understanding a range of future water availability patterns under climate change is essential for the future of hydropower operations. Especially as some regions become more water-stressed, and others may experience increases in water availability.

Several studies examine hydropower generation and variable water availability under climate change. Most use complex hydrological models[12–20], like the Variable Infiltration Capacity (VIC) model[21]. Such models have high data requirements that limit their applicability to data-sparse countries or regions. While some studies have used simpler semi-lumped

hydrological models to project climate change impacts on hydropower generation[22–28], the main regions studied include the continental U.S. and Europe[13,15–20,22–24,27–29]. Some studies focused on the worldwide impacts of climate change on hydropower generation[12,14], while others concentrated on specific regions such as the Niger Basin in Western Africa[26]. Studies show mixed increases and decreases in hydropower generation during the 21st century depending on the region studied. Van Vliet et al. 2016, concluded that regions with "considerable (>20%) declines" on hydropower generation potential include Southern Europe, Northern Africa, the Southern U.S., parts of South America, Southern Africa, and Southern Australia[14]. However, these studies do not address individual power plants, leaving a gap in the literature regarding climate impacts on hydropower projects in many developing countries. Further analyses for the Global South are needed[30,31].

Another aspect understudied in the literature is the impact of glacier melt on hydropower operations. Climate change, specifically increasing temperatures, will likely result in glacier shrinkage across the globe[32–44]. In the case of one of the case studies presented in this dissertation: Peru, the Peruvian Cordillera Blanca, contains 71% of the world's tropical glaciers[45]. Therefore, Peru is an interesting case study for glacier retreat and its effect on hydropower operations. According to a study conducted by the Peruvian Meteorological Service (SENAMHI) in 2015, most glaciers in the Peruvian Andes have already retreated between 57% to 100% and are now only considered seasonal snow cover[44]. Projections show these glaciers disappearing by the end of the century[11,46]. Accelerated melting has contributed to increases in dry season water supply[33–35,37,39,47], but this will only be a transitory effect. Glacier "peak" discharge has most likely already occurred in the Peruvian Andes[35,37], so the contribution of glacier melt to streamflow is likely to decrease in the future. These effects can also be present in other glacierized and snow-dominated basins in other regions of the world, such as the Swiss Alps and the Sierra Nevada in California, USA[16,23,48].

Given the limited research on climate-induced risks to hydropower plants in developing countries, this dissertation contributes to the literature by first: creating a simple water balance hydrological model paired with a hydropower operations model to evaluate climate-induced risks to hydropower generations in regions where extensive hydrological data may not be available; second: characterizing future hydropower availability across the Global South; and third:

developing an interactive visualization tool for multi-model ensemble results of future hydropower availability using open-sourced software.

1.1 Using Downscaled Global Climate Models

Climate Change is already affecting temperature and rainfall patterns across the globe[3]. The IPCC Assessment Report 6 Working Group I report expects the effects of climate change to broadly vary across different regions of the world[49,50]. Increasing temperatures and variation in rainfall will affect water availability. While some regions will become more water-stressed, other regions will experience increased water availability.

The development over time of large-scale global climate models (GCMs) contributes to a better understanding of the effects of climate change on a broad regional level. GCMs have become more complex over the past 20 years and now include more dynamics, biology, and chemistry of the atmosphere, biosphere, and oceans[51]. These models discretize the atmosphere, oceans, and land into cells with a resolution between 100 km^2 to 250 km^2 [51]. This resolution is too coarse to understand the dynamics on a smaller spatial resolution and shorter time frames than monthly climate variables. Downscaling is needed to be able to determine finer resolution changes. Climate scientists use dynamical and statistical downscaling methods to obtain these finer resolution results[52]. Dynamical downscaling methods consist of building models similar to GCMs, with a much smaller resolution (temporal and spatial) for a region of the world[52]. These models, mainly developed for North America and Europe, are usually known as Regional Climate Models (RCMs)[53].

On the other hand, statistical downscaling involves using statistical methods, such as regression, to relate global climate patterns to local climate patterns[52]. For other regions of the world, such as South America and Africa, the quality of the results obtained for RCMs is not the same as in Europe or North America[53]. Nevertheless, projections for the Global South from different GCMs and using other downscaling techniques exist[54,55] and, in the meantime, are the best available resources for climate studies in the region.

While global projections from the Coupled Model Intercomparison Project Phase 6 (CMIP6) are becoming available, regional, and statistically downscaled data were unavailable

when I conducted these analyses[56,57]. For the analyses undertaken in this dissertation, I thus use downscaled meteorological data from the Coupled Model Intercomparison Project Phase 5 (CMIP5). Specifically, I use NASA's Earth Exchange Global Daily Downscaled Projections (NEX-GDDP) dataset[55]. NEX-GDDP consists of comprehensive high-resolution climate data (0.25 degrees), which includes retrospective (control) and prospective runs from 21 General Circulation Models (GCMs) under Representative Concentration Pathways (RCPs) 4.5 and 8.5[58] from CMIP5. To capture the uncertainty of the climate models I use all 21 GCMs and report their simulation results in all three chapters of this dissertation.

Currently, the NEX-GDDP dataset provides consistently downscaled projections at a higher spatial resolution than other dynamically downscaled projection datasets, such as the Coordinated Regional Climate Downscaling Experiment (CORDEX), for the entire globe. As of December 2021, the update for the NEX-GDDP (NEX-GDDP-CMIP6) dataset now includes CMIP6 runs and encompasses more climatic variables than the previous version[59]. While the work presented in this dissertation uses CMIP5 runs, future work should use this newer version of the dataset.

As previously mentioned, the emissions scenarios used in this dissertation include RCP 4.5 and 8.5. RCP 4.5 represents a mid-emissions scenario (an increase of 2.5°C global average temperature by the end of the century), and RCP 8.5 a high emissions scenario (an increase of 5 °C global average temperature by the end of the century). I use RCPs 4.5 and 8.5 to quantify physical climate risk and note that RCP 8.5 encompasses the cumulative CO_2 emissions that occur under other RCPs[60,61] (they just happen sooner under RCP 8.5). I do not ascribe likelihood to one scenario over another.

1.2 The Hydropower Sector in the Global South

The hydropower sector generates more than 4,300 TWh of electricity annually (4,370 TWh in 2020)[62]. The regions with the largest installed capacity include Southeast Asia and the Pacific (~501 GW), followed by Europe (~254 GW), North and Central America (~205 GW), and South America (~177 GW)[62]. Furthermore, hydropower installed capacity worldwide continues to grow, and in 2020 a total of 21 GW of new hydropower capacity came online around the world[62]. The biggest installations include the Wudongde hydropower plant in China (6,800

MW), followed by the Lauca power plant in Angola (2,071 MW), and the Jixi (PSH) power plant also in China (1,800 MW). The regions with the largest new installations were Southeast Asia and the Pacific (14.5 GW of new installed capacity), followed by Europe (3.0 GW of new installed capacity), and South and Central Asia (1.6 GW of new installed capacity)[62].

While South America was the region with the least capacity additions in 2020, it remains the second-largest hydropower producer in the world[62–64]. With ~38 GW of hydropower installed capacity; Africa remains the region with the least hydropower capacity. Currently, more than half a billion people still lack access to modern electricity services in this region, specifically in Sub-Saharan Africa[65]. According to the Programme for Infrastructure Development in Africa (PIDA), hydropower will play an essential role in the region's electrification[66]. Therefore, Africa will be an important region for future hydropower developments.

Additionally, some countries rely more on hydropower generation than others. Reliance on hydropower, more than 50% of a country's electricity generation coming from hydropower, will play a key role in individual countries' vulnerability to climate change impacts. For example, South America is a region that is heavily reliant on hydropower generation. In 2020, the region produced an estimated 690 TWh of hydroelectricity[62], representing around 75% of its total electricity generation[67]. Analogously, in Sub-Saharan Africa, hydropower typically represents around half of the electricity generated each year [68]. Furthermore, this dependence can make regions highly susceptible to changes in hydropower availability under a changing climate.

For this dissertation, I identified five regions in the Global South with high hydropower growth potential[10,69]. First, I focus on regions with high hydropower dependence (South America and Africa), and then I extend the work to encompass most of the Global South. The countries in these regions serve as case studies for the following chapters. I include *1. Mexico and Central America, 2. South America, 3. Africa, 4. The Middle East*, and *5. Southeast Asia and the Pacific*. Table 1-1 describes the key characteristics of the hydropower systems in each of the five regions mentioned. I analyze a total of ~250 GW of hydropower installed capacity (56 countries and 542 hydropower plants) in this dissertation. Figure 1-1 shows a map of all the hydropower plants included, scaled by their installed capacity, in the five regions.

Table 1-1 – Main hydropower characteristics of regions included. I obtain the current installed capacity for each region and the largest producing country[62,63]. The proportion of the population with electricity access represents the level of electrification in the region[65,70].

Region	Current Installed Capacity	Country with Highest Installed Capacity (GW)	Proportion of Population with Electricity Access
Mexico and Central America	21 GW	Mexico (12 GW)	94.8% (Mexico, Central, and South America)
South America	177 GW	Brazil (101 GW)	
Africa	38 GW	Ethiopia (4 GW)	North Africa: 99+% Sub-Saharan Africa: 47.9%
Middle East	22 GW	Iran (12 GW)	92.3%
East Asia and the Pacific*	501 GW	China (370 GW)	96.0%

* For our analysis, I include the region Southeast Asia and the Pacific, which excludes China.

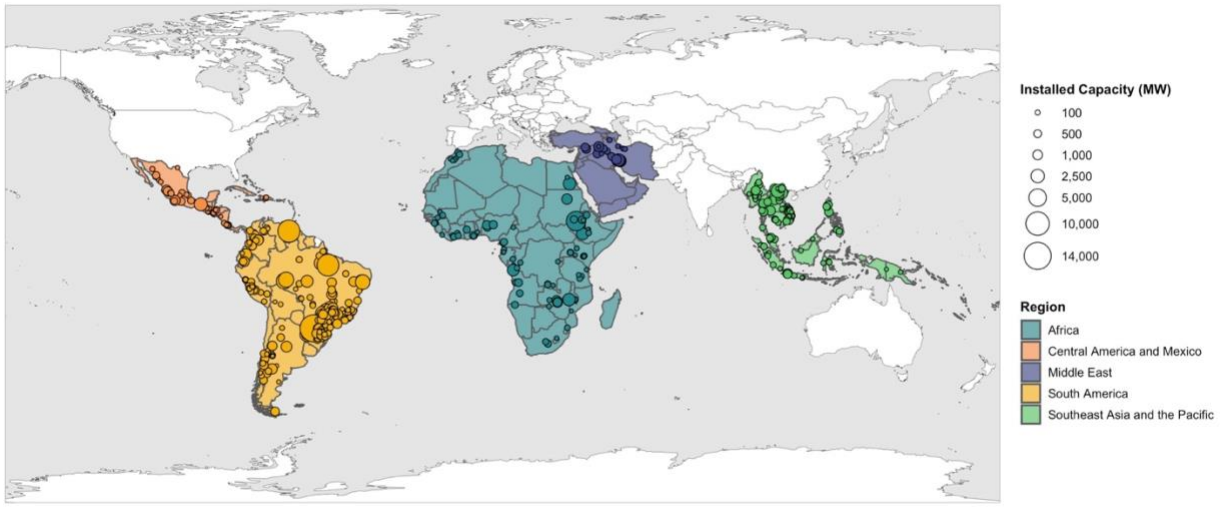

Figure 1-1 – Hydropower plants included in the case studies presented in this dissertation. I include 542 hydropower plants across five regions of the Global South. The regions include Mexico and Central America, South America, Africa, the Middle East, and Southeast Asia and the Pacific. I do not include China, Japan, or Korea in Southeast Asia and the Pacific.

1.3 Water Availability and Hydropower in a Changing Climate

Several studies exist on the matter of hydropower generation and variable water availability. In this section, I present a brief summary of some of the studies reviewed for this dissertation. Some studies address water availability and electricity generation sources[12–15,18,71,72], and others exclusively focus on hydropower generation[16,17,20,22–27,29]. Ganguli, Kumar, and Ganguly focus on water stress and its impact on thermoelectric power plants in the contiguous US[71]. They use a simple approach for modeling water availability: a water balance model that considers available precipitation (difference between precipitation and evapotranspiration). A "multivariate water stress index" is developed using projections from 45 models of CMIP5 and all representative concentration pathways (RCP): 2.6, 4.5, 6, and 8.5. This index evaluates scarcer and warmer conditions that could lead to compromised operations of wet-cooled thermal power plants. They highlight the need to develop an index for the near and midterm future instead of using projections for the end of the century.

Van Vliet et al. (2012) also analyzes future climate change impacts on thermoelectric facilities for Europe and the US[13]. It evaluates 61 thermoelectric power plants in the US and 35 in Europe. The study aims to test the vulnerability of these plants to Climate Change. Using three global climate models (GCM) projections and two Special Report Emissions Scenarios (SRES), and the Variable Infiltration Capacity (VIC) model, the variations on streamflow and streamflow temperature are determined. On the contrary to the previous study, instead of using a simple water balance, van Vliet et al. use this complex hydrologic model, the VIC, to estimate streamflow. The authors use the gross output of thermoelectric power plants under these future conditions to determine the vulnerability of electricity generation to climate change.

Other studies evaluate multiple sources of electricity generation and the effect of variations in water availability[12,14,15,18]. Van Vliet et al. (2016a) evaluate thermoelectric and hydroelectric power generation worldwide[12]. This study assesses 24,515 hydropower plants and 1,427 thermoelectric power plants and uses the VIC for streamflow calculation (1971-2099, including historical calibration data from the Global Runoff Data Centre – GRDC). The authors use 5 GCMs and 2 RCPs: 2.6 and 8.5. They evaluate system vulnerability through potential hydroelectric and thermoelectric reductions calculated with the streamflow and streamflow.

Bartos and Chester evaluate climate change impacts on the Western United States electricity production. They consider thermoelectric, hydroelectric, wind, and solar facilities. Similar to the previous study, they use the VIC to determine streamflow with CMIP3 downscaled projections (SRES A2, A1B, and B1). The study analyzed a historical period between 1949-2010 and a future period between 2010-2060 for 978 Western US power plants. The authors use peak load conditions to evaluate the impacts on generating capacity.

Voisin et al. evaluate thermoelectric, geothermal, hydropower, wind, solar, and pumped hydroelectric vulnerability in the Western United States with a historical perspective[18]. The study used a 30-year dataset between 1985 to 2015 to run the Land Surface Hydrology Model and the Community Land Model coupled with a routing model MOSART to calculate streamflow. The authors obtain historical costs from the Western Electricity Coordinating Council (WECC). Coupling an integrated water model and this cost model, the authors identify hotspots and develop the Water Scarcity Grid Impact Factor (WSGIF) by aggregating the results from plant-level to grid-level.

A following 2016 study by van Vliet et al. used three different complex hydrological models for streamflow calculations, including the VIC. This study evaluated both thermoelectric and hydroelectric power plants using 5 GCMs and RCPs 2.6 and 8.5 on a global scale[14]. The control period used was 1971-2000, and the future periods analyzed were 2010-2039, 2040-2069, and 2070-2099. The metric used to evaluate vulnerability was gross hydropower potential harnessed down at sea level. Additionally, cooling water discharge capacity was the metric used for thermoelectric power plant impact assessment.

Lehner et al. use the global hydrological model WaterGAP (Water – Global Analysis and Prognosis) to calculate streamflow from projections and evaluate hydropower potential in Europe under climate change[22]. They used a baseline period of 1961-1990 and future periods representative of the 2020s and 2070s decades to assess run-of-river and storage hydropower plants. The study assumes storage power plants harness all the streamflow that runs through them. The projections used include two GCMs and the IPCC-IS92a scenario, the intermediate Baseline-A scenario by the Dutch National Institute of Public Health and Environment, and the SRES A1B.

Schaefli et al. use a semi-lumped water balance that separates snow-covered areas from non-snow-covered areas to evaluate streamflow and the impact of climate change on hydropower

production in the Swiss Alps[23]. Instead of using GCMs and scenarios, the study used a perturbation method to account for future climate alterations. The control period was 1961-1990, and the future period was between 2070 to 2099. The dam of Mauvoisin is the only facility analyzed by using two parallel balances: one for rainfall and one for snowmelt. The authors evaluated several metrics, including reliability, vulnerability, and resilience.

Vicuna et al. use the VIC paired with 4 GCMs and SRES A2 and B1 to evaluate the impacts of climate change on high elevation hydropower generation in California[16]. The study evaluates the impact of streamflow seasonality on hydropower generation. The analysis uses a historical unimpaired natural runoff period from 1960 to 1990 and a future conditions period from 2070 to 2099. The authors model 11 reservoirs using a linear program in the Sierra Nevada basin. The Sacramento Municipal Utility District operates these reservoirs.

Later on, Vicuna evaluated two high-elevation hydropower systems in California using the VIC again[17]. This study looked at the Upper American River Project and the Big Creek System under projections from 6 GCMs, and SRES A2 and B1. The analysis, performed on a project level with an optimization model, used daily time series of streamflow at various locations and calculated operations for the reservoirs in the systems. Later, the authors translated streamflow into hydropower generation and revenues and used them as evaluation metrics.

Maran et al. use the TOPKAPI model developed by the ETH Zurich, the ECHAM GCM with two RCMs for downscaling, and the SRES A1B to compute climate change impacts from 2011-2050 in an alpine catchment. The authors evaluated the Val D'Aosta region in Italy with an optimization model built-in for reservoir operations evaluation.

Kao et al. ran the VIC 5 times with RegCM3 downscaled data from the CCSM3 GCM using the SRES A1B. The study evaluated regional US hydropower generation in an aggregated manner. The analysis, performed on an annual basis, cannot capture the seasonality of flows. It uses only Federal US Hydropower plants. The authors correlated runoff with electricity production from historical records assuming capacity did not vary in the 20 years since they obtained the records.

Tarroja et al. used the VIC, ten climate models, RCPs 4.5 and 8.5 to evaluate climate impacts and the implication on grid-level carbon dioxide emissions from 2040 to 2050 in California[20]. They used electricity grid performance metrics, with streamflow as the main variable,

to assess the impacts of climate change. Additionally, the study discusses the implications of greenhouse gas emissions of the California electricity grid. In addition to using the VIC for streamflow, the study used an electric grid dispatch model to simulate actual grid operations.

More recent studies continue to use semi-lumped water balance models[25–27,29] for streamflow projections. Turner et al. 2017, presented the Global Water Availability Model (GWAM): a water balance model that accounts for soil fluxes on top of precipitation and evaporation fluxes. Guadard et al., Chilkotti et al., and Oyerinde et al. performed an analysis based on specific power plants[26,27,29]. Consistent with previous studies, these analyses look at the variation of streamflow due to climate change and its impact on hydropower production.

These studies represent a sample of the existing literature on climate change impacting hydropower generation. After this review, I can see that there is still a gap for regional studies in the Global South. The studies presented developed specific case studies or large-scale global assessments but, for the most part, did not perform comprehensive and consistent studies for the Global South. My dissertation attempts to fill this gap: assessing climate-induced vulnerabilities of hydropower plants in the Global South.

1.4 Research Objectives

This dissertation fills in the literature gap of understanding climate-induced risks and vulnerabilities on hydropower systems in the Global South. First, I developed a model to characterize climate-induced changes on hydropower usable capacity at the power plant level. Then, I performed case studies for South America and Africa. For Africa, I assessed current and future complementarities of hydropower resources and proposed interconnections scenarios for the region. Finally, I developed a visualization tool including the characterization of 542 hydropower plants in the Global South. This dissertation had three objectives, which correspond to Chapters 2 through 4. The objectives were as follows:

- **Chapter 2:** Understand and characterize the impacts of climate change on hydropower usable capacity in Brazil, Colombia, and Peru using a multi-model ensemble and two emissions scenarios.

    - How can we characterize future hydropower usable capacity in data-scarce regions of the Global South?
    - What factors affect hydropower usable capacity in a changing climate for medium to large hydropower plants in Brazil, Colombia, and Peru?
    - What are the differences in simulated future usable capacity under different emissions scenarios (RCP 4.5 and 8.5)?
- **Chapter 3:** Understand and characterize the impacts of climate change on hydropower usable capacity and variability in Africa using a multi-model ensemble and two emissions scenarios. Propose interconnection scenarios based on the complementarity of hydropower resources for the continent.
    - What are the changes in usable hydropower capacity under climate change for the African continent?
    - To which degree hydropower resources in Africa can complement each other based on seasonality and the size of the systems?
    - How does the variability of hydropower resources change under different climate change scenarios (RCP 4.5 and 8.5)?
    - Which interconnections for the African continent would benefit from the complementarity and changes in variability of hydropower resources?
- **Chapter 4:** Characterize, visualize, and communicate future hydropower usable capacity in a changing climate using a multi-model ensemble and two emissions scenarios for the Global South.
    - What are the changes in usable hydropower capacity for 542 hydropower plants across five regions of the Global South?
    - What type of climate information and metrics can I use to communicate the changes in usable hydropower capacity to stakeholders?
    - How can I develop an open-source interactive analysis tool for usable hydropower capacity in the Global South using a multi-model ensemble?
    - For a given hydropower plant, what could be the future hydropower usable capacity in three future time-frames (2010-2039, 2050-2069, and 2070-2099), under a multi-model ensemble of 21 GCMs, and two RCPs (4.5 and 8.5)?

1.5 Dissertation Structure

This dissertation consists of an introduction (Chapter 1) and three additional chapters, one of which was published (Chapter 2), one is currently under review for publication, and the third one will be submitted for publication in a peer-reviewed journal after the completion of the defense. Chapter 1, the introduction, presents the background information for the dissertation and the overall structure of this document. Chapter 2, published in 2021 in Energy for Sustainable Development[73], presents a model to evaluate climate-induced changes in river flows that affect hydropower availability. Further, this chapter tests the model with 134 hydropower plants with an installed capacity larger than 100 MW in Brazil, Colombia, and Peru. Chapter 3, currently under review for publication in Nature Climate Change, investigates the potential changes in hydropower usable capacity using a multi-model ensemble and two emissions scenarios for 87 hydropower plants in Africa. Additionally, this chapter explores the differences in interannual and seasonal variability of usable hydropower capacity at the power plant, country, and power pool level. It proposes interconnection scenarios for Africa based on the complementarity of the hydropower resources in the continent. Chapter 4, which I plan to submit for publication after the defense, aims to integrate all previous assessments (Chapters 2 and 3) and extend the work to visualize and interactively communicate the changes in usable hydropower capacity for 542 power plants in the Global South. In this chapter, I develop an interactive analysis tool named RICCH: Risks and Impacts of Climate Change on Hydropower, which is currently available through shinyapps.io (https://ricch.shinyapps.io/hydro-shiny/). Finally, Chapter 5 presents a summary, discussion, and the overall conclusions of this dissertation.

Chapter 2 – Hydropower under climate uncertainty: characterizing the usable capacity of Brazilian, Colombian, and Peruvian power plants under climate scenarios

The contents of this chapter and its supporting information (included as Appendix A) have been published as: Caceres, A. L., Jaramillo, P., Matthews, H. S., Samaras, C. & Nijssen, B. (2021) "Hydropower under climate uncertainty: Characterizing the usable capacity of Brazilian, Colombian and Peruvian power plants under climate scenarios," *Energy for Sustainable Development, **61:** 217-229.*

2.1 Abstract

Hydropower may be a low-carbon option to increase power generation in developing countries, but these countries are some of the most vulnerable to climate change. Climate change can affect hydropower generation through changes in the timing and magnitude of precipitation, rising temperatures, and glacier mass changes. Evaluating climate impacts on hydropower generally requires detailed local input data and hydrological models, which may not be available in many developing nations. Nevertheless, the need to understand the impacts is essential for the developing world. Here we present a modeling framework that relies on remotely sensed and global gridded datasets forced by an ensemble of 21 general circulation models (GCMs) under two representative concentration pathways (RCPs) to evaluate climate-induced impacts on hydropower through the 21st century. We include 134 hydropower plants (> 100 MW), representing 42% of hydropower installed capacity in South America, across five regions of Brazil, Colombia, and Peru. Our results suggest the median monthly usable capacity would increase for Colombia (+2.6% to +8.4% for RCP 4.5 and 8.5, respectively) and Peru (+6.7% to +9.3% for RCP 4.5 and 8.5, respectively) by 2100 relative to the late 20th century. For Brazil, we observe a mix of reductions and increases in usable capacity. While our results suggest potential reductions for the dry season usable capacity in the Parana, Paraguay, and Southeast Atlantic regions of Brazil, we also observe slight increases in usable capacity during the rainy months for all its regions. These results can help inform future planning decisions and potential interconnections between the three countries. Additionally, the proposed framework can contribute to an increased capability to evaluate climate-induced risks to power systems in developing countries, where data and computation resources can be limited.

2.2 Introduction

The power sector accounts for more than a third of worldwide greenhouse gas (GHG) emissions[1], making it one of the largest sectors contributing to anthropogenic climate change. GHG emissions have to eventually decrease to zero to avoid the most severe impacts of climate change[2,3]. At the same time, electricity demand continues to increase worldwide. In 2018, global demand rose by 4%, leading to an increase in 2.5% of power sector GHG emissions[4]. Still, more than 800 million people worldwide lack access to modern electricity services[5]. To meet the

United Nations' (UN) Sustainable Development Goal (SDG) of achieving universal sustainable electricity access, emerging economies need to expand their electricity infrastructure in urban and rural communities[6]. Unfortunately, these economies are also some of the most vulnerable to projected climate change impacts, such as extreme heat and precipitation[7]. Moreover, the expansion of their electricity systems will need to occur within a global power sector that requires substantial emission reductions, compounding climate mitigation, and resilience challenges.

Hydropower is the dominant renewable electricity source worldwide, and it is expected to play an essential role in the sector's decarbonization[8]. Hydropower can balance intermittent renewables (e.g., solar and wind) and be a low-carbon option (especially with run-of-river plants that do not require reservoirs) to meet growing energy demand in emerging economies[10]. Unfortunately, climate change can threaten the viability of future hydropower development and operations. Climate change can affect hydropower operations through changes in the timing and magnitude of precipitation patterns that directly affect streamflow. Additionally, rising temperatures increase evapotranspiration, reducing available water, which can lead to capacity deratings (reductions in usable capacity). Changes in seasonal snow, as well as glacier mass, also have the potential to change the magnitude and seasonality of streamflow. All of these changes can directly affect hydropower operations and the usable capacity of hydropower plants[11].

In prior work, researchers estimated impacts of climate change on global hydropower resources[12,14,74,75], as well as impacts in specific countries and power pools[26,76–78]. Some of these studies report that climate change could reduce usable hydropower capacity in 60-75% of hydropower plants worldwide by 2040-2069[12]. Van Vliet et al. (2016) conclude that regions with "considerable (>20%) decline" of hydropower generation potential include Southern Europe, Northern Africa, the Southern U.S., parts of South America, Southern Africa, and Southern Australia[14]. In the context of South America, prior research has found decreased streamflow and future hydropower potential, mostly in northern Brazil, where there has been an expansion of Amazonian hydropower in recent years[79–84]. Previous studies for Colombia and Peru found a mix of increases and decreases in usable hydropower capacity[85–88]. Finally, some work in Brazil and Colombia included streamflow projections to develop least-cost pathways for expanding the countries' power capacity, concluding that hydropower alone would not meet the increasing energy demand in these countries[89,90].

Earlier studies of climate impacts on hydropower have several limitations in the context of developing countries in the Global South, and further regional studies are needed[30]. The majority of prior research relied on complex hydrological models[12–20], like the Variable Infiltration Capacity (VIC) model[21]. These models typically have high data and computational requirements, making them difficult to apply in data-sparse regions[91]. Furthermore, the bulk of the studies using complex and simpler semi-lumped hydrological models focused on the continental US and Europe[13,15–20,22–29,75].

The expansion of run-of-the-river hydropower in developing countries also requires a better accounting of seasonal streamflow variability and the effects of climate change at seasonal to sub-seasonal time scales. Similarly, there is a gap in the literature about the role of glacier melt on hydropower generation in glacierized catchments in tropical regions (like the Tropical Andes). Prior work on the importance of glacier runoff on hydropower has traditionally not included such tropical catchments and has instead focused on regions outside the Global South[16,17,23,24,92,93]. A recent study that did include the Global South examined hydropower potential in areas where glaciers have already retreated but did not include the retreat's effect on existing downstream power plants[94]. Finally, prior work with a specific focus in developing countries like Peru and Colombia relied on projections from the third version of the Coupled Model Intercomparison Project (CMIP3)[85–88], so there is a need to update such work to include more recent climate projections.

Increasing infrastructure resilience requires a characterization of future climate and its impacts, which has been an inhibiting challenge in data-sparse regions. Lack of reliable records leads to inefficient system design even when using historical climate conditions. If we add the uncertainty of the timing and magnitude of climate change, then the lack of impact assessments and characterizations of future conditions might lead to assets that are inadequate to withstand changing climatic conditions. This paper presents and demonstrates a modeling framework to assess the risk of reductions in usable capacity at individual hydropower plants under climate change. The framework's main appeal is its ability to process publicly available remotely sensed datasets and global gridded datasets', enabling modeling efforts for regions of the world with limited data.

Furthermore, the framework pairs a water balance model with a hydropower model and a reservoir operations model in a consistent manner. The flexibility and use of open access coding languages allow using multiple types of raster files and coupling with other existing models. The hydrological processes in the model are simplified compared to other large-scale hydrological models. This simplification might come at the expense of a detailed representation of the hydrological processes in the system. Still, our results are sufficiently robust to identify patterns that may be of concern to hydropower plants' future operations. Furthermore, power plant operators and decision-makers can use the results to screen the potential risk in yet-to-be-developed sites as emerging economies plan for low-carbon electricity capacity expansion. We apply the framework to 134 hydropower plants across three countries in South America (Brazil, Colombia, and Peru) and discuss the framework's potential to better inform hydropower planning decisions under climate change in these countries and the region.

2.3 Materials and Methods

2.3.1 Water Balance Model

The modeling framework proposed in this paper relies on a water balance model that accounts for runoff from three water sources: precipitation, seasonal snowpack, and glaciers[54,95,96]. We develop our own lumped water balance model to gain greater flexibility of data requirements. The model (developed in R and Python) provides flexibility to use various input data types, including remotely sensed datasets, climate projections, and global gridded products of soil properties and flow characteristics.

Using Python's pysheds[97] and R's spatial analysis packages, we can obtain watershed shapefiles corresponding to individual hydropower plant outlet locations and their upstream glacier area when applicable. The model then processes historical control experiments and projected precipitation, maximum temperature, and minimum temperature using R's raster and NetCDF packages for each of the hydropower plants of interest. The mean elevation from a digital elevation model, average soil moisture, and average soil depth from remotely sensed data for the watershed of interest serve as input to the water balance described in Equation (2.1):

$$Q_t = P_t + Gl_t + \Delta Sn_t - AET_t + \Delta S_t \quad (2.1)$$

Where Q_t is the runoff volume generated in a basin at month t, P_t is the total precipitation for month t, Gl_t is the glacier melt for month t, ΔSn_t is the snowmelt for month t, AET_t is the actual evapotranspiration for month t, and ΔS_t is the change in the soil moisture storage component compared to the previous month. The model calculates the Potential Evapotranspiration (PET) using the FAO's Penman-Monteith Method[98] and then determines AET[99] using the maximum soil moisture constraint. All the components in Equation (2.1) are in million m^3 per month. The model converts the monthly flow to streamflow (m^3/s) for the power calculations.

The model calculates glacier melt and snowmelt using a degree-day method in which it differentiates the degree-day coefficient (mm/degree-day °C) for ice and snow[100]. The model divides each basin of interest into elevation bands and calculates glacier and snowmelt for each elevation band separately. The model assumes glaciers are in equilibrium during the reference period (1970-2005), and there is no seasonal snow cover at the start of the model runs. The original glacier ice volume for the projection calculations relies on a scaling function (Equation A.1.5 in Appendix A.1)[101,102].

When using the model, we initiate the simulations with the initial soil moisture, S_0, set to half the maximum soil moisture capacity, and no seasonal snow. We spin the model for at least five years before the start of the analysis period. Finally, model calibration relies on the Shuffle Complex Evolution (SCE) optimization algorithm[103,104]. This algorithm compares the climatology of historical streamflow to the water balance simulated streamflow and adjusts different parameters to match the time series. Appendices A.1 and A.2 provide additional details concerning the water balance model and the calibration process.

Climate projections of temperature and precipitation are the key drivers of future water availability for the model. While global projections from the Coupled Model Intercomparison Project Phase 6 (CMIP6) are becoming available, regionally and statistically downscaled data are currently unavailable[56,57]. For this analysis, we thus use downscaled meteorological data from the Coupled Model Intercomparison Project Phase 5 (CMIP5). Specifically, we use NASA's Earth Exchange Global Daily Downscaled Projections (NEX-GDDP) dataset[55]. NEX-GDDP consists of comprehensive high-resolution climate data (0.25 degrees), which includes retrospective (control) and prospective runs from 21 General Circulation Models (GCMs) under

Representative Concentration Pathways (RCPs) 4.5 and 8.5[58] from CMIP5. Currently, the NEX-GDDP dataset provides consistently downscaled projections at a higher spatial resolution than other dynamically downscaled projection datasets, such as the Coordinated Regional Climate Downscaling Experiment (CORDEX), for the entire globe. RCP 4.5 represents a mid-emission scenario with atmospheric CO_2 concentrations decreasing after 2040, leading to an increase of 1.8 °C of surface mean temperature by 2100[105]. RCP 8.5 represents an extreme scenario with atmospheric CO_2 concentrations increasing throughout the century leading to an annual mean temperature increase of 3.7 °C[105]. We present a full list of the 21 GCMs included in the dataset in Table A.3-1 of Appendix A.

2.3.2 Hydropower Variables and Model Formulation

To calculate potential hydroelectricity, the model relies on the specifications of each hydropower plant in the analysis. The data required include each power plant's reservoir maximum and usable capacity (volume of water in million m^3), the power plant turbines' installed capacity (MW), the design flow (m^3/s), and the effective height (m). The operations of the plant depend on the type of hydropower project. Run-of-river hydropower plants have limited storage capacity and do not require operating a reservoir. Impoundment plants with storage capacity require the operations of a reservoir. Equation (2.2) describes the potential output power of run-of-river hydropower plants.

$$P_t = Q_t \cdot H \cdot \rho_w \cdot g \cdot \eta \qquad (2.2)$$

Where P_t is the potential average power output of each power plant (MW) in month t, Q_t is the input flow (m^3/s) in month t, H is the effective head of the turbine (m), ρ_w is the water's density (1,000 kg/m^3), g is the gravitational acceleration (9.8 m/s^2), and η is the turbine efficiency (90%).

To model reservoir operations in impoundment power plants, we relied on R's Reservoir package[106–108]. This model assumes that reservoir operations maximize hydropower generation and rely on the basic mass balance equation presented in Equation (2.3).

$$S_{t+1} = S_t + Q_t - R_t \qquad (2.3)$$

$$where\ 0 \leq S \leq S_{cap}$$

Where S_t is the volume of water stored in the reservoir, Q_t is the inflow to the reservoir, and R_t is the controlled release at time step t. S_{t+1} is the remaining stored water in the reservoir after the releases in the time step, and we use it for the future calculations of releases. The capacity of the reservoir ($S_{cap)}$ is the constraint for Equation (2.3). The Reservoir package calculates the optimal water releases to maximize hydropower generation using this basic formulation. In our modeling framework, we simulate water releases with the dynamic programming option for optimal hydropower generation.

2.3.3 Robustness Assessment

To perform robust analyses of climate change's impact on hydropower operations, we need to understand the spread across the climate projections we use. We refer to the spread as the wide range of possible futures that arise from using a multi-model ensemble of 21 GCMs. To understand where the spread is coming from and how the selection of RCPs and GCMs affect the model simulations results, we conduct a two-way analysis of variance (ANOVA) paired with an Internal Variability (IV) assessment. We perform this assessment following Chegwidden et al., 2019[109]. We use annual streamflow as a proxy for hydropower generation. We quantify the contributions of different factors to the annual streamflow changes between the control period (1970-2005) and the end of the century (2070-2099) projections with GCM and RCP as the ANOVA drivers.

Additionally, we perform an IV assessment that aims to capture the Earth system's natural fluctuations that deviate from an externally forced long-term trend such as greenhouse gas emissions. We conduct this analysis assuming a linear model for the predicted annual streamflow and the annual radiative forcing values corresponding to each RCP. We calculate the IV variance with the residuals of the change in the 30-year means. Finally, we calculate the total variance following Equation (2.4).

$$TV = IV + MV \tag{2.4}$$

Where TV is the total variance, IV is the internal variability, and MV is the model variability. We define MV as:

$$MV = RCP + GCM + Residual \tag{2.5}$$

Where RCP and GCM are the proportions of variance, explained by the representative concentration pathway and general circulation model selection (the residual from Equation (2.5) is different from the residual of the IV assessment previously mentioned).

2.4 Case studies

This paper demonstrates the use of the modeling framework described in the previous sections through three case studies for hydropower-dependent countries (>50% of electricity generation from hydropower) in South America. This region has traditionally relied on hydropower to meet its electricity demand. Brazil, Colombia, and Peru plan to continue expanding their hydropower generating capacity in the upcoming years through the construction of new projects[63,64,110–112]. Brazil is the largest hydropower producer in the region with an installed hydropower capacity of 109 GW (62 GW of which are in the country's southern region and included in this assessment)[63,113]. Colombia, which neighbors Peru and Brazil, is the third-largest hydropower producer in the region with 11 GW of installed hydropower capacity[114]. Finally, Peru has 5 GW of installed hydropower capacity. The Peruvian Andes contain 71% of the world's tropical glaciers, which are already experiencing dramatic changes[32–46,115,116]. These glaciers' disappearance poses threats such as decreased water supply and glacier lake outburst floods to downstream communities[117–119]. As a result, Peru is a good case study to explore the role of glacier retreat on hydropower operations[95,120]. Finally, Brazil, Colombia, and Peru are neighboring countries, offering opportunities to assess their hydropower resources' complementarity. While their power systems are not currently interconnected, there are discussions about pursuing such interconnection. For example, in 2010, Brazil signed an interconnection plan with Peru, which would have led Peru to sell its excess hydropower generation to Brazil[121]. Although these plans are currently halted, future interconnections in the region could either result in benefits through the complementary of their hydro resources or result in increased vulnerabilities due to correlated capacity reductions.

2.4.1 Power Plants

Our analysis focuses on medium to large hydropower plants with an effective installed capacity larger than 100 MW in the Colombian National Interconnected System (SIN), the Peruvian

National Electric Interconnected System (SEIN), and the southern part of the Brazilian National Interconnected System (SIN). The total number of power plants includes 19 in the entire territory of Colombia and 18 in Peru's entire territory. For Brazil, we include 97 plants in five regions in the south of the country: Parana, Paraguay, South Atlantic, Southeast Atlantic, and Uruguay. Table 2-1 includes the sources for the data needed to run the model for the power plants in the case study. Table 2-2 presents a summary of the main characteristics of the systems studied and the power plants in the analysis. Finally, Figure 2-1 shows the power plant locations within each country and their installed capacity. Appendix A.4 (Table A.4-1) includes the full list of the power plants in the analysis.

Table 2-1 – Remotely sensed, global gridded, and georeferenced datasets needed for the case studies.

Model Component	*Details*	*Temporal Resolution*	*Spatial Resolution*	*Period*	*Data Source for Case Study*
Major Basin Outlines	Basin outlines for Peruvian and Brazilian Major Hydrological Units	Static	Polygon outlines with information (GIS)	Static	Peruvian Water Authority (ANA), Brazilian National Electricity Agency (ANEEL)
Digital Elevation Model	Elevation (m)	Static	1 arc degree	Static	Shuttle Radar Topography Mission (SRTM)[122]
Soil Information	Soil moisture capacity (mm/m) Effective soil depth (cm)	Static	Polygon outlines with information (GIS)	Statics	FAO's Digital Soil Map [123]
Flow Characteristics	Flow accumulation and drainage direction raster files	Static	15 arc-second	Static	Shuttle Elevation Derivatives at multiple Scales (HydroSHEDS) dataset [124]
Control Climate Experiments	Precipitation ($kg/m^2/s$) Temperature (K)	Daily	0.25 degrees	1950 – 2005*	NASA Earth Exchange Global Daily Downscaled Projections (NEX-GDDP)[55]
Future Climate Experiments	Precipitation ($kg/m^2/s$) Temperature (K)	Daily	0.25 degrees	2006 – 2099*	
Glacier Information	Area (km^2) Median elevation (meters above sea level) and glacier area (km^2)	Collected at different times	Polygon outlines with information (GIS)	Static	Randolph Glacier Inventory (RGI) [95]

* We subset the results from NASA's NEX-GDDP to 1970-2005 for the historical experiment and 2010-2099 for the projection runs.

Table 2-2 – Summary of Power Plants in Brazil, Colombia, and Peru. Peak demand represents the maximum instantaneous demand in Megawatts for 2019. The total installed capacity in the analysis is the sum of all power plants included, and the range presented shows the smallest and the largest hydropower plant.

Country	*Population (million)*	*Peak Demand (MW)*	*Installed Capacity in the Analysis (MW) – Total and Range*	*Number of Power Plants in the Analysis*
Brazil	209.5 [125]	90,500 [126]	61,700 (100 – 14,000)	97
Colombia	49.6 [125]	10,600 [127]	9,000 (130 – 1,200)	19
Peru	32.0 [125]	7,200 [128]	4,200 (80 – 800)	18

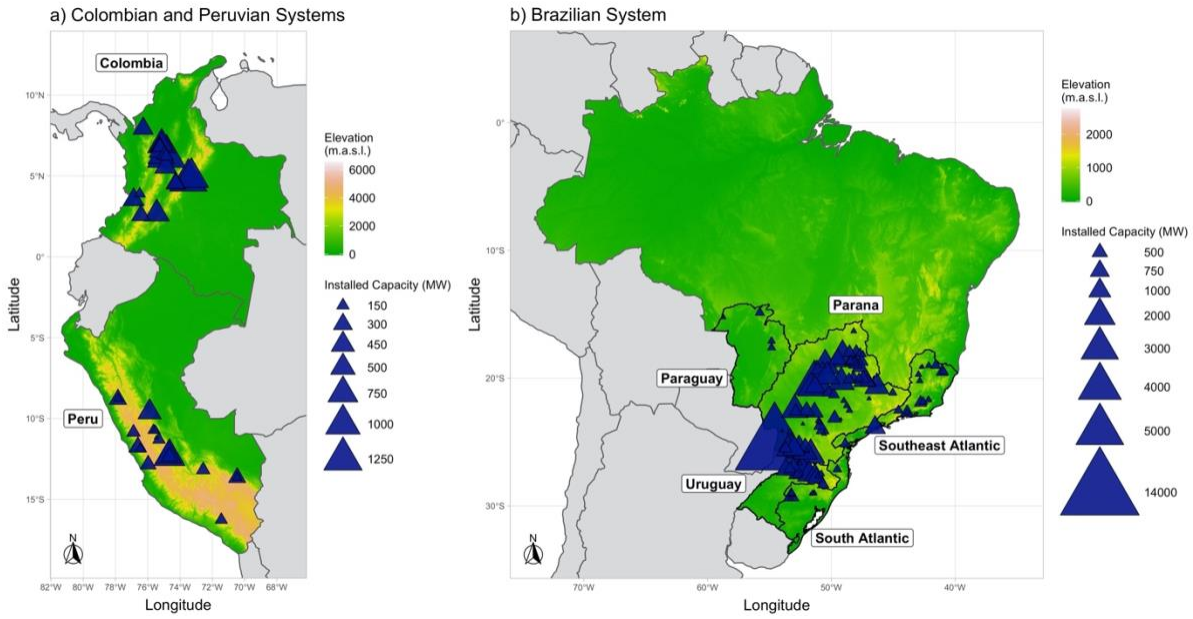

Figure 2-1 – Power plants included in the analysis located in a) Colombia and Peru, and b) Brazil. 134 power plants with a total installed capacity of 75 GW.

We obtain power plant characteristics from government institutions in each country. The National Energy Agency's Electric Sector Geographic Information System (SIGEL) provides georeferenced information of all hydropower plants in Brazil's SIN. The information included power plant and adjacent reservoir characteristics required for Equations (2.2) and (2.3). Additionally, we download historical streamflow data from the National Electric System

Operator (ONS) for each hydropower plant in the analysis. The length of the records varies depending on the year the power plant came online. For Colombia, we obtain the power plant's characteristics from the Colombian Electric System Operator (XM) and complement the information with data from Macías Parra & Andrade, (2014)[87]. Finally, for Peru, we obtain the power plant characteristics from the Ministry of Energy and Mines (MINEM) and the Supervising Organism of Energy and Mines (OSINERGMIN)[129–132]. Historical operating data comes from the information portal of the Economic Operator of the Peruvian National Interconnected System (COES)[133,134].

All the Peruvian hydropower plants in the analysis are run-of-river hydropower plants with limited storage[129–132]. As a result, we excluded the reservoir operations module described in Equation (2.3) for Peru's case study. In contrast, the Colombian and Brazilian hydropower plants include a mix of reservoir hydropower plants and run-of-river hydropower plants. Based on data from the power plant operators in these countries, we confirmed that they maximize generation in their power plants. Thus, we used Equation (2.3) to model reservoir operations of the impoundment power plants in Brazil and Colombia's case studies.

2.4.2 Analysis of Usable Hydropower Capacity

We obtain time series of usable capacity at the power plant level from the model for seven scenarios. These scenarios include a control run (1970-2005) and three future time frames (2010-2039, 2040-2069, and 2070-2099) under two RCPs (RCP 4.5 and RCP 8.5). We define usable capacity as the maximum monthly capacity in MW, constrained by the power plant's installed capacity, the simulated streamflow can maintain for a specific time frame. We analyze the changes in usable capacity (MW) for each month of the system considered between the projection runs and the control run. Each of the seven scenarios mentioned contains 21 time series corresponding to each GCM in the NEX-GDDP dataset. We aggregate power plants to the national level, and in Brazil's case, aggregate the five regions included. We perform this aggregation by summing the usable capacity time series for all power plants for each GCM and each climate scenario. We refer to the aggregated results as the system results. Once we have the systems' aggregated time series, we combine the 21 GCMs and perform the combined datasets' quantile analysis. This combination includes all possible results for the different months within the time frame specified. We obtain the 10^{th}, 25^{th}, median, $75^{th,}$ and 90^{th} percentile for each

month in each climate scenario. We compare the changes in usable capacity between each of the future scenarios quantiles with the control run quantiles. Using the combined datasets allows us to incorporate the GCMs' full spread and evaluate changes in the system's usable capacity. Consequently, we can determine the vulnerability of a power plant to changes in usable capacity.

2.4.3 Calibration for Case Study Results

As noted in the methods section, we used the Shuffle Complex Evolution (SCE) optimization algorithm[103,104] for model calibration. To calibrate the results for the case studies in Brazil, Colombia, and Peru, we use the average monthly streamflow for the reference period and historical streamflow records from government institutions at power plant locations or a historical global gridded runoff dataset when historical streamflow records were not available[135–138].

2.5 Results

2.5.1 Changes in usable capacity at individual power plants

After applying the model to 134 power plants in Brazil, Colombia, and Peru, we quantify the usable capacity changes for each power plant throughout the 21st century. To control for biases in the GCMs, we compare future climate projections with the models' historical reference simulations (instead of using empirical historical data)[139]. Figures 2-2, 2-3, and 2-4 show the relative change in the average normalized usable capacity at each power plant between RCP8.5 and the historical reference by season (rainy or dry). The normalized usable capacity reported is the ratio of the usable capacity to the installed capacity of the power plants. The figures for the results for RCP4.5 are available in Appendix Figures A.5-2 through A.5-4. Similarly, files with the monthly results for each power plant are available online[140].

Figure 2-2 shows that relative changes in the normalized usable capacity of power plants in Brazil under RCP 8.5 vary considerably by region. The normalized usable capacity for power plants in the South Atlantic and Uruguay regions likely increases. Not surprisingly, the largest increases in normalized usable capacity are higher during the rainy season and in the 2070-2099 period. Conversely, power plants in the Paraguay and Parana regions face relative reductions in the normalized usable capacity, particularly during the dry season. The largest power plant in the

Brazilian system (the Itaipu Dam in the Parana region) could face reductions of up to 4 percentage points in its normalized usable capacity during the dry season by 2070-2099.

In Colombia, most hydropower plants see no changes or increases of up to 6 percentage points in their normalized usable capacity during the rainy and dry season across all periods under RCP 8.5, as shown in Figure 2-3. Figure 2-4 shows that the largest relative increases and decreases in the normalized usable capacity occur in the Peruvian system. Most power plants in the country could experience increased normalized usable capacity but this is not noticeable in Figure 2-4. The power plants' installed capacity constrains the magnitude of the relative changes in the normalized usable capacity. Power plants can't generate electricity beyond this capacity regardless of the amount of water available. While this paper focuses on future usable capacity changes, it is important to recognize that increases in streamflow above the plant's design specifications can lead to other implications such as flooding. These potential effects have not been included in the analysis but are essential for each country's planning decisions.

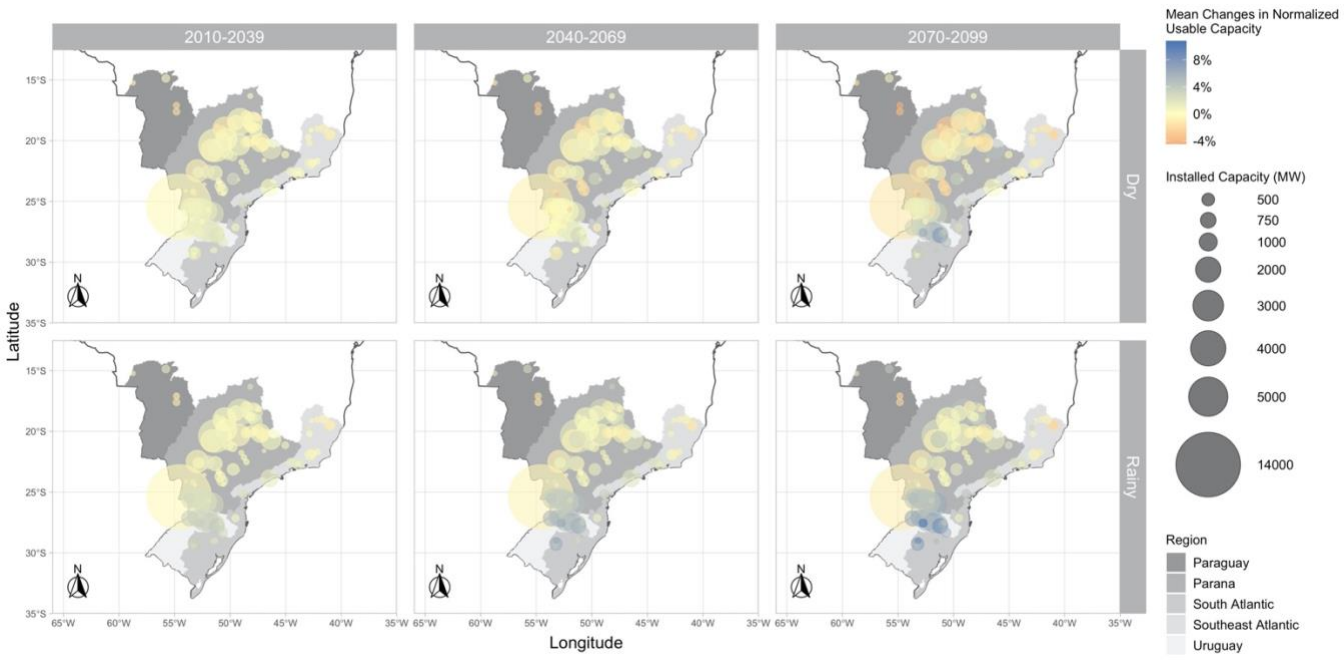

Figure 2-2 – Brazil's mean relative changes in normalized usable capacity for RCP 8.5 between the historical reference (1970-2005), the near future (2010-2039), the mid-century (2040-2069), and the end-of-the-century (2070-2099). The top panel presents the dry season (April to September) and the bottom panel the rainy season (October to March).

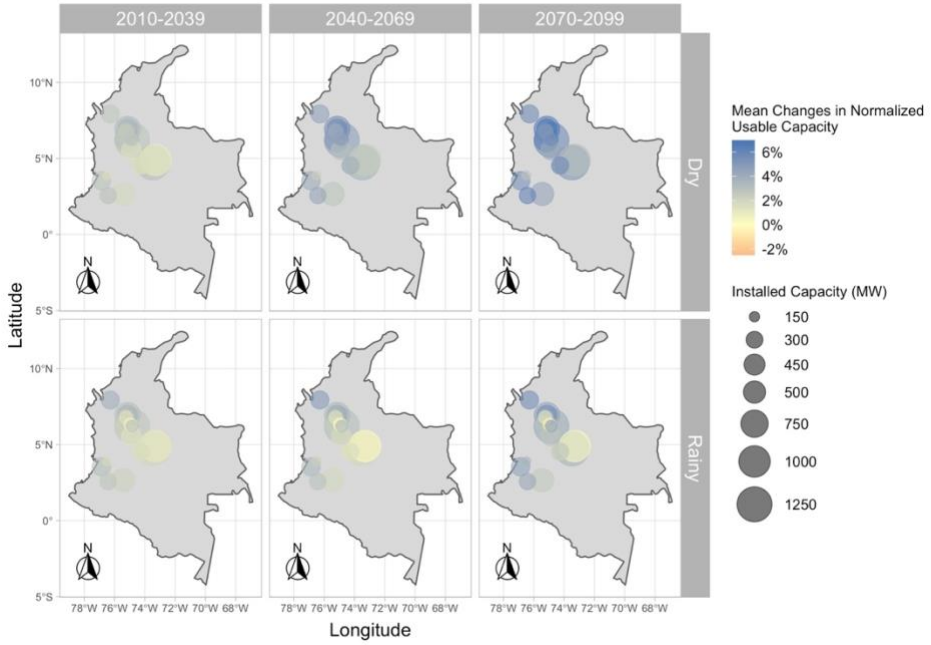

Figure 2-3 – Colombia's mean relative changes normalized usable capacity for RCP 8.5 between the historical reference (1970-2005), the near future (2010-2039), the mid-century (2040-2069), and the end-of-the-century (2070-2099). The top panel presents the dry season (December to March, July to August) and the bottom panel the rainy season (April to June, September to November).

Peru contains the largest number of glacierized catchments in tropical regions, and glaciers are located upstream, all but one of the hydropower plants studied (Appendix A.5.1 – Table A.5-1). As a result, our model includes the effect of glaciers on hydropower generation in Peru. Glacier runoff in the Tropical Andes is known to have more significant contributions to streamflow, and therefore usable hydropower capacity in smaller upstream catchments rather than larger downstream ones[32,34,39,47]. Our results show a considerable decrease in glacier area by the end of the century for all basins in Peru (Appendix Figure A.5-1) with considerable repercussions for the smallest upstream catchment. The Quitaracsa power plant has the largest concentration of glaciers (13.5% of the basin area covered by glaciers) and the smallest basin area (~370 km^2). This power plant experiences the largest reduction in usable capacity throughout the century caused by reductions in glacier runoff. As glaciers deplete, glacier runoff typically increases until the glacier reaches "peak" runoff. After this peak, glacier runoff decreases. Our results suggest that the Quitaracsa power plant is beyond "peak" runoff. The largest decreases at this site occur during the drier months when precipitation cannot compensate for the loss of the glaciers[34,141]. All other power plants in Peru are either still experiencing

increased glacier runoff, or the projected increases in precipitation could balance the decreased glacier contribution. Furthermore, all other power plants in the Peruvian system are in larger downstream catchments with smaller glacier runoff contributions, so they are less vulnerable to glacier retreat. Overall, our results suggest that glacier retreat does not jeopardize the Peruvian system's aggregate usable capacity in the 21st century, as described in the next section.

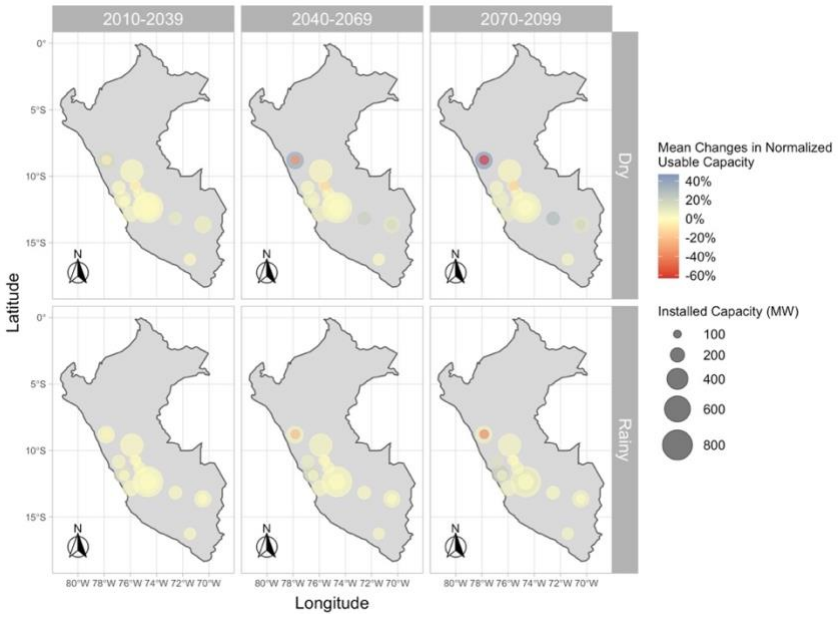

Figure 2-4 – Peru's mean relative changes in normalized usable capacity for RCP 8.5 between the historical reference (1970-2005), the near future (2010-2039), the mid-century (2040-2069), and the end-of-the-century (2070-2099). The top panel presents the dry season (May to November) and the bottom panel the rainy season (December to March).

2.5.2 Changes in usable capacity at the system level

The results for individual hydropower plants can be informative for making operating decisions at the plant level. They can also inform the scheduling of system reserves within a transmission zone to meet reliability standards. The aggregate climate impacts on all the power plants in the system also have relevant implications for power system design and operations. Figure 2-5 shows the distribution of monthly usable capacity in each region in the Brazilian system for the two climate scenarios in three time periods. The projected changes in usable capacity vary considerably for the five regions. Some regions are more likely to see increased usable capacity (e.g., South Atlantic, Uruguay), while others most likely decrease. The projected changes, either increasing or decreasing, become more significant as the century progresses and for the higher

emissions scenario (RCP 8.5). Specifically, the results show reductions of up to 5% in the lower quantiles (10% and 25%) of usable capacity for the Parana, Paraguay, and Southeast Atlantic regions. The Parana region results show a small percentage increases for the median to 90th percentile usable capacity for all time frames and climate scenarios. Conversely, results show percentage reductions in usable capacity for the Paraguay region.

The top panel in Figure 2-6 shows the aggregate results for the interconnected system in Southern Brazil. Figure 2-6 shows a slight increase in usable hydropower capacity during the wet months (October to April) in Brazil. Conversely, there is a slight reduction in usable hydropower capacity for the interconnected Brazilian system during the drier months (May to September). It is worth noting that the differences in installed capacities across the five regions drive the interconnected system results. The Parana region, which sees reductions in the lower quantiles of usable capacity (Figure 2-5), has 48.5 GW of installed capacity. In comparison, the Uruguay region, which sees increases in these quantiles (Figure 2-5), only has 7 GW of installed capacity. As a result, the climate effect on the Parana region's available capacity dominates the aggregate results for the entire interconnected system in Southern Brazil. While interconnection could balance some of the regional differences in climate impacts on usable capacity, the reductions in usable capacity in the much larger (by capacity) Parana region surpass the increases in usable capacity in the smaller (by capacity) regions. Thus, the dependence on the Parana region increases the climate vulnerability of the interconnected system.

Reductions in usable capacity during the dry periods are of particular concern to power system operators, as they imply a reduction in firm capacity. Firm capacity is the amount of power capacity that is available at all times during the year. A reduction in hydropower firm capacity due to decreased usable capacity in the dry season would increase the need for other (more expensive and higher polluting) generation assets to operate when hydropower is not available. Similarly, Figure 2-6 shows that the spread usable hydropower capacity within each month increases in future scenarios. The spread of the results for the end of the century is larger than for earlier periods. Increased variability in usable hydropower capacity would also increase the need for generating assets to balance such variability. Increased variability in the utilization rates for those assets would likely affect the costs of meeting reliability standards. While a full analysis of such costs is beyond this paper's scope, our results could inform such future work.

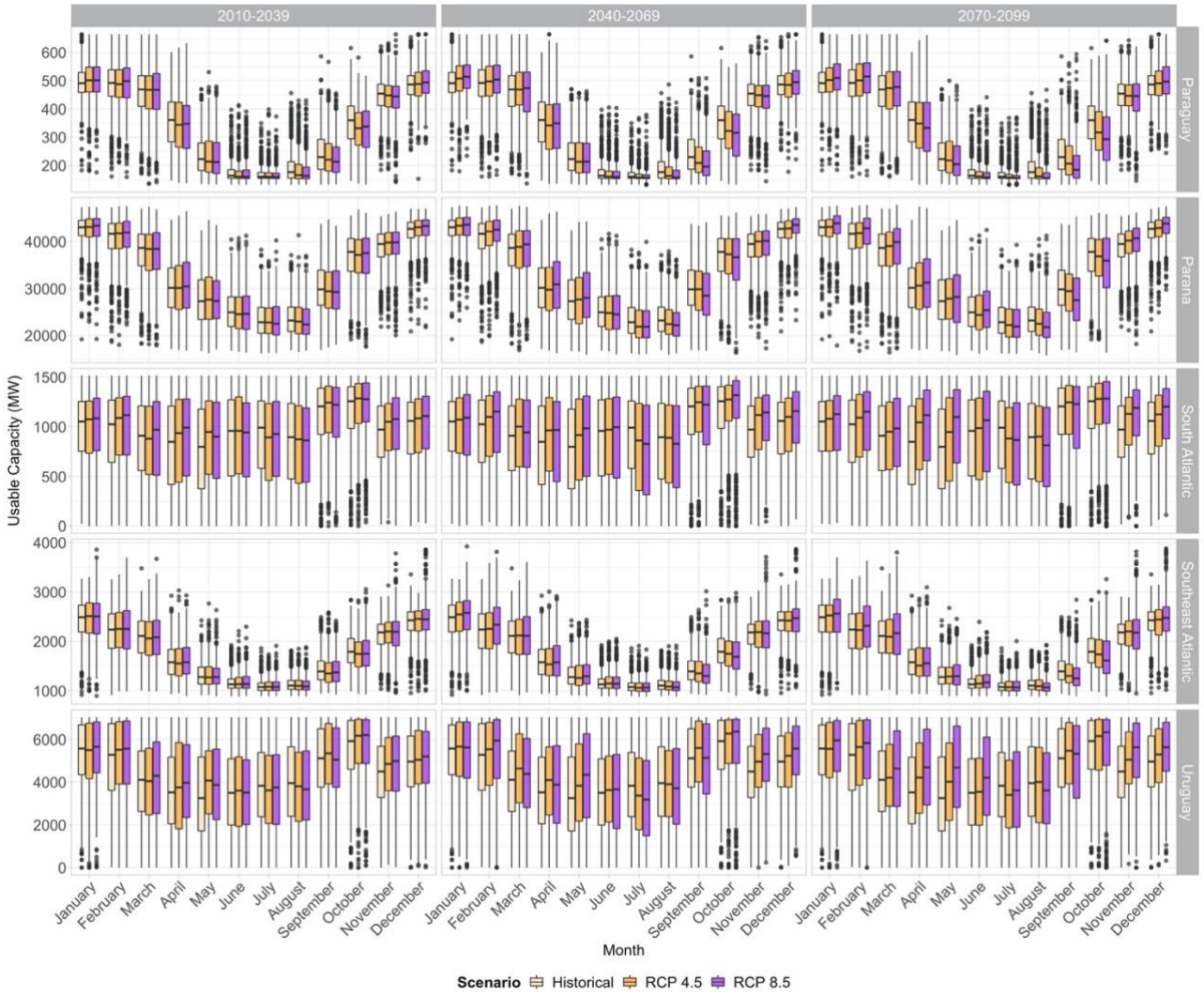

Figure 2-5 – Aggregated usable capacity (MW) for the regions in Brazil. The boxplots present the full spread of the 21 GCM experiments for the historical period (wheat), RCP 4.5 (orange), and RCP 8.5 (purple). Each column shows one of the analysis time frames, while each row presents the analyzed hydropower plants within each region.

Our results broadly agree with prior analyses of the Brazilian hydropower sector that also suggested a mix between increases and decreases in potential future generation depending on the region of study[79–81,90,142,143]. These results are similar to prior literature showing firm energy (power that is guaranteed 100% of the time) decreases for the Parana, Paraguay, and Southeast Atlantic regions[90]. Similarly, previous studies show that changes become more significant as the century progresses and under higher emissions scenarios. When comparing our results with Silva et al., (2020), Silva's results present higher anomalies for the Southeast and Midwest (Paraguay) regions leading to higher reductions on annual hydropower potential[81].

For the Colombian system, Figure 2-6 shows that the total usable capacity increases. Specifically, the results suggest a percentage increase in median usable capacity by the end of the century of 2.6% under RCP 4.5 and 8.4% under RCP 8.5. Figure 2-6 shows slight shifts in the drier months towards increased usable capacity while at the same time, the spread of the results for each month increases. Unlike Brazil's case, increased usable capacity (limited to the installed capacity) would benefit the system by increasing the firm capacity available from hydropower resources. However, the increase in the spread of usable capacity within a month would increase the variability in utilization rates for other generating assets, which can affect the costs of meeting reliability standards. Previous literature explored the potential effects of climate on Colombian hydropower plants using CMIP3 results and found decreases in streamflow in the region. Such changes in streamflow led to a reduction of simulated usable hydropower[87]. In contrast, our results obtained using CMIP5 and NASA NEX-GDDP downscaled projections show increases of usable capacity throughout the century when considering all 21 GCMs. The previous study used average precipitation results from GCMs, while we use the whole spread of the 21 GCM multi-model ensemble, making our results more robust.

Finally, for the Peruvian system, we observe the highest increases in usable capacity for the 10th percentile, followed by the 25th and to a lesser degree for the median, 75^{th,} and 90th. As shown in Figure 2-6, during the historical period, the country's ability to supply electricity from hydropower is considerably lower between May and September (dry months). Such seasonal differences in usable capacity remain under RCP4.5 and RCP8.5. However, the increases in usable capacity during the dry months are larger than in wet months and more impactful. Such an increase in usable capacity during the dry months could increase the firm capacity available from hydropower plants. Previous results from a study performed with CMIP3's SRES scenarios

showed inconclusive results for the direction of potential change in available capacity63. Using newer climate science outputs and a larger ensemble of GCMs allows us to capture a wider range of possible futures for the Peruvian system. Based on these results, the Peruvian hydropower system would most likely experience annual increases in usable capacity and increased firm hydropower capacity under both emission scenarios.

As noted earlier, there have been discussions about power system interconnection in South America. While an analysis of the effects of power system interconnection is beyond this paper's scope, our results can offer insights. Brazil's and Peru's dry seasons, which translate to lower usable capacity than the annual average, align, making energy exports less attractive between the two countries. On the other hand, there is a negative correlation between Brazil's and Colombia's dry seasons, which could open possibilities for future interconnections (negative Pearson correlation for usable capacity time series -0.62). We can also say this for Colombia and Peru (negative Pearson correlation for usable capacity time series -0.54). Analyzing these effects can better inform future interconnection plans within the region.

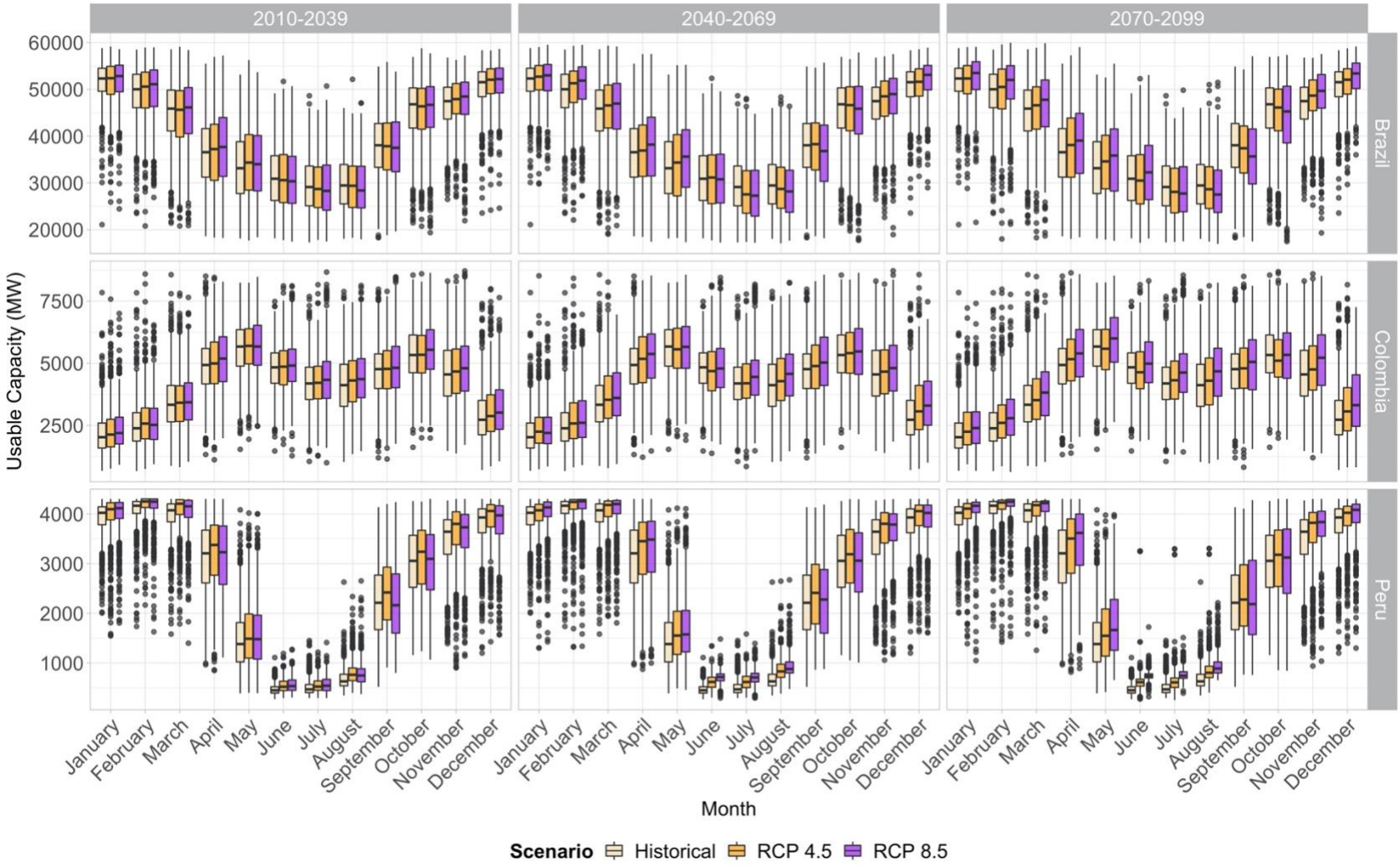

Figure 2-6 – Aggregated usable capacity (MW) for the Brazilian, Colombian, and Peruvian systems. The boxplots present the full spread of the 21 GCM experiments for the historical period (wheat), RCP 4.5 (orange), and RCP 8.5 (purple). Each column shows one of the analysis time frames, while each row presents the analyzed hydropower plants within a country.

2.5.3 Robustness Analysis

Additionally, we quantify the contributions of different factors to the spread in the projected changes in hydropower availability by conducting a two-way ANOVA paired with an Internal Variability Assessment (IV)[109]. For Brazil and Colombia, the largest source of variability for all power plants was the choice of GCM (75% and 78%, respectively). In Peru, the importance of selecting a particular GCM decreases to 53%, while the choice of RCP's increases to 26% compared to 2.8% for Brazil and 6.4% for Colombia (Appendix Figures A.5-6 and A.5-7). The main contributor to streamflow for Brazil and Colombia was precipitation. In Peru, glacier melt, which is driven by temperature in the model, also plays an important role. GCMs have a higher consensus on temperature changes than precipitation changes. As a result, the choice of GCM is the primary driver of variability in the countries where precipitation is the main contributor to streamflow, and the importance of the RCP increases when temperature becomes a key driver[115,144–147]. On the other hand, IV plays a lesser role in driving the spread of the results. The importance of the IV increases when precipitation is not the main driver of streamflow. Still, it would seem that the choice of GCM explains most of the variation in possible futures for all countries and power plants. Therefore, as GCMs and downscaling improve for these regions, the importance of GCMs as significant sources of variability should decrease. However, this is currently an important limitation on impact analyses.

2.6 Conclusions

This paper uses remotely sensed datasets and climate projections, with a versatile coupling of a hydrological model and a hydropower operations models to estimate future power generation under climate change in data-constrained regions of the world. Our results suggest that climate change will affect operations in the Brazilian, Colombian, and Peruvian hydropower sectors. In general, these systems may see increases in usable capacity due to increased water flows under climate change. Such increases in usable capacity would have positive implications for the Colombian SIN, the Peruvian SEIN, and to some extent, the Brazilian SIN. Increased usable capacity in these hydropower plants, particularly during the dry seasons, could reduce the need for new generating capacity that increasingly comes in the form of fossil-based thermoelectric power plants[67,148,149]. Reducing the need for fossil-based generation would, in turn, help meet the

greenhouse gas mitigation targets set by these countries under the Paris climate agreement. Further detailed assessments, including benefit-cost analyses that estimate the potential revenues or losses of generation changes under climate change, could be warranted for hydropower expansion plans. Additionally, future power plant design should use frameworks like the one applied in this paper to incorporate climate change in planning decisions by using potential changes in quantiles for power plant design. Unfortunately, Brazil and Peru's dry seasons mostly align, which would make a case for interconnection between the countries less strong. For Brazil and Colombia, or Peru and Colombia, there might be synergistic opportunities for interconnections as the neighboring countries have different rainy seasons.

Increases in streamflow that do not translate to further increases in usable capacity for the power plants could also have negative implications. Persistent increased streamflow, past the power plant's design flow, does not lead to increased generation and, in turn, could pose risks of flooding and landslides downstream of the power plant as well as structural damage to the power plant itself. Most of the power plants in Peru do not have significant storage capacity, making them more vulnerable to streamflow increases. Adding storage capacity could allow the use of the reservoir for flood management. The storage capacity could also manage seasonal flows and allow for more consistent power generation throughout the year, shifting generation from the rainy season to the dry season. However, reservoir expansion can be costly and could have negative externalities, including increases in methane emissions from the degradation of organic biomass[150–152]. While we do not perform a thorough analysis of the risks associated with increased flow, it is clear that such analysis should be the focus of future work.

In considering our results, it is important to be aware of some of the modeling work's limitations. To calibrate the hydrological model, we rely on historical flow data for basins and a global gridded dataset (GRUN)[137]. Using this gridded dataset allows the calibration of all basins in the study, but the dataset's performance varies significantly depending on the region. Another aspect is uncertainty in climate projections. As seen in the robustness check, climate model selection is the major contributor to the model's results variance. Consistent with best practices in climate impact analysis, we use multiple general circulation models and perform a variability analysis. By using an ensemble of general circulation models, we aim to capture the best understanding of the effect of climate change on meteorological variables available for scientific

research. As climate science continues to evolve and new data from climate simulation efforts becomes available, new simulations could be developed using the model presented in this paper.

Future work could expand the power generation model to include reservoir management features and hydropower generation optimization under different demand scenarios. Currently, the reservoir operations model maximized hydropower generation when available. The model developed for this paper is flexible and allows the exploration of hydropower plants around the world. Incorporating these assessments into planning decisions is the next step for the sector's future resilience to climate change. Hydropower could be a crucial component of a low-carbon power generation system in emerging economies, where electricity demand is expected to continue to increase throughout the 21st century. The model described in this paper can also be used as a screening tool to inform siting decisions for new hydropower plants under climate change.

Chapter 3 – Mitigating climate-induced risks and increasing resilience of hydropower systems in Africa

This chapter is being revised for publication in Nature Climate Change (February 2022) as: Caceres, A. L., Jaramillo, P., Matthews, H. S., Samaras, C. & Nijssen, B. "Mitigating climate-induced risks and increasing resilience of hydropower systems in Africa."

3.1 Abstract

More than half a billion people in Africa still lack access to modern electricity services, and hydropower will play an essential role in meeting the region's growing energy needs. Climate change can impact hydropower operations by altering annual usable capacity and variability of supply. Herein, we assess future hydropower usable capacity, variability, and complementarities (i.e., the extent to which different hydropower systems can complement each other through electricity trading) under a changing climate for 87 hydropower plants across five African power pools. Further, we generate seven power pool interconnection scenarios. Our results confirm that interconnecting the African power pools could benefit the most variable hydropower resources and mitigate the risks of potential decreases in usable capacity resulting from climate change. Additionally, these interconnections could decrease future interannual and seasonal variability by operating as joint systems and help balance new additions of variable renewable generation.

3.2 Main

Despite considerable economic growth in Africa during the past decade[153], more than half a billion people still lack access to modern electricity services: less than 1 million in North Africa and 578 million in Sub-Saharan Africa (SSA) (2019)[65]. To achieve universal electricity access (United Nations Sustainable Development Goal 7)[6], infrastructure development will need to accelerate in the coming years. The Programme for Infrastructure Development in Africa (PIDA) expects electricity consumption to increase more than fivefold by 2050, with hydropower playing an essential role in meeting increased electricity demand[66,154]. Furthermore, current peak electricity demand is already higher than installed capacity in most countries, so there is a pressing need to upgrade and further expand the region's electricity infrastructure[155].

Africa's electricity supply consists of 245 GW of installed capacity (870 TWh annual generation in 2018)[63], with 35 GW from hydropower plants (14% capacity and 16% generation)[62] which are heavily dependent on climate conditions. However, the contribution of hydropower varies across the continent and with that the corresponding climate-induced risks. In Sub-Saharan countries (excluding South Africa), hydropower accounted for more than a third of installed capacity and more than half of generation in 2018[156]. Indeed, 160 million people in SSA

currently live in hydropower-dependent countries (i.e., more than 50% of their electricity generation comes from hydropower plants). The Democratic Republic of Congo, Ethiopia, Malawi, Mozambique, Uganda, and Zambia produce more than 75% of their electricity from hydropower, making these countries particularly vulnerable to potential climate change impacts on hydropower systems[157,158].

Climate change can affect hydropower operations through changes in the timing and magnitude of precipitation patterns, as well as increases in evapotranspiration due to rising temperatures[12,75]. Previous studies have investigated the potential impacts of climate change on water and hydropower resources worldwide and in the African continent, mainly agreeing that East Africa would likely experience wetter conditions in a warming climate. At the same time, West, Southern, and Northern (Morocco) Africa would most likely experience drying, while the climate impacts in Central Africa are mixed[14,25,78,157–165]. The continent is already experiencing some of the effects of climate change, with droughts causing major power disruptions in the past decades in Kenya, Tanzania, Ghana, Zimbabwe, and Zambia[166,167]. Although previous assessments look at pooling other energy sources, no previous assessment has looked at the opportunities of pooling hydropower resources in the continent.

According to a report by the International Renewable Energy Agency (IRENA), by 2030, installed hydropower capacity in Africa could reach 100 GW[168], and Haffner et al. suggest that the hydropower generation potential in the region could be as high as 350 GW[169]. However, increased hydropower reliance in Africa could increase the continent's climate-induced vulnerability. Furthermore, concentrating hydropower resources in a small number of basins increases vulnerability to changes in basin-specific hydrological regimes. For example, most hydropower development in East Africa will likely remain in the Nile basin, while hydropower plants in Southern Africa will likely remain concentrated in the Zambezi basin. This lack of spatial diversity in hydropower plant siting could compound the risks of climate-induced disruptions in each region's electricity systems if extreme weather events were to occur[162]. Therefore, engineers and hydropower infrastructure planners need to account for climate change and the spatial patterns of hydrological regimes in planning decisions[77]. One way to mitigate these risks is diversifying the electricity systems by developing other renewable energy sources, such as solar and wind, and pursuing regional interconnections to balance energy resources[170,171].

Plans for regional transmission lines and electricity flows between African countries are a priority of the PIDA and other initiatives such as the Africa Clean Energy Corridor (ACEC)[155,172,173]. Power pools interconnect groups of countries in each region and create electricity markets and trading between them. Currently, there are five power pools in Africa: North Africa Power Pool (officially known as the Maghreb Electricity Committee – COMELEC), West African Power Pool (WAPP), Central Africa Power Pool (CAPP), Eastern Africa Power Pool (EAPP), and Southern African Power Pool (SAPP). The energy mix and degree of electrification vary significantly from power pool to power pool (see Table 3-1). The COMELEC has the highest electrification rate (97% in 2016) and the CAPP the lowest (25% in 2016)[153]. The existing transmission infrastructure connecting the power pools is still limited, preventing significant electricity transactions between countries[167,172].

The expansion and interconnection of power pools may offer opportunities to develop complementary energy resources in the continent. Complementary energy sources can work in combination and balance each other on both spatial and temporal scales[174]. For example, a few studies identified the potential for wind-solar and hydro-wind-solar complementarities in West Africa and across the African Clean Energy Corridor (includes countries in Eastern and Southern Africa)[171,174–178]. These studies find that exploiting potential synergies and using multicriteria analyses for siting decisions between hydro-wind-solar systems could increase the competitiveness of these energy sources in the continent. In the context of hydropower, complementarities could occur when a hydropower plant can operate at full capacity in one region, balancing another hydropower plant unable to operate in another region during the same period. To date, there has not been an assessment of cross country and cross power pool complementarities of hydropower resources in the continent or how to leverage them to mitigate the impacts of climate change on future hydropower operations. As previously mentioned, hydropower will remain an important source of electricity as the continent electrifies [66], therefore consistently assessing the impacts throughout the continent remains essential for the future resilience of the African electricity sector. Previous literature assessed the impacts of climate change on multiple African countries' hydropower systems[167], but studies use inconsistent multi-model ensembles and did not assess how pooling hydropower resources in the continent could improve the reliability of hydropower and benefit the countries.

Table 3-1 – African power pools' electrification rate, total hydropower installed capacity, and hydropower installed capacity included in the analysis. The table presents all five power pools included in the study. The electrification rate represents the percentage of the population with access to electricity for each of these power pools (combination of urban and rural access)[179]. The existing installed capacity represents the net installed capacity of all power plants (fossil and renewable) from the United Nations Energy Statistics Database[180]. The total hydropower installed capacity is the sum of the installed capacity in each country in the power pool[181]. The hydropower installed capacity included is the sum of all power plants included in the analysis (excludes power plants with an installed capacity smaller than 100 MW). For the EAPP, the hydropower installed capacity includes the not yet online Grand Renaissance Dam (6.45 GW) in Ethiopia (currently being filled). The difference between the SAPP's existing hydropower installed capacity and the capacity included in the analysis is due to a lack of data on the characteristics of the hydropower plants in Angola.

Power Pool	Electrification Rate (%)	Existing Installed Capacity [GW]	Existing Hydropower Installed Capacity [GW] (% of total capacity)	Hydropower Installed Capacity Included in the Analysis [GW]*
COMELEC	97%	99.9	5.0 (5%)	3.7
WAPP	52%	24.3	5.9 (24%)	4.7
CAPP	25%	6.9	4.3 (62%)	3.9
EAPP	54%	11.5	15.1 (75%)	13.7
SAPP	86%	66.4	14.0 (21%)	7.7
All Power Pools	46.8% (SSA) 97.2% (NA)	209.0	44.3 (21%)	33.7

* Excludes ~3.4 GW of pumped hydropower installed in Morocco and South Africa.

Here, we evaluate and generate seven potential interconnection scenarios for the five African power pools (COMELEC, WAPP, CAPP, EAPP, and SAPP) based on the potential complementary relationships between hydropower resources in the continent. To build the interconnection scenarios, we perform a hydropower climate impact assessment on 87 hydropower plants in 27 African countries (Figure 3-1, Appendix B Supplementary Table B-1) with an installed capacity ranging from 43 to 6,450 MW. Together, these 87 plants represent more than 75% of the total installed hydropower capacity on the continent. The impact assessment uses a consistent multi-model ensemble of 21 Global Climate Models (GCMs) from the Coupled Model Intercomparison Project 5 (CMIP5) and two emission scenarios (RCP 4.5 and 8.5) through 2099. We pair a water balance model with a reservoir operations model and a hydropower model to simulate future usable capacity under climate change at the power plant

level. Using the usable capacity time series for each hydropower plant, we assess the complementarity of hydropower resources at the power plant, country, and power pool levels. We then generate seven interconnection scenarios by combining the power pools in the continent that would allow electricity flows between the most complementary systems. We argue that these interconnection scenarios would help alleviate the effects of climate change on usable hydropower capacity and decrease the variability (interannual and seasonal) of the most vulnerable power pools. Our study analyzes current installed capacity in the continent, and it can be used in conjunction with capacity expansion models to evaluate future deployment of electricity sources in the continent under multiple climate conditions. Our analysis aims to understand how hydropower reliability in the continent could benefit pooled hydropower resources. Our results lay the groundwork for future studies that incorporate other existing and potential energy sources.

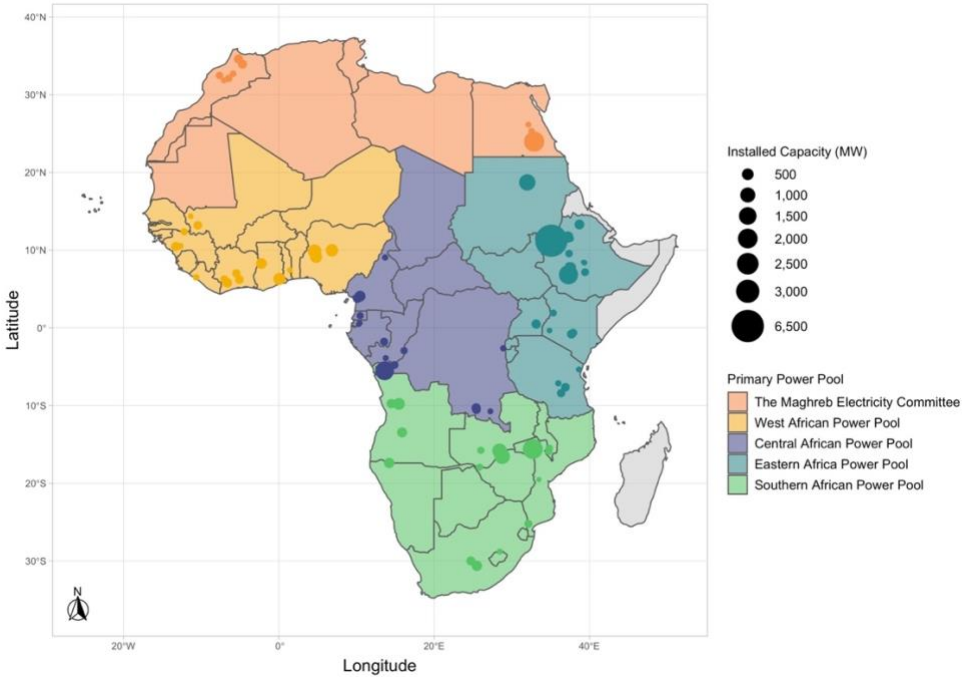

Figure 3-1 – Existing hydropower plants in the COMELEC, CAPP, WAPP, EAPP, and SAPP included in the analysis. We analyze all hydropower plants with an installed capacity larger than 40 MW. This represents 75% of current hydropower installed capacity in the continent plus 6 GW from the Grand Renaissance Dam in Ethiopia. The Grand Renaissance Dam is not currently online but has already been completed and is being filled. The size of the circle in the figure corresponds to the power plant's installed capacity (MW), and the color-coding denotes the corresponding power pool. We present details about the power plants in Appendix B Supplementary Table B-1.

3.3 Results

3.3.1 Assessing future power plant and country-level changes to usable hydropower capacity

To assess each power plant's changes in usable capacity (the maximum monthly capacity the simulated streamflow can maintain in MW), we perform an analysis using a multi-model ensemble of 21 GCMs and two emissions scenarios (RCP 4.5 and RCP 8.5) (see Methods). Our results present a comparison of three future time frames: near future (2010 – 2039), mid-century (2040 – 2069), and end-of-the-century (2070 – 2099), and the historical reference (1970 – 2005) (Figure 3-2, and Appendix B Supplementary Figures B-1 through B-12). The multi-model mean annual usable capacity varies depending on the power pool and location, with a mix of potential increases and decreases at the power plant and the country level compared to the historical reference. These results are consistent with previous analyses[182–184]. We further extend the work to present individual hydropower plant results, aggregated country-level results, and the effects of interconnecting the continent's power pools.

Figure 3-2 presents the mean normalized changes in hydropower usable capacity for the 87 power plants and 27 countries included in the analysis. These results suggest opposing trends in annual usable capacity for the two countries included in the COMELEC. For hydropower plants in Egypt, increases in annual usable capacity could be as high as 9% relative to the historical reference period (High Aswan Dam), while the usable capacity of power plants in Morocco decreases up to 12% (Almassira power plant), by the end-of-the-century and under RCP 8.5. When looking at the aggregated country-level changes, the overall increases and decreases in usable capacity are lower compared to the individual power plants (Figure 3-2, Panel B.). For Egypt, the potential increases in usable capacity at the country level are 4%, and for Morocco the potential decreases in usable capacity are 6% (end of the century and under RCP 8.5).

For the WAPP, the simulation results suggest reductions in annual usable hydropower capacity (Figure 3-2). The power plants located in Gambia, Guinea, Liberia, and Mali could experience declines up to 3%, on average, by the end of the century and under RCP 8.5. Results for RCP 4.5 are similar but of a lesser magnitude (-1% by the end of the century). These reductions could be greater when looking at monthly usable capacity between April and June

(monthly usable capacity reductions larger than 10% for some power plants) (Appendix B Supplementary Figures B-4 through B-6). The overall decreases are lower when looking at the country-level changes (Figure 3-2, Panel B.).

The CAPP results suggest increases in annual usable capacity for all power plants (up to 9% by the end of the century and RCP 8.5 – Figure 3-2, Panel A.). Most increases occur in the Democratic Republic of the Congo (7% by the end of the century under RCP 8.5 – Figure 3-2 Panel B). These increases are likely driven by changes in the Inga II power plant, which has an installed capacity of 1,775 MW and represents 64% of the country's installed capacity.

The fourth power pool we analyze is the EAPP, where most hydropower plants are in the Nile River Basin. In this basin, 9.7 GW of installed capacity (out of 13.7 GW for the power pool) are in the Blue Nile, Victoria Nile, and the main Nile rivers (Figure 3-2, Panel A.). The results suggest the highest increases in annual power plant usable capacity, ranging from 8% to 11%, for Melka Wakena (153 MW) in Ethiopia, Gilgel Gibe I, II, and III (2,485 MW in total) in Ethiopia, and Merowe (1,250 MW) in Sudan by the end of the century and under RCP 8.5. When looking at the overall country-level changes, Tanzania is the only country in the EAPP where our results suggest potential decreases in annual usable capacity (up to 7% for the country-level results for the end-of-the-century – Figure 3-2, Panel B.).

Finally, in the SAPP, all but one power plant could experience potential reductions in usable capacity throughout the 21st century under both emissions scenarios (Figure 3-2, Panel A). The annual power plant level reductions range from negligible ~0% for the Cambambe power plant (260 MW) in Angola, to -5% for the Van der Kloof power plant (240 MW) in South Africa (end of the century and under RCP 8.5). The largest monthly reductions in the SAPP occur between September and November in Zambia and Zimbabwe, where usable capacity at individual hydropower plants could decrease by up to 30% (Appendix B Supplementary Figures B-9 through B-11). Overall, for all countries in the SAPP, the results suggest reductions in usable hydropower capacity under both emissions scenarios (Figure 3-2, Panel B). Consistently, the largest potential reductions in usable capacity, for both power plant and country levels, are by the end of the century and under RCP 8.5.

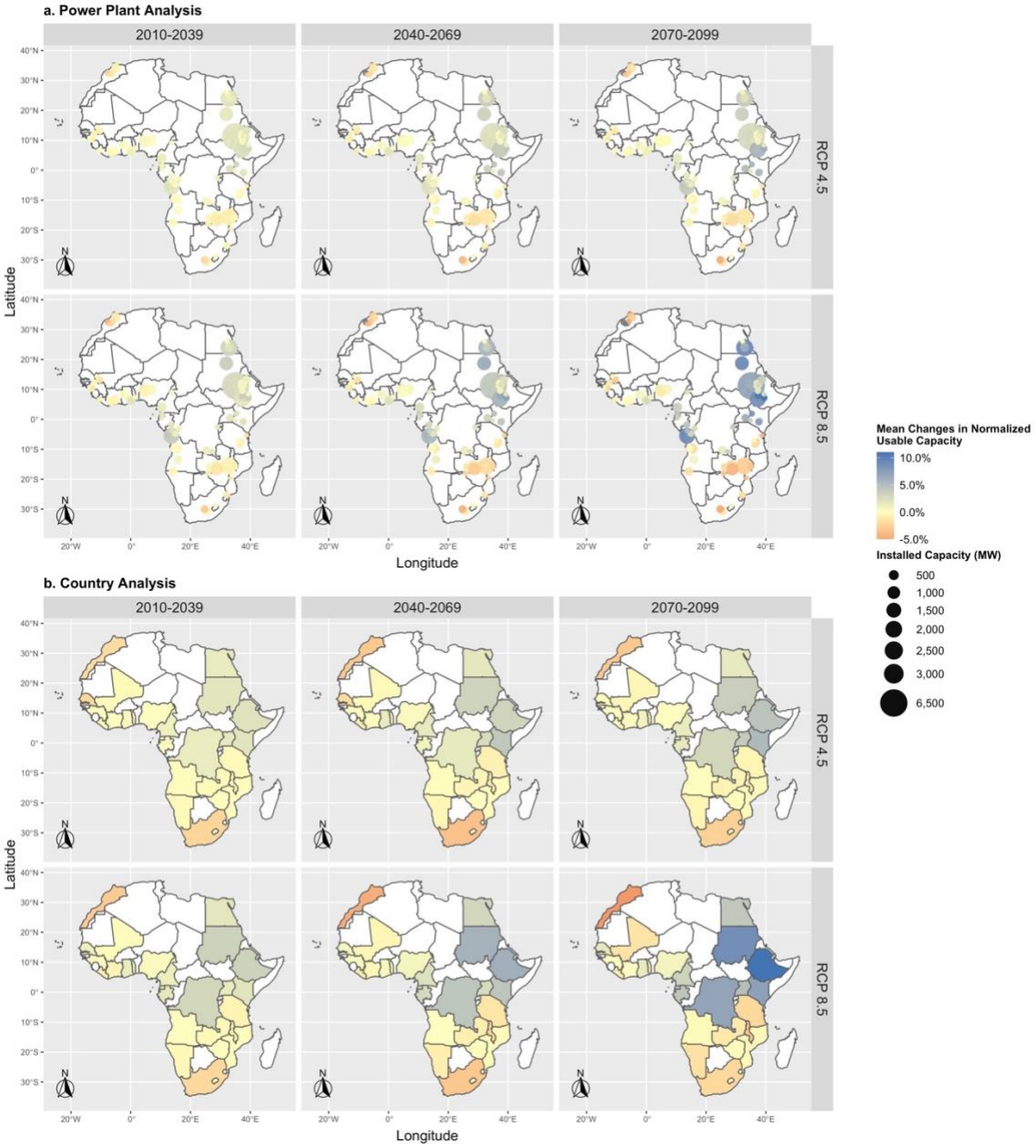

Figure 3-2 – Mean relative changes in annual normalized usable capacity for RCP 4.5 and RCP 8.5. A. Panels show the differences in percentage points for each power plant in the analysis between the historical reference (1970 – 2005) and the near future (2010 – 2039), the mid-century (2040 – 2069), and the end-of-the-century (2070 – 2099). The circle's size represents the installed capacity (MW) of the hydropower plants, and the intensity of the color shows the direction of the change (blue increases and red decreases). We present the changes at the power plant level for each month in Supplementary Figs. B-1 through B-12. B. Panels show the differences in percentage points for each country between the historical reference (1970 – 2005) and the near future (2010 – 2039), the mid-century (2040 – 2069), and the end-of-the-century (2070 – 2099). Each countries' installed capacity can be found in Supplementary Table B-1.

3.3.2 Assessing future power pool changes to usable hydropower capacity

After analyzing changes in usable capacity at the power plant and country level, we explore the changes in usable capacity when interconnecting countries into their corresponding power pools. For four of the five power pools, we find that the projected reductions in annual usable capacity at the individual country level are no longer projected at the power pool level (Figure 3-3). The SAPP is the only power pool experiencing small declines in mean annual usable capacity (up to -1% under RCP 8.5 by the end of the century). On the other hand, the power pool experiencing the largest increases is the EAPP, with up to 9% mean changes by the end of the century under RCP 8.5. The results suggest that the second largest increases would occur in the CAPP, also by the end of the century and under RCP 8.5 (6%). The two other power pools experience almost no changes. Overall, we find that operating the hydropower systems jointly as part of a power pool would mitigate the projected potential decreases in usable capacity at the individual power plant or country levels.

Furthermore, when looking at the monthly usable capacity for each power pool (Appendix B Supplementary Figure B-13), once again, the results suggest increases in monthly usable capacity for those power pools for which we project annual increases. Appendix B Supplementary Figure B-13 shows the full spread of the multi-model ensemble for the monthly usable capacity of each power pool. Furthermore, Appendix B Supplementary Figures B-14 and B-15 present the probability density function and the inverse cumulative density function of the monthly usable capacity time series for each power pool. These figures allow exploring the exceedance probability and the change in the distribution of the monthly capacities of the full multi-model ensemble. For the SAPP, the results suggest decreases in monthly usable capacity between May and November. During these months, the countries in this power pool might need to rely on alternative electricity sources to meet demand. Still, the potential decreases are lower when operating as a power pool than in the isolated country-level system.

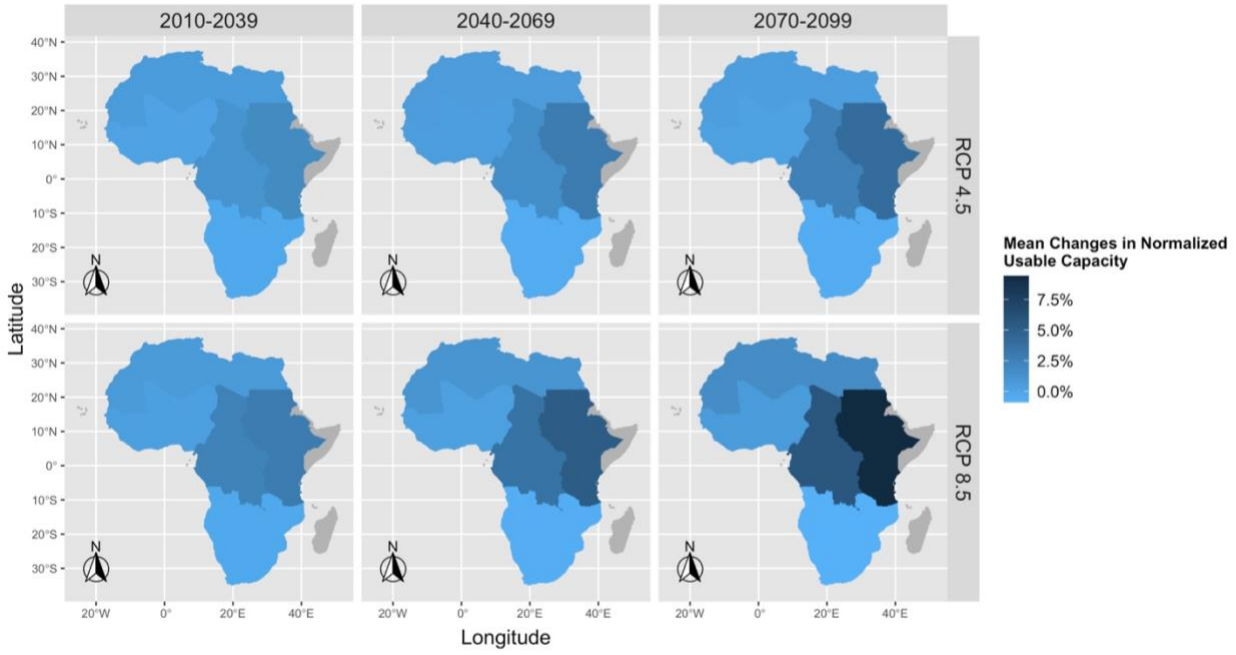

Figure 3-3 – Mean relative changes in annual normalized usable capacity for RCP 4.5 and RCP 8.5 at the power pool level. Panels show the differences in percentage points for each power pool in the analysis between the historical reference (1970 – 2005) and the near future (2010 – 2039), the mid-century (2040 – 2069), and the end-of-the-century (2070 – 2099). We present the boundaries of each power pool in Fig. 3.1 and their installed capacities in Supplementary Table B-1.

3.3.3 Changes in the variability of usable capacity at the country and power pool levels

To further understand future climate change patterns on usable capacity at the country and power pool levels, we compute interannual variability and seasonal variability metrics for each country and power pool (see Methods, Table 3-2 and Table 3-3, and Supplementary Tables B-2 and B-3). The interannual variability is the coefficient of variation of annual usable capacity between years, and the seasonal variability estimates the within-year effects. These metrics, which we adapt from the hydrology literature to our analysis of usable hydropower capacity[185], can illustrate the variability between years and months of the studied hydropower systems. Table 3-2 and Table 3-3 show the interannual and seasonal variability coefficients for individual countries and the five power pools under RCP 8.5 (Supplementary Tables B-2 and B-3 for RCP 4.5). Coefficients closer to zero indicate lower variability across and within years.

The countries with the highest interannual variability in the historical reference period are South Africa (SAPP), Morocco (COMELEC), and Lesotho (SAPP). Additionally, the climate-

induced increases in the interannual variability are statistically significant (p-value < 0.05) for Morocco and South Africa until the mid-century. In all but COMELEC, the interannual variability at the power pool level may increase by the end of the century and RCP 8.5. However, the variability increases at the power pool level are generally lower than the variability increases in individual countries. Results are similar under RCP 4.5 (Supplementary Table B-2). These results suggest that by completing the interconnection of countries within the power pools, there is a potential to smooth the variability of the individual countries, making the hydropower systems more reliable as the effects of climate change become more noticeable. It is important to recognize that the power pool operations assumed here would require the construction of additional transmission capabilities to allow for the electricity flows described in this section.

Table 3-2 – Interannual variability of usable capacity by country and power pool, measured as the coefficient of variation in usable capacity. We aggregate (sum) the annual usable hydropower capacity of each power plant and country to calculate the country and power pool level usable capacity and coefficients of variation (CV)—the closer to 0 the interannual variability metric, the less variable the hydropower supply across years. The direction of changes column represents increases (orange up arrow) and decreases (purple down arrow) by the end of the century. We present gradients of purple in the "Historical" column that correspond to the variability of the country or power pool. We present the interannual variability under RCP 4.5 in Supplementary Table B-2.

Country [MW]	Historical	RCP 8.5			Direction of Changes
	1970 – 2005	2010 – 2039	2040 – 2069	2070 – 2099	
Egypt [2,842]	0.06	0.05*	0.04***	0.04*	↓
Morocco [902]	0.26	0.24***	0.25***	0.36*	↑
COMELEC [3,744]	**0.05**	**0.04*** **	**0.04*** **	**0.04**	↓
Cote d'Ivoire [824]	0.05	0.05	0.05	0.06	↑
Ghana [1,100]	0.05	0.04*	0.06***	0.05***	↓
Guinea [315]	0.09	0.12	0.13	0.15	↑
Liberia [88]	0.09	0.09	0.10	0.12	↑
Mali [262]	0.02	0.03*	0.04**	0.06***	↑
Nigeria [1,920]	0.10	0.09***	0.11***	0.13	↑
Senegal [120]	0.02	0.03	0.04**	0.06***	↑
Togo [66]	0.02	0.03	0.03	0.04	↑
WAPP [4,695]	**0.05**	**0.05*** **	**0.06*** **	**0.06**	↑
Cameroon [750]	0.12	0.12	0.12	0.13	↑

Democratic Republic of the Congo [2,756]	0.13	0.13	0.14	0.15	↑
Equatorial Guinea [120]	0.17	0.30	0.29	0.29	↑
Gabon [286]	0.13	0.20	0.20	0.22	↑
CAPP [3,912]	**0.11**	**0.12**	**0.12**	**0.13**	↑
Ethiopia [10,164]	0.16	0.16***	0.16***	0.19	↑
Kenya [721]	0.12	0.12	0.13	0.14**	↑
Sudan [1,665]	0.15	0.14*	0.14*	0.13	↓
Tanzania [528]	0.03	0.04	0.05	0.05	↑
Uganda [630]	0.1	0.10	0.11	0.11*	↑
EAPP [13,708]	**0.12**	**0.13*** **	**0.12*** **	**0.14**	↑
Angola [1,100]	0.03	0.04*	0.04	0.05	↑
Lesotho [72]	0.24	0.29	0.31	0.36	↑
Malawi [374]	0.10	0.10	0.11	0.12	↑
Mozambique [2,293]	0.01	0.01	0.01	0.01***	-
Namibia [347]	0.02	0.02	0.03	0.03*	↑
South Africa [600]	0.26	0.26***	0.29***	0.35	↑
Zambia [2,208]	0.02	0.03	0.03	0.03	↑
Zimbabwe [750]	0.00	0.00	0.00	0.00***	↑
SAPP [7,744]	**0.01**	**0.02*** **	**0.02***	**0.02***	↑

Statistical significance for the interannual variability compared to the historical reference: '***' 0.001 '**' 0.01 '*' 0.05

The country-level seasonal variability (in Table 3-3) shows a mix of increases and reductions in variability across the power pools. In the COMELEC, Morocco is likely to experience statistically significant declines in seasonal variability throughout the century under both emissions scenarios (p-value < 0.05 for the near-future and mid-century). In the CAPP, Cameroon and the Democratic Republic of the Congo also experience reductions in seasonal variability under both emissions scenarios, leading to an overall variability reduction in the aggregated power pool. Finally, in the EAPP, Ethiopia and Sudan would likely experience less seasonal variability under climate change (statistically significant). As with the results for interannual variability, Table 3-3 shows that changes in seasonal variability under climate change are lower when the countries operate together as an aggregated power pool than

individually (Supplementary Table B-3 for RCP 4.5). In the SAPP, Mozambique drives the reductions in the overall seasonal variability of the power pool, smoothing the increases of the most variable countries in the power pool (Lesotho, Malawi, and South Africa).

The countries that benefit the most from the power pools interconnection are in the CAPP and the EAPP, where reductions in seasonal variability under climate change are statistically significant (p-value < 0.001). On the other hand, the seasonal variability increases under RCP 4.5 and RCP 8.5 for the COMELEC power pool (p-value < 0.01). This increase in seasonal variability under climate change by the end of the century is driven by increased seasonal variability in Egypt (76% of the COMELEC's installed capacity). Beyond Egypt and Morocco, there are no other medium to large hydropower plants in the COMELEC, leading to very geographically concentrated hydropower resources (in either Morocco or the Nile River basin in Egypt). If more countries in the COMELEC had hydropower resources, the seasonal variability could decrease. The results for this region highlight the potential benefits of spatial heterogeneity and cross power pool electricity trading.

Table 3-3 – Seasonal variability of usable capacity by country and power pool, measured as the coefficient of variation in usable capacity. We aggregate (sum) the monthly usable hydropower capacity of each power plant and country to calculate country and power pool level usable capacity and coefficients of variation (CV)—the closer to 0 the seasonal variability metric, the less variable the hydropower supply within a year. The direction of changes column represents increases (orange up arrow) and decreases (purple down arrow) by the end of the century. We present gradients of purple in the "Historical" column that correspond to the variability of the country or power pool. We present the seasonal variability under RCP 4.5 in Supplementary Table B-3.

Country [MW]	Historical	RCP 8.5			Direction of Changes
	1970 – 2005	2010 – 2039	2040 – 2069	2070 – 2099	
Egypt [2,842]	0.08	0.08	0.07	0.08	↑
Morocco [902]	0.42	0.42*	0.40**	0.36	↓
COMELEC [3,744]	**0.06**	**0.06**	**0.06**	**0.07****	↑
Cote d'Ivoire [824]	0.31	0.31	0.32	0.31	↓
Ghana [1,100]	0.09	0.09	0.09	0.09	↓
Guinea [315]	0.39	0.39	0.46	0.47	↑
Liberia [88]	0.54	0.54	0.56	0.56	↑
Mali [262]	0.08	0.08	0.09	0.10	↑

Nigeria [1,920]	0.69	0.69	0.68	0.68	↓
Senegal [120]	0.08	0.08	0.09	0.10	↑
Togo [66]	0.08	0.08	0.09	0.08	↑
WAPP [4,695]	**0.34**	**0.34**	**0.34**	**0.34**	-
Cameroon [750]	0.70	0.70	0.67	0.66	↓
Democratic Republic of the Congo [2,756]	0.49	0.49	0.45*	0.42***	↓
Equatorial Guinea [120]	0.62	0.62	0.72	0.71	↑
Gabon [286]	0.57	0.57	0.64	0.63	↑
CAPP [3,912]	**0.33**	**0.32**	**0.31***	**0.30*****	↓
Ethiopia [10,164]	0.53	0.53	0.48*	0.42***	↓
Kenya [721]	0.27	0.27	0.27	0.27**	↑
Sudan [1,665]	0.45	0.45	0.39***	0.35***	↓
Tanzania [528]	0.33	0.33	0.34	0.35	↑
Uganda [630]	0.30	0.30	0.30	0.29	↓
EAPP [13,708]	**0.37**	**0.36**	**0.34****	**0.30*****	↓
Angola [1,100]	0.27	0.27	0.28	0.29	↑
Lesotho [72]	0.78	0.78	0.87	0.94	↑
Malawi [374]	0.81	0.81	0.84	0.86	↑
Mozambique [2,293]	0.03	0.03	0.03	0.03	-
Namibia [347]	0.18	0.18	0.18	0.18	-
South Africa [600]	0.53	0.53	0.69*	0.71**	↑
Zambia [2,208]	0.24	0.24	0.25	0.25	↑
Zimbabwe [750]	0.00	0.00	0.01	0.01	↑
SAPP [7,744]	**0.16**	**0.16**	**0.16**	**0.16**	-

Statistical significance for the interannual variability compared to the historical reference: '***' 0.001 '**' 0.01 '*' 0.05

3.3.4 Assessing future changes to usable hydropower capacity and variability under power pool interconnection scenarios

Following the findings for each individual power pool, we explore whether further interconnections could mitigate the variability of the isolated systems and the effects of climate change on their usable capacity. We perform a complementarity assessment to develop

interconnection scenarios for the power pools in the continent (see Methods, Appendix B Supplementary Notes B-1 and B-2, Supplementary Figures B-16 through B-19, and Supplementary Tables B-4 through B-6). We base the interconnection scenarios on the potential complementarities of the individual country and power pool hydropower resources (based on temporal correlations and usable capacity time series, see Appendix B Supplementary Figures B-16 through B-19). With the country-level results, we determine which power pools could benefit the most from interconnecting. We define seven groups of power pools as the interconnection scenarios. Currently, such sharing of resources is not possible in the continent. Thus, our scenarios are exploratory, and their viability depends on a large-scale expansion of transmission capabilities across the continent to allow for the necessary electricity flows. We determine six combinations of interconnection scenarios between two or more power pools and a whole interconnection scenario of all five African power pools (Appendix B Supplementary Table B-6). We analyze the effects of seven interconnection scenarios, in total, on mean annual usable capacity and the seasonal and interannual variability of the systems.

Table 3-4 presents the relative changes in the mean annual usable capacity for each of the seven interconnection scenarios. These results are driven by the individual power plants, countries, and power pools' usable capacity as presented in Figures 3-2 and 3-3. All seven interconnection scenarios show increases in usable capacity that are larger by the end of the century and under RCP 8.5, compared to RCP 4.5. We find the largest relative increases driven by the interconnection of the EAPP to other power pools (scenarios 2, 4, 6, and 7). Combining the CAPP with the EAPP yields the largest relative increases in annual usable capacity by the end of the century (9%). While interconnecting power pools is generally beneficial for the reliability of all systems, the SAPP would benefit the most. The previous sections showed that the SAPP was the only power pool that would experience slight decreases in its mean annual usable capacity under climate change. Scenarios 1 and 5 show that interconnections between the SAPP and complementary power pools would result in increases of usable hydropower capacity for the aggregate system compared to the SAPP operating in isolation. Such increase is lower than for the other scenarios, thus reducing the vulnerability of the SAPP to climate change. While this study shows that electricity trade across power pools could mitigate the impacts of variability in usable capacity in the importing power pools, such trade is only feasible if it is mutually beneficial. Furthermore, the value of trading electricity to manage the variability of

hydropower will also depend on other factors like the demand for electricity in each power pool and the availability of non-hydro generation, which are not included in this analysis. Finally, agreements between power pools should be drafted to ensure that electricity trade is benefiting all involved parties.

Table 3-4 – Mean relative changes in annual normalized usable capacity for RCP 4.5 and RCP 8.5 when looking at the seven interconnection scenarios. Columns present the differences in percentage points for each of the interconnection scenarios between the historical reference (1970 – 2005) and the near future (2010 – 2039), the mid-century (2040 – 2069), and the end-of-the-century (2070 – 2099). We present different shadings of blue, corresponding to the increases in mean annual usable capacity. The installed capacity of the individual power pools is presented in Supplementary Table B-1.

Scenario	Interconnection Scenarios [GW]	RCP 4.5			RCP 8.5		
		2010 – 2039	2040 – 2069	2070 - 2099	2010 – 2039	2040 – 2069	2070 - 2099
1	CAPP & SAPP [11.7]	0.2%	0.1%	0.4%	0.6%	0.7%	1.3%
2	CAPP & EAPP [17.6]	1.7%	2.6%	3.7%	2.8%	4.9%	8.6%
3	WAPP & CAPP [8.6]	0.4%	0.6%	0.8%	0.9%	1.2%	2.0%
4	EAPP & SAPP [21.5]	1.1%	1.7%	2.4%	1.7%	3.1%	5.7%
5	WAPP, CAPP, & SAPP [16.4]	0.1%	0.2%	0.4%	0.5%	0.6%	1.1%
6	WAPP, CAPP, & EAPP [22.3]	1.2%	1.8%	2.5%	2.0%	3.4%	5.9%
7	All Power Pools [33.8]	0.9%	1.4%	1.9%	1.5%	2.6%	4.6%

The final piece of our analysis examines the seasonal and interannual variability of the proposed interconnection scenarios. We present the coefficient of variation in usable capacity for the aggregated interconnection scenarios under RCP 8.5 in Tables 3-5 and 3-6 (Appendix B Supplementary Tables B-7 and B-8 for RCP 4.5).

By operating power pools jointly, we find that the interannual and seasonal variabilities tend to decrease compared to the independent operation of the most variable power pools. For example, in scenario 2, under historical climate conditions, interconnecting CAPP and the EAPP would reduce the interannual and seasonal variability compared to operating each system independently. Furthermore, by interconnecting the power pools, the seasonal variability of the interconnected scenario significantly decreases (p-value < 0.001) by the end of the century under RCP 8.5. The interconnection scenario smooths the individual variability of the power pools and mitigates the effects of climate change. We include a discussion of the statistical significance meaning in Appendix B Supplementary Note B-3.

Table 3-5 – Interannual variability of usable capacity by power pool interconnection scenario, measured as the coefficient of variation in usable capacity. We aggregate (sum) each power pool's monthly usable hydropower capacity to calculate the interconnection scenario usable capacity and coefficients of variation—the closer to 0 the interannual variability metric, the less variable the hydropower supply across years. The direction of changes column represents increases (orange arrow) and decreases (purple arrow) by the end of the century. We present gradients of purple in the "Historical" column that correspond to the variability of the country or power pool. We present the interannual variability under RCP 4.5 in Supplementary Table B-7.

Scenario	Interconnection Scenarios [GW]	Historical	RCP 8.5			Direction of Changes
		1970 – 2005	2010 – 2039	2040 – 2069	2070 – 2099	
-	COMELEC [3.7]	0.05	0.04***	0.04***	0.04	↓
-	WAPP [4.7]	0.05	0.05***	0.06***	0.06	↑
-	CAPP [3.9]	0.11	0.12	0.12	0.13	↑
-	EAPP [13.7]	0.12	0.13***	0.12***	0.14	↑
-	SAPP [7.7]	0.01	0.02***	0.02*	0.02*	↑
1	CAPP & SAPP [11.7]	0.03	0.03	0.04	0.04	↑

2	CAPP & EAPP [17.6]	0.10	0.10***	0.11***	0.12	↑
3	WAPP & CAPP [8.6]	0.06	0.07**	0.07**	0.08	↑
4	EAPP & SAPP [21.5]	0.07	0.07***	0.07***	0.09	↑
5	WAPP, CAPP, & SAPP [16.4]	0.03	0.03***	0.04**	0.04	↑
6	WAPP, CAPP, & EAPP [22.3]	0.08	0.08***	0.09***	0.10	↑
7	All Power Pools [33.8]	0.05	0.05***	0.06***	0.07	↑

Statistical significance for the interannual variability compared to the historical reference: '***' 0.001 '**' 0.01 '*' 0.05

Table 3-6 – Seasonal variability of usable capacity by power pool interconnection scenario, measured as the coefficient of variation in usable capacity. We aggregate (sum) each power pool's monthly usable hydropower capacity to calculate the interconnection scenario usable capacity and coefficients of variation—the closer to 0 the seasonal variability metric, the less variable the hydropower supply within a year. The direction of changes column represents increases (orange arrow) and decreases (purple arrow) by the end of the century. We present gradients of purple in the "Historical" column that correspond to the variability of the country or power pool. We present the seasonal variability under RCP 4.5 in Supplementary Table B-8.

Scenario	Power Pools Interconnected [GW]	Historical	RCP 8.5			Direction of Changes
		1970 – 2005	2010 – 2039	2040 – 2069	2070 – 2099	
-	COMELEC [3.7]	0.06	0.06	0.06	0.07**	↑
-	WAPP [4.7]	0.34	0.34	0.34	0.34	-
-	CAPP [3.9]	0.33	0.32	0.31*	0.30***	↓
-	EAPP [13.7]	0.37	0.36	0.34**	0.30***	↓
-	SAPP [7.7]	0.16	0.16	0.16	0.16	-
1	CAPP & SAPP [11.7]	0.19	0.18	0.19	0.18	↓
2	CAPP & EAPP [17.6]	0.24	0.24	0.23**	0.21***	↓
3	WAPP & CAPP [8.6]	0.19	0.19	0.19	0.18	↓
4	EAPP & SAPP [21.5]	0.13	0.13	0.12**	0.12***	↓

5	WAPP, CAPP, & SAPP [16.4]	0.09	0.09	0.09	0.09	-
6	WAPP, CAPP, & EAPP [22.3]	0.27	0.26	0.25*	0.23***	↓
7	All Power Pools [33.8]	0.12	0.12	0.12	0.12**	-

Statistical significance for the interannual variability compared to the historical reference: '***' 0.001 '**' 0.01 '*' 0.05

Another example that presents benefits for at least 2 of the power pools in the interconnection is scenario 5. When the WAPP is operated together with the CAPP and the SAPP, the aggregated system's seasonal variability decreases compared to any individual power pool under historical climate conditions. Additionally, there are no significant changes in variability (interannual or seasonal) of the interconnected system by the end of the century under climate change.

Our final scenario 7 assumes the complete interconnection of all the African power pools. Under all climate conditions evaluated, interannual and seasonal variabilities of the fully interconnected system are smaller than the variability of four of the five power pools when operated in isolation. Therefore, interconnecting the power pools can make the systems' hydropower supply more stable and reliable within and across years, even when considering the effects of climate change. The continent still needs to expand the transmission infrastructure to make the most out of these interconnection scenarios.

3.4 Discussion

To achieve the universal electrification of the African continent while at the same time minimizing carbon emissions, the region will likely continue to rely on hydropower. Indeed, the PIDA plans on expanding hydropower resources in the continent to meet the electrification goals and interconnect regions through power pools. We analyze 27 countries in this study, 14 of them hydropower-dependent countries (more than 50% of their electricity generation in 2019 came from hydropower)[186,187]. Moreover, ten produced more than 75% of their electricity from this energy source in 2019.

Our analysis of climate change impacts on hydropower plants in five African power pools shows differences in the direction of usable capacity changes under two emissions scenarios. Our results suggest dryer conditions in the SAPP, the WAPP, and the COMELEC (Morocco) under climate change. On the other hand, countries in the EAPP could experience increased usable capacity for all months under climate change. We find mixed results for the CAPP, with potential increases in usable capacity for the Democratic Republic of Congo driven by the Inga II power plant. The wetter conditions in some areas of the continent could balance the drying in others. The potential additions of large hydropower projects in Africa further reinforce the need for the power pools' interconnection. Currently, electricity trade between power pools and even inside the power pools is limited[162,167,172,173]. In this assessment, we focus on hydropower as it is one of the renewable energy sources with the highest potential to serve as a baseload for low-carbon electricity sector planning.

We find that the interannual variability of usable hydropower capacity is likely to increase for all but three countries in the study under climate change. Additionally, seasonal variability increases for more than half of the countries studied. For the most part, the variability increases at the country level are higher than the changes in variability at the power pool level. Increased interannual and seasonal variability under climate change could jeopardize the system and deter an individual country's ability to transition to carbon-neutral electricity sources such as solar and wind. If the countries balance their hydropower resources through electricity trading, they could improve the reliability of their systems and achieve a smoother transition to low-carbon electricity system[171,178]. While this study focuses on hydropower generation potential across a wide range of countries in Africa, other renewable energy sources will likely penetrate the national grids. Furthermore, electricity demand will play a role in the future deployment of capacity in the continent. In this work, we aimed to characterize hydropower resources in a consistent manner across power pools and countries and limited our analysis to current installed capacity. Future work can incorporate our results into capacity expansion models that account for supply of multiple energy sources, power generation technologies, end-use technologies, and demand for end-use services.

We explore the potential interconnections across power pools using a complementarity assessment to generate interconnection scenarios. Previous work suggests the potential for interconnection to decrease the risk of power disruptions based on hydropower variability[154,170].

Our results confirm that interconnecting the power pools in the continent could benefit the most variable hydropower resources and mitigate the potential decreases in usable capacity resulting from climate change impacts in the individual countries' systems. At the same time, interconnection could decrease the variability of hydropower resources making it more attractive as a baseload source of electricity.

Although we do not incorporate the potential synergies between hydropower, solar and wind, there is potential for these energy sources to drive a low-carbon electrification for Africa. The potential for solar and wind resources, just like hydropower, is spatially heterogenous in the continent. There is large Solar photovoltaics (PV) potential in parts of Southern Africa, Sudan, Libya, Egypt, and Ethiopia, but is more limited in Central Africa (e.g., the DRC). Similarly, Southern Africa is suitable for concentrated solar power (CSP). On the other hand, wind is relatively more limited in the continent but could be synergistic with solar resources in West Africa[176,171]. As shown in this study, hydropower in the African continent has the potential to remain a reliable source of electricity throughout the 21st century. Pairing hydropower with wind and solar, and at the same time expanding the transmission infrastructure to allow for the power pool operations, would enable Africa to electrify using low-carbon energy sources. Detailed local analysis of the interannual and seasonal variability of hydropower, solar, and wind resources and potential complementarities under demand scenarios is an important next step in achieving widespread low-carbon electrification across the continent.

In this study, we analyze 87 power plants, including 37 reservoir hydropower plants. While large hydropower reservoirs can have detrimental impacts on ecological systems and produce biogenic greenhouse emissions[152,188,189], they could help balance competing water uses and improve the resilience to flooding[190]. Previous work, including a study of the Grand Renaissance Dam in Ethiopia, illustrates how balancing reservoir operations with other renewables (e.g., solar and wind) can improve the resiliency of the power system while at the same time achieving decarbonization goals and renewable penetration[170]. Furthermore, optimizing the use of existing reservoirs in the region in conjunction with power pool operation could enhance the systems' resilience to the future impacts of climate change. Although we do not include optimal operations of reservoirs with competing water uses or cascading power plants, we argue that our work provides the baseline for the assessment of optimal reservoir operation while looking at multiple power pools and temporal scales.

Appendix B provides the complete list of georeferenced pairs of power plants and potential attractive interconnections between countries, including preliminary distance estimates for interconnection. This information could be useful but not sufficient for decision-makers evaluating interconnection plans. Such investment decisions should assess the benefits of interconnection as well as the costs of building and operating the transmission lines. Finally, the analysis in this paper could be applied to other regions of the world. Current global databases for hydropower and water resources do not incorporate climate change impacts on usable capacity, potential generation variability, and potential synergies between countries and power plants based on seasonality[185,191].

The challenges for Africa's electrification efforts extend beyond the potential impacts of climate change. Still, we suggest there is an opportunity for future synergies based on hydropower generation in the continent. Additionally, there is large untapped hydropower potential[192] that could help achieve electrification goals while balancing climate change impacts in parts of the continent if planning decisions consider these impacts. Furthermore, expanding hydropower systems in the continent could strengthen the complementarities between and inside power pools. Hydropower can provide stability to the grid as solar and wind installations increases[9]. Other challenges the region will face while pursuing electrification and interconnection include aging infrastructure and the lack of strong institutions, regulations, and policies[193]. These countries will need to overcome these compounding challenges to achieve universal electricity access in the continent under a changing climate.

3.5 Methods

3.5.1 Streamflow calculation

We rely on a monthly water balance and hydropower operations model[194–196] to model usable hydropower capacity. We previously developed the lumped water balance model using R and Python to evaluate hydropower plants in South America[73]. We include a total of 87 hydropower plants across 27 countries and five African Power Pools.

We delineate the watersheds for each hydropower plant using Python's pysheds192 package and R's spatial analysis packages and data from Hydrosheds[198] for the African continent.

We obtain the watershed's mean elevation from a digital elevation model[199] and the average soil moisture[200] and soil depth[200] from remotely sensed data. The extracted data serve as input to the water balance model. We use temperature data from NCEP-DOE Reanalysis 2[201] dataset, precipitation from the CPCC dataset[202], and runoff data from the GRDC[203] and GRUN[204] for the model calibration. We calibrate the model using the Shuffle Complex Evolution (SCE) algorithm and the Nash Sutcliffe Efficiency Coefficient (NSE).

We use climate projections as the model's key drivers of future usable capacity from NASA's Earth Exchange Global Daily Downscaled Projections (NEX-GDDP) dataset[55]. NEX-GDDP consists of comprehensive high-resolution climate data (0.25 degrees), which includes retrospective (control) and prospective runs from 21 Global Climate Models (GCMs) under Representative Concentration Pathways (RCPs) 4.5 and 8.5[58] from the Coupled Model Intercomparison Project Phase 5 (CMIP5). RCP 4.5 represents a mid-emissions scenario (increase of 2.5°C global average temperature by the end of the century), and RCP 8.5 a high emissions scenario (increase of 5 °C global average temperature by the end of the century). We use RCPs 4.5 and 8.5 to quantify physical climate risk and note that RCP 8.5 encompasses the cumulative CO_2 emissions that occur under other RCPs[60,61] (they just happen sooner under RCP 8.5). We do not ascribe likelihood to one scenario over another. We use CMIP5 in lieu of CMIP6 as there was still no consistently downscaled CMIP6 dataset for Africa at the time of the study[56,57].

3.5.2 Hydropower formulation, usable capacity assessment, and variability analysis

Using the time series obtained from the water balance model, we calculate monthly future usable capacity. We obtain the characteristics of the power plants from different sources, including the West African Renewable Power Database[205], Global Reservoir and Dam Database (GRanD)[206], and Conway et al., 2017[207] (for the full list, see Appendix B Supplementary Table B-1). The model's inputs include the power plant's geographic location (latitude and longitude), the installed capacity (P, in MW), the design flow (Q, in m^3/s), the reservoir's maximum and usable capacities (V_{max} and V_{use}, where max is the maximum volume and use the usable capacity in million m^3), the reservoir's maximum area (A_{max}, in km^2), and the power plant's effective height

(H, in m). We include only online power plants in the analysis, except for the Grand Renaissance Dam in Ethiopia, which is currently being filled.

We define usable capacity as the maximum monthly capacity in MW, constrained by the power plant's installed capacity, the simulated streamflow can maintain for a specific time frame. To model the usable capacity, we determine if power plants are run-of-river or impoundment hydropower plants. For both formulations, we assume 1,000 kg/m^3 for the density of water (ρ_{water}), 90% for the efficiency (η) of the power plant turbines, and 9.8 m/s^2 for the gravity constant (g). Run-of-river hydropower plants have limited storage capacity and do not require operating a reservoir (Equation (3.1)). On the other hand, reservoir power plants require simulating water releases, for which we use the Reservoir package in R[208–210]. This formulation optimizes water releases through a dam by maximizing hydropower generation (using V_{max}, V_{use}, and A_{max} in addition to the parameters used for run-of-river hydropower plants).

$$P_t = Q_t \times H \times \rho_{water} \times g \times \eta \qquad \text{Equation (3.1)}$$

We obtain 42 futures, and 21 historical reference runs using the multi-model ensemble (two RCP's and the GCMs historical control run) for each hydropower location. We divide the time series into four time slices: historical reference (1970 – 2005), near-future (2010 – 2039), mid-century (2040 – 2069), and end-of-the-century (2070 – 2099). We find the multi-model annual and monthly usable capacity mean for each time frame and each power plant. We calculate the annual usable capacity as the mean of the monthly values for each year. The normalized usable capacity is the ratio of the usable capacity time series with the power plant's installed capacity. We assess the normalized usable capacity changes as the difference in percentage points between the future time frame multi-model mean (annual or monthly) and the historical reference mean for both scenarios.

We aggregate time series to the country and power pool level by summing each power plant's corresponding time series in the system. Then, using the 63 aggregated time series of usable hydropower capacity (upc_i, annual mean for the period i, and $upc_{m,i}$, monthly mean for the period i) corresponding to each country, we calculate the coefficients of variation across years (interannual variability) and within year (seasonal variability) as described in equations (3.2) and (3.3), respectively ($i_v \geq 0$ and $s_v \geq 0$). The closer each value is to 0, the smaller the

standard deviation compared to the mean of the population and, therefore, the smaller the variation within and across years.

$$i_v = \frac{sd(upc_i)}{mean(upc_i)} \qquad \text{Equation (3.2)}$$

$$s_v = \frac{sd(upc_{m,i})}{mean(upcm_{,i})} \qquad \text{Equation (3.3)}$$

Finally, to calculate the statistical significance of the differences between the coefficients of variation for the interannual and seasonal variability and their corresponding time-frames and scenarios, we perform an asymptotic test using the "cvequality" package in R[211]. With this package, we test the differences in the coefficients of variation of two sample populations for statistical significance. We derive p-values for the multi-model ensemble coefficient of variation of annual (IV) and seasonal (SV) usable capacity time series at their corresponding geographic scales (country, power pool, and interconnection scenario).

3.5.3 Generating interconnection scenarios via complementarity indexes and metrics

We calculate complementarity indexes to identify the potential synergies between power plants, countries, and power pools. This analysis aims to determine the most relevant interconnection scenarios for the power pools in the continent. We define complementarity as a measure of how much different renewable energy sources can complement each other to provide a reliable power profile[175,212]. We can measure complementarity spatially and/or temporally. Spatial complementarity is presented when sources complement each other in a certain region[175]. Temporal complementarity occurs when sources complement each other during different periods of time[175]. Here, we assess the complementarity between hydropower resources at the power plant and country-level using the usable capacity time series obtained from the previous framework. We define two indexes to capture temporal and spatial complementarities based on the monthly usable capacity of a pair of power plants or countries: the temporal complementarity index calculated as the Pearson correlation coefficient (shown in equation (3.4)) and the monthly usable capacity complementarity (shown in equation (3.5)). We calculate these indexes for a pair x,y of power plants or countries using the monthly usable capacity (upc) for a given period i. The Pearson correlation coefficient (-1 to +1) presents high complementarity the closer the values get

to -1. On the other hand, the usable capacity complementarity metric (0 to +1) shows a higher degree of complementarity the closer it is to 1.

$$r = \frac{\sum(upc_{x,m.i} - \overline{upc_{x,m.\iota}})(upc_{y,m.i} - \overline{upc_{y,m.\iota}})}{\sqrt{\sum(upc_{x,m.i} - \overline{upc_{x,m.\iota}})^2 \sum(upc_{y,m.i} - \overline{upc_{y,m.\iota}})^2}} \qquad \text{Equation (3.4)}$$

$$UCI = 1 - \sqrt{\left(\frac{\overline{upc_{x,m,\iota}} - \overline{upc_{y,m,\iota}}}{\overline{upc_{x,m,\iota}} + \overline{upc_{y,m,\iota}}}\right)^2} \qquad \text{Equation (3.5)}$$

We calculate an index by combining the previous two metrics (r and UCI) using equation (3.6). We call this metric the Complementarity Index (CI). The CI (-1 to +1) presents higher complementarity for a given pair the closer the value gets to 1. We consider highly complementary pairs when the values are higher than +0.5.

$$CI = -1 \times r \times UCI \qquad \text{Equation (3.6)}$$

Using this index and the previous two metrics, we identify potential interconnection scenarios between countries and power pools by identifying the highest complementary countries (CI > 0.5). We present the results of the complementarity analysis and the details for the scenarios in Appendix B Supplementary Notes B-1 and B-2.

3.6 Data Availability

The datasets generated and analyzed during the current study are available in the Zenodo repository (https://doi.org/10.5281/zenodo.5020878)[213].

Chapter 4 – RICCH: An Interactive Analysis Tool for Risk and Impacts of Climate Change on Hydropower Plants in the Global South

The contents of this chapter will be submitted for publication. This chapter should be referred to as: Caceres, A. L., Jaramillo, P., Matthews, H. S., Samaras, C., Huang, L. & Nijssen, B. (2022) "RICCH: An Interactive Analysis Tool for Risk and Impacts of Climate Change on Hydropower Plants in the Global South."

4.1 Abstract

Climate change can threaten the viability of future hydropower development and operations. Identifying climate impacts and the potential risks on hydropower plants is the first step towards the future adaptation of the hydropower sector. Further regional assessments for the Global South are still needed. With RICCH, we combine the results of hydropower climate assessments with an interactive analysis tool. First, we identify future hydropower usable capacity for 542 hydropower plants across 56 countries using a consistent multi-model ensemble of 21 GCMs and 2 RCPs. Then, we build the RICCH database, which includes power plant characteristics and these time series of usable capacity. Finally, we build the RICCH tool using the database and R-Shiny. We publish the source code in GitHub and the tool in shinyapps.io, enabling it to remain open-sourced and publicly available. This publication allows users to download and modify the code when needed and update the database with personalized results from other studies. RICCH allows users to interact with multiple hydropower plants in different regions and countries and explore the changes in usable hydropower capacity in a changing climate. The future steps for RICCH will be to survey key stakeholders to improve how we present the information and allow RICCH to become a valuable tool for the future planning of the hydropower sector.

4.2 Introduction

Currently, a third of worldwide greenhouse gas emissions (GHG) comes from electricity generation around the world[1]. The power sector is one of the largest contributors to the increases in atmospheric concentrations of GHG. A few countries, including the United States and China, are responsible for more than 50% of these emissions[214]. At the same time, more than 800 million people worldwide, almost two-thirds in Sub-Saharan Africa, still lack access to modern electricity services[5]. The United Nations (UN) Sustainable Development Goal (SDG) 7 aims to achieve universal sustainable electricity access[6]. In turn, global electricity demand is expected to continue to increase over the following decades, and there is a pressing need to decrease the carbon intensity of its sources[215]. Therefore, emerging economies in the Global South will need to expand their electricity infrastructure while cutting emissions, and at the same time, adapt to some of the potentially detrimental impacts of climate change[6,215,216].

Hydropower is the largest renewable source of electricity generation worldwide, accounting for 16% of electricity generation in 2019[217]. Although there has been a recent trend towards increasing the capacity of other renewable electricity sources, such as solar and wind, hydropower will remain one of the most important sources of renewable electricity globally and should play an important role in the sector's decarbonization[8,218]. Furthermore, hydropower can help balance the intermittent nature of other renewables (e.g., solar and wind) as they continue to penetrate national grids. Hydropower assets, particularly run-of-river designs, still have considerable potential to be a low-carbon option to meet the growing energy demand in emerging economies (e.g., in South America, Africa, and Asia)[10,69]. For example, Africa will continue to rely on hydropower as its electricity demand increases throughout the 21st century[66].

On the other hand, climate change can threaten the viability of future hydropower development. Climate change could alter the timing and magnitude of precipitation which directly influences water availability and streamflow. Accelerated melting of glaciers in the mid-latitudes, e.g., the Tropical Andes, creates unsustainable streamflow in glacierized basins that will likely disappear as glaciers continue to retreat[32,34,40,219]. Rising temperature will increase evaporative demand within basins and could reduce river flows directly affecting power plant operations[11]. Some studies suggest that climate change could reduce usable hydropower capacity in more than half of the basins studied by mid-century[12]. However, there is a gap in the literature regarding climate impacts on individual hydropower projects in the Global South, and further regional studies are needed. Nonetheless, as previously mentioned, hydropower poses opportunities to decarbonize the electricity sector in many economies. Power plants with storage can provide flood control and mitigate the effects of droughts. However, reservoir expansion can be costly and could have negative externalities, including increases in methane emissions from the degradation of organic biomass, and social conflicts product of the displacement of communities to build the reservoirs[152,188,189,220].

Identifying climate impacts and the potential risks on hydropower plants in the Global South effectively is the first step towards future climate adaptation and improving the resilience of the electricity sector in a changing climate. Communicating assessment results to relevant decision-makers will be crucial, yet effective communication tools for climate adaptation are severely lacking[221,222]. The use of interactive visuals can improve the understanding and dissemination of scientific information[223]. In this regard, some efforts aim to create compelling

visualizations using geographic information systems (GIS) to convey climate impacts and adaptation strategies to stakeholders[224–226]. However, these tools typically lack interactive features and fail to communicate the most relevant information to their users[225]. While climate scientists might be used to dealing with multiple climate change scenarios and their effects on hydropower systems, actual decision-makers might find this information too complex.

Currently, no global database or tool allows the identification of vulnerability and risk to climate change for hydropower plants located anywhere in the world. Nonetheless, some databases include useful information for evaluating climate change impacts on hydropower generation. Table 4-1 describes some of the most relevant open access (free) existing databases. Additionally, some existing power plant databases include hydropower. For example, the World Bank has georeferenced datasets for power plants in several African countries (e.g., South Africa, Zambia, and others) as part of their data catalog[227]. Unfortunately, these datasets are outdated (from 2006), and the newer version (World Electric Power Plants Database 2018, developed by S&P Platts) is not freely accessible[228]. The World Resources Institute also has a Global Power Plant Database[229]. This database is freely accessible, and it includes geographic coordinates and characteristics of the power plants, but it has significant data gaps for numerous countries in the Global South. Furthermore, they do not incorporate the potential impacts of climate change on the power plants. Our current study expands on these existing databases. Using a water balance and a hydropower operations model, we complement existing databases by incorporating simulated future usable hydropower capacity under two emissions scenarios for medium to large (> 40 MW) hydropower plants in the Global South. We build "RICCH: Risk and Impacts of Climate Change on Hydropower" for 542 hydropower plants across 56 countries in five regions of the world (Mexico and Central America, South America, Africa, the Middle East, and Southeast Asia and the Pacific). Our main objectives for RICCH are to (i) generate an interactive assessment tool for hydropower in the Global South that could help inform future adaptation of the hydropower sector and (ii) perform regional and country-specific assessments of future hydropower availability under climate change.

Table 4-1 – Existing Hydropower, Reservoir, and Dam Databases. The following table describes the main hydropower and reservoir databases with their corresponding key characteristics and extent.

Database	*Power Plants Included*	*Capacity Included*	*Key Attributes Included*	*File Type*	*Open-sourced*
Global Hydropower Database (GHD) *Wan et al., 2021*[230]	8,716 georeferenced hydropower plant records (134 countries)	91.8% of the world's hydropower installed capacity	Installed capacity, reservoir characteristics, and other relevant information.	Shapefile (.shp)	Yes
Global Reservoir and Dam (GRaND) *Lehner et al., 2011 (updated to version1.3 – 2019)*[231]	7,320 georeferenced reservoir and dam records (140 countries)	Does not specify installed capacity of hydropower dams	Name, river, primary use, height, area, and reservoir volume.	Shapefile (.shp)	Yes
FAOAQUASTAT *FAOAQUASTAT, 2016*[232]	>14,000 georeferenced records for dams (9 regions globally)	Does not specify installed capacity of hydropower dams	Date completed, dam height, reservoir capacity, reservoir area, sedimentation, and uses.	Microsoft Excel Spreadsheet (.xlsx)	Yes
Existing US Hydropower Assets *Johnson, Kao, Samu, & Uria-Martinez, 2019*[233]	2,298 georeferenced records (in the United States)	~6.0% of the world's hydropower installed capacity	Key characteristics of operational hydropower plants (total capacity, annual net hydropower generation, and others).	Microsoft Excel Spreadsheet (.xlsx)	Yes
West Africa and India Hydropower Dams *Ivanescu, 2018*[234]	3,262 georeferenced records of hydropower dams in West Africa and India	~1.8% of the world's hydropower installed capacity	Reservoir capacity, installed capacity, location, others.	Comma-separated values delimited text file (.csv)	Yes

Pumped Storage Tool *International Hydropower Association, 2019*[235]	Number of records unclear.	-	Location, installed capacity, and energy stored by pumped storage hydropower plants worldwide.	Interactive Website	No
Hydropower Potential Dataset *Hoes et al., 2017*[10]	11.8 million theoretical locations	52 PWh/year potential	Global hydropower potential database with high spatial resolution (global gridded dataset).	Shapefile (.shp)	Yes
Future Global Dams and Hydropower Projects *Zarfl et al., 2015*[236]	3,700 georeferenced records (101 countries)	725 GW of future capacity	Location and installed capacity.	Microsoft Excel Spreadsheet (.xlsx)	Yes
RICCH Tool and Database *Current publication**	542 georeferenced records of hydropower plants (56 countries)	~18.8 % of the world's hydropower installed capacity	Location, installed capacity, hydropower usable capacity (21 GCMs and 2 RCPs).	R-Shiny (.R) and Comma-separated values delimited text file (.csv)	Yes

* The entirety of the contents are not available at the moment.

4.3 Methods

4.3.1 The Water Balance and Hydropower Operations Model

Previously, we developed a hydropower risk and vulnerability assessment model consisting of a hydrological water balance paired with optional reservoir operations[106] and hydropower operations[73]. The water balance accounts for three water sources (precipitation[54,96], snowpack, and glaciers[95]), a water storage component, and water losses for each power plant system analyzed[123]. The model requires processing and analyzing large georeferenced datasets and developing various data analysis tools using R and Python. We input downscaled global climate projections[55], remotely sensed soil properties and digital elevation models[122,123,237], hydropower

plants locations[89,113,231,238], and other complementary information[95,239,240] to obtain future hydropower usable capacity time series for every power plant analyzed. Equation (4.1) presents the water balance model basic configuration.

$$Q_t = S_{t-1} + P_t + Gl_t + Sn_t - AET_t - S_t \qquad (4.1)$$

Where Q_t is the runoff generated at month t, S_{t-1} is the previous month's soil moisture storage component, P_t is the precipitation at month t, Gl_t is the glacier melt at month t, Sn_t is the snowmelt at month t, AET_t is the actual evapotranspiration at month t and S_t is that month's soil moisture storage component. The glacier component is optional.

We obtain the streamflow at the power plant level for a multi-model ensemble of 21 Global Climate Models (GCMs) from NASA's Earth Exchange Global Daily Downscaled Projections (NEX-GDDP)[55] dataset under two Representative Concentration Pathways (RCPs) from the Coupled Model Intercomparison Project 5 (CMIP5). For each of the climate models, we include a retrospective control run (1970-2005) and two future simulations under RCP 4.5 (mid-emissions scenario) and RCP 8.5 (business-as-usual scenario). We use NASA's NEX-GDDP dataset because it provides a consistently downscaled product for all GCMs and the entire globe.

With the projected streamflow and the power plant characteristics obtained from multiple sources, including global databases and governmental entities from multiple countries[114,129,131,135,136,162,178,229–231,241], we simulate hydropower operations through 2099 using either Equation (4.2) and optionally a reservoir optimization model in the R Reservoir Package[106] for hydropower plants with large storage capabilities. We apply the models to each hydropower plant independently.

$$P_t = Q_t \cdot H \cdot \rho_w \cdot g \cdot \eta \qquad (4.2)$$

Where P_t is the potential average power output of each power plant (MW) in month t, Q_t is the input flow (m^3/s) in month t, H is the effective head of the turbine (m), ρ_w is the water's density (1,000 kg/m^3), g is the gravitational acceleration (9.8 m/s^2), and η is the turbine efficiency (90%). We obtain time series of usable capacity (MW) at the hydropower plant level from this module. For each power plant included in the analysis, there are 21 corresponding time series, one for every GCM, for the two emissions scenarios (RCP 4.5 and 8.5) and the retrospective run. Each power plant will have 63 time series in total when considering all models and scenarios. With these results, we start building the database and interface for RICCH.

4.3.2 RICCH R-Shiny Dashboard Development

4.3.2.1 Developing the RICCH Complementary Database

4.3.2.1.1 Identifying hydropower plants in the Global South

In 2020, a total of 21 GW of new hydropower installed capacity came online around the world[62]. The biggest installations happened in Southeast Asia and the Pacific (14.5 GW), followed by Europe (3.0 GW) and South and Central Asia (1.6 GW)[62]. The increase in new installations in South America stalled in 2020, but the region remains the second-largest hydropower generator in the world[63]. The largest capacity concentration is in Southeast Asia and the Pacific, followed by Europe, North America, and South America. The African continent remains the region with the least hydropower installed capacity, and currently, there are still more than half a billion people without electricity access in Sub-Saharan Africa[65,242]. Nevertheless, hydropower is expected to play an essential role in the electrification of Africa[66]. We identify five regions in the Global South with high hydropower growth potential[10,69]. These regions include Mexico and Central America, South America, Africa, the Middle East, and Southeast Asia and the Pacific. Table 4-2 describes the key characteristics of these regions, including their hydropower resources and electrification rates.

Additionally, some countries within these regions rely more on hydropower generation than others. For example, South America is a region that is heavily reliant on hydropower generation. In 2020, the region produced an estimated 690 TWh of hydroelectricity[62], representing around 75% of its electricity generation[67]. Analogously, in Sub-Saharan Africa, hydropower typically represents around half of the electricity generated each year [68]. Furthermore, hydropower dependence (more than 50% of your electricity generation coming from hydropower) can make regions highly susceptible to any changes in hydropower availability under a changing climate.

Table 4-2 – Main hydropower characteristics in the fastest growing regions of the Global South. We obtain the current installed capacity for each region and the largest producing country from the International Hydropower Association 2020 and 2021 Hydropower Status Reports[62,63]. The proportion of the population with electricity access represents the level of electrification in the region, and we obtain this information from the International Energy Agency and the World Bank [65,70].

Region	Current Installed Capacity	Country with Highest Installed Capacity (GW)	Proportion of Population with Electricity Access
Mexico and Central America	21 GW	Mexico (12 GW)	94.8% (Mexico, Central, and South America)
South America	177 GW	Brazil (101 GW)	
Africa	38 GW	Ethiopia (4 GW)	North Africa: 99+% Sub-Saharan Africa: 47.9%
Middle East	22 GW	Iran (12 GW)	92.3%
East Asia and the Pacific*	501 GW	China (370 GW)	96.0%

* For our analysis, we include the region Southeast Asia and the Pacific, which excludes China.

Once we identify these five regions, we proceed to characterize the hydropower plants in each one. We obtain hydropower plant characteristics from multiple sources, including Global Hydropower Database (GHD)[230], the Global Reservoir and Dam Database (GRanD)[231], the Global Energy Observatory[243], and other sources presented in Table 4-2. We include medium to large hydropower plants (> 40 MW in installed capacity). RICCH consists of 542 hydropower plants ranging from 43 MW (Koka hydropower plant in Ethiopia) to 14,000 MW (Itaipu hydropower plant between Brazil and Paraguay). These power plants span 56 countries across the five mentioned regions. Figure 4-1 shows the locations of all the hydropower plants included in RICCH, and Table 4-3 describes the main characteristics of the power plants by region. We refer to the compilation of the 542 hydropower plants with their key design characteristics as the "Hydropower Plants Database." Supplementary Tables D-1 and D-2 present the list of countries, the number of power plants included in each region, and the key attributes in the database. We run the water balance and hydropower operations models for each power plant and obtain future hydropower usable capacity time series. The following section describes how we incorporate the time series results into the RICCH database and the interactive tool.

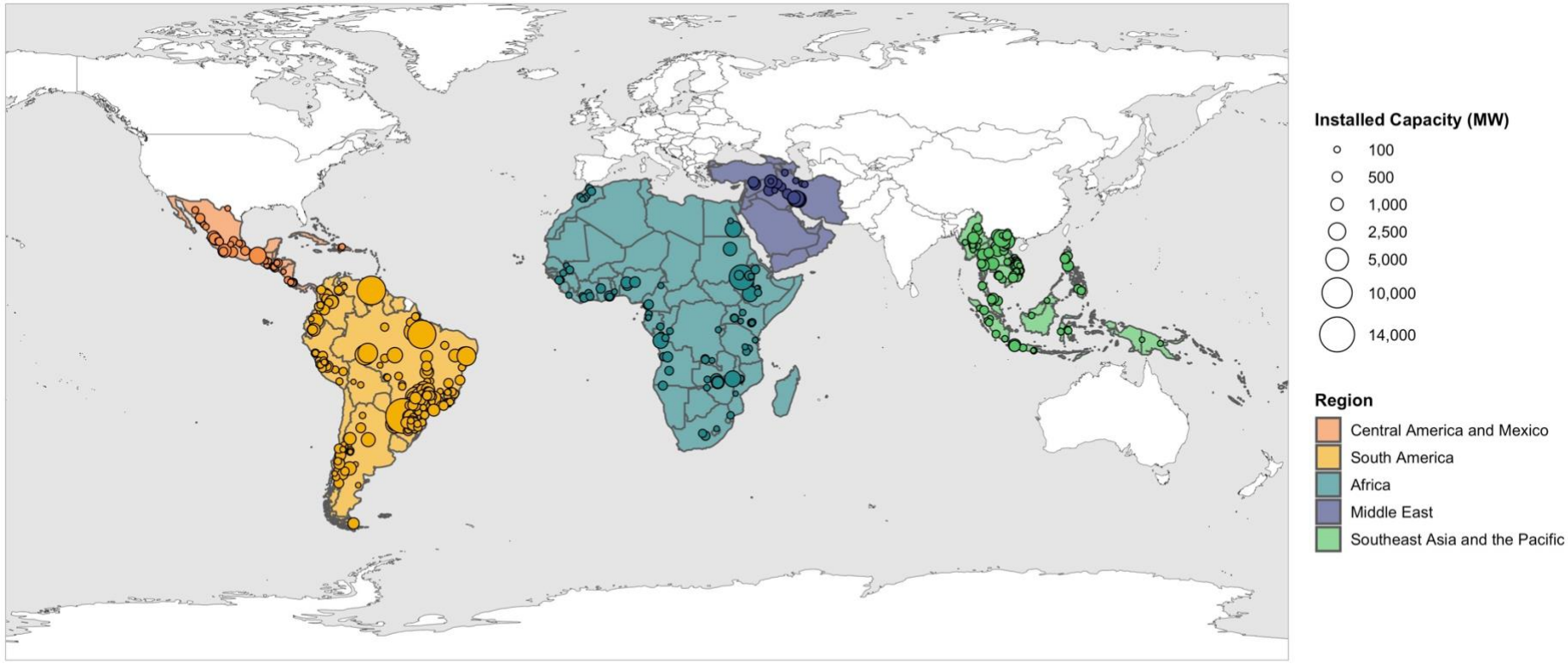

Figure 4-1 – Distribution of hydropower plants included in RICCH. We include 542 hydropower plants across five regions of the Global South. The regions include Mexico and Central America, South America, Africa, the Middle East, and Southeast Asia and the Pacific. We do not include China, Japan, or Korea in Southeast Asia and the Pacific. Hydropower plants installed capacity ranges from 43 MW (Koka hydropower plant in Ethiopia) to 14,000 MW (Itaipu hydropower plant in Brazil).

Table 4-3 – Summary of hydropower plants included in RICCH. We present all five regions included in the interactive tool. The installed capacity included in each region represents the net installed capacity for the hydropower plants in RICCH. Supplementary Table D-1 presents a list of the countries and the number of power plants included in each region. Supplementary Table D-2 shows the key attributes of the "Hydropower Plant Database." The installed capacity included is the sum of the installed capacity in each of these countries. For Southeast Asia and the Pacific, we do not include China, Korea, or Japan.

Region	Countries Included	Power Plants Included	Installed Capacity Included (GW)	Range of Installed Capacity (MW)
Africa	28	87	27*	43 – 2,100
Southeast Asia and the Pacific	9	132	35	51 – 2,400
Central America and Mexico	7	49	15	51 – 2,400
Middle East	3	22	14	62 – 2,000
South America	9	252	154	51 – 14,000
Total	**56**	**542**	**245***	

* We include the Grand Renaissance Dam for Ethiopia (currently being filled) for a total of ~34 GW in Ethiopia and ~250 GW overall.

4.3.2.1.2 Incorporating Future Usable Capacity Results

We obtain future hydropower usable capacity for each of the hydropower plants included in our original database. We run the water balance and hydropower operations model based on the design characteristics and locations of the power plants as described in the schematic presented in Figure 4-2. We aggregate each usable hydropower capacity (MW) time series corresponding to a GCM simulation to four main periods: historical (1970-2005), early century (2010-2039), mid-century (2040-2069), and end-of-the-century (2070-2099). The result of this aggregation is the mean monthly hydropower usable for each of the 542 hydropower plants and 21 GCMs, two RCPs, and the historical control run. Every hydropower plant in the RICCH database has a corresponding monthly mean usable capacity (MW) for every GCM for each of the time-frames mentioned and the corresponding RCPs. For example, the Itaipu power plant in Brazil has a record for its simulated mean monthly usable capacity for January in the early century (2010-2039), under GCM ACCESS1_0 and RCP 4.5. The same applies to all other combinations of months, GCMs, and RCPs.

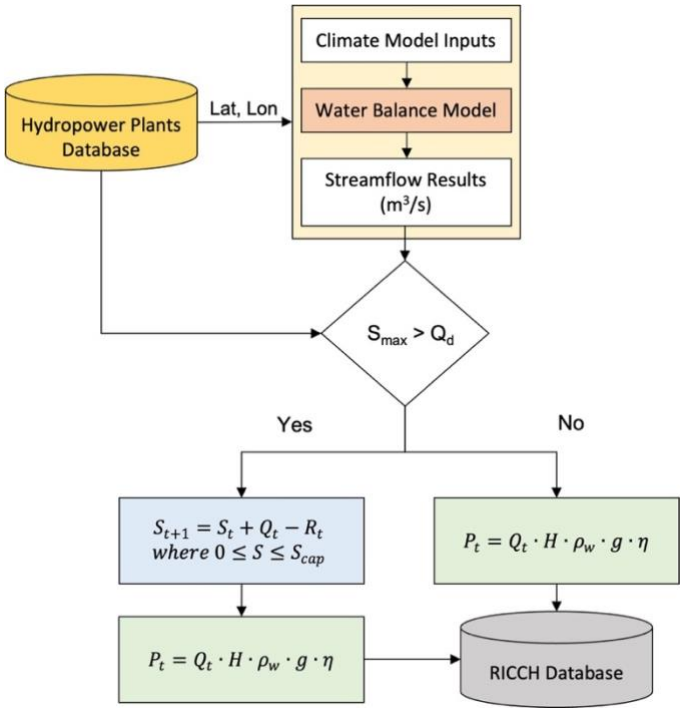

Figure 4-2 – Schematic for the creation of the RICCH Database. With the water balance and hydropower operations model described in the section under the same name, we generate simulated time series of future hydropower usable capacity for all the hydropower plants included in the Hydropower Plants Database (542 records). We incorporate the results from assessing the future usable capacity time series for each hydropower plant and generate the RICCH Database. This database includes all 542 records of power plants with the future usable capacity under 21 GCMs, two emissions scenarios (RCP 4.5 and RCP 8.5), and a retrospective control run.

Table 4-4 presents the key attributes included in the RICCH database. For every hydropower plant, a designated name refers to the corresponding shapefile for the water balance model (name_shp) and the full name of the power plant (long_name). All hydropower plants are georeferenced with their longitude (lon) and latitude (lat) locations. We include the installed capacity in Megawatts (MW) (power_mw), the region (e.g., South America), country, administrative unit name (adm_unit), the type of administrative unit (name_adm_unit), the GCM used for the simulation, the scenario (historical, RCP 4.5, or RCP 8.5), the time frame (time_frame), the month for the simulation (month_factor), and the usable capacity value for the given record in MW (mean_period). The database contains a total of 956,088 records corresponding to each of the 542 hydropower plants. For every power plant, a total of 1,764 records exists, corresponding to every month (January through December), time-frame (historical, 2010-2039, 2040-2069, and 2070-2099), scenario (historical, RCP 4.5, and RCP 8.5), and GCM (21 models in NASA's NEX-GDDP). We export the database to a Comma-separated

Values file which can be displayed using Geographic Information Systems (GIS) software (e.g., ArcGIS or QGIS), R, Python, or other software which allows displaying georeferenced datasets.

Table 4-4 – Overview of the key attributes and content included in the RICCH Database. We present the names of the hydropower plants, their locations, and the results from the future hydropower usable capacity simulation runs. We provide the units when appropriate and an example of the presentation of the information in the database.

Key attributes	Description	Units	Example
name_shp	The abbreviated name of the hydropower plant used as a reference for shapefile documents.	-	guadalupe_IV
long_name	The full name of the hydropower plant.	-	Guadalupe IV
power_mw	The installed capacity of the hydropower plant in MW.	MW	202
lon	The longitude location of the power plant.	°	-75.25
lat	The latitude location of the power plant.	°	6.78
country_code	The ISO Alpha-3 code for the country where the power plant is located.	-	COL
country	The full name of the country where the power plant is located.	-	Colombia
adm_unit	The full name of the administrative unit.	-	Antioquia
name_adm_unit	The type of administrative unit in the specific country (e.g., state, region, province, etc.).	-	Departamento
climate_model	The name of the Global Climate Model (GCM) for the simulation.	-	ACCESS1_0
scenario	The scenario for the simulation. There are three options for this field: rcp45 corresponding to RCP 4.5, rcp85 corresponding to RCP 8.5, and the historical corresponding to the retrospective control run.	-	rcp45
time_frame	The time frame for the simulation results. There are four options for this field: historical corresponding to the control run between 1970 and 2005, 2010-2039 corresponding to the early century, 2040-2069 corresponding to the mid-century, and 2070-2099 corresponding to the end of the century.	-	2010-2039
month_factor	Represents the month of the year for the simulation. January is 1, February 2, and so on.	-	1

mean_period	This field corresponds to the simulation results for the specific climate model, scenario, time-frame, and month. The value represents the usable capacity in MW.	MW	117.7

4.3.2.2 Developing the RICCH Dashboard User Interface Using R-Shiny

Using the records in the RICCH Database, we develop the RICCH User Interface using R-Shiny. We refer to the tool, which incorporates the interface and the database, as RICCH. As previously mentioned, RICCH displays the usable capacity of 542 hydropower plants across the Global South under two different emissions scenarios and for a multi-model ensemble of 21 GCMs. Figure 4-3 presents a schematic for RICCH. The interactive tool aims to provide an interface for the hydropower operations model results. RICCH is an interactive dashboard that merges the original RICCH Database with the GIS shapefile data files. Our target audience for RICCH includes decision-makers, hydropower planners, operators, and any potential stakeholder of the hydropower and electricity sectors. We aim for decision-makers to use the information we present to inform future climate change adaptation of the hydropower and electricity sectors in their corresponding countries and regions.

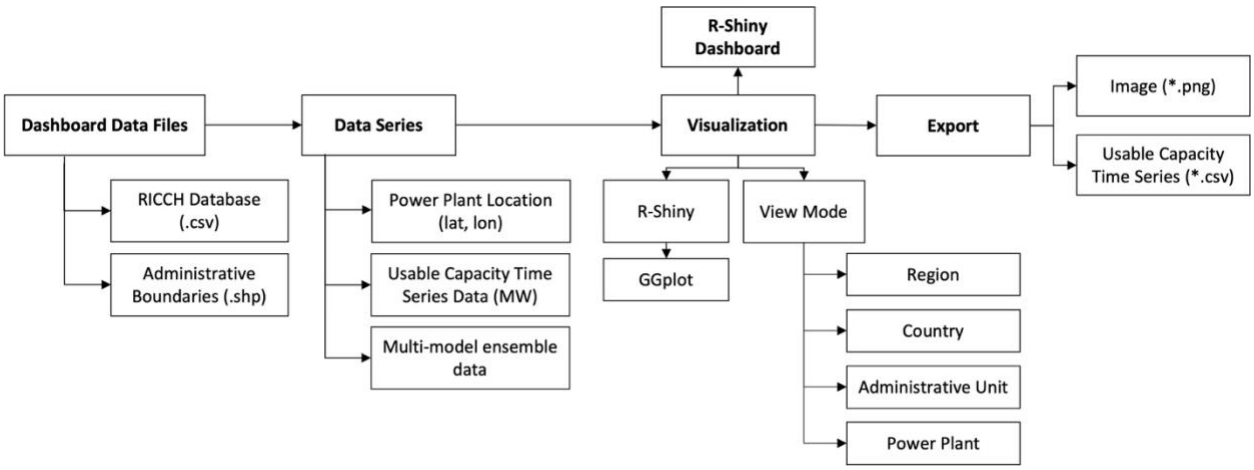

Figure 4-3 – Scheme for the creation of the RICCH visualization tool. The input data files to the dashboard include the original RICCH database (>900k records) and Global Administrative Areas database (GADM)[244]. We process the records for every power plant and display them using R-Shiny and GGplot. RICCH displays the usable capacity curves for every power plant in a region, country, and administrative unit. Users can export the results as an image or a CSV file.

We implement the dashboard using R-Shiny in R-Studio. R-Shiny is a package in the statistical software R, which allows the creation of interactive visualizations of datasets[245]. We implement subsets of maps from the regional to the country, administrative unit, and power plant levels using R-Shiny. For every hydropower plant, we present monthly usable capacity curves for every scenario and time-frame. We plot these curves using the packages GGplot (for the static curves) and Plotly (to implement the interactive capabilities) in R[246]. Users can export the results to a CSV or an image (.png) file.

4.3.2.3 Web Implementation – Using Shiny Apps

For the web implementation of RICCH, we use "shinyapps.io." This online service allows hosting R-Shiny applications and publishing them online. The integration of RICCH into shinyapps.io is seamless because the dashboard's source code uses shiny. We publish the source code for RICCH in GitHub (https://github.com/acaceres93/RICCH)[247]. The RICCH database is publicly available for download in the Zenodo repository titled "RICCH: An Interactive Analysis Tool for Risk and Impacts of Climate Change on Hydropower Database" (https://doi.org/10.5281/zenodo.5714446). Users interested in running the application in their local machines can download the source code and the database. The application is available using this URL: https://ricch.shinyapps.io/hydro-shiny/ (shinyapps.io[248]).

4.3.3 RICCH

4.3.3.1 Demonstration of RICCH Visualizations and Results

Previously, we identified 542 hydropower plants in the Global South and performed a water balance and hydropower operations assessment under a multi-model ensemble of 21 GCMs. In this section, we describe how RICCH displays the information for these hydropower plants. Figure 4-4 shows the main views for RICCH using South America and subsequently Peru as the example. The default view for RICCH (Panel A), includes all five regions delineated in the world map. The color coding represents the total installed capacity (MW) included in each region. When the user clicks on the region, the tools zooms into a country level view (Panel B). Then, the user can click on the desired country and the tool now zooms in to reveal the power plants in the country that correspond to the different administrative units (Panel C). For all panels, the color coding of the regions, countries, and administrative units correspond to the installed capacity (MW). Once the power plants are visible, users can then select any of them and the usable capacity curves appear. We base the size of the circles on the installed capacity of the power plant. The default average usable capacity curve displayed is for the ACCESS1_0 GCM. Figure 4-4 shows the aggregated results for all power plants in Peru using the ACCESS1_0 GCM simulation results.

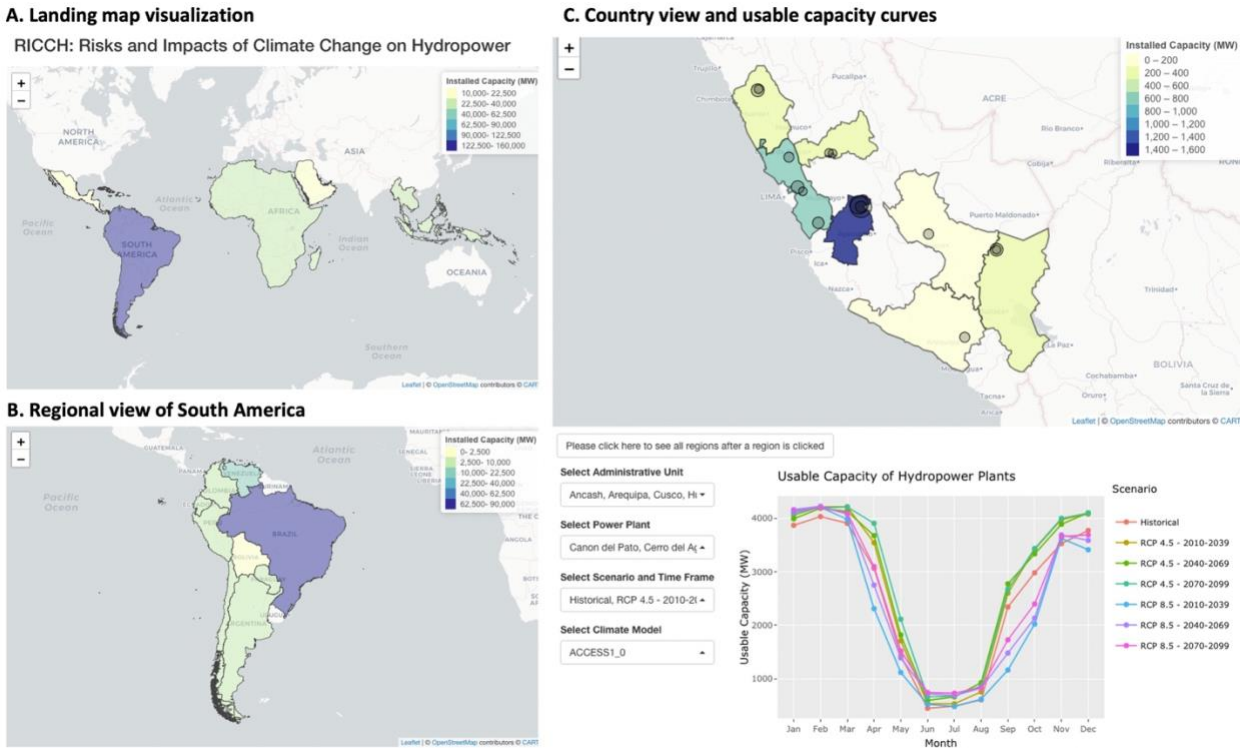

Figure 4-4 – Screenshot of RICCH visualization interface. Users can select a region, country, and power plant to display usable capacity curves for every combination of power plants, GCMs, time-frames, and scenarios. Panel A shows the landing visualization, which includes the five regions in RICCH. The color-coding of the regions represents their total installed capacity (MW). Panel B shows an example of the visualization for the South America region. Again, the color-coding represents the installed capacity (MW) of each country. Finally, Panel C presents the full view of an example country, Peru, and the monthly usable capacity (MW) curves for a subset of administrative units, power plants, scenarios, and time- frames, and one climate model. The color-coding in the map of the administrative units corresponds to the installed capacity (MW) of the power plants included in the unit.

In Figure 4-5, we present the views of the multiple drop-down lists included in RICCH. Users can choose an Administrative Unit, followed by a power plant, a scenario and time frame, and a GCM (climate model). Users can also zoom back out to the country or region level by clicking on a button. Furthermore, when users select more than one GCM, the plot shows the minimum and maximum values of the GCM ensemble. When all GCMs are selected, users can observe the multi-model ensemble mean and their full spread as bands (Figure 4-6). The last functionality of RICCH is the ability to export the results either as an image (.png) or a Comma Separated Values file (.csv). At the top of the Usable Capacity curves, users can click on six different buttons. Two allow exporting the results in the mentioned formats, and the other four allow for zooming in, zooming out, autoscaling the content, and resetting the axis for the plots.

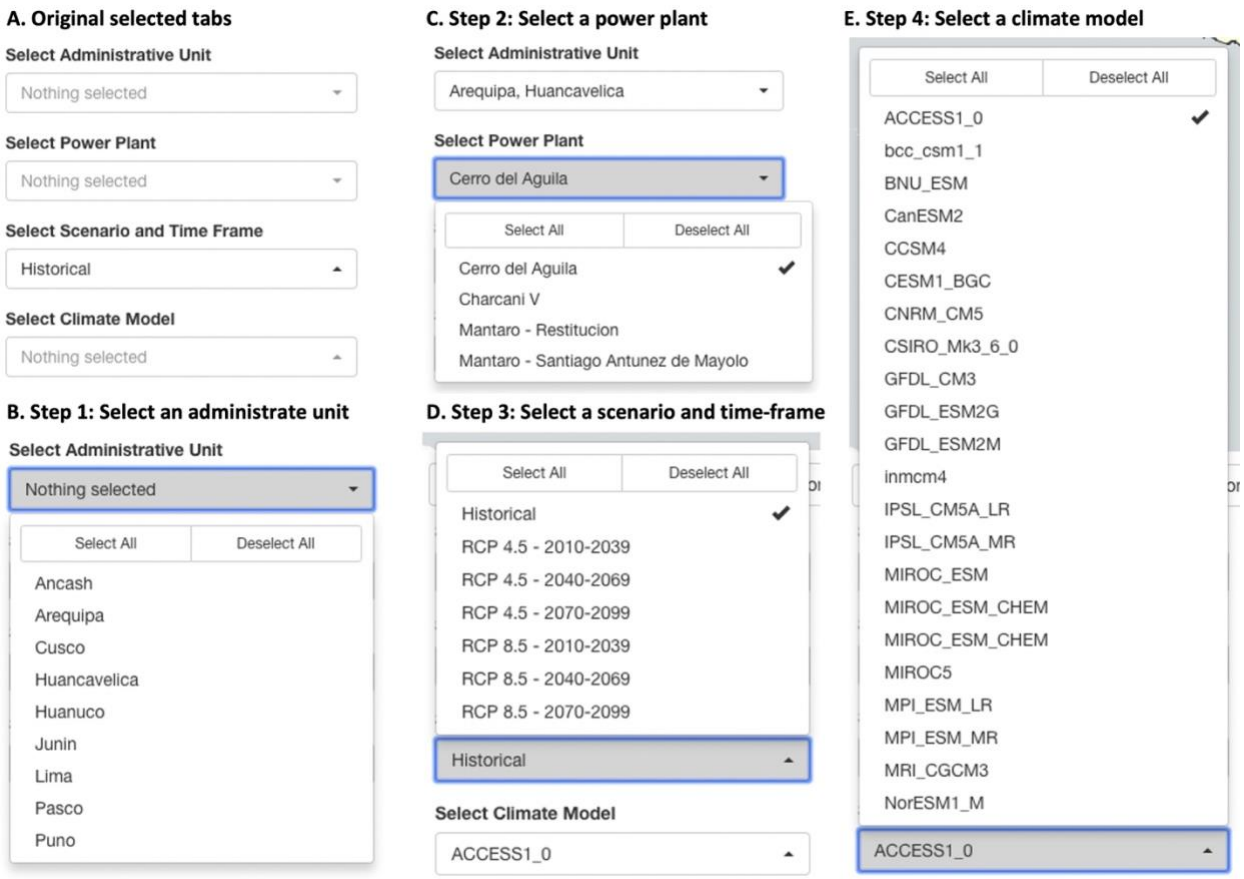

Figure 4-5 – Screenshot of drop-down selections for RICCH. Users can select multiple power plants, scenarios, and climate models in different regions in a country to display average usable capacity curves. Panel A shows the original tabs with no default selections. Panel B shows the options when selecting an administrative unit. This subset will be dependent on the country the user selects. Panel C presents the list of power plants available based on the selection of administrative units. Panel D shows all possible scenarios and time-frames users can select. Finally, Panel D shows the full ensemble of the 21 GCMs users can select. If all options are selected, the multi-model ensemble mean will be plotted.

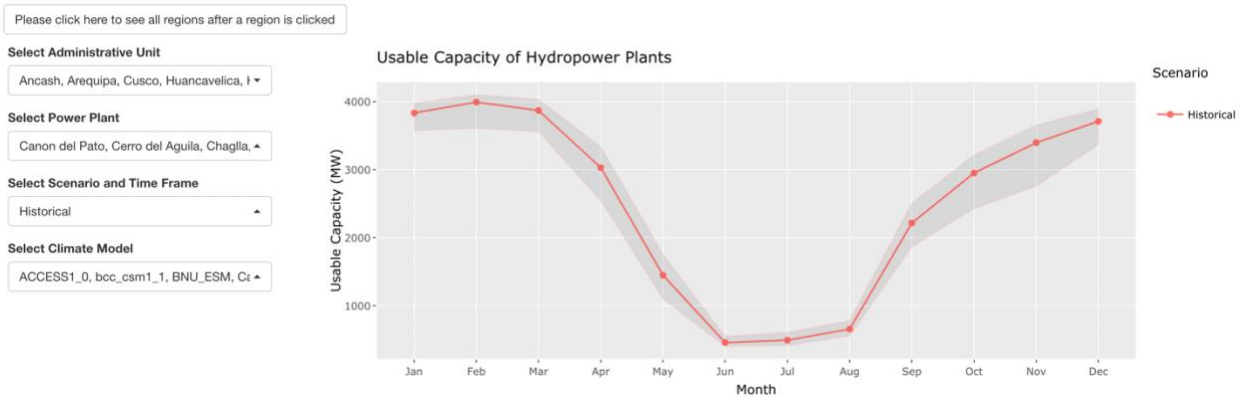

Figure 4-6 – Multi-model ensemble Usable Capacity Plots. When users select multiple climate models, the display shows the multi-model spread. Users can observe the ensemble mean and the spread of the selection of climate models (minimum and maximum values for usable capacity). Multiple selections of models, scenarios, and time-frames are possible.

4.4 Results and discussion

4.4.1 RICCH Interactive Interface

This study develops RICCH, an interactive tool for displaying climate impacts on hydropower plants in the Global South. RICCH allows users to explore the changes in usable hydropower capacity for 542 hydropower plants across 56 countries and five regions. Users can select a specific region in the Global South, followed by a country, an administrative unit, and a power plant. Users can also choose multiple power plants within a country and region to assess the aggregated monthly usable capacity curves for every GCM in the ensemble. RICCH allows for the combination of power plants, GCMs simulations, and time-frames. Our tool aims to effectively convey climate impacts on usable hydropower capacity across the Global South.

To our knowledge, there is no existing tool publicly available that displays the impacts on hydropower usable capacity for all medium to large hydropower plants in the Global South (> 40 MW). Furthermore, RICCH is the first to include a global database of usable hydropower capacity using a multi-model ensemble and two emissions scenarios consistent across all hydropower plants. Additionally, we present a complementary database, previously referred to as the “Hydropower Plants Database,” that includes the key characteristics of the hydropower

plants in RICCH. We publish the base code for RICCH and the water balance and hydropower operations model in GitHub (https://github.com/acaceres93/RICCH). Users can also find the time series of usable hydropower capacity for every hydropower plant in our Zenodo repository (https://doi.org/10.5281/zenodo.5714446).

Decision-makers can use the information we present to inform future climate change adaptation of the hydropower and electricity sectors in their corresponding countries and regions. Our usable capacity curves are meant to be used as a guideline for future hydropower availability and to be complemented with more extensive studies. Figure 4-7 presents a summary of the results included in RICCH. We present the mean normalized changes in usable capacity at the country level for every country analyzed. We can see that climate change's effects on usable hydropower capacity are larger by the end of the century and under a higher emissions scenario (RCP 8.5).

Additionally, we can see the differences in the distribution of impacts, with potential increases in some countries (e.g., Ethiopia) and decreases in others (e.g., Argentina). With this information, decision-makers and stakeholders can identify critical regions, countries, and power plants under different scenarios and GCMs. For hydropower plants experiencing increases in usable capacity, potential flooding studies could be suggested. On the other hand, alternative energy sources could be explored for hydropower plants and countries experiencing decreases. Additionally, our results can be used in conjunction to examine future synergies between hydropower and other renewable energy sources (e.g., complementary analysis).

Figure 4-7 – Mean relative changes in annual normalized usable capacity for RCP 4.5 and RCP 8.5. Panels show the differences in percentage points for each country between the historical reference (1970 – 2005) and the near future (2010 – 2039), the mid-century (2040 – 2069), and the end-of-the-century (2070 – 2099). The intensity of the color shows the direction of the change (blue increases and red decreases). Supplementary Table D-1 presents each country's total installed capacity. Supplementary Figures D-1 through D-4 show the mean changes at the power plant level for Central America and Mexico, South America, Africa and the Middle East, and Southeast Asia and the Pacific, respectively.

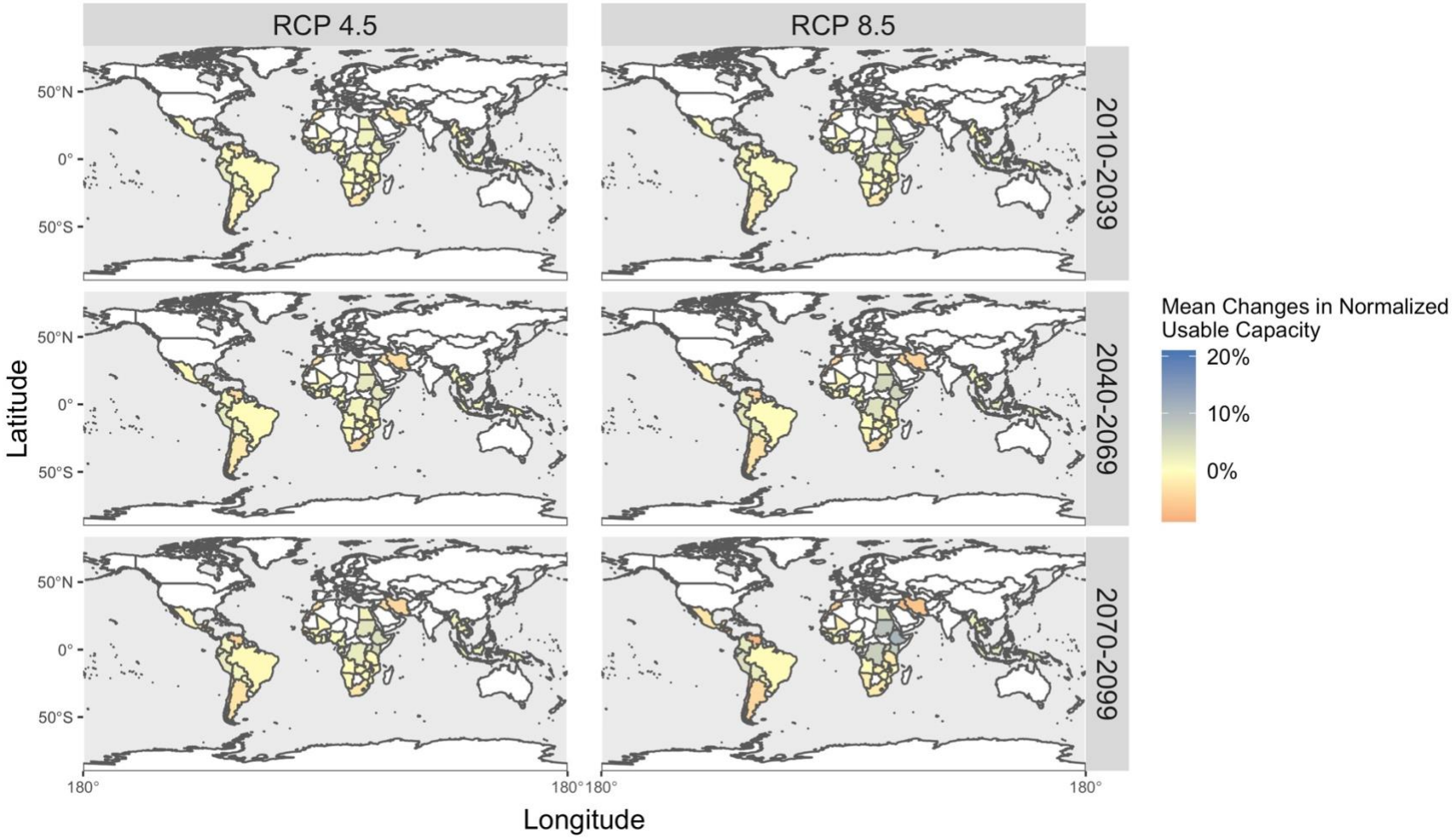

4.4.2 Future directions

One of the future directions for RICCH is to complement existing databases and tools such as the World Resources Institute Aqueduct Water Risk Atlas[185,249] and GRanD[231]. Incorporating the results of RICCH into these databases and tools can improve the way electricity sector planners incorporate climate change into their planning processes. Users should be able to input data from other databases and hydrological models and visualize and compare the results to the baseline RICCH simulations. Additionally, we have not yet tested the current version of RICCH with potential users. One of the missing components for climate adaptation communications is user engagement. Therefore, the following step for RICCH would be to involve potential users to improve the tool. Conducting surveys and working together with stakeholders would be a key component for this phase. Getting feedback from stakeholders and decision-makers can improve the way we convey the information to them and the effectiveness of the communication of climate change impacts on hydropower plants. Future versions of RICCH can incorporate these features, and constant feedback is welcome for the improvement of the tool.

4.5 Conclusions

There is no existing global hydropower climate impact interactive tool publicly available. RICCH aims to fill this gap and provide users with multiple scales of usable hydropower capacity under a consistent multi-model ensemble of 21 GCMs and two emissions scenarios. Conducting and communicating the results of these analyses using consistent datasets can help inform future country-level and regional planning. RICCH aims to become a guideline for future climate adaptation planning for decision-makers and stakeholders in the electricity sector. Additionally, users should complement the results presented in RICCH with further studies that would increase the future resilience of the hydropower sector in a changing climate. In this study, we developed a climate impact assessment database, followed by an interactive, open-sourced user interface to communicate the impacts of climate change on hydropower plants in the Global South. Users worldwide can access the tool and the source code for customization and adapt it to meet their needs better. RICCH aims to provide a first step towards an adaptive future for hydropower plants across the Global South.

Chapter 5 – Conclusions and Contributions

5.1 Summary and Conclusions

Currently, a third of worldwide greenhouse gas emissions (GHG) comes from electricity generation around the world[1]. The power sector is one of the most significant contributors to increasing GHG atmospheric concentrations. At the same time, more than 800 million people worldwide still lack access to modern electricity services[5]. Furthermore, global electricity demand is expected to continue to increase over the following decades, and there is a pressing need to decrease the carbon intensity of its sources[215]. Therefore, to achieve the UN's Sustainable Development Goal 7 of universal electricity access, emerging economies in the Global South will need to expand their electricity infrastructure while cutting emissions, and at the same time, adapting to some of the potentially detrimental impacts of climate change[6,215,216]. Hydropower can be a crucial player in the electrification of the Global South. Hydropower is the largest renewable source of electricity worldwide, and it will continue to play an essential role in the electricity sector's expansion in the Global South and decarbonization[8,217,218]. Unfortunately, climate change can threaten the viability of future hydropower development. Climate change could alter the timing and magnitude of precipitation which directly influences water availability and streamflow. Rising temperatures could increase evapotranspiration within basins, reducing the expected water volumes available and directly affecting power plant operations[11].

The objectives of this thesis were to fill in the gap on regional climate impact assessments of hydropower resources in the Global South by characterizing the impacts of climate change on usable hydropower capacity and developing visualization and analysis tools to improve the effectiveness of climate impacts communications to stakeholders and policymakers. I achieved these objectives by reviewing the current literature on hydrology and hydropower generation, developing a hydropower assessment model, conducting climate impact studies for existing hydropower plants in the Global South, and creating an interactive analysis tool for displaying the results of the mentioned studies.

Chapter 2 introduced a water balance model coupled with a hydropower operations model to assess usable hydropower capacity at the power plant level for data-scarce regions of the Global South. Further, I assessed future hydropower usable capacity under two emissions scenarios and a

multi-model ensemble of 134 hydropower plants in Brazil, Colombia, and Peru. The study used remotely sensed datasets and climate projections from NASA's NEX-GDDP dataset and coupled the mentioned water balance hydrological model with a hydropower operations model. My results suggest potential changes in usable capacity for all three hydropower systems: Brazil, Colombia, and Peru. Overall, I saw a potential increase in usable capacity due to increased water flow under both emissions scenarios (RCP 4.5 and 8.5) studied. Such increases could positively affect the Colombian SIN and the Peruvian SEIN. For the Brazilian SIN, the changes depend on the region studied. The increases in usable capacity for hydropower plants, particularly during low generation periods such as the dry season, could reduce the need for new capacity, which increasingly comes from thermoelectric power plants in the Global South[67,148,149]. I also found that increases in streamflow could not always translate to increases in usable capacity. Large increases during the rainy seasons could also have negative implications for the hydropower plants and the electricity systems. Increases beyond the power plant's design characteristics could pose risks of flooding and downstream landslides, as well as potential structural damage to the power plant. In the case of Peru, the low storage capabilities of its hydropower plants make the country particularly vulnerable to these increases. Flood management through the addition of reservoirs could be beneficial. However, reservoirs can be costly and have negative externalities such as increased biogenic methane emissions[150–152]. The results presented in this chapter could help decision-makers and electricity operators in these countries start planning the adaptation of their hydropower sectors to a changing climate. Furthermore, the model I developed and described in this chapter can be applied to other countries and continents worldwide and further be used as a screening tool to inform siting decisions of new hydropower projects.

With the model developed in Chapter 2 and keeping in mind the gap in the literature on regional impact assessments for the Global South, Chapter 3 concentrated on the African hydropower sector. This chapter looks at 87 hydropower plants across all five African power pools. It explores the differences in usable hydropower capacity using the same climate projections dataset from Chapter 2 (NASA's NEX-GDDP) and the two emissions scenarios (RCP 4.5 and 8.5). I found a potential for dryer conditions in the SAPP, the WAPP, and the COMELEC (Morocco). For the EAPP, I saw potential increases in usable capacity for all months and for the CAPP mixed results, with some potential increases driven by the Inga II power plant in the DRC. Further, I found that the wetter conditions in some areas of Africa could help

balance the drying in others. In the second part of this chapter, I explored the changes in two variability metrics: interannual and seasonal variability at the country and power pool levels. I found that the interannual and seasonal variabilities of usable hydropower capacity were likely to increase for more than half the countries in the study. For the most part, the results showed higher variability at the country level than when aggregated to the power pool level. These results reinforce the case for the interconnection of the African power pools. In the final section of this chapter, I explored the potential interconnections of power pools using a complementarity assessment and generated seven interconnection scenarios. The results confirm that the interconnection of the African power pools, based on their hydropower resources alone, could benefit the most variable resources and mitigate the potential decreases in usable capacity resulting from a changing climate. At the same time, interconnection could decrease the variability of hydropower resources making it more attractive as a baseload source of electricity. Balancing hydropower resources through electricity trading could improve the reliability of African electricity generation[171,178]. I suggest there is an opportunity for future synergies in Africa based on their hydropower resources. Interconnections coupled with the still sizeable untapped hydropower potential[192] could help achieve the continent's electrification goals while adapting to climate change impacts.

Finally, Chapter 4 aimed to synthesize and expand the research done in Chapters 2 and 3. RICCH collected the results from the impact assessments performed for Chapters 2 and 3 and further expanded the analysis to include a total of 542 hydropower plants across the Global South. In this chapter, I developed an interactive analysis tool to display the changes in the usable capacity of hydropower plants under a multi-model ensemble of 21 GCMs and two emissions scenarios (RCP 4.5 and 8.5) for 56 countries in five regions of the Global South. RICCH allows users to select specific regions, countries, administrative units, and power plants. Users can combine power plants, GCMs simulations, and time-frames and display the results accordingly. This tool aims to be a first step to effectively convey climate impacts on usable hydropower capacity across the Global South. In this chapter, I also developed a global database of usable hydropower capacity under a changing climate using the same hydrological model coupled with the hydropower operations model first presented in Chapter 2. Additionally, I compiled a database of the 542 hydropower plants presented in RICCH, including their design characteristics and geographic locations. For the power plants included in RICCH, I found that

the effects of climate change, whether increases or decreases, on usable hydropower capacity, are consistently larger for the individual countries by the end of the century under a higher emissions scenario (RCP 8.5). Additionally, I observed differences in the distribution of changes in usable capacity, with some countries showing increases (e.g., Ethiopia) and others showing decreases (e.g., Argentina). The information presented decision-makers and stakeholders could identify critical regions, countries, and power plants under a large ensemble of climate models. RICCH could inform future climate change adaptation of the hydropower electricity sectors across these five regions. These results could also be used in conjunction with other studies, such as capacity expansion models, to examine future energy mixes with other sources of electricity.

In conclusion, I conducted numerous climate impact assessments for the hydropower sector across the Global South over the previous three chapters. These studies furthered the understanding of how climate change could impact hydropower usable capacity over a large variety of regions and continents. All the products from this dissertation, listed in the following section, including the model, results, datasets, code, and tool, are meant to improve the understanding stakeholders and policymakers have of the effect of climate change on hydropower generation and help inform the future adaptation and resilience of the sector.

5.2 Research and Data Contributions

This dissertation aimed to characterize and understand how climate change can impact usable hydropower capacity in the Global South. The following publications, including open-sourced datasets, are products of the research and methods used in this dissertation. Please make sure to cite the datasets appropriately when used.

- Chapter 2: *"Hydropower under climate uncertainty: Characterizing the usable capacity of Brazilian, Colombian and Peruvian power plants under climate scenarios"*
    - Journal Publication: Caceres, A. L., Jaramillo, P., Matthews, H. S., Samaras, C. & Nijssen, B. (2021) "Hydropower under climate uncertainty: Characterizing the usable capacity of Brazilian, Colombian and Peruvian power plants under climate scenarios," *Energy for Sustainable Development, **61:** 217-229.* (https://doi.org/10.1016/j.esd.2021.02.006)

- Dataset: Caceres, A. L., Jaramillo, P., Matthews, H. S., Samaras, C. & Nijssen, B. Climate Forced Hydropower Simulations Using NASA NEX-GDDP. https://doi.org/10.5281/zenodo.4009505 (2020).

- Chapter 3: "*Mitigating climate-induced risks and increasing resilience of hydropower systems in Africa"*
  - Journal Publication (under review in Nature Climate Change): Caceres, A. L., Jaramillo, P., Matthews, H. S., Samaras, C. & Nijssen, B. (2022) *"Mitigating climate-induced risks and increasing resilience of hydropower systems in Africa."*
  - Dataset: Cáceres, A. L., Jaramillo, P., Matthews, H. S., Samaras, C. & Nijssen, B. Climate Forced Hydropower Simulations for the African Continent Using NASA NEX GDDP. https://doi.org/10.5281/zenodo.5020878 (2021).
- Chapter 4: *"RICCH: An Interactive Analysis Tool for Risk and Impacts of Climate Change on Hydropower Plants in the Global South"*
  - Journal Publication (to be submitted after defense to Environmental Modelling and Software): Caceres, A. L., Jaramillo, P., Matthews, H. S., Samaras, C., Huang, L. & Nijssen, B. (2022) "*RICCH: An Interactive Analysis Tool for Risk and Impacts of Climate Change on Hydropower Plants in the Global South."*
  - Dataset: Cáceres, A. L., Jaramillo, P., Matthews, H. S., Samaras, C. & Nijssen, B. RICCH: An Interactive Analysis Tool for Risk and Impacts of Climate Change on Hydropower Database. https://doi.org/10.5281/zenodo.5714446 (2022).
  - Code: Cáceres, A. L., Jaramillo, P., Matthews, H. S., Samaras, C. & Nijssen, B. RICCH. https://github.com/acaceres93/RICCH.git (2021).
  - Software: Cáceres, A. L. *et al.* RICCH: Risks and Impacts of Climate Change on Hydropower. *v1.0* https://ricch.shinyapps.io/hydro-shiny/ (2021).

Outside the work of the dissertation, there was a collaboration with the Rwanda Energy Group (REG). I assessed the impacts of climate change on usable hydropower capacity in Rwanda, which was published by Rebecca Mutesi in REG's Least Cost Power Development Plan[250] for the country.

5.3 Recommendations for Future Work

5.3.1 Updating Hydropower Usable Capacity Simulations with CMIP6 Projection Runs

In Chapters 2 through 4, I used CMIP5 Projection Runs from NASA's NEX-GDDP dataset[55]. This dataset was the only consistently downscaled dataset for the whole world when I conducted the studies presented in this dissertation. For a matter of consistency, I used the same dataset for all three main chapters of the dissertation (Chapters 2 – 4). On December 21st, 2021, NASA published a new update to the dataset. The current version of the NEX-GDDP dataset now includes CMIP6 runs[59]. These simulations constitute the latest climate science and are part of Working Group 1's contribution to IPCC's Assessment Report 6[49]. The NEX-GDDP CMIP6 dataset includes two Shared Socioeconomic Pathways (SSPs) simulations that correspond to the radiative forcing of RCP 4.5 and 8.5 like in the previous CMIP5 version. The SSPs included are: SSP5 (fossil fuel development) with a radiative forcing of 8.5 W/m^2 corresponding to the radiative forcing in RCP 8.5 and SSP2 (middle of the road) with a radiative forcing of 4.5 W/m^2 corresponding to the radiative forcing in RCP 4.5. Furthermore, this dataset includes more climatic variables to force the water balance and stop using historical averages than the previous dataset, which only had precipitation, maximum near-surface temperature, and minimum near-surface temperature. All the variables included in the new CMIP6 version are: near-surface relative humidity percentage (hurs – %), near-surface specific humidity dimensionless ratio (huss – kg/kg), precipitation (pr – kg/m^2s^1), surface dowelling longwave radiation (rlds – W/m^2), surface downwelling shortwave radiation (rsds – W/m^2), daily-mean near-surface wind speed (sfcWind – m/s), daily near-surface air temperature (tas – Degrees Kelvin), daily maximum near-surface air temperature (tasmax – Degrees Kelvin), and daily minimum near-surface air temperature (tasmin – Degrees Kelvin). Future research could re-run the simulations used to inform the results and datasets presented in this dissertation and compare the differences in the results with the latest climate science.

5.3.2 Using Hydropower Usable Capacity Simulations for Capacity Expansion Modelling of the African Continent and the Global South

The results and datasets produced in Chapter 3 can inform capacity expansion modeling and planning. While Chapter 3, and the entirety of this thesis, focused only on hydropower resources, other energy sources will likely play an essential role in the electrification of the Global South and the transition to a low-carbon electricity sector. For Chapter 3 specifically, the research analyzed current installed capacity in Africa. These results can be used in conjunction with capacity expansion models to evaluate the future deployment of electricity sources in Africa under multiple climate conditions and constraints. While our analysis was limited to understanding how hydropower reliability could benefit from pooled hydropower resources, modeling other energy resources in Africa is important for electricity planners. Modeling multiple energy sources for the whole continent will be challenging, and it can be part of future dissertations. Conducting realistic capacity expansion models for Africa will require building specific databases for supply options (renewables and non-renewable supply curves), power generation technologies (performance and costs), end-use technologies (performance and costs), and end-use demands (across all end-use sector) specific for each country in the continent. The datasets produced in Chapter 3 can serve as inputs for capacity expansion models, complemented, as previously mentioned, by other databases that include other energy sources. The same applies to other regions of the Global South presented in this dissertation.

5.3.3 Include Temperature and Precipitation from GCMs to RICCH Online Interface and Implement New Query Capabilities

The current version of RICCH presented in Chapter 4 includes only hydropower usable capacity for the 542 power plants in the database. Future work could incorporate other climatic variables such as precipitation and temperature from the multi-model ensemble presented in the current version. Users could then find relationships between changes in these variables and how they relate to usable hydropower capacity. Furthermore, this includes possibly implementing new query capabilities. For example, in the current version of RICCH, users select climate models and RCPs to visualize the subset of usable hydropower capacity for the power plant(s) selected. The new query feature could allow the user to choose a period mean change (Δ) in temperature,

for example (e.g., between 2°C and 4°C) and a precipitation increase and see the range of possible hydropower usable capacity. Future research could implement these features and others to improve the user experience.

5.3.4 Further Documentation of RICCH Database and Publishing R-Shiny Dashboard Code

The current version of the RICCH Database (https://doi.org/10.5281/zenodo.5714446) is a preliminary version. At the moment, this database does lacks proper data description and documentation files. After the defense, I will be working to build the complete documentation of the database, including all references, and add a "Data Description" file to the repository. Additionally, I will be including a second file with only the main characteristics of the power plants. This will exclude the time series of usable capacity which are part of the current published version of the database. Based on other suggested work other variables can be added to the repository for the final version. Therefore, the final version of the database will include multiple files with the power plant characteristics, the usable hydropower capacity time series, and any other relevant variables for the power plants and countries.

In addition to the RICCH Database, after the defense I will be working to publish the R-Shiny Dashboard code and its underlying data. The code and data will be published using CMU's Kilthub repository. Kilthub has the option to allow for the repository to remain as part of the department after I leave CMU which would ensure the continuation of the work. I will publish the code using this service after the defense and it will remain as part of the Engineering and Public Policy Department repository.

5.3.5 Run Variability Metrics for RICCH Hydropower Plants and Incorporate Them into RICCH's Online Interface at Multiple Geographic Scales

Other features to incorporate to RICCH include variability metrics such as those included in Chapter 3 for the African continent. As previously mentioned, the current version of RICCH only presents usable hydropower capacity. Future work could run seasonal variability and interannual variability metrics, like the ones used in Chapter 3, for all the time series included in

Chapter 4 Zenodo repository[213]. These metrics could be incorporated into the user interface as another layer of variables, same as the precipitation and temperature mentioned in 5.3.3. Currently, we only have these metrics for the African continent and the country-level results. Ideally, I could add results at multiple geographic to RICCH. Adding these results requires calculating the metrics at the power plant, country, and in some cases, such as the African continent, power pool, and potentially region of the Global South. New features to allow the user to explore these multiple geographic scales for the variability metrics could display in conjunction the hydropower usable capacity results for the same scales. This information could then be presented to potential users and stakeholders to improve the usefulness of RICCH and its applications (see 5.3.5).

5.3.6 User Engagement for RICCH

One of the missing components when developing tools for climate adaptation communications is user engagement. Therefore, future work could involve potential users and stakeholders to conduct surveys. The first task would be to identify potential stakeholders, which could be done through snowball sampling[251]. Then, surveys to get feedback on RICCH could be designed. Finally, the surveys could be conducted, and the feedback could improve the tool. The objective is to improve the communication of climate change impacts on usable hydropower capacity. Ideally, future researchers could present to potential users' different options for the GUI, the reports, and the interactive visualizations RICCH might have. With this, a new version of RICCH could be created. This work could be done under the guidance of experts and work to achieve better science communication of adaptation measures under climate change.

Chapter 6 – References

1. World Resources Institute. Historical GHG Emissions. *ClimateWatch* https://www.climatewatchdata.org/ghg-emissions?breakBy=sector&filter=380%2C378%2C404%2C405%2C381%2C398&source=33&version=1 (2018).
2. Stocker, T. F. *et al. Global warming of 1.5°C. Report of the Intergovernmental Panel on Climate Change* (2018) doi:10.1017/CBO9781107415324.
3. IPCC. Climate Change 2014 Synthesis Report Summary Chapter for Policymakers. *IPCC* 31 (2014) doi:10.1017/CBO9781107415324.
4. OECD/IEA. *Global Energy & CO2 Status Report 2019*. *Global Energy & CO2 Status Report* (2019).
5. International Energy Agency. *SDG7: Data and Projections*. (2019).
6. United Nations. Sustainable Development Goals. *United Nations* https://sustainabledevelopment.un.org/?menu=1300 (2015).
7. Allen, M. *et al.* Chapter 1 — Global Warming of 1.5 ºC. *IPCC* (2019).
8. IEA. Hydropower. https://www.iea.org/fuels-and-technologies/hydropower (2019).
9. International Energy Agency. *Hydropower Special Market Report: Analysis and forecast to 2030*. https://www.iea.org/reports/hydropower-special-market-report (2021).
10. Hoes, O. A. C., Meijer, L. J. J., van der Ent, R. J. & van de Giesen, N. C. Systematic high-resolution assessment of global hydropower potential. *PLOS ONE* **12**, e0171844 (2017).
11. Bradley, R. S., Vuille, M., Diaz, H. F. & Vergara, W. CLIMATE CHANGE: Threats to Water Supplies in the Tropical Andes. *Science* **312**, 1755–1756 (2006).
12. van Vliet, M. T. H., Wiberg, D., Leduc, S. & Riahi, K. Power-generation system vulnerability and adaptation to changes in climate and water resources. *Nature Climate Change* **6**, 375–380 (2016).
13. van Vliet, M. T. H. *et al.* Vulnerability of US and European electricity supply to climate change. *Nature Climate Change* **2**, 676–681 (2012).

14. van Vliet, M. T. H. *et al.* Multi-model assessment of global hydropower and cooling water discharge potential under climate change. *Global Environmental Change* **40**, 156–170 (2016).
15. Bartos, M. D. & Chester, M. V. Impacts of climate change on electric power supply in the Western United States. *Nature Climate Change* **5**, 748–752 (2015).
16. Vicuna, S., Leonardson, R., Hanemann, M. W., Dale, L. L. & Dracup, J. A. Climate change impacts on high elevation hydropower generation in California's Sierra Nevada: a case study in the Upper American River. *Climatic Change* **87**, 123–137 (2008).
17. Vicuña, S., Dracup, J. A. & Dale, L. Climate change impacts on two high-elevation hydropower systems in California. *Climatic Change* **109**, 151–169 (2011).
18. Voisin, N. *et al.* Vulnerability of the US western electric grid to hydro-climatological conditions: How bad can it get? *Energy* **115**, 1–12 (2016).
19. Kao, S.-C. *et al.* Projecting changes in annual hydropower generation using regional runoff data: An assessment of the United States federal hydropower plants. *Energy* **80**, 239–250 (2015).
20. Tarroja, B., AghaKouchak, A. & Samuelsen, S. Quantifying climate change impacts on hydropower generation and implications on electric grid greenhouse gas emissions and operation. *Energy* **111**, 295–305 (2016).
21. Liang, X., Lettenmaier, D. P., Wood, E. F. & Burges, S. J. A simple hydrologically based model of land surface water and energy fluxes for general circulation models. *Journal of Geophysical Research* (1994) doi:10.1029/94JD00483.
22. Lehner, B., Czisch, G. & Vassolo, S. The impact of global change on the hydropower potential of Europe: a model-based analysis. *Energy Policy* **33**, 839–855 (2005).
23. Schaefli, B., Hingray, B. & Musy, A. Climate change and hydropower production in the Swiss Alps: quantification of potential impacts and related modelling uncertainties. *Hydrology and Earth System Sciences* **11**, 1191–1205 (2007).
24. Maran, S., Volonterio, M. & Gaudard, L. Climate change impacts on hydropower in an alpine catchment. *Environmental Science & Policy* **43**, 15–25 (2014).

25. Turner, S. W. D., Hejazi, M., Kim, S. H., Clarke, L. & Edmonds, J. Climate impacts on hydropower and consequences for global electricity supply investment needs. *Energy* **141**, 2081–2090 (2017).
26. Oyerinde, G. *et al.* Quantifying Uncertainties in Modeling Climate Change Impacts on Hydropower Production. *Climate* **4**, 34 (2016).
27. Chilkoti, V., Bolisetti, T. & Balachandar, R. Climate change impact assessment on hydropower generation using multi-model climate ensemble. *Renewable Energy* **109**, 510–517 (2017).
28. Ganguli, P., Kumar, D. & Ganguly, A. R. US Power Production at Risk from Water Stress in a Changing Climate. *Scientific Reports* **7**, 11983 (2017).
29. Gaudard, L., Avanzi, F. & De Michele, C. Seasonal aspects of the energy-water nexus: The case of a run-of-the-river hydropower plant. *Applied Energy* **210**, 604–612 (2018).
30. Cronin, J., Anandarajah, G. & Dessens, O. Climate change impacts on the energy system: a review of trends and gaps. *Climatic Change* **151**, 79–93 (2018).
31. Solaun, K. & Cerdá, E. Climate change impacts on renewable energy generation. A review of quantitative projections. *Renewable and Sustainable Energy Reviews* **116**, 109415 (2019).
32. Kaser, G., Grosshauser, M. & Marzeion, B. Contribution potential of glaciers to water availability in different climate regimes. *Proceedings of the National Academy of Sciences* **107**, 20223–20227 (2010).
33. Schaner, N., Voisin, N., Nijssen, B. & Lettenmaier, D. P. The contribution of glacier melt to streamflow. *Environmental Research Letters* **7**, 034029 (2012).
34. Huss, M. & Hock, R. Global-scale hydrological response to future glacier mass loss. *Nature Climate Change* **8**, 135–140 (2018).
35. Baraer, M. *et al.* Glacier recession and water resources in Peru's Cordillera Blanca. *Journal of Glaciology* **58**, 134–150 (2012).
36. Engelhardt, M., Schuler, T. V. & Andreassen, L. M. Contribution of snow and glacier melt to discharge for highly glacierised catchments in Norway. *Hydrology and Earth System Sciences Discussions* **10**, 11485–11517 (2013).

37. Mark, B. G. *et al.* Glacier loss and hydro-social risks in the Peruvian Andes. *Global and Planetary Change* **159**, 61–76 (2017).
38. Van Tiel, M. *et al.* The role of glacier changes and threshold definition in the characterisation of future streamflow droughts in glacierised catchments. *Hydrology and Earth System Sciences* **22**, 463–485 (2018).
39. Vuille, M. *et al.* Rapid decline of snow and ice in the tropical Andes – Impacts, uncertainties and challenges ahead. *Earth-Science Reviews* **176**, 195–213 (2018).
40. Mark, B. G. Hot ice: glaciers in the tropics are making the press. Tropical glaciers. International Hydrology Series by Georg Kaser and Henry Osmaston (Eds.) Cambridge University Press, UNESCO, Cambridge, UK, 207 pp ISBN 0-521-6333-8 (hardcover) Published 2002. *Hydrological Processes* **16**, 3297–3302 (2002).
41. Mark, B. G. & Seltzer, G. O. Evaluation of recent glacier recession in the Cordillera Blanca, Peru (AD 1962–1999): spatial distribution of mass loss and climatic forcing. *Quaternary Science Reviews* **24**, 2265–2280 (2005).
42. Mark, B. G. & Seltzer, G. O. Tropical glacier meltwater contribution to stream discharge: a case study in the Cordillera Blanca, Peru. *Journal of Glaciology* **49**, 271–281 (2003).
43. Racoviteanu, A. E., Arnaud, Y., Williams, M. W. & Ordoñez, J. Decadal changes in glacier parameters in the Cordillera Blanca, Peru, derived from remote sensing. *Journal of Glaciology* **54**, 499–510 (2008).
44. SENAMHI Perú. *Evolución de la cobertura glaciar de las cuencas Chillón, Rímac, Lurín y parte alta del Mantaro*. (2015).
45. Kaser, G. A review of the modern fluctuations of tropical glaciers. *Global and Planetary Change* **22**, 93–103 (1999).
46. Rabatel, A. *et al.* Current state of glaciers in the tropical Andes: a multi-century perspective on glacier evolution and climate change. *The Cryosphere* **7**, 81–102 (2013).
47. Buytaert, W. *et al.* Glacial melt content of water use in the tropical Andes. *Environmental Research Letters* **12**, 114014 (2017).

48. Schwartz, M., Hall, A., Sun, F., Walton, D. & Berg, N. Significant and inevitable end-of-21 st -century advances in surface runoff timing in California's Sierra Nevada. *Journal of Hydrometeorology* JHM-D-16-0257.1 (2017) doi:10.1175/JHM-D-16-0257.1.
49. IPCC *et al. Climate Change 2021: The Physical Science Basis. Contribution of Working Group I to the Sixth Assessment Report of the Intergovernmental Panel on Climate Change*. *Cambridge University Press* https://www.ipcc.ch/report/ar6/wg1/#FullReport (2021).
50. IPCC. IPCC: Climate Change 2021: The Physical Science Basis (Summary for Policymakers). *Cambridge University Press. In Press.* **Sixth Asse**, (2021).
51. Kotamarthi, R., Mearns, L., Hayhoe, K., Castro, C. L. & Wuebbles, D. *Use of Climate Information for Decision-Making and Impacts Research: State of Understanding*. (2016).
52. Mearns, L. O., Bukovsky, M. S., Pryor, S. C. & Magaña, V. Downscaling of Climate Information. in 201–250 (2014). doi:10.1007/978-3-319-03768-4_5.
53. Solman, S. A. Regional Climate Modeling over South America: A Review. *Advances in Meteorology* **2013**, 1–13 (2013).
54. CCAFS, CIAT, ILRI, I. CCAFS Climate. *GCM Downscaled Data Portal* http://ccafs-climate.org/ (2016).
55. Climate Analytics Group & NASA Ames Research Center. NEX-GDDP Dataset. (2018).
56. The CMIP6 landscape. *Nature Climate Change* **9**, 727–727 (2019).
57. World Climate Research Programme. FAQ Data and ACCESS - WCRP CORDEX. *CORDEX* https://cordex.org/faq/faq-data-and-access/ (2020).
58. van Vuuren, D. P., Edmonds, J. A., Kainuma, M., Riahi, K. & Weyant, J. A special issue on the RCPs. *Climatic Change* **109**, 1–4 (2011).
59. Thrasher, B., Wang, W., Michaelis, A. & Nemani, R. NEX-GDDP-CMIP6. (2021).
60. Schwalm, C. R., Glendon, S. & Duffy, P. B. RCP8.5 tracks cumulative CO_2 emissions. *Proceedings of the National Academy of Sciences* **117**, 19656–19657 (2020).

61. Stocker, T. F. *et al. IPCC, 2013: Summary for Policymakers. In: Climate Change 2013: The Physical Science Basis. Contribution of Working Group I to the Fifth Assessment Report of the IPCC*. *Cambridge University Press* https://www.ipcc.ch/site/assets/uploads/2018/02/WG1AR5_SPM_FINAL.pdf (2013).
62. International Hydropower Association. *2021 Hydropower Status Report*. https://assets-global.website-files.com/5f749e4b9399c80b5e421384/60c37321987070812596e26a_IHA 2021240 5-status-report-02_LR.pdf (2021).
63. International Hydropower Association. *Hydropower Status Report*. https://www.hydropower.org/sites/default/files/publications-docs/2020_hydropower_status_report.pdf (2020).
64. International Hydropower Association. *Hydropower Status Report*. https://www.hydropower.org/sites/default/files/publications-docs/2019_hydropower_status_report_0.pdf (2019).
65. International Energy Agency. *Report extract: Access to electricity*. https://www.iea.org/reports/sdg7-data-and-projections/access-to-electricity (2020).
66. The Programme for Infrastructure Development in Africa. *The PIDA Energy Vision*. https://www.afdb.org/fileadmin/uploads/afdb/Documents/Generic-Documents/PIDA brief Energy.pdf (2016).
67. Arango-Aramburo, S., Ríos-Ocampo, J. P. & Larsen, E. R. Examining the decreasing share of renewable energy amid growing thermal capacity: The case of South America. *Renewable and Sustainable Energy Reviews* **119**, 109648 (2020).
68. International Energy Agency. *Africa Energy Outlook 2019*. (2019).
69. Gernaat, D. E. H. J., Bogaart, P. W., Vuuren, D. P. van, Biemans, H. & Niessink, R. High-resolution assessment of global technical and economic hydropower potential. *Nature Energy* **2**, 821–828 (2017).
70. World Bank. Access to electricity (% of population) - Latin America & Caribbean. *The World Bank Data* https://data.worldbank.org/indicator/EG.ELC.ACCS.ZS?locations=ZJ (2021).

71. Ganguli, P., Kumar, D. & Ganguly, A. R. US Power Production at Risk from Water Stress in a Changing Climate. *Scientific Reports* **7**, 11983 (2017).
72. Roy, S. B., Summers, K. V. & Goldstein, R. A. Water Sustainability in the United States and Cooling Water Requirements for Power Generation. *Water Resources Update* (2003).
73. Caceres, A. L., Jaramillo, P., Matthews, H. S., Samaras, C. & Nijssen, B. Hydropower under climate uncertainty: Characterizing the usable capacity of Brazilian, Colombian and Peruvian power plants under climate scenarios. *Energy for Sustainable Development* **61**, 217–229 (2021).
74. Zhou, Q., Hanasaki, N., Fujimori, S., Masaki, Y. & Hijioka, Y. Economic consequences of global climate change and mitigation on future hydropower generation. *Climatic Change* **147**, 77–90 (2018).
75. Yalew, S. G. *et al.* Impacts of climate change on energy systems in global and regional scenarios. *Nature Energy* (2020) doi:10.1038/s41560-020-0664-z.
76. Carvajal, P. E., Anandarajah, G., Mulugetta, Y. & Dessens, O. Assessing uncertainty of climate change impacts on long-term hydropower generation using the CMIP5 ensemble—the case of Ecuador. *Climatic Change* **144**, 611–624 (2017).
77. Sridharan, V. *et al.* Resilience of the Eastern African electricity sector to climate driven changes in hydropower generation. *Nature Communications* **10**, 302 (2019).
78. Spalding-Fecher, R., Joyce, B. & Winkler, H. Climate change and hydropower in the Southern African Power Pool and Zambezi River Basin: System-wide impacts and policy implications. *Energy Policy* **103**, 84–97 (2017).
79. de Lucena, A. F. P. *et al.* The vulnerability of renewable energy to climate change in Brazil. *Energy Policy* **37**, 879–889 (2009).
80. de Souza Dias, V., Pereira da Luz, M., Medero, G. & Tarley Ferreira Nascimento, D. An Overview of Hydropower Reservoirs in Brazil: Current Situation, Future Perspectives and Impacts of Climate Change. *Water* **10**, 592 (2018).
81. Silva, M. V. M. da *et al.* Projections of climate change in streamflow and affluent natural energy in the Brazilian hydroelectric sector of CORDEX models. *RBRH* **25**, (2020).

82. Arias, M. E. *et al.* Impacts of climate change and deforestation on hydropower planning in the Brazilian Amazon. *Nature Sustainability* (2020) doi:10.1038/s41893-020-0492-y.
83. Mohor, G. S., Rodriguez, D. A., Tomasella, J. & Siqueira Júnior, J. L. Exploratory analyses for the assessment of climate change impacts on the energy production in an Amazon run-of-river hydropower plant. *Journal of Hydrology: Regional Studies* **4**, 41–59 (2015).
84. Lucena, A. F. P. *et al.* Interactions between climate change mitigation and adaptation: The case of hydropower in Brazil. *Energy* **164**, 1161–1177 (2018).
85. Ospina Noreña, J. E., Gay García, C., Conde, A. C. & Magaña, V. Vulnerability of water resources in the face of potential climate change: generation of hydroelectric power in Colombia. *Atmósfera* **22**, 229–252 (2009).
86. Güiza-Villa, N., Gay-García, C. & Ospina-Noreña, J. E. Effects of Climate Change on Water Resources, Indices, and Related Activities in Colombia. in *Resources of Water [Working Title]* (ed. Chandrasekaran, Dr. P. T.) (Intechopen, 2019). doi:10.5772/intechopen.90652.
87. Macías Parra, A. M. & Andrade, J. *Estudio de Generación Eléctrica bajo Escenario de Cambio Climático*. (2014).
88. CEPAL - BID. *La economía del cambio climático en el Perú*. (2014).
89. Arango-Aramburo, S. *et al.* Climate impacts on hydropower in Colombia: A multi-model assessment of power sector adaptation pathways. *Energy Policy* **128**, 179–188 (2019).
90. de Lucena, A. F. P., Schaeffer, R. & Szklo, A. S. Least-cost adaptation options for global climate change impacts on the Brazilian electric power system. *Global Environmental Change* **20**, 342–350 (2010).
91. Magaju, D., Cattapan, A. & Franca, M. Identification of run-of-river hydropower investments in data scarce regions using global data. *Energy for Sustainable Development* **58**, 30–41 (2020).
92. Schaefli, B., Manso, P., Fischer, M., Huss, M. & Farinotti, D. The role of glacier retreat for Swiss hydropower production. *Renewable Energy* **132**, 615–627 (2019).

93. Puspitarini, H. D., François, B., Zaramella, M., Brown, C. & Borga, M. The impact of glacier shrinkage on energy production from hydropower-solar complementarity in alpine river basins. *Science of The Total Environment* **719**, 137488 (2020).
94. Farinotti, D., Round, V., Huss, M., Compagno, L. & Zekollari, H. Large hydropower and water-storage potential in future glacier-free basins. *Nature* **575**, 341–344 (2019).
95. RGI Consortium. Randolph Glacier Inventory – A Dataset of Global Glacier Outlines: Version 6.0: Technical Report. 71 (2017) doi:10.7265/N5-RGI-60.
96. Abatzoglou, J. T., Dobrowski, S. Z., Parks, S. A. & Hegewisch, K. C. TerraClimate, a high-resolution global dataset of monthly climate and climatic water balance from 1958-2015. *Scientific Data* **5**, (2018).
97. Bartos, M. D. Pysheds: a fast, open-source digital elevation model processing library. (2018).
98. Daly, E., Porporato, A. & Rodriguez-Iturbe, I. Coupled Dynamics of Photosynthesis, Transpiration, and Soil Water Balance. Part I: Upscaling from Hourly to Daily Level. *Journal of Hydrometeorology* **5**, 546–558 (2004).
99. Yates, D. N. WatBal: An Integrated Water Balance Model for Climate Impact Assessment of River Basin Runoff. *International Journal of Water Resources Development* **12**, 121–140 (1996).
100. Hock, R. Temperature index melt modelling in mountain areas. *Journal of Hydrology* **282**, 104–115 (2003).
101. Grinsted, A. An estimate of global glacier volume. *The Cryosphere* **7**, 141–151 (2013).
102. Bahr, D. B., Meier, M. F. & Peckham, S. D. The physical basis of glacier volume-area scaling. *Journal of Geophysical Research: Solid Earth* **102**, 20355–20362 (1997).
103. Duan, Q. Y., Gupta, V. K. & Sorooshian, S. Shuffled complex evolution approach for effective and efficient global minimization. *Journal of Optimization Theory and Applications* **76**, 501–521 (1993).
104. Shin, M.-J. & Choi, Y. Combining an R-Based Evolutionary Algorithm and Hydrological Model for Effective Parameter Calibration. *Water* **10**, 1339 (2018).

105. Hartmann, D. L., Tank, a. M. G. K. & Rusticucci, M. *IPCC Fifth Assessment Report, Climatie Change 2013: The Physical Science Basis*. *IPCC* vol. AR5 (2013).
106. Turner, S. W. D. & Galelli, S. Water supply sensitivity to climate change: An R package for implementing reservoir storage analysis in global and regional impact studies. *Environmental Modelling & Software* **76**, 13–19 (2016).
107. Wu, X., Cheng, C., Lund, J. R., Niu, W. & Miao, S. Stochastic dynamic programming for hydropower reservoir operations with multiple local optima. *Journal of Hydrology* **564**, 712–722 (2018).
108. Feng, Z., Niu, W., Cheng, C. & Lund, J. R. Optimizing Hydropower Reservoirs Operation via an Orthogonal Progressive Optimality Algorithm. *Journal of Water Resources Planning and Management* **144**, 04018001 (2018).
109. Chegwidden, O. S. *et al.* How do modeling decisions affect the spread among hydrologic climate change projections? Exploring a large ensemble of simulations across a diversity of hydroclimates. *Earth's Future* 2018EF001047 (2019) doi:10.1029/2018EF001047.
110. International Energy Agency. Country Profile: Colombia. *The Energy Mix* https://www.iea.org/countries/Colombia (2020).
111. International Energy Agency. Peru. *Country Profile* https://www.iea.org/countries/peru (2020).
112. International Energy Agency. Brazil. *Country Profile* https://www.iea.org/countries/brazil (2020).
113. Agência Nacional de Energia Elétrica. Sistema de Informações Geográficas do Setor Elétrico - SIGEL. https://sigel.aneel.gov.br/portal/home/index.html (2020).
114. XM. Capacidad Efectiva Neta. *Descripción del Sistema Eléctrico Colombiano* http://informesanuales.xm.com.co/2015/SitePages/operacion/2-6-Capacidad-efectiva-neta.aspx (2020).
115. Urrutia, R. & Vuille, M. Climate change projections for the tropical Andes using a regional climate model: Temperature and precipitation simulations for the end of the 21st century. *Journal of Geophysical Research* **114**, D02108 (2009).
116. Mernild, S. H. *et al.* The Andes Cordillera. Part I: snow distribution, properties, and trends (1979-2014). *International Journal of Climatology* **37**, 1680–1698 (2017).

117. Palmer, J. The Dangers of Glacial Lake Floods: Pioneering and Capitulation. *Eos* **100**, (2019).
118. Drenkhan, F., Huggel, C., Guardamino, L. & Haeberli, W. Managing risks and future options from new lakes in the deglaciating Andes of Peru: The example of the Vilcanota-Urubamba basin. *Science of the Total Environment* **665**, 465–483 (2019).
119. Buytaert, W. *et al.* Glacial melt content of water use in the tropical Andes. *Environmental Research Letters* **12**, 114014 (2017).
120. Ministerio de Energía y Minas. *Capítulo 3: Anuario Estadístico de Electricidad 2016*. (2017).
121. Gobierno de la República del Perú & Gobierno de la República Federativa del Brasil. Acuerdo entre el gobierno de la República del Perú y el gobierno de la República Federativa del Brasil para el suministro de electricidad al Perú y Exportación de Excedentes al Brasil. 9 (2010).
122. Jarvis, A., Reuter, H. I. I., Nelson, A. & Guevara, E. Hole-filled seamless SRTM data V4. *International Centre for Tropical Agriculture (CIAT)* available from http://srtm.csi.cgiar.org (2008) doi:http//srtm.csi.cgiar.org.
123. Sanchez, P. A. *et al.* Digital Soil Map of the World. *Science* **325**, 680–681 (2009).
124. Lehner, B., Verdin, K. & Jarvis, A. New global hydrography derived from spaceborne elevation data. *Eos* **89**, 93–94 (2008).
125. World Bank. Population, total. *Indicators* https://data.worldbank.org/indicator/SP.POP.TOTL?name_desc=false (2020).
126. Operador Nacional do Sistema Elétrico. Demanda Máxima 2019. *Resultados da Operação: Histórico da Operação* http://www.ons.org.br/Paginas/resultados-da-operacao/historico-da-operacao/demanda_maxima.aspx (2020).
127. XM. Demanda Máxima de Potencia 2019. *Portal BI: Información Inteligente* http://portalbissrs.xm.com.co/dmnd/Paginas/Historicos/Historicos.aspx (2020).
128. Comité de Operación Económica del Sistema Interconectado Nacional. Demanda. *Portal de Información* http://www.coes.org.pe/Portal/portalinformacion/demanda (2020).

129. OSINERGMIN Perú. *Centrales de Generación Eléctrica - En Operación*. https://www.osinergmin.gob.pe/seccion/centro_documental/electricidad/Documentos/PROYECTOS GFE/Generación/2-EN-OPERACION.pdf (2017).
130. OSINERGMIN Perú. *Supervisión de Contratos de Proyectos de Generación y Transmisión de Energía Eléctrica en Construcción*. (2017).
131. OSINERGMIN Perú. *Compendio de Centrales de Generación Eléctrica del Sistema Interconectado Nacional Despachado por el Comité de Operación Económica del Sistema - 2014*. https://issuu.com/osinergmin/docs/compendio_centrales_2014 (2015).
132. Ministerio de Energía y Minas. *Anuario Estadístico de Electricidad 2015 - Capítulo 3*. (2016).
133. Comité de Operación Económica del Sistema Interconectado Nacional. Portal de Indicadores. http://www.coes.org.pe/Portal/portalinformacion/generacion (2018).
134. Comité de Operación Económica del Sistema Interconectado Nacional. Indicadores BI. https://www.coes.org.pe/Portal/portalinformacion/VisorPowerBI (2020).
135. XM. Hidrología: Aportes. *Portal BI: Información Inteligente* http://portalbissrs.xm.com.co/hdrlg/Paginas/Historicos/Historicos.aspx (2020).
136. Operador Nacional do Sistema Elétrico. Dados Hidrológicos/Vazaões. *Resultados da Operação: Histórico da Operação* http://www.ons.org.br/Paginas/resultados-da-operacao/historico-da-operacao/dados_hidrologicos_vazoes.aspx (2020).
137. Ghiggi, G., Humphrey, V., Seneviratne, S. I. & Gudmundsson, L. GRUN: An observations-based global gridded runoff dataset from 1902 to 2014. *Earth System Science Data Discussions* 1–32 (2019) doi:10.5194/essd-2019-32.
138. Ambiand: Ambiental Andina. *Estudio de series sintéticas para los modelos de mediano y largo plazo*. (2014).
139. Wood, A. W. & Maurer, E. P. Long-range experimental hydrologic forecasting for the eastern United States. *Journal of Geophysical Research* **107**, 4429 (2002).
140. Caceres, A. L., Jaramillo, P., Matthews, H. S., Samaras, C. & Nijssen, B. Climate Forced Hydropower Simulations Using NASA NEX-GDDP. (2020) doi:10.5281/zenodo.4009505.

141. Hock, R. & Rasul, G. *Special Report on the Ocean and Cryosphere in a Changing Climate Chapter 2: High Mountain Areas*. (2019).
142. de Queiroz, A. R., Faria, V. A. D., Lima, L. M. M. & Lima, J. W. M. Hydropower revenues under the threat of climate change in Brazil. *Renewable Energy* **133**, 873–882 (2019).
143. de Oliveira, V. A., de Mello, C. R., Viola, M. R. & Srinivasan, R. Assessment of climate change impacts on streamflow and hydropower potential in the headwater region of the Grande river basin, Southeastern Brazil. *International Journal of Climatology* **37**, 5005–5023 (2017).
144. Vuille, M., Franquist, E., Garreaud, R., Lavado Casimiro, W. S. & Cáceres, B. Impact of the global warming hiatus on Andean temperature. *Journal of Geophysical Research: Atmospheres* **120**, 3745–3757 (2015).
145. Lavado Casimiro, W. S., Labat, D., Ronchail, J., Espinoza, J. C. & Guyot, J. L. Trends in rainfall and temperature in the Peruvian Amazon-Andes basin over the last 40 years (1965-2007). *Hydrological Processes* n/a-n/a (2012) doi:10.1002/hyp.9418.
146. Marengo, J. A., Jones, R., Alves, L. M. & Valverde, M. C. Future change of temperature and precipitation extremes in South America as derived from the PRECIS regional climate modeling system. *International Journal of Climatology* **29**, 2241–2255 (2009).
147. Jones, R. G. *et al.* Generating high resolution climate change scenarios using PRECIS. 40 (2004).
148. Ministerio de Energía y Minas. *Plan Energético Nacional 2014-2025*. (2014).
149. OSINERGMIN Perú. *Proyectos Relevantes de Generación y Transmisión de Energía Eléctrica en Construcción*. (2017).
150. de Faria, F. A. M., Jaramillo, P., Sawakuchi, H. O., Richey, J. E. & Barros, N. Estimating greenhouse gas emissions from future Amazonian hydroelectric reservoirs. *Environmental Research Letters* **10**, 124019 (2015).
151. Deemer, B. R. *et al.* Greenhouse Gas Emissions from Reservoir Water Surfaces: A New Global Synthesis. *BioScience* **66**, 949–964 (2016).

152. Barros, N. *et al.* Carbon emission from hydroelectric reservoirs linked to reservoir age and latitude. *Nature Geoscience* (2011) doi:10.1038/ngeo1211.
153. Pappis, I. *et al. Energy projections for African countries*. https://publications.jrc.ec.europa.eu/repository/bitstream/JRC118432/jrc118432_jrc118432_reviewed_by_ipo.pdf (2019) doi:10.2760/678700.
154. Cervigni, R., Liden, R., Neumann, J. E. & Strzepek, K. M. *Enhancing the Climate Resilience of Africa's Infrastructure: The Power and Water Sectors*. *Enhancing the Climate Resilience of Africa's Infrastructure: The Power and Water Sectors* (2015). doi:10.1596/978-1-4648-0466-3.
155. IRENA. *Africa Clean Energy Corridor: Analysis of Infrastructure for Renewable Power in Eastern and Southern Africa*. (International Renewable Energy Agency, 2015).
156. International Energy Agency. *Africa Energy Outlook 2019*. https://iea.blob.core.windows.net/assets/2f7b6170-d616-4dd7-a7ca-a65a3a332fc1/Africa_Energy_Outlook_2019.pdf (2019).
157. Falchetta, G., Gernaat, D. E. H. J., Hunt, J. & Sterl, S. Hydropower dependency and climate change in sub-Saharan Africa: A nexus framework and evidence-based review. *Journal of Cleaner Production* **231**, 1399–1417 (2019).
158. International Energy Agency. *Climate Impacts on African Hydropower*. https://www.iea.org/reports/climate-impacts-on-african-hydropower (2020).
159. Turner, S. W. D., Ng, J. Y. & Galelli, S. Examining global electricity supply vulnerability to climate change using a high-fidelity hydropower dam model. *Science of The Total Environment* **590–591**, 663–675 (2017).
160. Kling, H., Stanzel, P. & Preishuber, M. Impact modelling of water resources development and climate scenarios on Zambezi River discharge. *Journal of Hydrology: Regional Studies* **1**, 17–43 (2014).
161. Stanzel, P., Kling, H. & Bauer, H. Climate change impact on West African rivers under an ensemble of CORDEX climate projections. *Climate Services* **11**, 36–48 (2018).

162. Conway, D., Dalin, C., Landman, W. A. & Osborn, T. J. Hydropower plans in eastern and southern Africa increase risk of concurrent climate-related electricity supply disruption. *Nature Energy* **2**, 946–953 (2017).
163. Sidibe, M. *et al.* Near-term impacts of climate variability and change on hydrological systems in West and Central Africa. *Climate Dynamics* **54**, 2041–2070 (2020).
164. Kling, H., Stanzel, P. & Fuchs, M. Regional Assessment of the Hydropower Potential of Rivers in West Africa. *Energy Procedia* **97**, 286–293 (2016).
165. Cole, M. A., Elliott, R. J. R. & Strobl, E. Climate Change, Hydro-Dependency, and the African Dam Boom. *World Development* **60**, 84–98 (2014).
166. van Vliet, M. T. H., Sheffield, J., Wiberg, D. & Wood, E. F. Impacts of recent drought and warm years on water resources and electricity supply worldwide. *Environmental Research Letters* **11**, 124021 (2016).
167. Busch, S., de Felice, M. & Hidalgo Gonzalez, I. *Analysis of the water-power nexus in the Southern African Power Pool*. (Publications Office of the European Union, 2020). doi:10.2760/920794.
168. International Renewable Energy Agency. *Scaling Up Renewable Energy Deployment in Africa: Detailed Overview of IRENA's Engagement and Impact*. https://www.irena.org/-/media/Files/IRENA/Agency/Publication/2020/Feb/IRENA_Africa_Impact_Report_2020.pdf?la=en&hash=B1AD828DFD77D6430B93185EC90A0D1B72D452CC (2020).
169. Hafner, M., Tagliapietra, S. & de Strasser, L. Prospects for Renewable Energy in Africa. in *Energy in Africa: Challenges and Opportunities* 47–75 (Springer International Publishing, 2018). doi:10.1007/978-3-319-92219-5_3.
170. Sterl, S., Fadly, D., Liersch, S., Koch, H. & Thiery, W. Linking solar and wind power in eastern Africa with operation of the Grand Ethiopian Renaissance Dam. *Nature Energy* (2021) doi:10.1038/s41560-021-00799-5.
171. Sterl, S., Liersch, S., Koch, H., Lipzig, N. P. M. van & Thiery, W. A new approach for assessing synergies of solar and wind power: implications for West Africa. *Environmental Research Letters* **13**, 094009 (2018).

172. Pavičević, M. & Quoilin, S. *Analysis of the water-power nexus in the North, Eastern and Central African Power Pools*. (Publications Office of the European Union, 2020). doi:10.2760/12651.
173. de Felice, M., Gonzalez Aparicio, I., Huld, T., Busch, S. & Hidalgo Gonzalez, I. *Analysis of the water-power nexus in the West African Power Pool*. (2019). doi:10.2760/362802.
174. Jurasz, J., Canales, F. A., Kies, A., Guezgouz, M. & Beluco, A. A review on the complementarity of renewable energy sources: Concept, metrics, application and future research directions. *Solar Energy* **195**, 703–724 (2020).
175. Jurasz, J., Canales, F. A., Kies, A., Guezgouz, M. & Beluco, A. A review on the complementarity of renewable energy sources: Concept, metrics, application and future research directions. *Solar Energy* **195**, 703–724 (2020).
176. Wu, G. C. *et al.* Strategic siting and regional grid interconnections key to low-carbon futures in African countries. *Proceedings of the National Academy of Sciences* **114**, E3004–E3012 (2017).
177. Wu, G. C., Deshmukh, R., Ndhlukula, K., Radojicic, T. & Reilly, J. *Renewable Energy Zones for the Africa Clean Energy Corridor*. https://www.irena.org/-/media/Files/IRENA/Agency/Publication/2015/IRENA-LBNL_Africa-RE-_CEC_2015.pdf (2015).
178. Sterl, S. *et al.* Smart renewable electricity portfolios in West Africa. *Nature Sustainability* **3**, 710–719 (2020).
179. Pappis, I. *et al. Energy projections for African countries*. (2019) doi:10.2760/678700.
180. United Nations Statistics Division. Electricity, net installed capacity of electric power plants. *Energy Statistics Database* http://data.un.org/Data.aspx?d=EDATA&f=cmID%3aEC%3btrID%3a133 (2021).
181. International Hydropower Association. Africa (2020 Data). https://www.hydropower.org/region-profiles/africa (2020).
182. Falchetta, G., Gernaat, D. E. H. J., Hunt, J. & Sterl, S. Hydropower dependency and climate change in sub-Saharan Africa: A nexus framework and evidence-based review. *Journal of Cleaner Production* **231**, 1399–1417 (2019).

183. International Energy Agency. *Climate Impacts on African Hydropower*. (2020).
184. Gernaat, D. E. H. J. *et al.* Climate change impacts on renewable energy supply. *Nature Climate Change* **11**, (2021).
185. Rutger Willem Hofste, Samantha Kuzma, Sara Walker, Edwin H. Sutanudjaja, Marc F.P. Bierkens, Marijn J.M. Kuijper, Marta Faneca Sanchez, Rens Van Beek, Yoshihide Wada, S. G. R. and P. R. *Aqueduct 3.0: Updated Decision-Relevant Global Water Risk Indicators*. https://www.wri.org/publication/aqueduct-30 (2019).
186. BP. *Statistical Review of World Energy*. https://www.bp.com/en/global/corporate/energy-economics/statistical-review-of-world-energy.html (2021).
187. Our World in Data. Share of electricity production from hydropower. https://ourworldindata.org/grapher/share-electricity-hydro?tab=chart&stackMode=absolute&time=earliest..latest&region=Africa (2021).
188. de Faria, F. A. M., Jaramillo, P., Sawakuchi, H. O., Richey, J. E. & Barros, N. Estimating greenhouse gas emissions from future Amazonian hydroelectric reservoirs. *Environmental Research Letters* **10**, 124019 (2015).
189. Deemer, B. R. *et al.* Greenhouse Gas Emissions from Reservoir Water Surfaces: A New Global Synthesis. *BioScience* **66**, 949–964 (2016).
190. Boulange, J., Hanasaki, N., Yamazaki, D. & Pokhrel, Y. Role of dams in reducing global flood exposure under climate change. *Nature Communications* **12**, 417 (2021).
191. Lindersson, S., Brandimarte, L., Mård, J. & di Baldassarre, G. A review of freely accessible global datasets for the study of floods, droughts and their interactions with human societies. *WIREs Water* **7**, (2020).
192. Gernaat, D. E. H. J., Bogaart, P. W., Vuuren, D. P. van, Biemans, H. & Niessink, R. High-resolution assessment of global technical and economic hydropower potential. *Nature Energy* **2**, 821–828 (2017).
193. Bishoge, O. K., Kombe, G. G. & Mvile, B. N. Renewable energy for sustainable development in sub-Saharan African countries: Challenges and way forward. *Journal of Renewable and Sustainable Energy* **12**, 052702 (2020).

194. RGI Consortium. Randolph Glacier Inventory – A Dataset of Global Glacier Outlines: Version 6.0: Technical Report. 71 (2017) doi:10.7265/N5-RGI-60.
195. Abatzoglou, J. T., Dobrowski, S. Z., Parks, S. A. & Hegewisch, K. C. TerraClimate, a high-resolution global dataset of monthly climate and climatic water balance from 1958-2015. *Scientific Data* **5**, (2018).
196. CCAFS, CIAT, ILRI, I. CCAFS Climate. *GCM Downscaled Data Portal* http://ccafs-climate.org/ (2016).
197. Bartos, M. D. Pysheds: a fast, open-source digital elevation model processing library. (2018).
198. Lehner, B., Verdin, K. & Jarvis, A. New global hydrography derived from spaceborne elevation data. *Eos* **89**, 93–94 (2008).
199. Jarvis, A., Reuter, H. I. I., Nelson, A. & Guevara, E. Hole-filled seamless SRTM data V4. *International Centre for Tropical Agriculture (CIAT)* available from http://srtm.csi.cgiar.org (2008) doi:http//srtm.csi.cgiar.org.
200. Sanchez, P. A. *et al.* Digital Soil Map of the World. *Science* **325**, 680–681 (2009).
201. Kanamitsu, W. Ebisuzaki, J. Woollen, S-K Yang, J.J. Hnilo, M. Fiorino, and G. L. Potter. NCEP-DOE AMIP-II Reanalysis (R-2). (2020).
202. Ziese, Markus; Rauthe-Schöch, Armin; Becker, Andreas; Finger, Peter; Meyer-Christoffer, Anja; Schneider, U. GPCC Full Data Daily Version.2018 at 1.0°: Daily Land-Surface Precipitation from Rain-Gauges built on GTS-based and Historic Data. (2018) doi:10.5676/DWD_GPCC/FD_D_V2018_100.
203. BfG. Global Runoff Data Centre (GRDC) Reference Dataset.
204. Ghiggi, G., Humphrey, V., Seneviratne, S. I. & Gudmundsson, L. GRUN: An observations-based global gridded runoff dataset from 1902 to 2014. *Earth System Science Data Discussions* 1–32 (2019) doi:10.5194/essd-2019-32.
205. Sterl, S. *et al.* Smart renewable electricity portfolios in West Africa. *Nature Sustainability* **3**, 710–719 (2020).
206. Lehner, B. *et al.* Global Reservoir and Dam Database, Version 1 (GRanDv1): Technical Documentation. *NASA Socioeconomic Data and Applications Center (SEDAC)*

http://www.gwsp.org/fileadmin/downloads/GRanD_Technical_Documentation_v1_1.pdf (2011).

207. Conway, D., Dalin, C., Landman, W. A. & Osborn, T. J. Hydropower plans in eastern and southern Africa increase risk of concurrent climate-related electricity supply disruption. *Nature Energy* **2**, 946–953 (2017).
208. Turner, S. W. D. & Galelli, S. Water supply sensitivity to climate change: An R package for implementing reservoir storage analysis in global and regional impact studies. *Environmental Modelling & Software* **76**, 13–19 (2016).
209. Wu, X., Cheng, C., Lund, J. R., Niu, W. & Miao, S. Stochastic dynamic programming for hydropower reservoir operations with multiple local optima. *Journal of Hydrology* **564**, 712–722 (2018).
210. Feng, Z., Niu, W., Cheng, C. & Lund, J. R. Optimizing Hydropower Reservoirs Operation via an Orthogonal Progressive Optimality Algorithm. *Journal of Water Resources Planning and Management* **144**, 04018001 (2018).
211. Marwick, B. & Krishnamoorthy, K. cvequality: Tests for the Equality of Coefficients of Variation from Multiple Groups. (2019).
212. Yan, J. *et al.* Reviews on characteristic of renewables: Evaluating the variability and complementarity. *International Transactions on Electrical Energy Systems* (2020) doi:10.1002/2050-7038.12281.
213. Cáceres, A. L., Jaramillo, P., Matthews, H. S., Samaras, C. & Nijssen, B. Climate Forced Hydropower Simulations for the African Continent Using NASA NEX GDDP. https://doi.org/10.5281/zenodo.5020878 (2021).
214. Friedlingstein, P. *et al.* Global Carbon Budget 2020. *Earth System Science Data* **12**, (2020).
215. IPCC. Summary for Policymakers. in *Climate Change 2021: The Physical Science Basis. Contribution of Working Group I to the Sixth Assessment Report of the Intergovernmental Panel on Climate Change* (eds. Masson-Delmotte, V. et al.) (Cambridge University Press. In Press., 2021).
216. United Nations/Framework Convention on Climate Change. Paris Agreement. in *21st Conference of the Parties* 3 (2015). doi:FCCC/CP/2015/L.9.

217. International Energy Agency. Electricity: Data Browser. https://www.iea.org/fuels-and-technologies/electricity (2021).
218. IEA. Hydropower has a crucial role in accelerating clean energy transitions to achieve countries' climate ambitions securely. *Press Release* (2021).
219. Huss, M. & Hock, R. A new model for global glacier change and sea-level rise. *Frontiers in Earth Science* **3**, (2015).
220. Ansar, A., Flyvbjerg, B., Budzier, A. & Lunn, D. Should we build more large dams? The actual costs of hydropower megaproject development. *Energy Policy* **69**, 43–56 (2014).
221. Leal Filho, W., Manolas, E., Azul, A. M., Azeiteiro, U. & McGhie, H. *Handbook of climate change communication. Vol. 3, Case studies in climate change communication. Case studies in climate change communication* (2018).
222. Henderson, A. N. Reflections on Science Communication in the Context of Global Climate Policy. in *Global Consensus on Climate Change: Paris Agreement and the Path Beyond* 107–118 (2019). doi:10.1021/bk-2019-1313.ch012.
223. Nayak, S. & Iwasa, J. H. Preparing scientists for a visual future. *EMBO reports* **20**, (2019).
224. Terrado, M., Christel, I., Bojovic, D., Soret, A. & Doblas-Reyes, F. J. Climate Change Communication and User Engagement: A Tool to Anticipate Climate Change. in *Handbook of Climate Change Communication: Vol. 3. Climate Change Management.* (ed. Leal Filho W., Manolas E., Azul A., Azeiteiro U., M. H.) 285–302 (Springer, Cham, 2018). doi:10.1007/978-3-319-70479-1_18.
225. Neset, T.-S., Opach, T., Lion, P., Lilja, A. & Johansson, J. Map-Based Web Tools Supporting Climate Change Adaptation. *The Professional Geographer* **68**, 103–114 (2016).
226. Glaas, E., Ballantyne, A. G., Neset, T.-S. & Linnér, B.-O. Visualization for supporting individual climate change adaptation planning: Assessment of a web-based tool. *Landscape and Urban Planning* **158**, 1–11 (2017).
227. World Bank. Data Catalog. https://datacatalog.worldbank.org (2020).
228. S&P Global Platts. World Electric Power Plants Database. (2018).

229. Global Energy Observatory, Google, KTH Royal Institude of Technology in Stockholm, Enipedia & World Resources Institute. Global Power Plant Database. *Published on Resource Watch and Google Earth Engine* (2018).
230. Wan, W., Zhao, J., Popat, E., Herbert, C. & Döll, P. Analyzing the Impact of Streamflow Drought on Hydroelectricity Production: A Global-Scale Study. *Water Resources Research* **57**, (2021).
231. Lehner, B. *et al.* Global Reservoir and Dam Database, Version 1 (GRanDv1): Technical Documentation. *NASA Socioeconomic Data and Applications Center (SEDAC)* http://www.gwsp.org/fileadmin/downloads/GRanD_Technical_Documentation_v1_1.pdf (2011).
232. FAOAQUASTAT. AQUASTAT. *Food and Agriculture Organization of the United Nations* (2016).
233. Johnson, M. M., Kao, S., Samu, N. M. & Uria-Martinez, R. Existing Hydropower Assets Plant Dataset FY19. (2019) doi:10.21951/EHA_FY2019/1508076.
234. Ivanescu, C. West Africa And India - Hydropower Dams. *World Bank Data Catalog* https://datacatalog.worldbank.org/dataset/west-africa-and-india-hydropower-dams-2018 (2018).
235. International Hydropower Association. Pumped Storage Tracking Tool. (2019).
236. Zarfl, C., Lumsdon, A. E., Berlekamp, J., Tydecks, L. & Tockner, K. A global boom in hydropower dam construction. *Aquatic Sciences* **77**, 161–170 (2015).
237. Myneni, R., Knyazikhin, Y. & Park, T. MOD15A2H MODIS/Terra Leaf Area Index/FPAR 8-Day L4 Global 500m SIN Grid V006 [Data set]. (2015) doi:10.5067/MODIS/MOD15A2H.006.
238. Comité de Operación Económica del Sistema Interconectado Nacional. Ficha Técnica: Listado de Centrales. http://sicoes.coes.org.pe/apppublico/FichaTecnica/FichaTecnica (2018).
239. Loeb, N. G. *et al.* Clouds and the Earth's Radiant Energy System (CERES) Energy Balanced and Filled (EBAF) Top-of-Atmosphere (TOA) Edition-4.0 Data Product. *Journal of Climate* **31**, 895–918 (2018).

240. Willett, K. M. *et al.* HadISDH land surface multi-variable humidity and temperature record for climate monitoring. *Climate of the Past* **10**, 1983–2006 (2014).
241. OSINERGMIN Perú. Mapa SEIN. https://www.osinergmin.gob.pe/newweb/uploads/Publico/MapaSEIN/ (2018).
242. International Energy Agency. *Report extract: Access to electricity*. (2020).
243. Global Energy Observatory. http://globalenergyobservatory.org (2017).
244. GADM. Global Administrative Areas Database. *v3.6* https://gadm.org/data.html (2021).
245. Chang, W. shiny: web application framework for R. *R package* vol. 1 (2021).
246. Sievert, C. *Interactive Web-Based Data Visualization with R, plotly, and shiny*. *Interactive Web-Based Data Visualization with R, plotly, and shiny* (2020). doi:10.1201/9780429447273.
247. Cáceres, A. L., Jaramillo, P., Matthews, H. S., Samaras, C. & Nijssen, B. RICCH. https://github.com/acaceres93/RICCH.git (2021).
248. Cáceres, A. L. *et al.* RICCH: Risks and Impacts of Climate Change on Hydropower. *v1.0* https://ricch.shinyapps.io/hydro-shiny/ (2021).
249. Reig, P., Shiao, T. & Gassert, F. *Aqueduct Water Risk Framework*. (2013).
250. Mutesi Bisangwa, R. *Rwanda: Least Cost Power Development Plan (LCPDP) 2020 - 2040*. https://www.reg.rw/fileadmin/user_upload/Least_Cost_Power_Development_Plan_2020-2024.pdf (2021).
251. Goodman, L. A. Snowball Sampling. *The Annals of Mathematical Statistics* (1961) doi:10.1214/aoms/1177705148.
252. Smith, A., Lott, N. & Vose, R. The Integrated Surface Database: Recent Developments and Partnerships. *Bulletin of the American Meteorological Society* **92**, 704–708 (2011).
253. Hejazi, M. I. *et al.* Integrated assessment of global water scarcity over the 21st century under multiple climate change mitigation policies. *Hydrology and Earth System Sciences* **18**, 2859–2883 (2014).

254. Natural Resources Conservation Service. Chapter 11 Snowmelt. in *Part 630 National Engineering Handbook* (United States Department of Agriculture, 2004).
255. Rango, A. & Martinec, J. REVISITING THE DEGREE-DAY METHOD FOR SNOWMELT COMPUTATIONS. *Journal of the American Water Resources Association* **31**, 657–669 (1995).
256. Martinec, J. The degree–day factor for snowmelt runoff forecasting. *IUGG General Assembly of Helsinki* **51**, 468–477 (1960).
257. Fernández, A. & Mark, B. G. Modeling modern glacier response to climate changes along the Andes Cordillera: A multiscale review. *Journal of Advances in Modeling Earth Systems* **8**, 467–495 (2016).
258. Hirabayashi, Y., Döll, P. & Kanae, S. Global-scale modeling of glacier mass balances for water resources assessments: Glacier mass changes between 1948 and 2006. *Journal of Hydrology* **390**, 245–256 (2010).
259. Andrews, F. T., Croke, B. F. W. & Jakeman, A. J. An open software environment for hydrological model assessment and development. *Environmental Modelling and Software* (2011) doi:10.1016/j.envsoft.2011.04.006.
260. BfG. Global Runoff Data Centre (GRDC) Reference Dataset.
261. Arderne, C. Africa - Electricity Transmission and Distribution Grid Map. (2017).
262. USAID. Power Africa: Rwanda Fact Sheet. https://www.usaid.gov/sites/default/files/documents/1860/Rwanda_-_November_2018_Country_Fact_Sheet.pdf (2020).

Appendix A – Supporting Information for Chapter 2

A.1 Water Balance Model Calculations

We calculated potential evapotranspiration (PET) using the FAO Penman Monteith Method[98] using temperature from historical or projection data, the Leaf Area Index for each area from MODIS[237], the average monthly relative humidity from the HadISDH version 4.0.0.2017f dataset[240,252], and the shortwave and longwave radiation from the CERES EBAF-TOA Ed. 4.0 dataset[239]. Shortwave and longwave radiation projections data was not available in the NEX-GDDP dataset. Once we calculated PET, we estimated actual Evapotranspiration (AET) using equations (A.1.1) and (A.1.2), defined by Kaczmarek (1993)[99].

$$AET_t = \beta \times PET_t \tag{A.1.1}$$

$$\beta = \left(\frac{5 \times \left(\frac{S_{t-1}}{S_t}\right) - 2 \times \left(\frac{S_{t-1}}{S_t}\right)^2}{3} \right) \tag{A.1.2}$$

Where AET_t is actual evapotranspiration in mm, β is a dimensionless parameter computed using equation (A.1.2), PET_t is potential evapotranspiration in mm, S_t is the soil moisture in this time-step in mm, and S_{t-1} is the soil moisture in the previous time-step in mm.

For soil moisture, equation (A.1.3) describes the formulation proposed by Hejazi et al. 2014[253].

$$S_t = \begin{cases} S_m & S_{t-1} + P_t + PET_t \geq S_m \\ \gamma \cdot S_{t-1} + P_t - AET_t & otherwise \\ 0 & \gamma \cdot S_{t-1} + P_t - AET_t \leq 0 \end{cases} \tag{A.1.3}$$

Where S_t and S_{t-1} are the same as in equation A.1.2, S_m is the maximum soil moisture capacity in mm, P_t is the precipitation in that time step in mm, and γ is a constant dependent on the soil moisture.

Additionally, we calculated the glacier melt and the snowmelt components using a degree day approach. As previously stated, most studies link glacier retreat in the tropical Andes to

increased temperature, which makes a degree day approach appropriate for estimating glacier melt and snowmelt. Equation (A.1.4) describes the degree day method used[254]:

$$M = C_m \cdot \max\{0, (T_a - T_b)\} \cdot D \qquad \text{(A.1.4)}$$

Where M represents the snowmelt in mm/month, C_m represents the degree-day coefficient or degree-day factor (mm/degree-day Celsius), T_a is the mean monthly temperature (°C), T_b is the base temperature (°C), which we assumed to be 0 °C[255,256], and D is the number of days in the month of the analysis. The existing literature suggests that the value of C_m varies for snow and ice. The values for snow typically range between 3-5 mm/degree-day °C and the values for ice can range between 3-20 mm/degree-day °C[100,257,258]. We used a value of 3.5 mm/degree-day °C snow and 20 mm/degree-day °C ice to account for the upper bound contribution of glaciers and snow to runoff as initial parameters. A temperature lapse rate of 0.0065°C/m is used to calculate the temperature at the glacier mean elevation.

Equation (A.1.5) describes a scaling relationship[101,102] used to determine the volume of the glacier (V), in km^3, based on its characteristic surface area (S), in km^2. Glaciers in the tropical Andes have small areas (~1 km^2)[95,118], therefore, the mean area of the glacier is used in the scaling relationship in lieu of the lumped glacier area in the basin, to avoid overestimating glacier volume. Glacier accumulation is tracked when the temperature at the glacier's altitude is below 0°C and there is precipitation in the time step.

$$V = S^{1.375} \qquad \text{(A.1.5)}$$

A key difference for calculating snowmelt versus glacier melt is that snowmelt calculations do not rely on the scaling relationship to determine melt. To track accumulation or melt, we used elevation bands. Every power plant sub-basin is divided into elevation bands of 100 meters. For every band, temperature is calculated using the same temperature lapse rate as previously mentioned. If the temperature in the elevation band is below 0°C, then it is assumed that snow falls and accumulates. Every period with temperature higher than 0°C is a potential melt period and depending on the accumulation in the previous time steps, snow melts with a rate depending on the degree day factor. The model is initialized assuming no snow accumulation in the previous time step.

Evapotranspiration and soil moisture obtained from equations (A.1.1) and (A.1.3), in units of mm, were multiplied over the area of the sub-basin to obtain their values in each time step. We multiplied precipitation (from downscaled climate data in units of mm per km^2) by the area of the sub-basin minus the glacier area, which is updated for every time step in the projection runs of the models. In order to determine the total contribution from snowmelt and glacier melt, we multiplied the values obtained from equation (A.1.4) by the sub-basin's elevation band areas, and the glacier area determined with the RGI values and the projected variations through the century. The elevation bands area is modified with the changing glacier area. The output of the water balance equation described in Equation (2.1) in Chapter 2 is the streamflow (Million m^3/month) through the each of the power plants analyzed which is converted into m^3/s for the analysis.

A.2 Hydrological Model Calibration

To improve the performance of the water balance model developed, we used the Shuffle Complex Evolution (SCE) optimization algorithm which has been widely applied in hydrological model calibration[103,104]. The calibration included six parameters: glacier degree day coefficient, snow degree day coefficient, maximum basin soil moisture, crop aerodynamic resistance, crop stomatal conductance, and canopy architectural resistance. Using monthly historical records, we calibrated the model at the sub-basin level, though data availability constrained the calibration in some basins. Additionally, we performed the calibrations with all the available historical data and were thus unable to perform a split sample calibration with further validation. We then used the calibrated parameters as inputs for the projection simulations. Finally, we further corrected the streamflow results using a linear parametric transformation.

We used the SCE optimization algorithm embedded in the R package hydromad[259] for the calibration. We selected the six parameters mention above, which have the ability to affect both the timing and the magnitude of the streamflow generated by the water balance model. The glacier degree day and snow degree day coefficients affect the timing of the flows while the maximum basin's soil moisture, the crop aerodynamic resistance, the crop stomatal conductance and the canopy architectural resistance affect the magnitude of the flows. In order to calibrate the model, the SCE algorithm compares the climatology of historical streamflow to the climatology generated by the water balance model with the historical experiments' data and alters the parameters to match the time series. We maximized the Nash-Sutcliffe model efficiency coefficient to calibrate the model. Equation (A.2.1) shows the formulation of the coefficient.

$$NSE = 1 - \frac{\sum_{t=1}^{T}(Q_m^t - Q_o^t)^2}{\sum_{t=1}^{T}(Q_o^t - \overline{Q_o})^2} \qquad \text{(A.2.1)}$$

Where Q_o is the mean of the observed discharges, and Q_m is the modeled discharge. Q_o^t is the observed discharge at time step t, and Q_m^t is the modeled discharge at time step t. The Nash-Sutcliffe efficiency ranges from -∞ to 1, where 1 is the perfect fit of the model.

We initialized all six parameters with the values described in the main text. Nine basins were calibrated with the SCE algorithm and their parameters applied to the basins showing similar characteristics. Additionally, we further corrected the calibrated simulations using a linear parametric transformation.

A.3 General Circulation Models Used

For the development of the hydropower model, the NASA NEX-GDDP dataset was used. Historical experiments, and projections under RCP 4.5 and 8.5 were used from 21 GCMS from CMIP5. The 21 GCMs runs used are presented in the following table.

Table A.3-1 – General Circulation Models (GCMs) obtained from NASA's NEX-GDDP dataset and used for streamflow simulations.

General Circulation Models
INCM4.0
BCC-CSM1-1
NorESM1-M
MRI-CGCM3
MPI-ESM-MR
MPI-ESM-LR
MIROC5
MIROC-ESM
MIROC-ESM-CHEM
IPSL-CM5A-MR
IPSL-CM5A-LR
GFDL-ESM2M
GFDL-ESM2G
GFDL-CM3
CanESM2
CSIRO-Mk3-6-0
CNRM-CM5
CESM1-BGC
CCSM4
BNU-ESM
ACCESS1-0

A.4 Power Plants in the Analysis

Table A.4-1 – Power Plant Characteristics

Country	*Power Plant*	*Effective Capacity (MW)*	*Hydraulic Head (m)*	*Design Flow (m^3/s)*	*Reservoir*	*Status*
Brazil	14 de Julho	100	34	339	No	Operating
	Agua Vermelha	1396	57	2780	Yes	Operating
	Aimores	330	32	1170	No	Operating
	Amador Aguiar I	240	58	467	No	Operating
	Amador Aguiar II	210	46	518	No	Operating
	Apertados	139	27	595	No	Under development
	Baguari	140	18	883	No	Operating
	Baixo Iguacu	350	16	2504	No	Operating
	Bariri	143	23	722	No	Operating
	Barra Bonita	141	24	680	No	Operating
	Barra Grande	690	167	469	Yes	Operating
	Bocaina	150	150	113	No	Approved
	Cachoeira Dourada	658	32	2311	No	Operating
	Campos Novos	880	190	526	Yes	Operating
	Capivara	619	49	1440	Yes	Operating
	Castro Alves	130	92	160	No	Operating
	Cebolao Medio	120	32	426	No	Identified
	Chavantes	414	75	624	Yes	Operating
	Comissario	105	37	326	No	Under development
	Corumba I	375	81	527	Yes	Operating
	Corumba IV	129	63	231	Yes	Operating
	Dona Francisca	125	40	353	No	Operating

Emborcacao	1192	44	3061	Yes	Operating
Estreito	1050	65	1842	No	Operating
Euclides Da Cunha	109	92	135	No	Operating
Fontes Nova	132	325	46	No	Operating
Foz Do Chapeco	855	52	1873	No	Operating
Foz Do Piquiri	101	16	718	No	Under development
Fundao	120	97	141	No	Operating
Funil Parana	180	35	584	No	Operating
Funil Southeast Atlantic	216	39	629	Yes	Operating
Furnas	1216	95	1451	Yes	Operating
Galileia	238	22	1228	No	Identified
Garibaldi	192	45	484	Yes	Operating
Governador Bento Munhoz Da Rocha Neto	1676	140	1359	No	Operating
Governador Jayme Canet Junior	361	122	336	No	Operating
Governador Jose Richa	1240	66	2120	No	Operating
Governador Ney Aminthas de Barros Braga	1260	117	1222	No	Operating
Governador Pedro Viriato Parigot de Souza	260	754	39	No	Operating
Guilman Amorim	140	68	234	No	Operating
Henry Borden	889	720	157	No	Operating
Ibitinga	131	22	694	No	Operating
Igarapava	210	17	1370	No	Operating
Ilha Dos Pombos	187	34	618	No	Operating
Ilha Solteira	3444	47	8334	Yes	Operating
Irai	330	15	2497	No	Under development
Ita	1450	106	1552	No	Operating

Itaguacu	151	59	292	No	Under development
Itaipu Parte Brasileira	14000	115	13864	No	Operating
Itaocara I	150	28	598	No	Construction not started
Itapiranga	725	28	2937	No	Under development
Itauba	500	91	622	No	Operating
Itiquira	157	231	77	No	Operating
Itumbiara	2082	84	2800	Yes	Operating
Jacui	180	98	209	No	Operating
Jaguara	424	46	1048	Yes	Operating
Jauru	122	107	129	No	Operating
Jupia	1551	21	8265	No	Operating
Jurumirim	101	17	686	Yes	Operating
Limoeiro	142	35	460	No	Identified
Machadinho	1140	105	1230	Yes	Operating
Manso	210	62	383	Yes	Operating
Marechal Mascarenhas de Moraes	476	44	1224	No	Operating
Marimbondo	1440	64	2574	Yes	Operating
Mascarenhas	198	21	1068	No	Operating
Miranda	408	71	652	Yes	Operating
Monte Claro	130	44	335	No	Operating
Nilo Pecanha	380	312	138	No	Operating
Nova Avanhandava	347	30	1314	No	Operating
Nova Ponte	510	119	486	Yes	Operating
Pai Quere	292	150	221	No	Construction not started
Paicandu	103	22	528	No	Identified
Passo Fundo	226	263	98	Yes	Operating

	Passo Real	158	48	376	Yes	Operating
	Ponte de Pedra	176	246	81	No	Operating
	Porto Colombia	320	24	1526	No	Operating
	Porto Estrela	112	50	253	Yes	Operating
	Porto Primavera	1540	20	8739	No	Operating
	Promissao	264	27	1093	Yes	Operating
	Quebra Queixo	120	122	111	Yes	Operating
	Risoleta Neves	140	58	275	No	Operating
	Rosana	354	20	2009	No	Operating
	Salto	116	51	258	No	Operating
	Salto Grande	102	44	263	No	Operating
	Salto Osorio	1078	73	1676	No	Operating
	Salto Pilao	192	194	112	No	Operating
	Salto Santiago	1420	109	1478	Yes	Operating
	Santa Clara	120	99	138	Yes	Operating
	Sao Jeronimo	340	90	429	No	Under development
	Sao Roque	142	54	301	No	Under construction
	Sao Simao	1710	73	2662	Yes	Operating
	Serra Do Facao	213	80	301	No	Operating
	Simplicio	334	115	329	No	Operating
	Taquarucu	525	26	2337	No	Operating
	Telemaco Borba	118	48	282	No	Under development
	Tres Irmaos	808	48	1909	Yes	Operating
	Volta Grande	380	28	1563	No	Operating
Colombia	*Alto Anchicaya*	355	370	103	Yes	*Operating*
	Betania	540	64	910	Yes	*Operating*

	Calima	132	197	72	Yes	*Operating*
	Chivor	1000	748	143	No	*Operating*
	Guaca	325	498	70	No	*Operating*
	Guadalupe III	*270*	*483*	*60*	No	*Operating*
	Guadalupe IV	*202*	*449*	*48*	No	*Operating*
	Guatape	560	828	73	No	*Operating*
	Guavio	1200	1015	127	Yes	*Operating*
	Jaguas	170	252	72	No	*Operating*
	La Tasajera	206	558	38	No	*Operating*
	Miel I	396	206	206	No	*Operating*
	Paraiso	276	423	70	No	*Operating*
	Playas	201	179	120	Yes	*Operating*
	Porce II	405	221	197	Yes	*Operating*
	Porce III	660	325	218	Yes	*Operating*
	Salvajina	285	107	285	Yes	*Operating*
	San Carlos	1240	573	232	No	*Operating*
	Urra	340	52	700	Yes	*Operating*
Peru	*El Platanal*	220	630	40	No	Operating
	Chaglla	450	340	130	No	Operating
	Cheves	170	600	30	No	Operating
	San Gaban II	110	660	20	No	Operating
	San Gaban III	250	620	40	No	Under construction
	Cerro del Aguila	550	300	210	No	Operating
	Restitucion	220	300	210	No	Operating
	Santiago Antunez de Mayolo	798	780	110	No	Operating
	Chimay	150	190	80	No	Operating

La Virgen	80	350	30	No	Under construction
Yaupi	110	530	30	No	Operating
Yuncan	130	550	30	No	Operating
Charcani V	145	700	25	No	Operating
Huinco	260	1250	35	No	Operating
Matucana	120	970	15	No	Operating
Cañon del Pato	260	380	40	No	Operating
Quitaracsa	110	860	15	No	Operating
Machu Picchu II	170	360	30	No	Operating

A.5 Supporting Figures and Tables Results Section

A.5.1 Glacier Area Variations

For all sub-basins in the Peruvian case study, Table A.5.1 presents the basin area, glacier area and what is the share of basin area covered by glaciers. Figure A.5.1 shows the estimated decrease in glacier area from 2006 to 2099. The ribbons surrounding the orange and purple lines show the variation in estimates of glacier decrease from the GCMs used to run the model. All models show a consistent trend in glacier area reductions by the end of the century for both RCPs (except for Huinco), accentuated for RCP 8.5. During our period of analysis, glacier melt remains an important contributor to flows during dry months for basins in which the complete retreat is not projected, but the decreased glacier area by the end of the analysis suggests increased vulnerability beyond 2100 if temperatures continue to increase in the 22nd century.

Table A.5-1 – Peruvian basin and glacier areas

Power Plant	Basin Area (km^2)	Glacier Area (km^2)	% Covered by Glaciers
Cerro del Aguila	27,900	20	0.1%
Restitucion	27,800	20	0.1%
Santiago Antunez de Mayolo	27,800	20	0.1%
Machu Picchu II	9,600	310	3.2%
Chaglla	7,300	10	0.1%
Cañon del Pato	5,300	430	8.1%
El Platanal	4,980	30	0.6%
Charcani V	4,100	0	0.0%
San Gaban II	2,770	120	4.3%
San Gaban III	2,770	120	4.3%
Chimay	2,700	8	0.3%
La Virgen	2,100	0	0.0%
Yaupi	1,800	7	0.4%
Yuncan	1,500	7	0.5%
Matucana	880	9	1.0%

Huinco	870	1	0.1%
Cheves	810	0	0.0%
Quitaracsa	370	50	13.5%

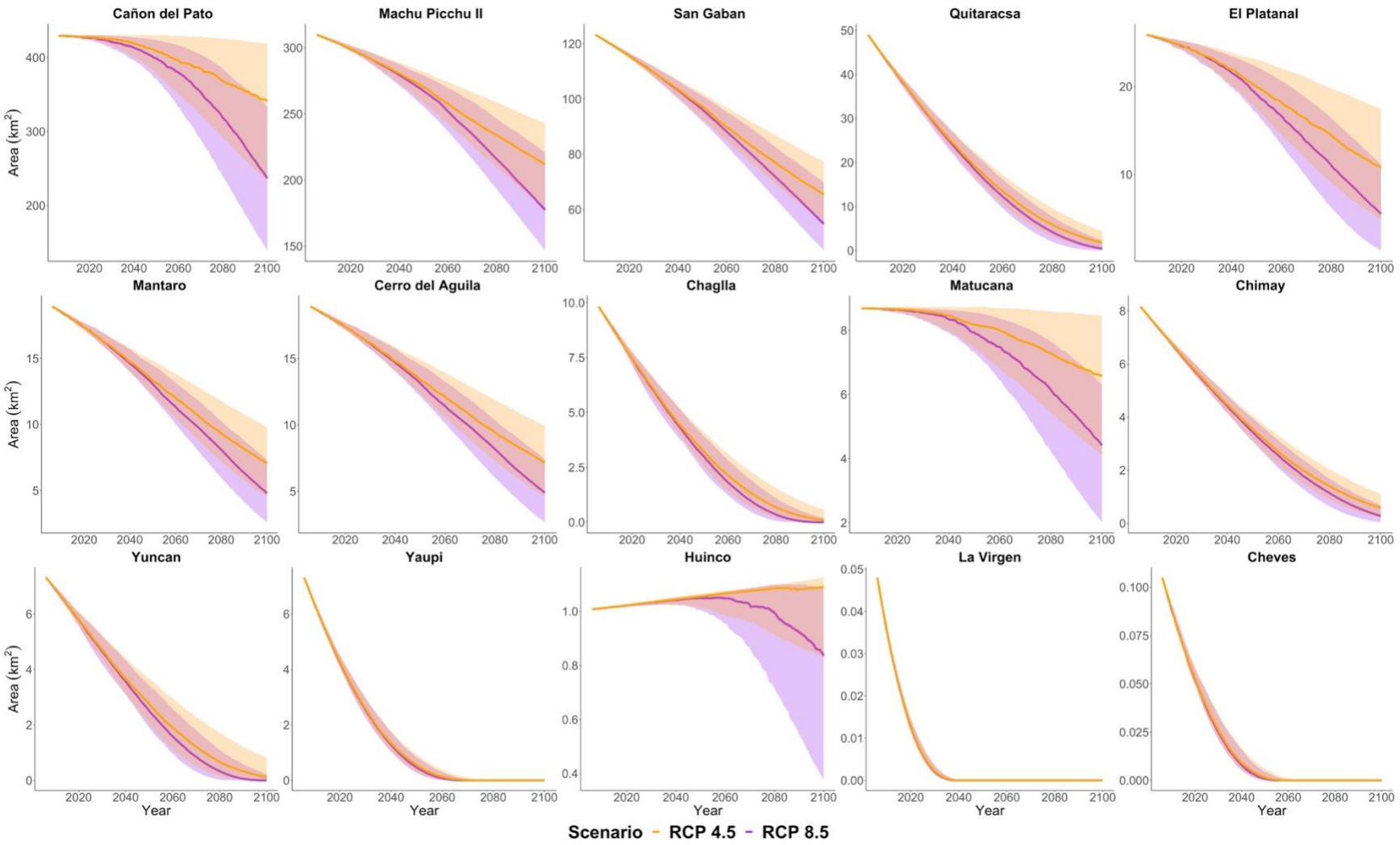

Figure A.5-1 – Projected glacier area for all power plants with initial glacier mass (2006-2099) under RCP 4.5 (orange) and RCP 8.5 (purple) ordered by largest initial glacier area. The ribbons, colored respectively to the emissions scenario, show the spread of the different GCMs used.

A.5.2 Normalized Usable Capacity for Each Power Plant Under RCP4.5

The figures presented below show the relative change in the average normalized usable capacity at each por plant between RCP 4.5 and the historical reference by season (rainy or dry). The normalized usable capacity reported is the ratio of the usable capacity to the installed capacity of the power plant. The results for RCP 4.5, compared to RCP 8.5, are less noticeable for all systems. Figures A.5.2 through A.5.4 present the results for all three systems under RCP 4.5. The increases and decreases in the specific power plants are lower under this emissions scenario than the one presented in the main article for all power plants analyzed.

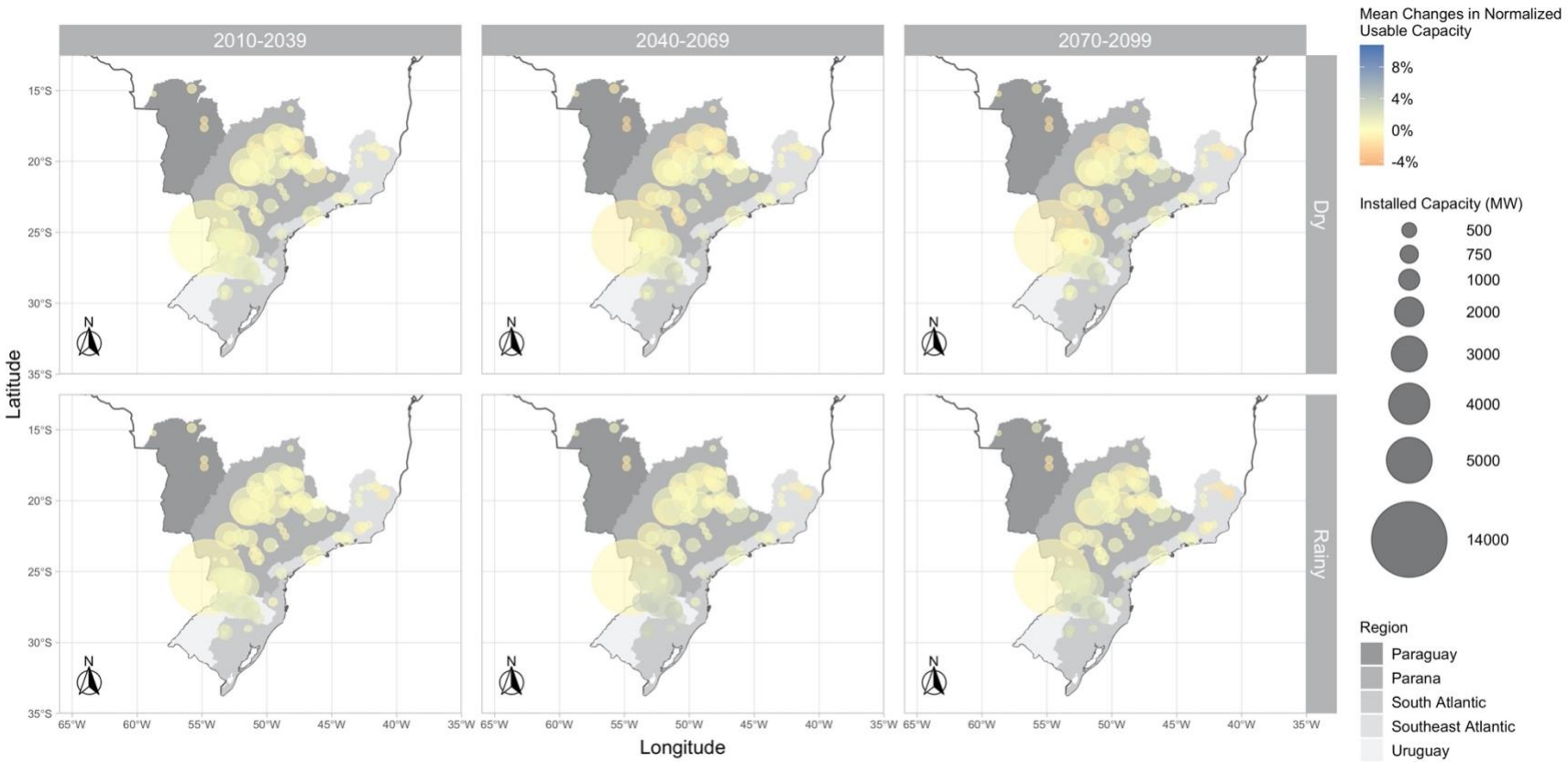

Figure A.5-2 - Brazil's mean relative changes in normalized usable capacity for RCP 4.5 between the historical reference (1970-2005), the near future (2010-2039), the mid-century (2040-2069), and the end-of-the-century (2070-2099). The top panel presents the dry season (April to September) and the bottom panel the rainy season (October to March).

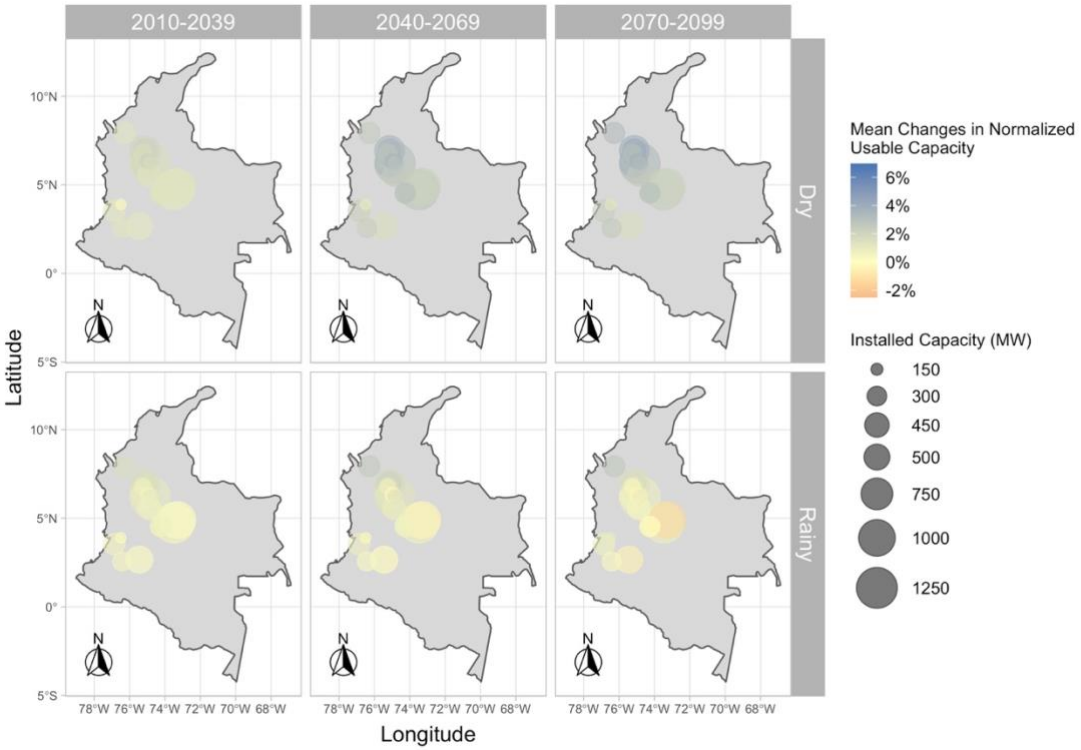

Figure A.5-3 – Colombia's mean relative changes in normalized usable capacity for RCP 4.5 between the historical reference (1970-2005), the near future (2010-2039), the mid-century (2040-2069), and the end-of-the-century (2070-2099). The top panel presents the dry season (December to March, July to August) and the bottom panel the rainy season (April to June, September to November).

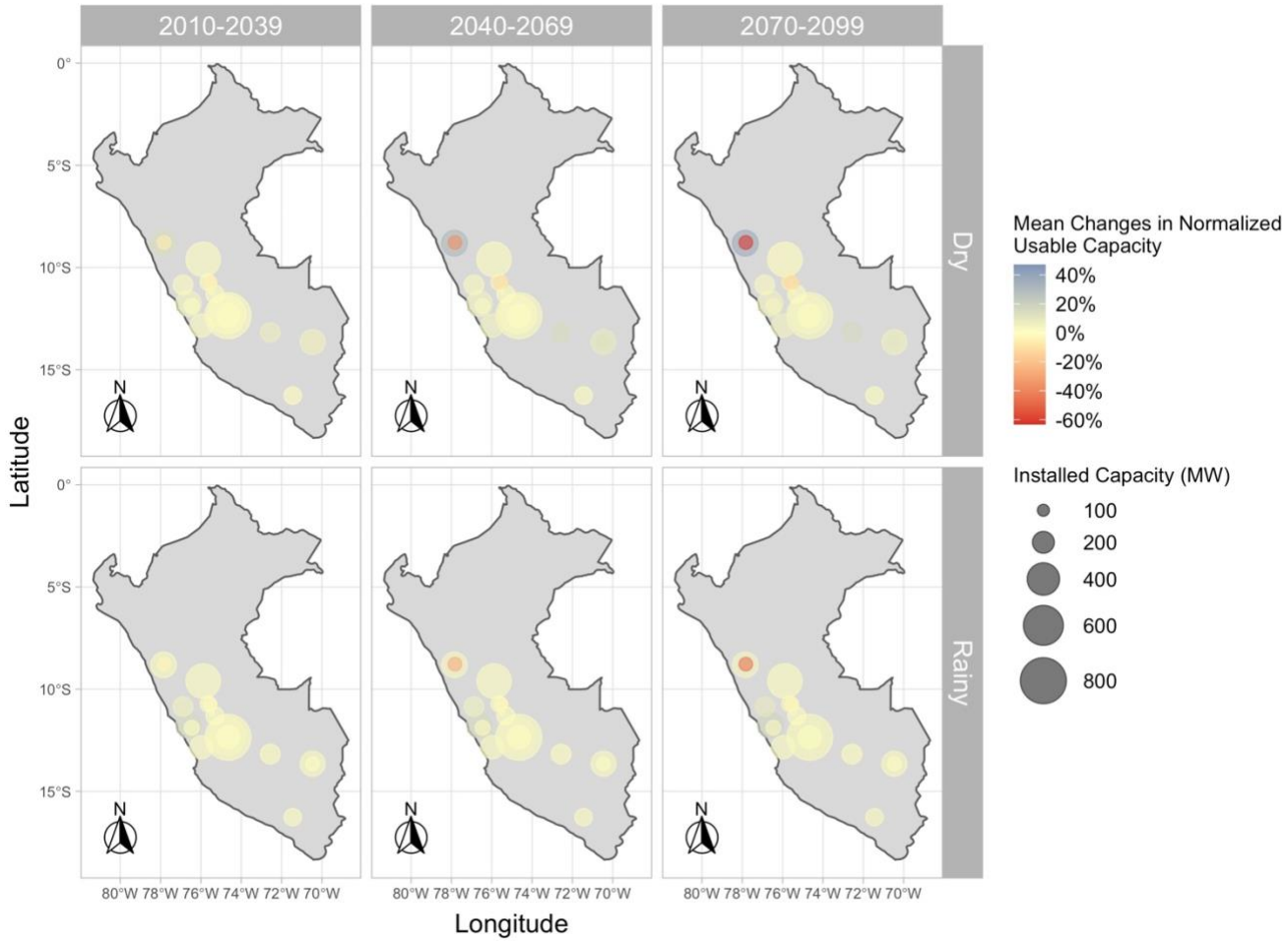

Figure A.5-4 – Peru's mean relative changes in normalized usable capacity for RCP 4.5 between the historical reference (1970-2005), the near future (2010-2039), the mid-century (2040-2069), and the end-of-the-century (2070-2099) for Peru. The top panel presents the dry season (May to November) and the bottom panel the rainy season (December to March).

Additionally, Figure A.5.4 presents the changes in mean seasonal usable capacity for all three periods and seasons (rainy or dry) for the Peruvian system. These results are analogous to the ones presented in Figure 2.4 in the main text.

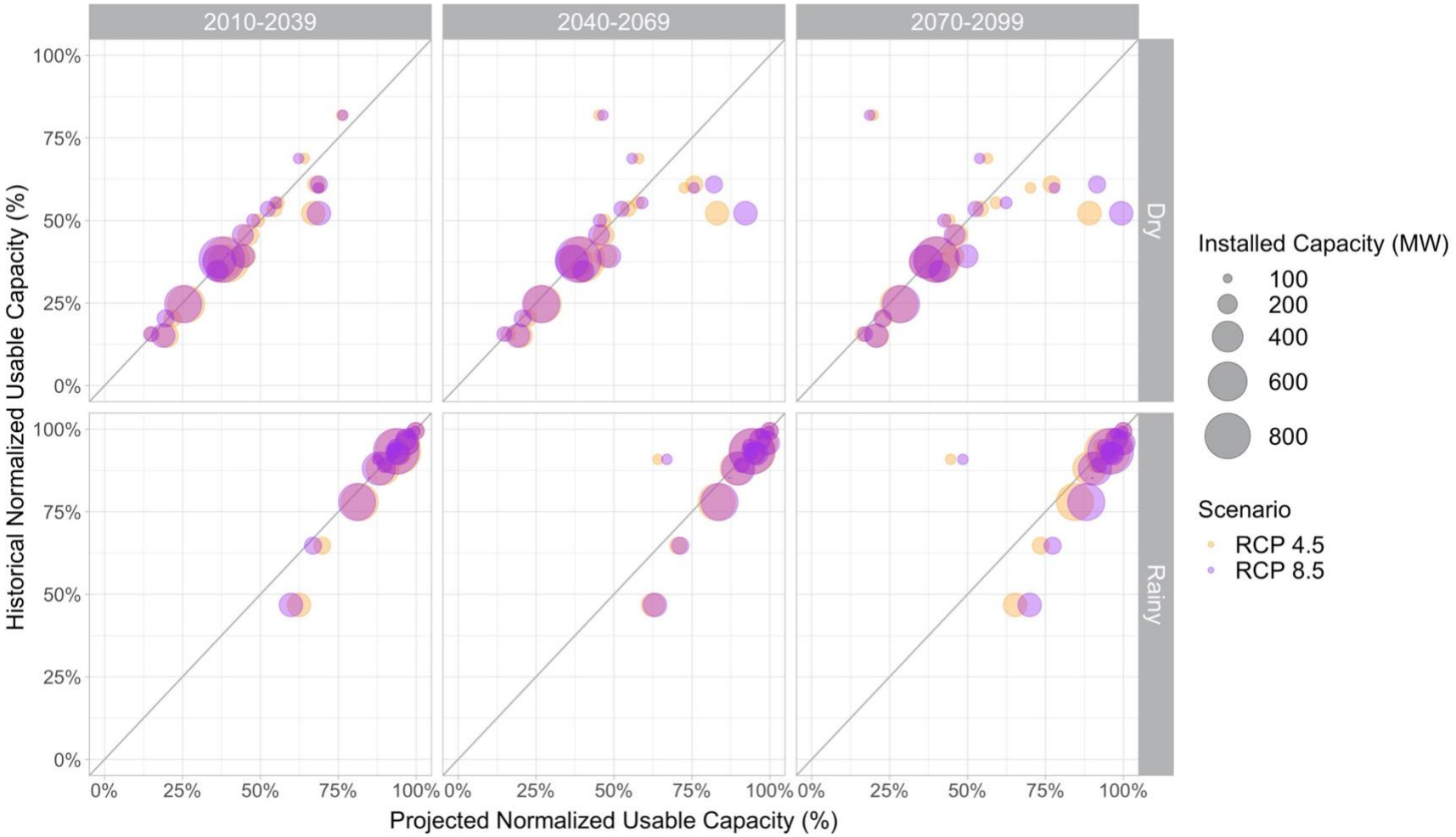

Figure A.5-5 – Comparison of mean seasonal normalized usable capacity (defined as the ratio between available capacity and installed capacity) for the near future (2010-2039), the mid-century (2040-2069), and the end-of-the-century (2070-2099) for Peru. The top panel presents the dry season (May to November) and the bottom panel the rainy season (December to March).

A.5.3 Robustness Analysis

To quantify the contributions of different factors to the spread in the projected changes in hydropower availability, we conducted a two-way ANOVA paired with an Internal Variability Assessment (IV)[109] on annual streamflow as a proxy for available hydropower capacity. Figure A.5.6 presents the results for Brazil, Colombia and Peru and Figure A.5.7 presents the results for the individual power plants.

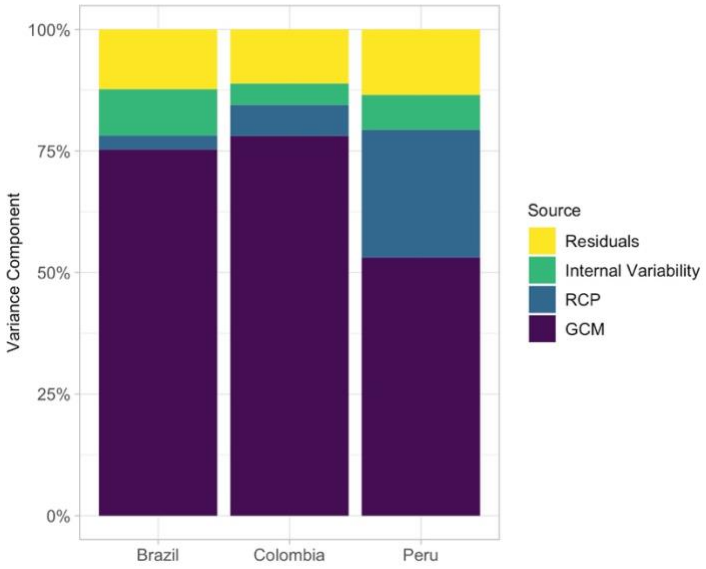

Figure A.5-6 – System average variability components. ANOVA paired with IV results representing the source of variation in the spread of the change of annual streamflow as a proxy for hydropower availability.

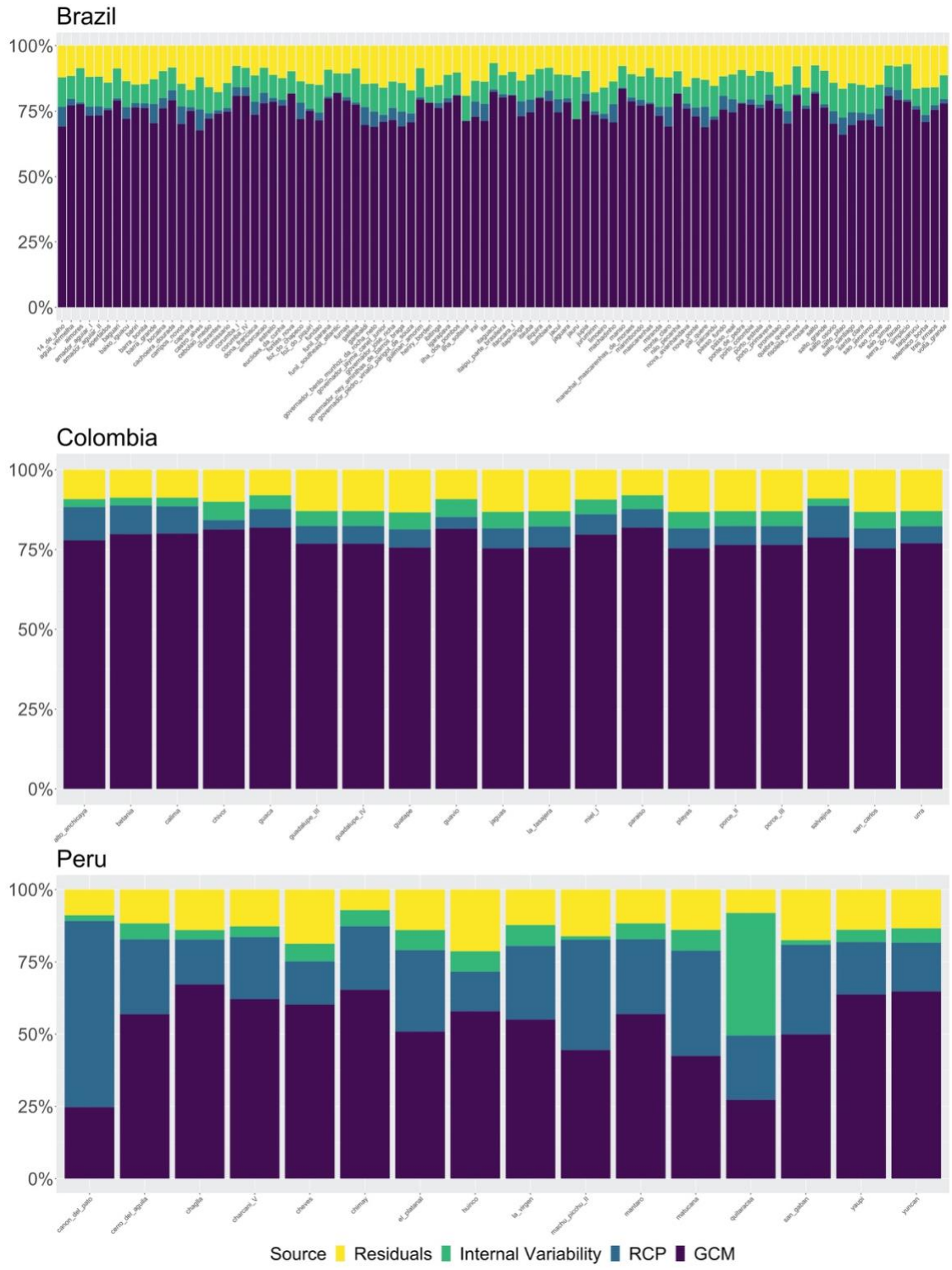

Figure A.5-7 – Power plant variability components. ANOVA and IV results representing the source of the variation in the spread of the change for each hydropower plant for annual streamflow, which in turn affects hydropower generation.

After pairing the ANOVA with the IV, we perform an additional check by analyzing the consensus of models on the change (increasing/decreasing) of annual streamflow and generation potential for the analysis periods. These assessments allow us to understand the key drivers for the spread in the ensemble and how our choices of GCM and RCP impact our results. Furthermore, they enable us to determine the ensemble's level of agreement on the impact of climate change. Table A.5.2 presents the model consensus on the direction of streamflow changes by the end of the century for all power plants in the analysis. Similar to what presented in the main article, the larger consensus in temperature changes across GCMs results in a larger consensus about the direction of streamflow changes and resulting available capacity in the glacierized basins in Peru than in Brazil or Colombia.

Table A.5-2 – Model Agreement of Annual Streamflow Changes Direction and Standard Deviation of Annual Volume. The model agreement includes the 21 GCMs under both RCP 4.5 and RCP 8.5 (total of 42 models)

Country	***Power Plant***	**Model Agreement Increases (RCP 4.5)**	**Model Agreement Increases (RCP 8.5)**
Brazil	14 de Julho	16	18
	Agua Vermelha	13	13
	Aimores	11	12
	Amador Aguiar I	12	13
	Amador Aguiar II	12	12
	Apertados	11	16
	Baguari	11	12
	Baixo Iguacu	12	18
	Bariri	14	14
	Barra Bonita	14	14
	Barra Grande	16	18
	Bocaina	12	13
	Cachoeira Dourada	12	13
	Campos Novos	16	18
	Capivara	15	15

Castro Alves	16	18
Cebolao Medio	12	15
Chavantes	15	15
Comissario	12	17
Corumba I	13	13
Corumba IV	14	13
Dona Francisca	14	18
Emborcacao	12	14
Estreito	12	13
Euclides Da Cunha	13	13
Fontes Nova	12	13
Foz Do Chapeco	15	18
Foz Do Piquiri	12	15
Fundao	12	17
Funil Parana	12	12
Funil Southeast Atlantic	13	13
Furnas	12	13
Galileia	11	12
Garibaldi	16	18
Governador Bento Munhoz Da Rocha Neto	14	18
Governador Jayme Canet Junior	12	15
Governador Jose Richa	12	18
Governador Ney Aminthas de Barros Braga	14	18
Governador Pedro Viriato Parigot de Souza	13	17
Guilman Amorim	11	12

Henry Borden	13	12
Ibitinga	14	14
Igarapava	12	13
Ilha Dos Pombos	13	13
Ilha Solteira	11	11
Irai	15	18
Ita	16	18
Itaguacu	13	13
Itaipu Parte Brasileira	13	13
Itaocara I	13	13
Itapiranga	15	18
Itauba	14	18
Itiquira	15	13
Itumbiara	12	13
Jacui	14	18
Jaguara	12	13
Jauru	14	14
Jupia	12	12
Jurumirim	15	15
Limoeiro	12	15
Machadinho	16	18
Manso	13	14
Marechal Mascarenhas de Moraes	12	13
Marimbondo	13	13
Mascarenhas	11	12
Miranda	12	13
Monte Claro	16	18
Nilo Pecanha	12	13

Nova Avanhandava	14	14
Nova Ponte	12	13
Pai Quere	16	18
Paicandu	11	16
Passo Fundo	14	18
Passo Real	14	18
Ponte de Pedra	15	13
Porto Colombia	12	13
Porto Estrela	11	12
Porto Primavera	12	12
Promissao	14	14
Quebra Queixo	15	18
Risoleta Neves	11	11
Rosana	15	15
Salto	13	13
Salto Grande	11	12
Salto Osorio	13	18
Salto Pilao	16	18
Salto Santiago	14	18
Santa Clara	12	17
Sao Jeronimo	12	15
Sao Roque	16	18
Sao Simao	13	12
Serra Do Facao	12	14
Simplicio	12	14
Taquarucu	15	15
Telemaco Borba	12	15
Tres Irmaos	14	14

	Volta Grande	12	13
Colombia	*Alto Anchicaya*	15	17
	Betania	12	16
	Calima	14	17
	Chivor	12	18
	Guaca	16	17
	Guadalupe III	15	14
	Guadalupe IV	15	14
	Guatape	15	16
	Guavio	12	17
	Jaguas	14	16
	La Tasajera	14	16
	Miel I	16	18
	Paraiso	16	17
	Playas	14	16
	Porce II	14	15
	Porce III	14	15
	Salvajina	13	17
	San Carlos	14	16
	Urra	15	16
Peru	*Canon del Pato*	21	21
	Cerro del Aguila	20	21
	Chaglla	17	20
	Charcani V	18	20
	Cheves	21	21
	Chimay	20	20
	El Platanal	20	21
	Huinco	21	21

La Virgen	20	20
Machu Picchu II	21	21
Mantaro (Restitucion & Santiago Antunez de Mayolo)	20	21
Matucana	21	21
Quitaracsa	0	0
San Gaban (II & III)	20	21
Yaupi	10	20
Yuncan	9	19

Appendix B – Supporting Information Chapter 3

B.1 Supplementary Figures

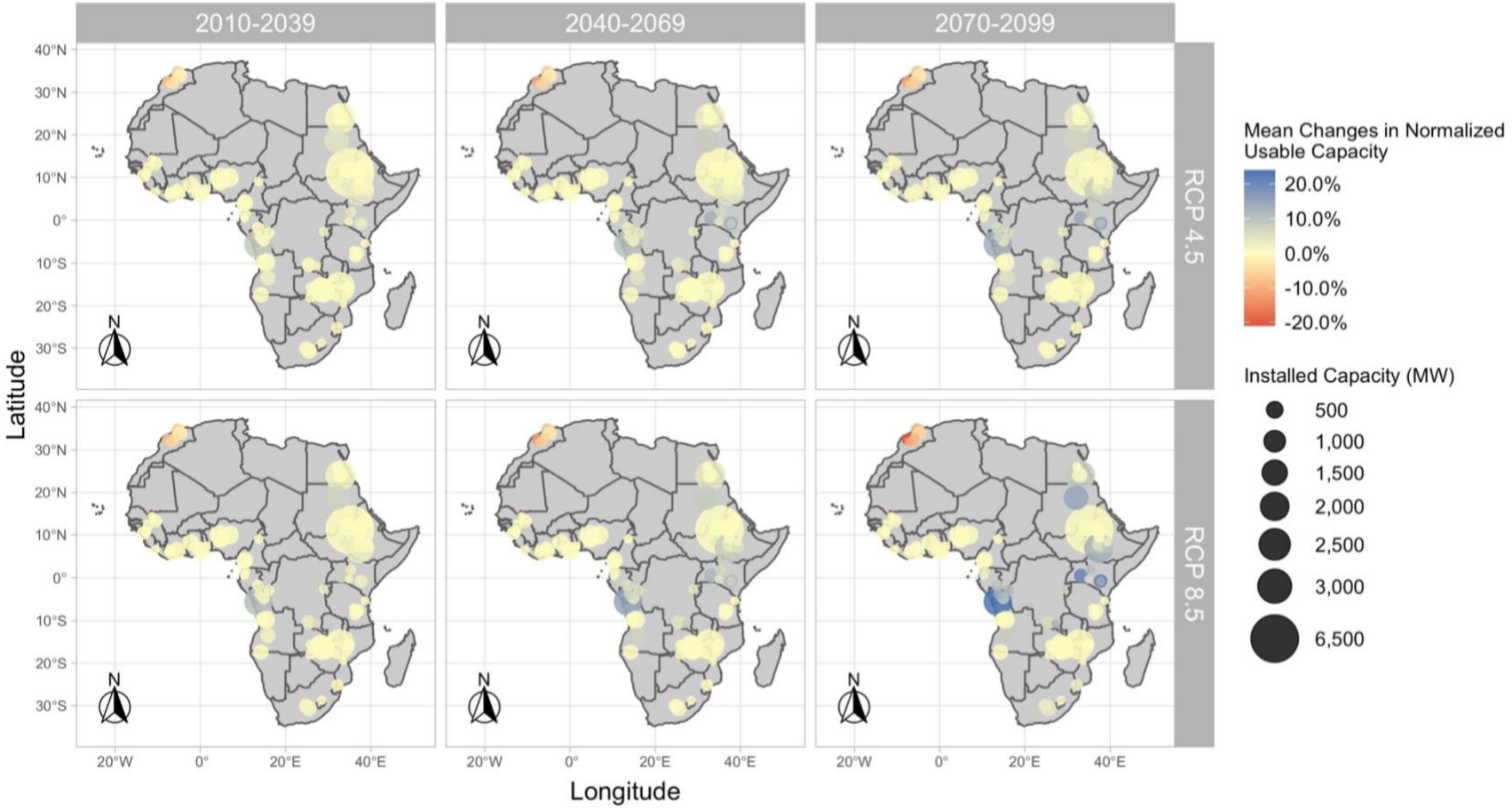

Supplementary Figure B-1 – Mean relative changes in monthly normalized usable capacity for January under RCP 4.5 and RCP 8.5. Panels show the differences in percentage points between the historical reference (1970 – 2005) and the near future (2010 – 2039), the mid-century (2040 – 2069), and the end-of-

the-century (2070 – 2099). The circle's size represents the installed capacity (MW) of the existing hydropower plants, and the intensity of the color the direction of the change (blue increases and red decreases).

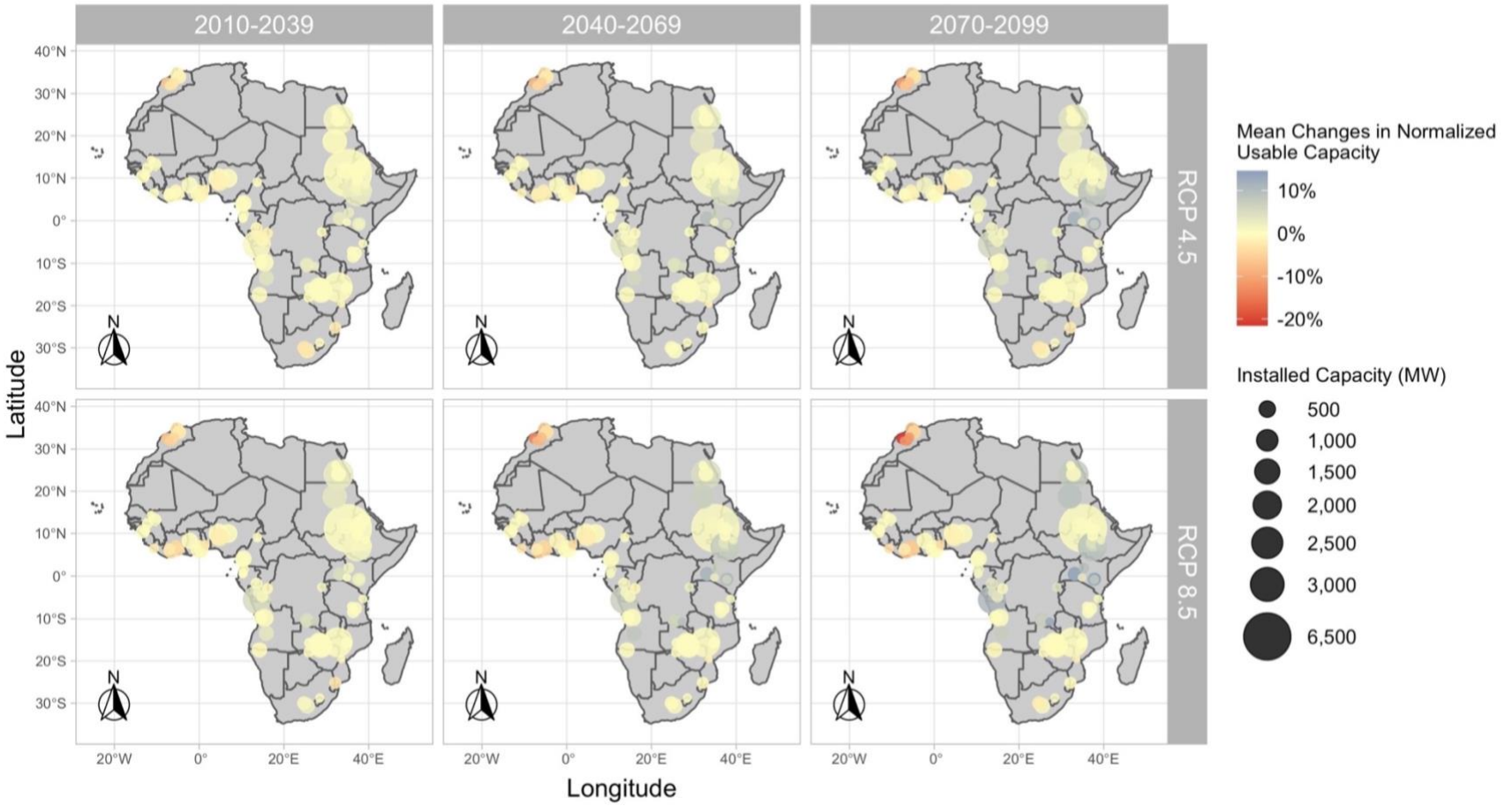

Supplementary Figure B-2 – Mean relative changes in monthly normalized usable capacity for February under RCP 4.5 and RCP 8.5. Panels show the differences in percentage points between the historical reference (1970 – 2005) and the near future (2010 – 2039), the mid-century (2040 – 2069), and the end-of-the-century (2070 – 2099). The circle's size represents the installed capacity (MW) of the existing hydropower plants, and the intensity of the color represents the direction of the change (blue increases and red decreases).

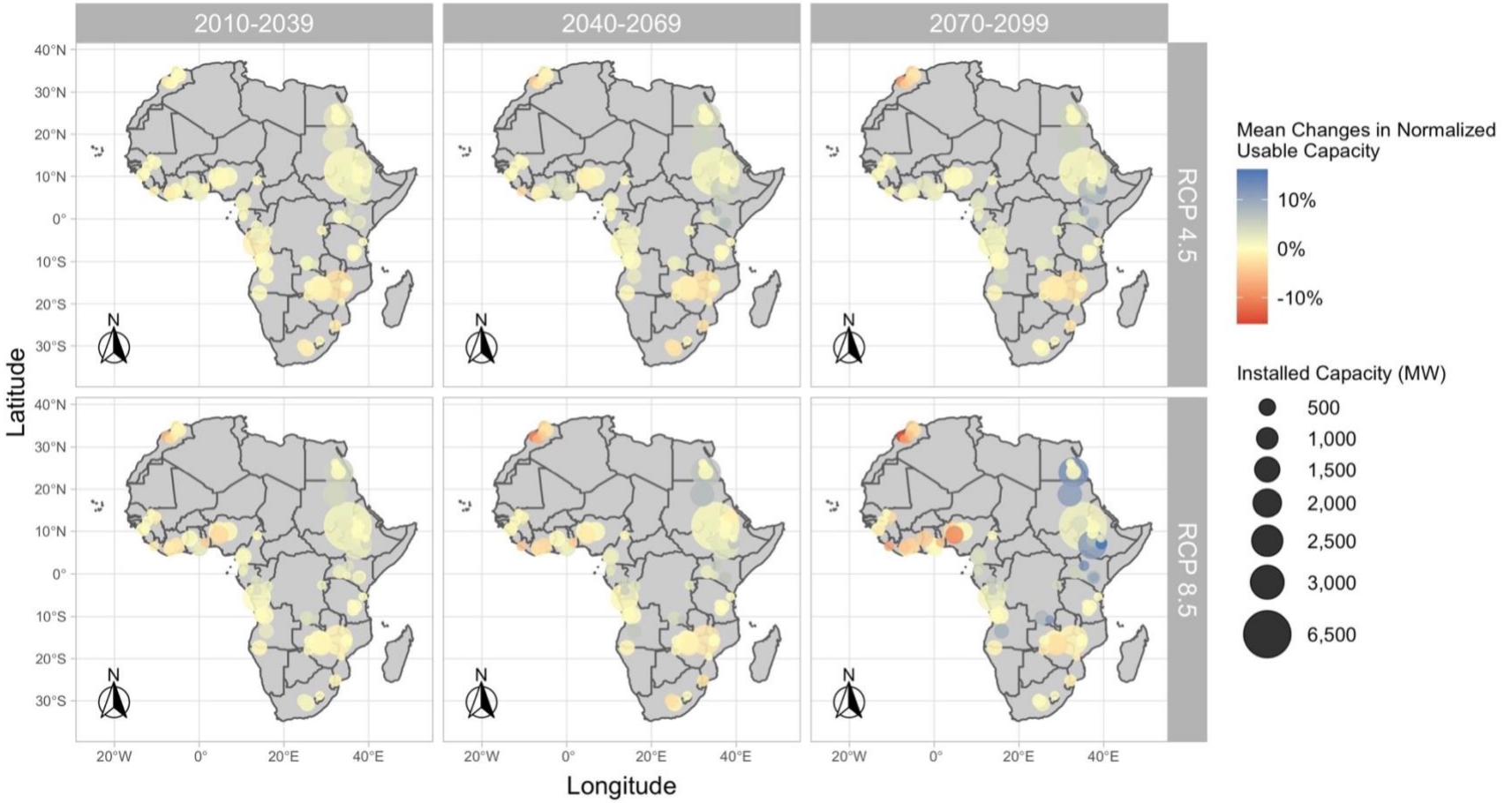

Supplementary Figure B-3 – Mean relative changes in monthly normalized usable capacity for March under RCP 4.5 and RCP 8.5. Panels show the differences in percentage points between the historical reference (1970 – 2005) and the near future (2010 – 2039), the mid-century (2040 – 2069), and the end-of-the-century (2070 – 2099). The circle's size represents the installed capacity (MW) of the existing hydropower plants, and the intensity of the color represents the direction of the change (blue increases and red decreases).

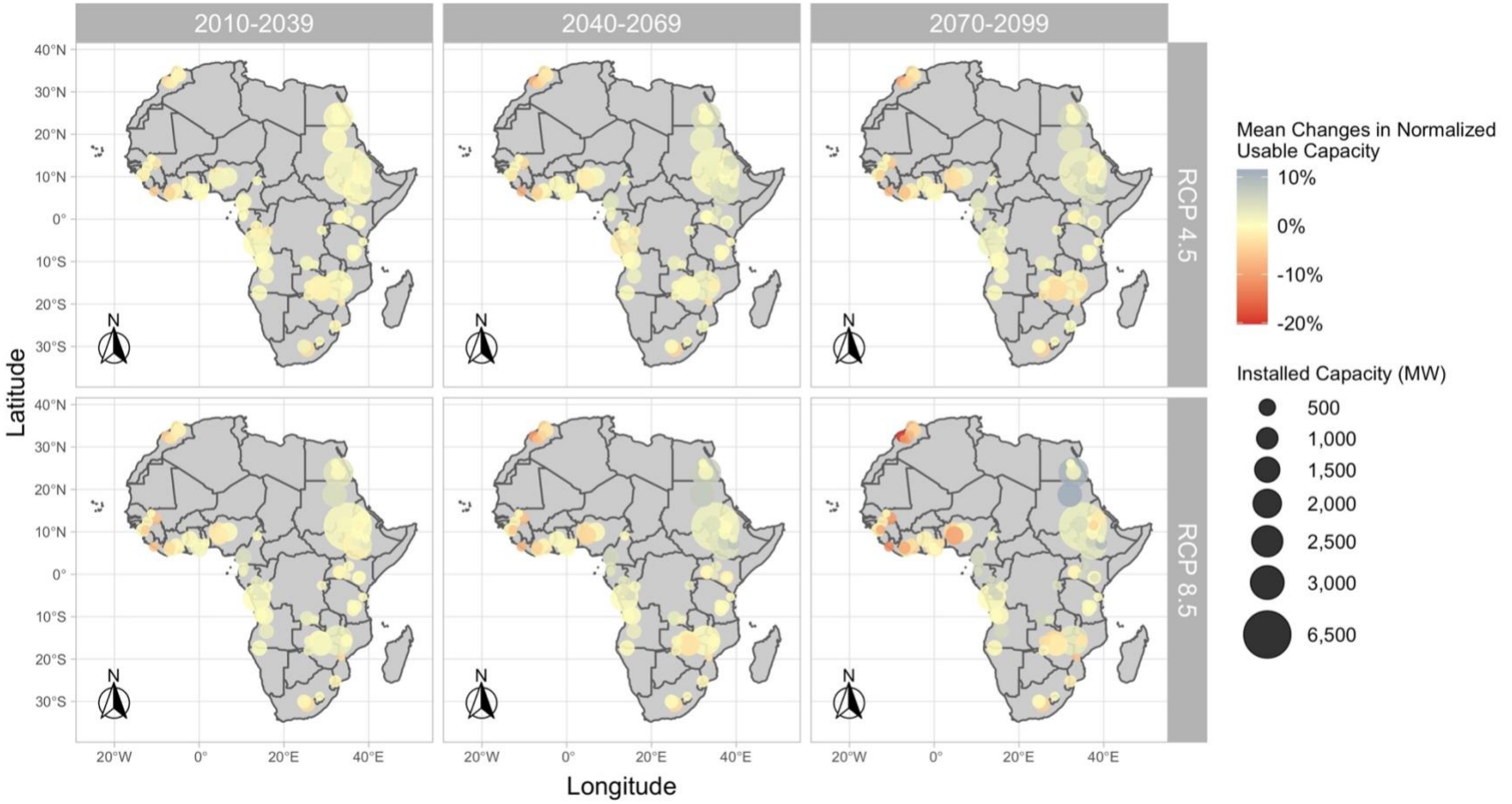

Supplementary Figure B-4 – Mean relative changes in monthly normalized usable capacity for April under RCP 4.5 and RCP 8.5. Panels show the differences in percentage points between the historical reference (1970 – 2005) and the near future (2010 – 2039), the mid-century (2040 – 2069), and the end-of-the-century (2070 – 2099). The circle's size represents the installed capacity (MW) of the existing hydropower plants, and the intensity of the color represents the direction of the change (blue increases and red decreases).

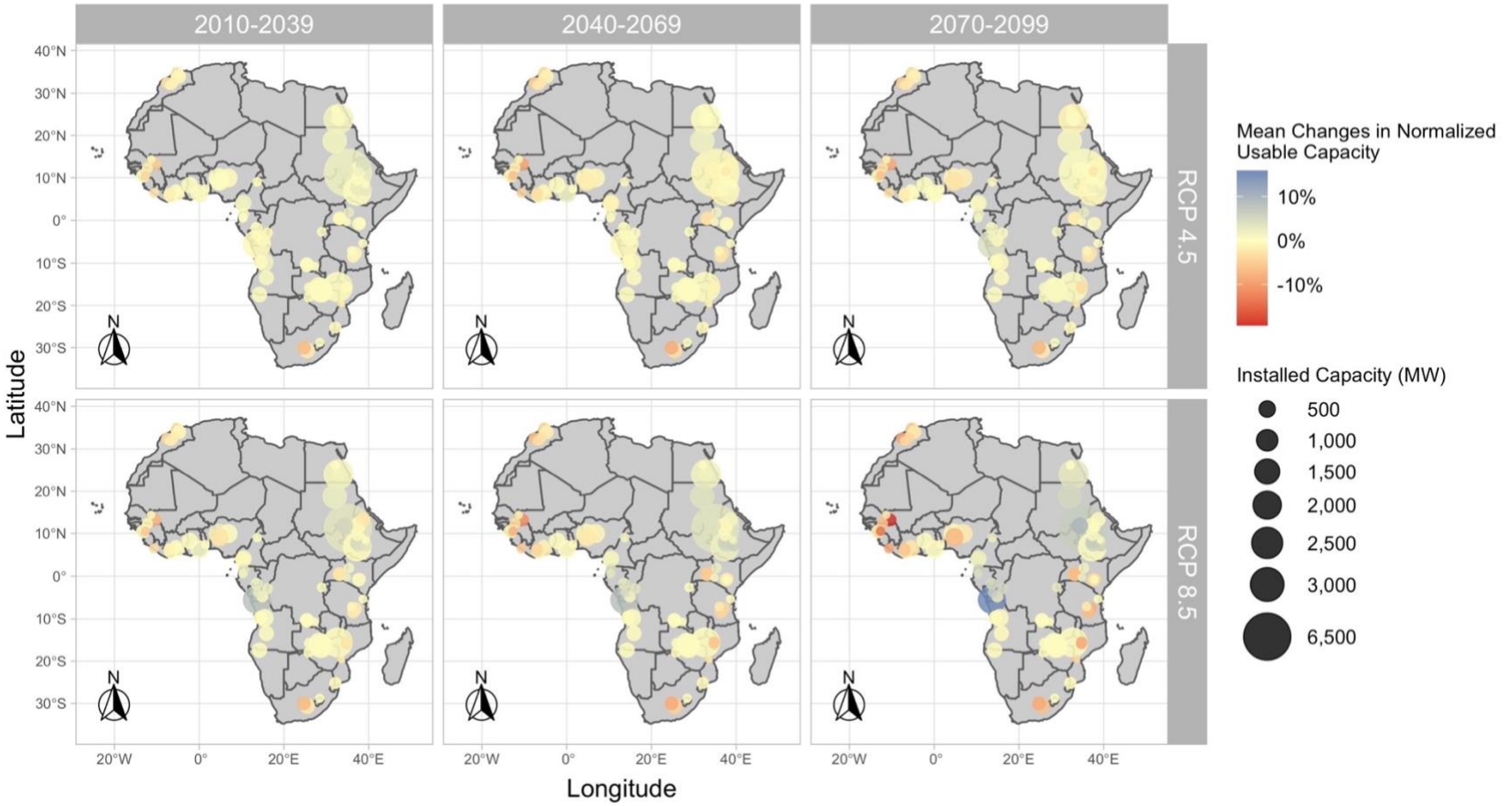

Supplementary Figure B-5 – Mean relative changes in monthly normalized usable capacity for May under RCP 4.5 and RCP 8.5. Panels show the differences in percentage points between the historical reference (1970 – 2005) and the near future (2010 – 2039), the mid-century (2040 – 2069), and the end-of-the-century (2070 – 2099). The circle's size represents the installed capacity (MW) of the existing hydropower plants, and the intensity of the color represents the direction of the change (blue increases and red decreases).

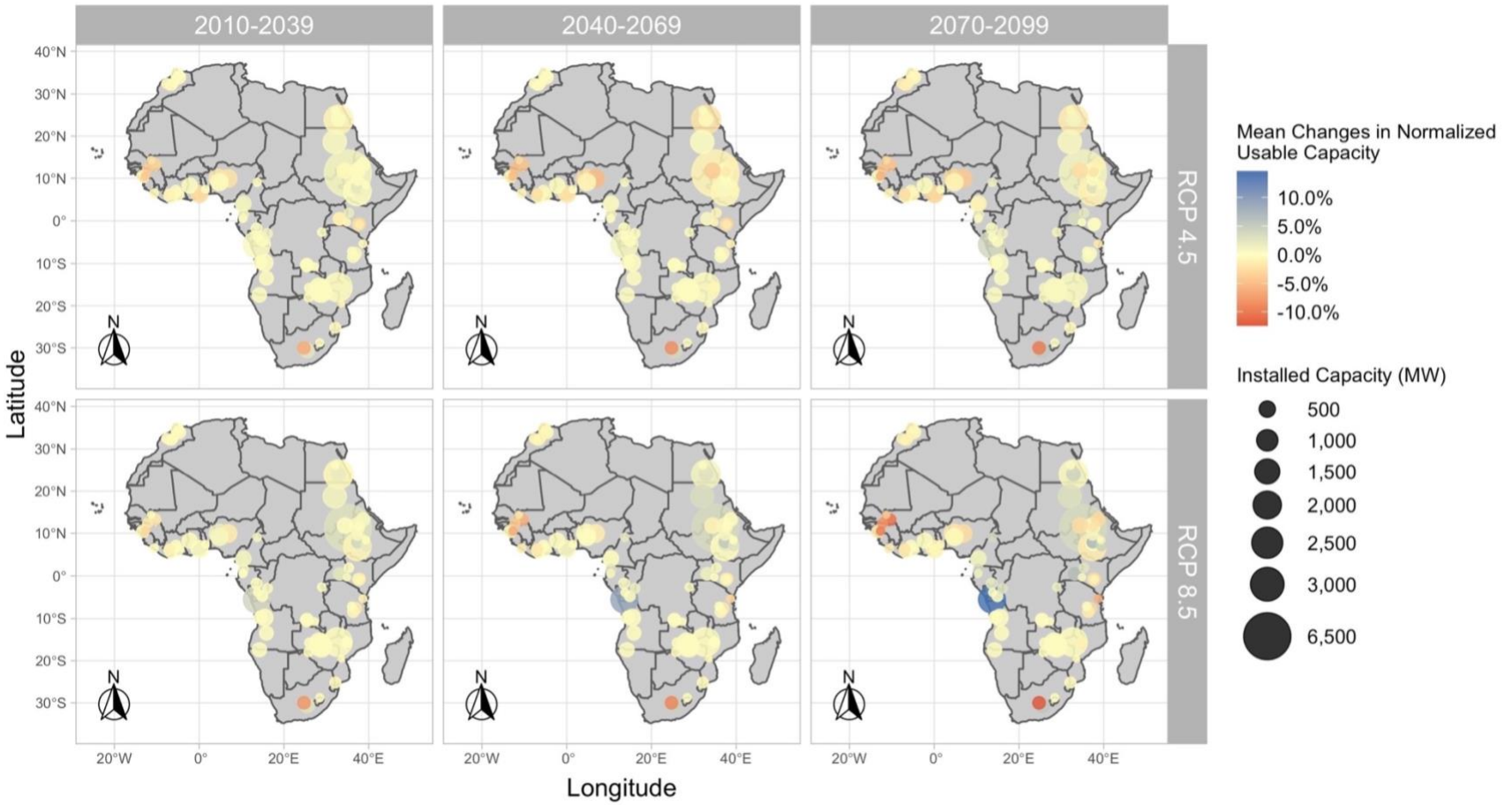

Supplementary Figure B-6 – Mean relative changes in monthly normalized usable capacity for June under RCP 4.5 and RCP 8.5. Panels show the differences in percentage points between the historical reference (1970 – 2005) and the near future (2010 – 2039), the mid-century (2040 – 2069), and the end-of-the-century (2070 – 2099). The circle's size represents the installed capacity (MW) of the existing hydropower plants, and the intensity of the color represents the direction of the change (blue increases and red decreases).

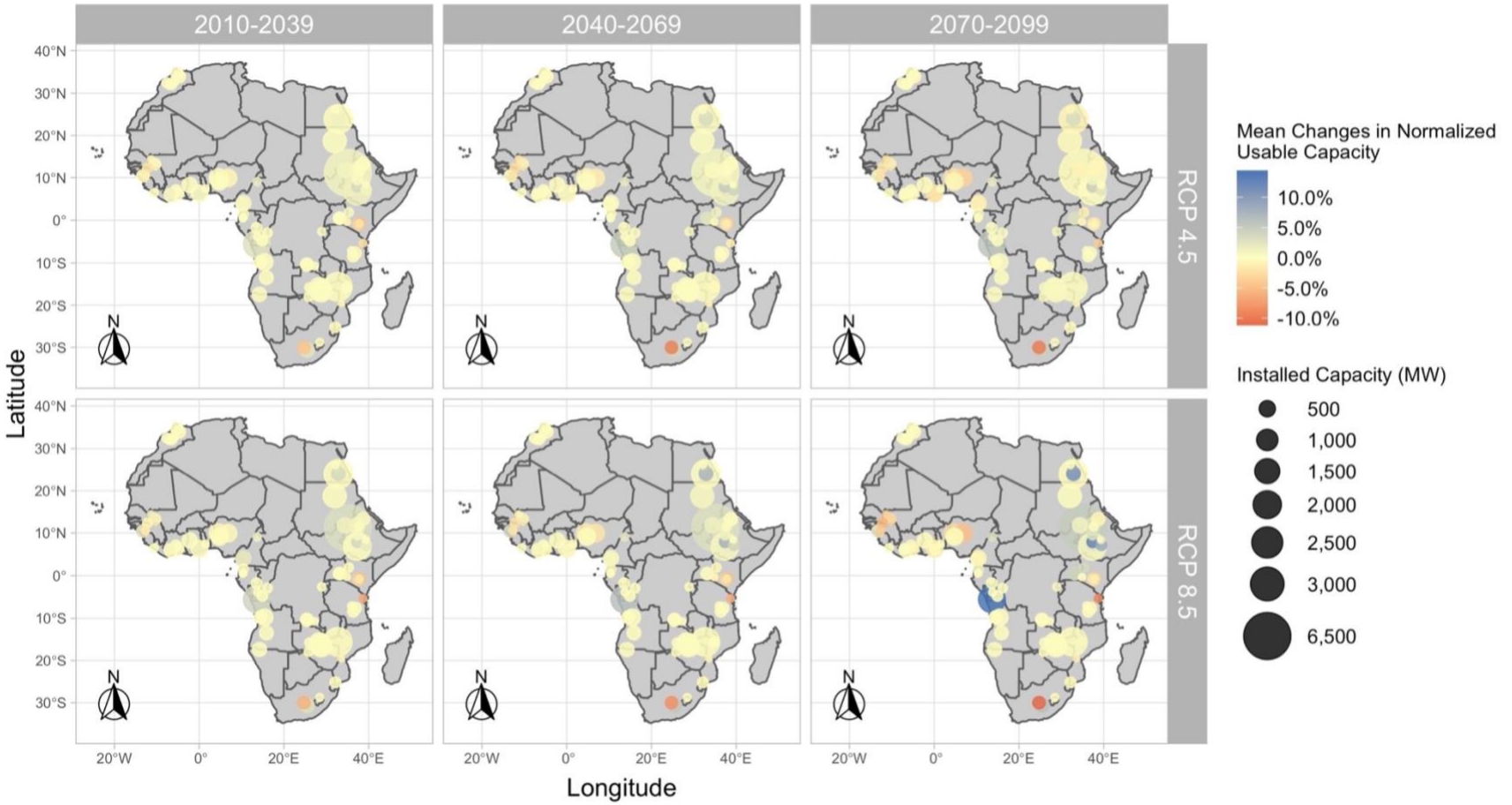

Supplementary Figure B-7 – Mean relative changes in monthly normalized usable capacity for July under RCP 4.5 and RCP 8.5. Panels show the differences in percentage points between the historical reference (1970 – 2005) and the near future (2010 – 2039), the mid-century (2040 – 2069), and the end-of-the-century (2070 – 2099). The circle's size represents the installed capacity (MW) of the existing hydropower plants, and the intensity of the color represents the direction of the change (blue increases and red decreases).

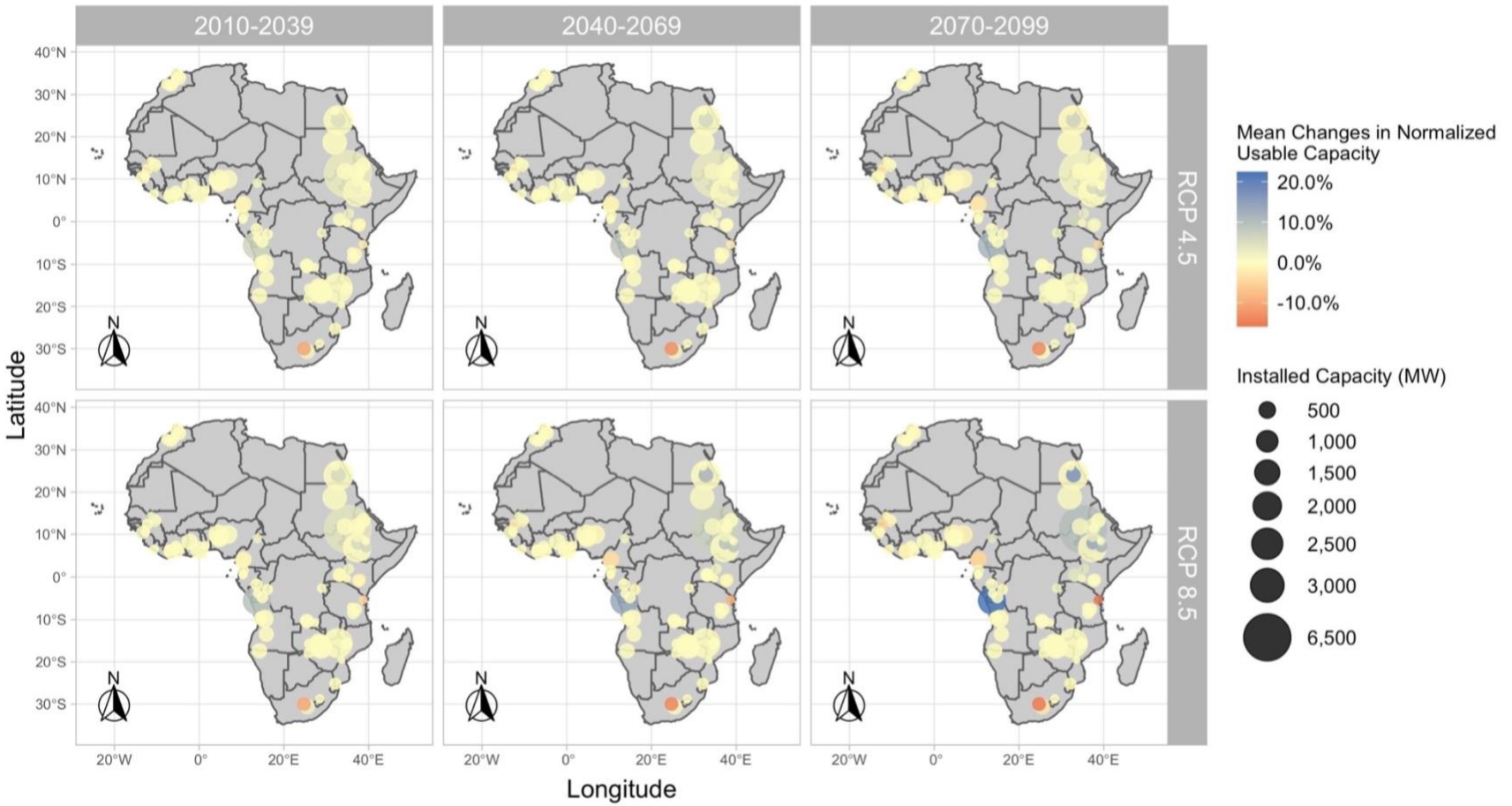

Supplementary Figure B-8 – Mean relative changes in monthly normalized usable capacity for August under RCP 4.5 and RCP 8.5. Panels show the differences in percentage points between the historical reference (1970 – 2005) and the near future (2010 – 2039), the mid-century (2040 – 2069), and the end-of-the-century (2070 – 2099). The circle's size represents the installed capacity (MW) of the existing hydropower plants, and the intensity of the color represents the direction of the change (blue increases and red decreases).

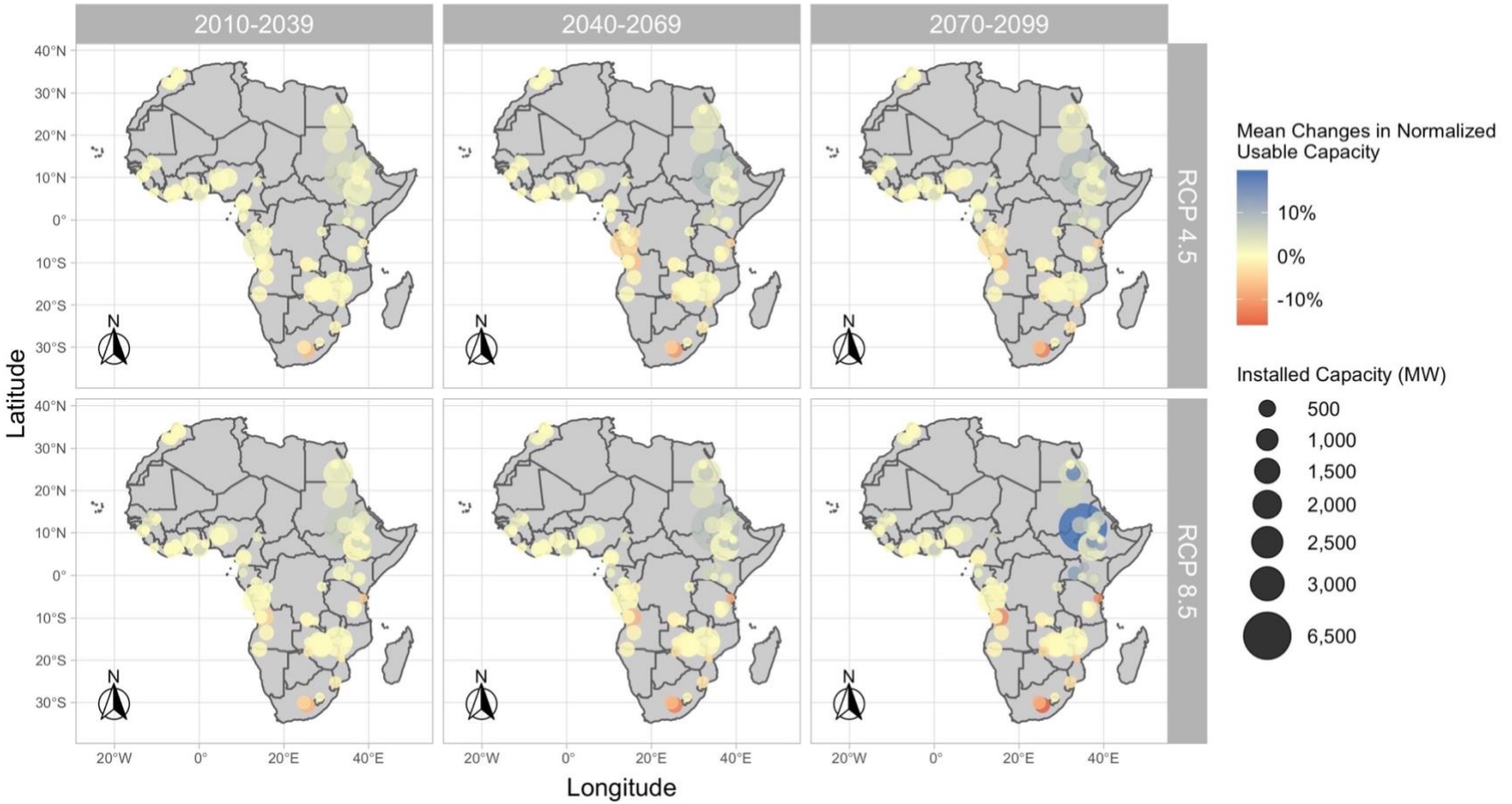

Supplementary Figure B-9 – Mean relative changes in monthly normalized usable capacity for September under RCP 4.5 and RCP 8.5. Panels show the differences in percentage points between the historical reference (1970 – 2005) and the near future (2010 – 2039), the mid-century (2040 – 2069), and the end-of-the-century (2070 – 2099). The circle's size represents the installed capacity (MW) of the existing hydropower plants, and the intensity of the color represents the direction of the change (blue increases and red decreases).

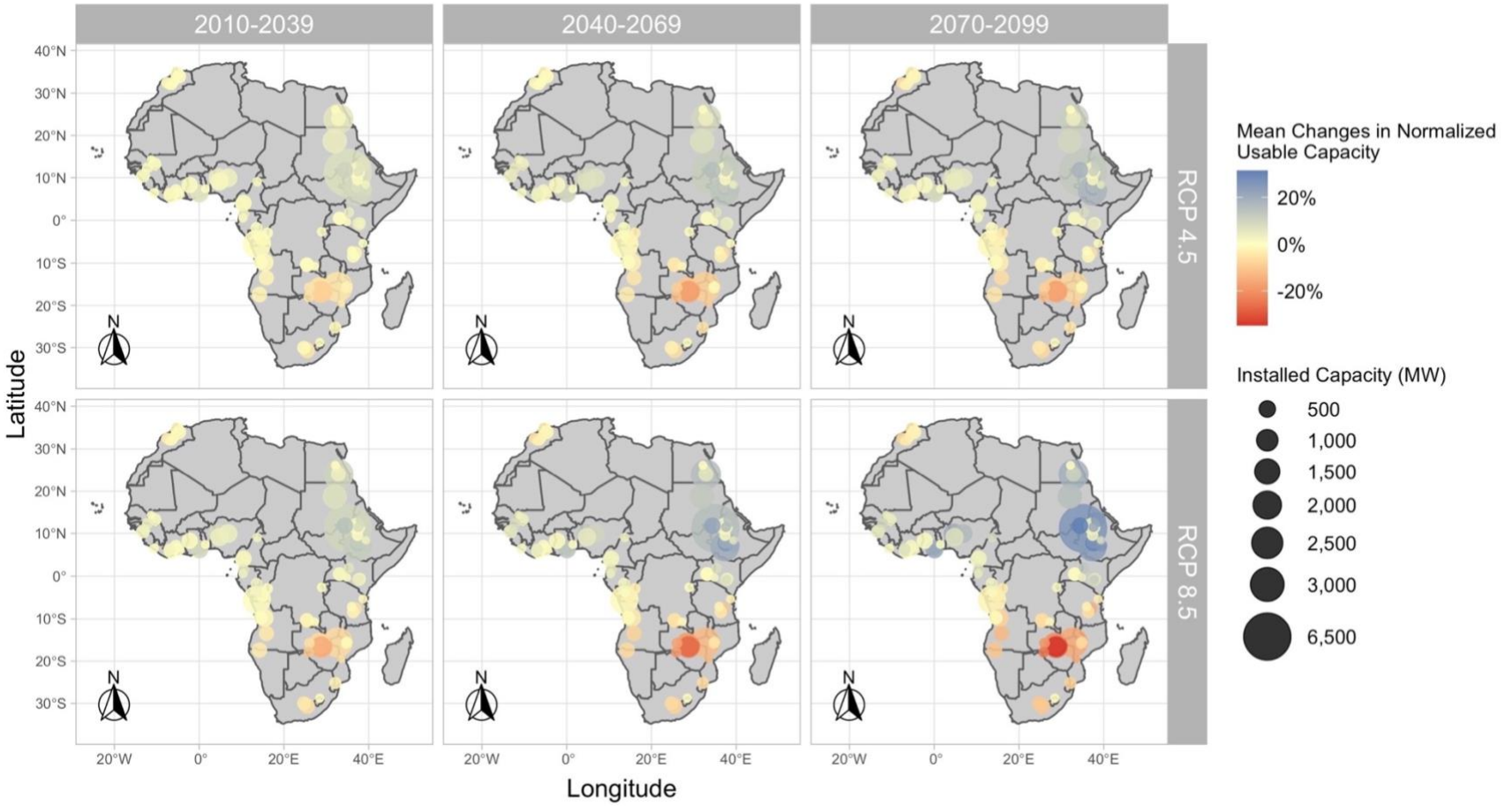

Supplementary Figure B-10 – Mean relative changes in monthly normalized usable capacity for October under RCP 4.5 and RCP 8.5. Panels show the differences in percentage points between the historical reference (1970 – 2005) and the near future (2010 – 2039), the mid-century (2040 – 2069), and the end-of-the-century (2070 – 2099). The circle's size represents the installed capacity (MW) of the existing hydropower plants, and the intensity of the color represents the direction of the change (blue increases and red decreases).

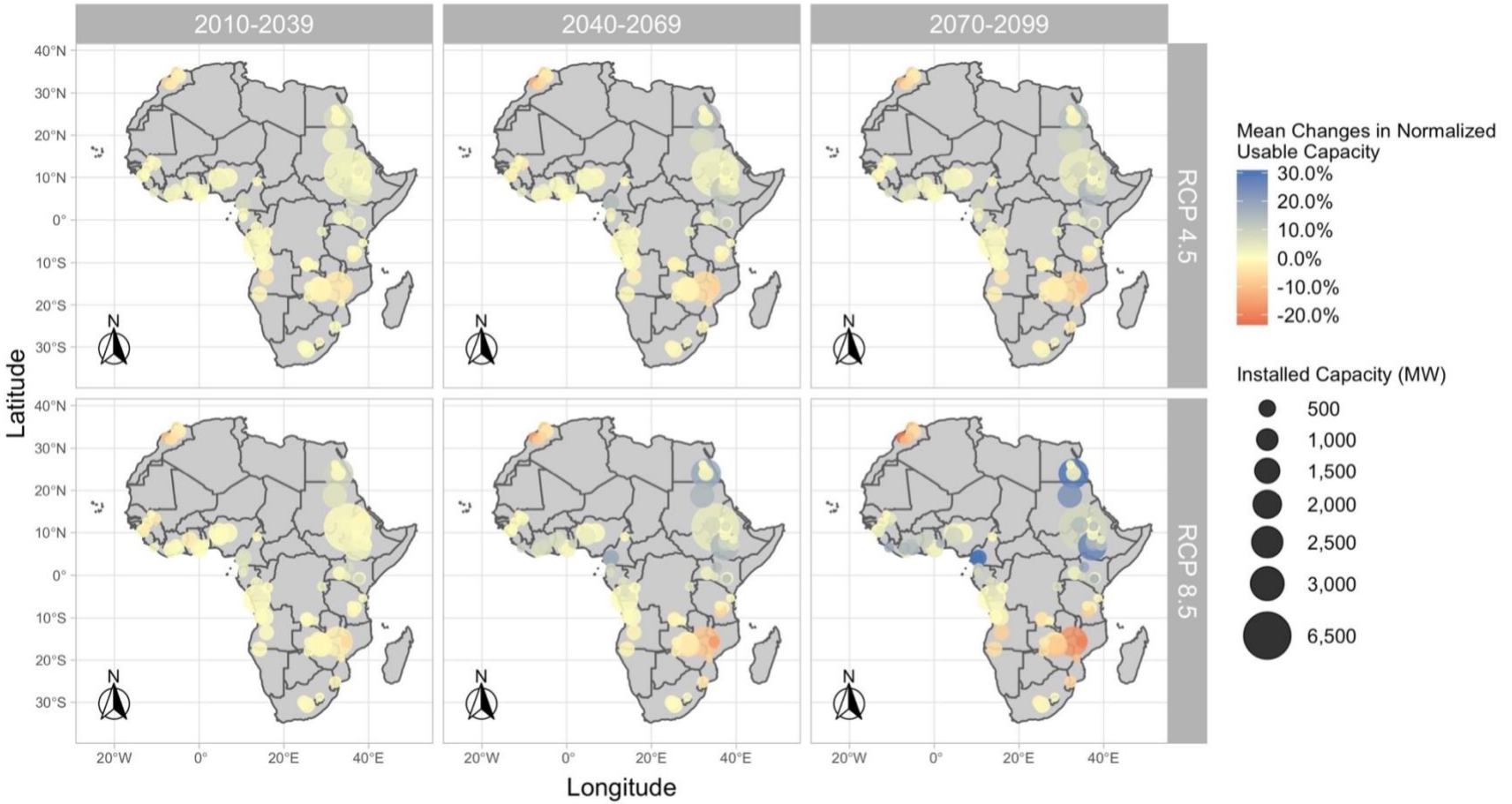

Supplementary Figure B-11 – Mean relative changes in monthly normalized usable capacity for November under RCP 4.5 and RCP 8.5. Panels show the differences in percentage points between the historical reference (1970 – 2005) and the near future (2010 – 2039), the mid-century (2040 – 2069), and the end-of-the-century (2070 – 2099). The circle's size represents the installed capacity (MW) of the existing hydropower plants, and the intensity of the color represents the direction of the change (blue increases and red decreases).

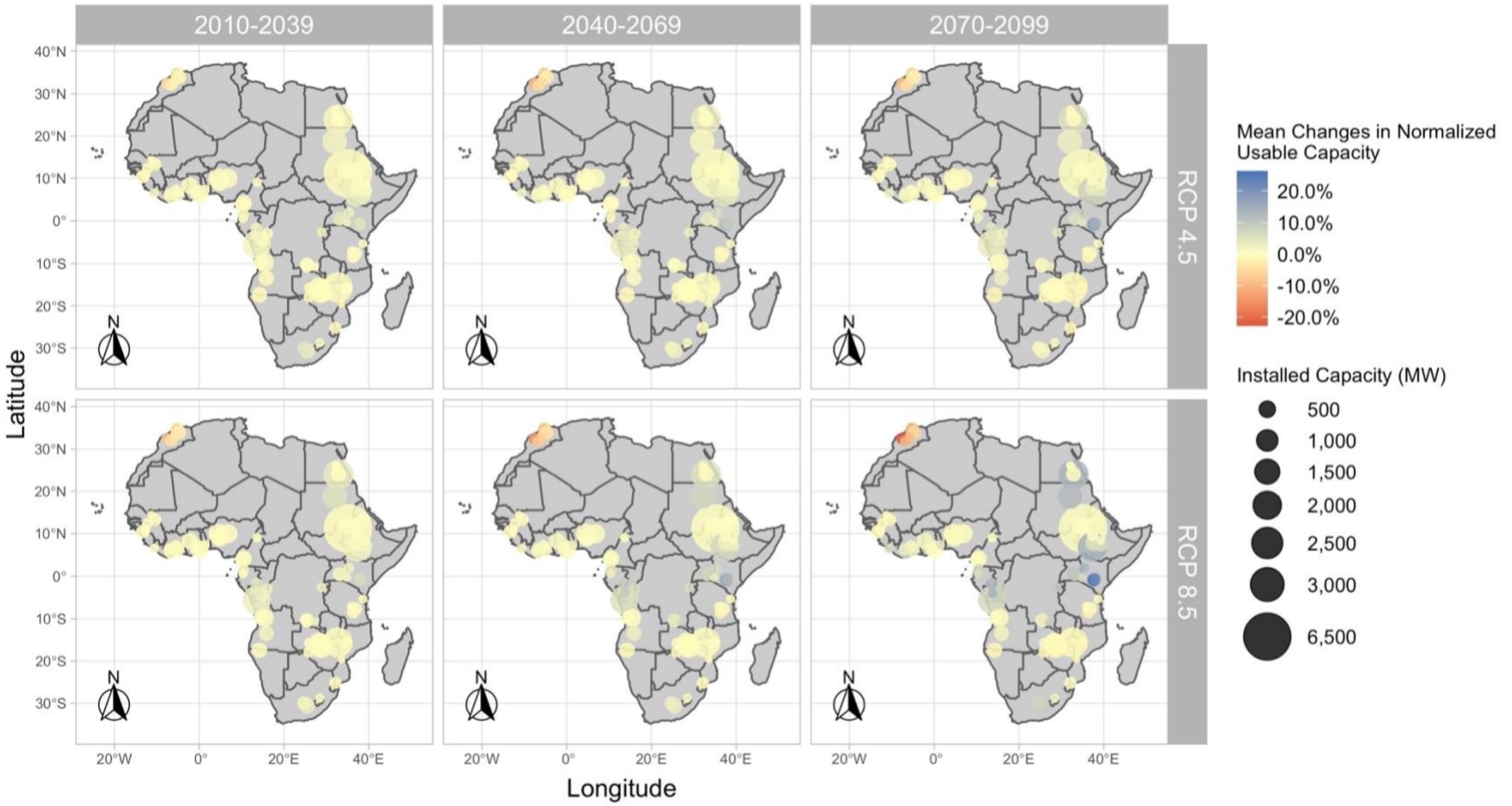

Supplementary Figure B-12 – Mean relative changes in monthly normalized usable capacity for December under RCP 4.5 and RCP 8.5. Panels show the differences in percentage points between the historical reference (1970 – 2005) and the near future (2010 – 2039), the mid-century (2040 – 2069), and the end-of-the-century (2070 – 2099). The circle's size represents the installed capacity (MW) of the existing hydropower plants, and the intensity of the color represents the direction of the change (blue increases and red decreases).

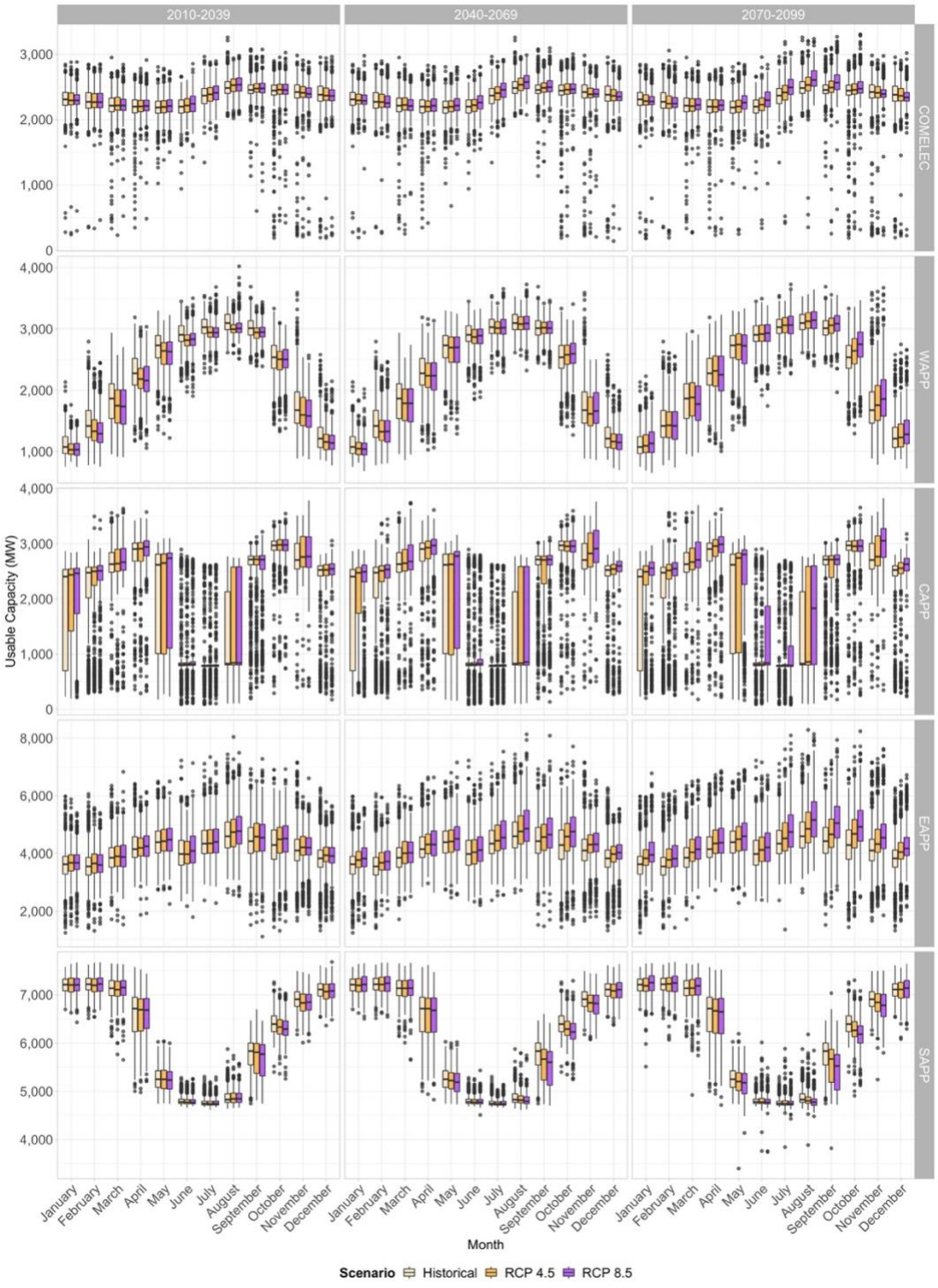

Supplementary Figure B-13 – Aggregated usable capacity for the COMELEC, CAPP, EAPP, SAPP, and WAPP. The boxplots present the results from the multi-model ensemble of 21 GCM experiments for the 1970-2005 historical reference (wheat), RCP 4.5 (orange), and RCP 8.5 (purple). Each column presents the time frame of the analysis: near future (2010 – 2039), mid-century (2040 – 2069), and end-of-century (2070 – 2099). The scales of each of the panels are different depending on the power pool.

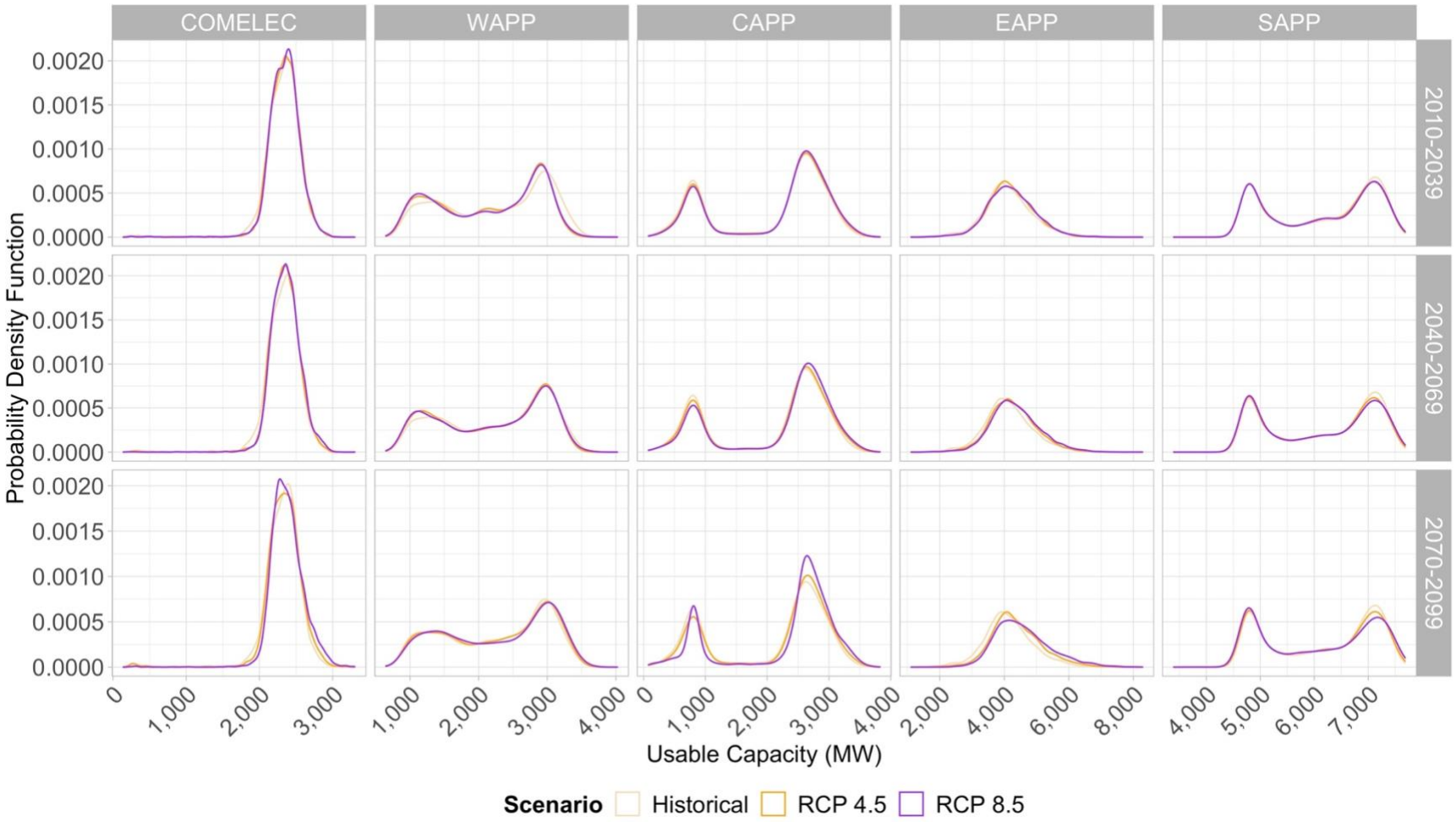

Supplementary Figure B-14 | Probability Density Function of Aggregated Multi-Model Ensemble Power Pool Usable Capacity Time Series. The Y axis of the plot represents the probability for a usable capacity (MW) value for the power pool. We include all five power pools in the analysis (COMELEC, WAPP, CAPP, EAPP, and SAPP). We present three scenarios (historical reference, RCP 4.5, and RCP 8.5) and three time-frames (early century – 2010-2039, mid-century – 2040-2069, and end of the century – 2070-2099). We present the historical reference in "wheat" color, RCP 4.5 in "orange" color, and RCP 8.5 in "purple" color.

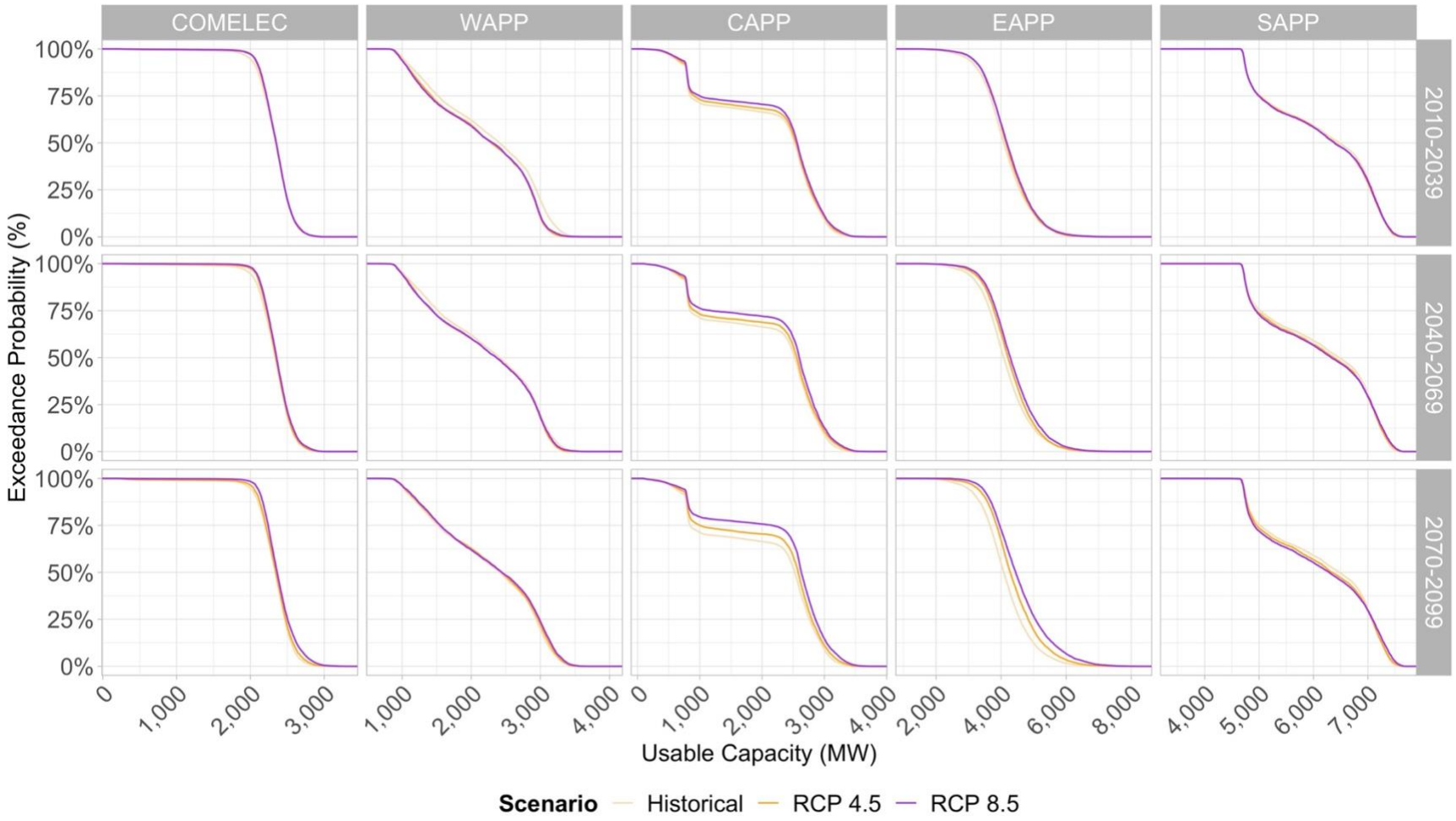

Supplementary Figure B-15 | Exceedance Probability of Aggregated Multi-Model Ensemble Power Pool Usable Capacity Time Series. The Y axis of the plot represents the exceedance probability of usable capacity (MW) for the power pool. We include all five power pools in the analysis (COMELEC, WAPP, CAPP, EAPP, and SAPP). We present three scenarios (historical reference, RCP 4.5, and RCP 8.5) and three time-frames (early century – 2010-2039, mid-century – 2040-2069, and end of the century – 2070-2099). We present the historical reference in "wheat" color, RCP 4.5 in "orange" color, and RCP 8.5 in "purple" color.

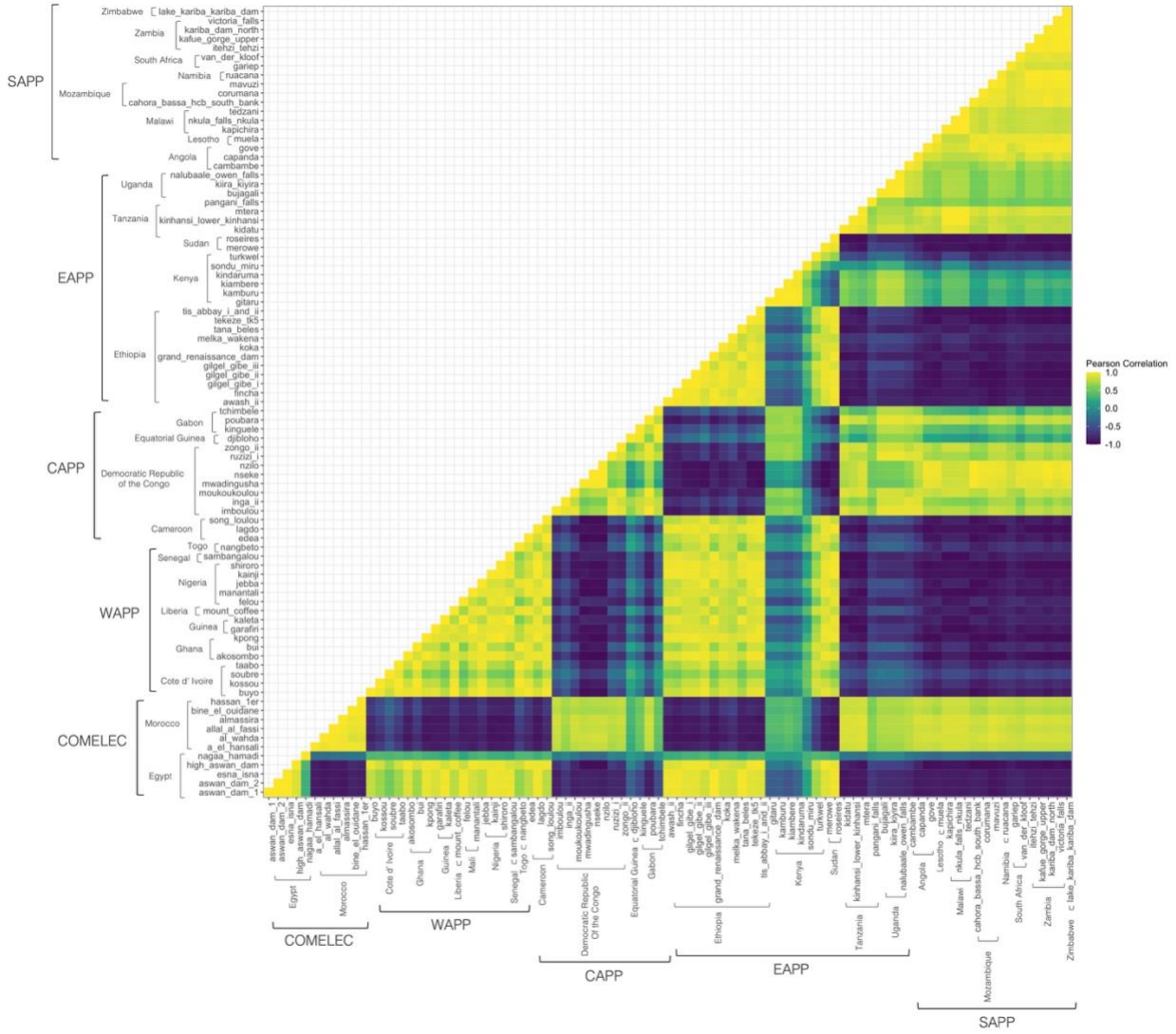

Supplementary Figure B-16 – Temporal correlations (Pearson correlation – Historical) for each pair of power plants in the analysis. The darker the color the higher the complements between power plants. Highly temporally complementary power plants have a Pearson correlation coefficient lower than -0.5.

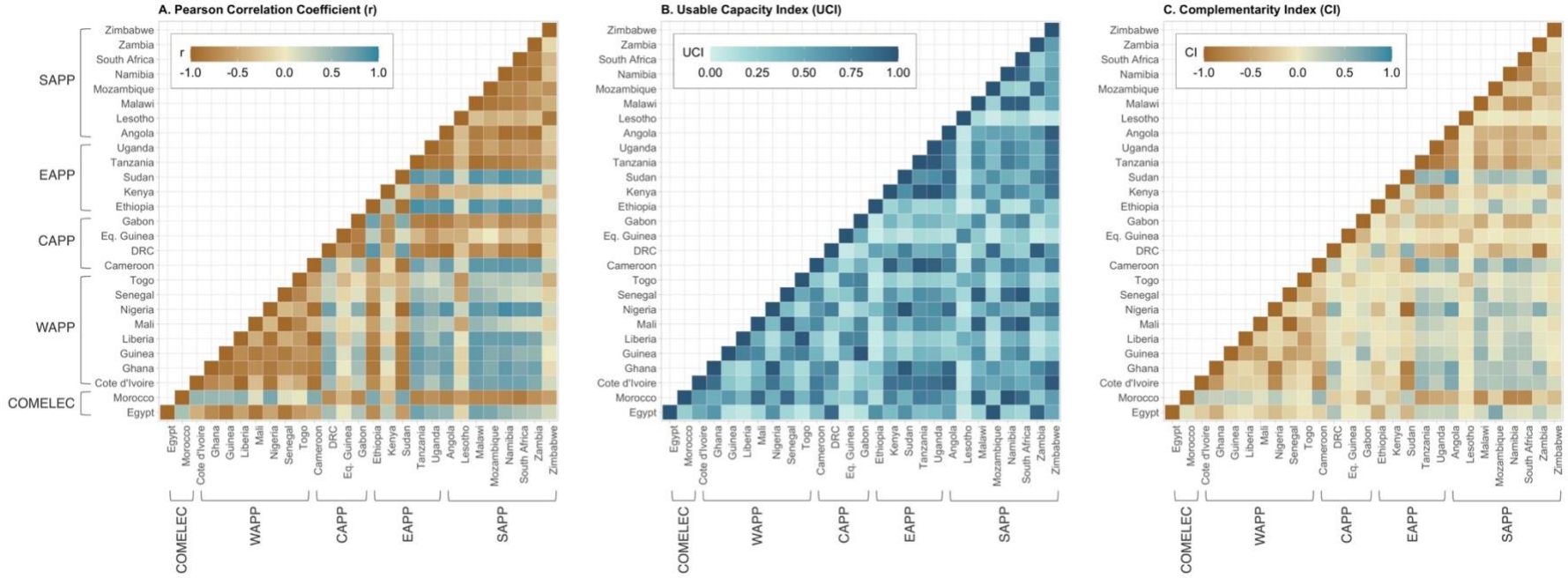

Supplementary Figure B-17 – Aggregated country-level complementarity indexes in the historical period (1970-2005). A. Country-level Pearson Correlation Coefficient (r). The values range from -1 to +1. The closer to -1, the more temporally complementary the pair of countries. B. Country-level Usable Capacity Complementarity (UCI). The values range from 0 to +1. The closer to +1, the more complementary the pair of countries. C. Country-level Complementarity Index (CI). The values range from -1 to +1. The closer to +1, the more complementary the countries are. See Methods and Supplementary Note B.3.1 for the description of each of the metrics.

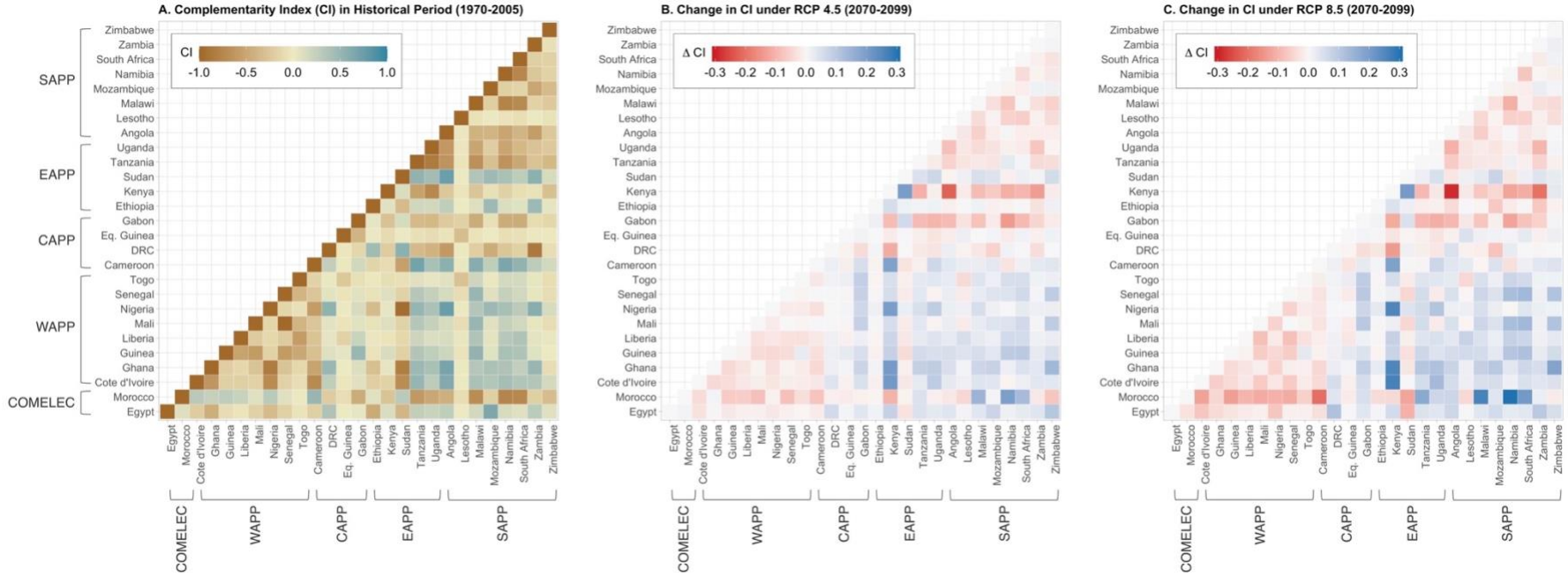

Supplementary Figure B-18 – Differences in the Complementarity Index (CI) between the historical reference and future projections under two emissions scenarios. A) We present the country-level complementarity index for each pair of countries in the analysis for the historical reference (1970 – 2005). Panel A is the same plot as in Supplementary Fig. B-15, panel C. The CI values range between -1 and +1—the closer to +1, the more appealing the relationship between countries. The complementarity index accounts for the usable capacity's timing (r) and the power plants' size within the country's electricity mix. (UCI). In B & C, we present the absolute change in the complementarity index for each pair presented in A. for the end of the century (2070-2099) under RCP 4.5 and 8.5, respectively. Positive changes (blue) represent an increase in the complementarity between the pair, while negative changes (red) represent decreases in complementary relationships. Note that each panel has its own legend and scale.

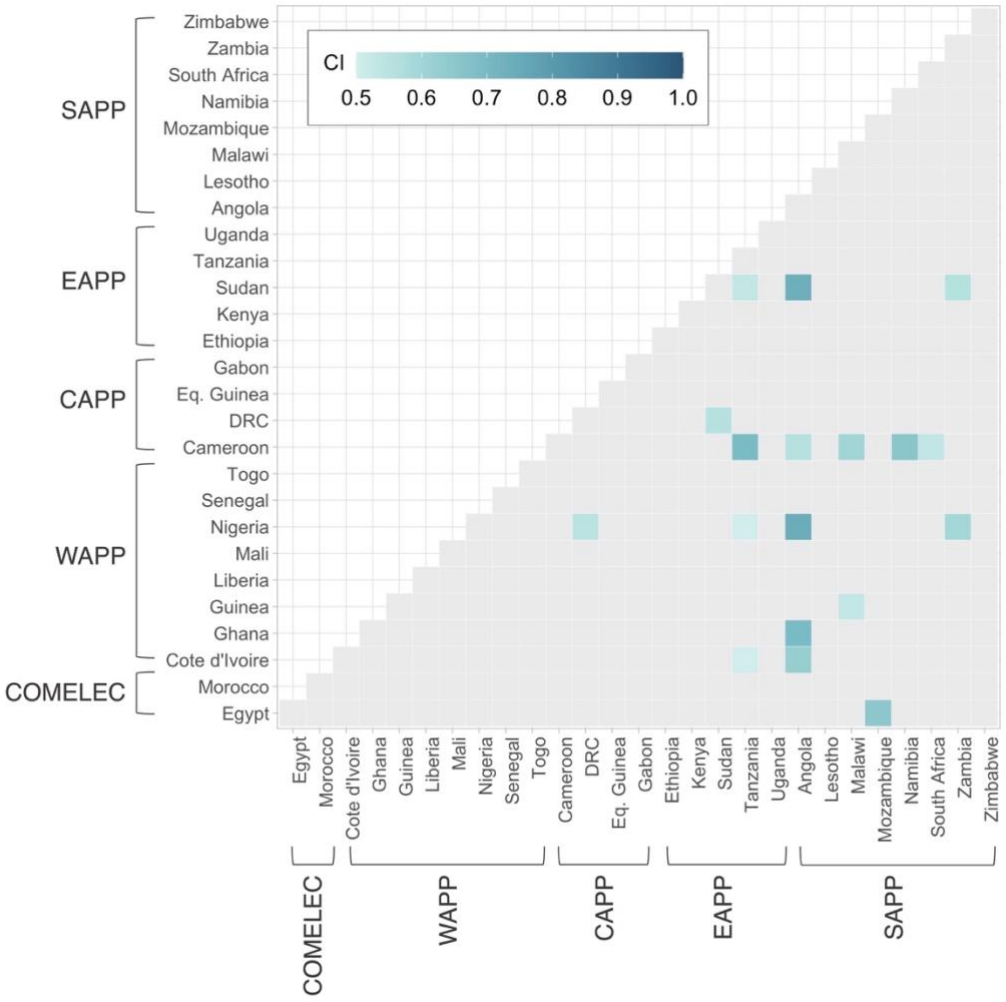

Supplementary Figure B-19 – Highly complementary countries in the historical reference period (1970-2005). We filter the results for the Complementarity Index (CI) shown in Supplementary Figs. B-15 and B-16, to obtain the highest complementary pairs of countries (CI > 0.5). We use these results paired with Supplementary Table B-4 to generate interconnection scenarios (Supplementary Note B.3.2). There are currently no existing interconnections between the countries that would allow for electricity flows between them.

B.2 Supplementary Tables

Supplementary Table B-1 – Power plants included in the analysis across the Maghreb Electricity Committee (COMELEC), Central African Power Pool (CAPP), Eastern Africa Power Pool (EAPP), Southern African Power Pool (SAPP), and West African Power Pool (WAPP). The table presents the list of power plants organized by power pool and country. Power plants are presented in descending order of installed capacity (in Megawatts).

Power Pool [MW]	Country [MW]	Power Plant	Longitude	Latitude	Installed Capacity (MW)
COMELEC [3,744]	Egypt [2,842]	High Aswan Dam	32.88	23.97	2,100
		Aswan Dam 1	32.86	24.03	322
		Aswan Dam 2	32.86	24.03	270
		Esna (Isna)	32.55	25.31	86
		Nagaa Hamadi	32.14	26.15	64
	Morocco [902]	Allal Al Fassi	-4.68	33.93	240
		Al Wahda	-5.20	34.60	240
		Bine El Ouidane	-6.46	32.11	135
		Almassira	-7.64	32.48	128
		A. El Hansali	-5.89	32.69	92
		Hassan 1er	-7.08	31.85	67
WAPP [4,695]	Cote d'Ivoire [824]	Soubre	-6.64	5.79	275
		Taabo	-5.08	6.21	210
		Kossou	-5.47	7.03	174
		Buyo	-7.03	6.24	165
	Ghana [1,100]	Akosombo	0.06	6.30	540
		Bui	-2.24	8.28	400
		Kpong	0.13	6.12	160
	Guinea [315]	Kaleta	-13.28	10.46	240
		Garafiri	-12.66	10.53	75
	Liberia [88]	Mount Coffee	-10.65	6.51	88
	Mali	Manantali	-10.43	13.20	200

	[262]	Felou Hydroelectric Power Plant Mali	-11.35	14.36	62
	Nigeria [1,920]	Kainji	4.61	9.86	760
		Shiroro	6.83	9.97	600
		Jebba	4.79	9.14	560
	Senegal [120]	Sambangalou	-12.19	12.37	120
	Togo [66]	Nangbeto	1.44	7.42	66
CAPP [3,912]	Cameroon [750]	Song Loulou	10.46	4.08	406
		Edea	10.13	3.81	264
		Lagdo	13.69	9.06	80
	Democratic Republic of the Congo [2,756]	Inga II	13.62	-5.53	1,775
		Nseke	25.41	-10.30	260
		Nzilo	25.45	-10.50	228
		Zongo II	14.91	-4.78	150
		Imboulou	16.13	-2.93	120
		Ruzizi I	28.90	-2.63	81
		Moukoukoulou	13.76	-3.89	74
		Mwadingusha	27.24	-10.75	68
	Equatorial Guinea [120]	Djibloho	10.47	1.58	120
	Gabon [286]	Poubara	13.55	-1.77	160
		Tchimbele	10.41	0.62	68
		Kinguele	10.28	0.46	58
EAPP [13,708]	Ethiopia [10,164]	Grand Renaissance Dam	35.09	11.22	6,450
		Gilgel Gibe III	37.30	6.84	1,870
		Tana Beles	37.21	11.68	460
		Gilgel Gibe II	37.56	7.75	420
		Tekeze/TK5	38.71	13.30	300
		Gilgel Gibe I	37.39	7.93	185

		Melka Wakena	39.43	7.17	153
		Fincha	37.37	9.56	134
		Tis Abbay I and II	37.59	11.48	85
		Awash II	39.35	8.39	64
		Koka	39.16	8.47	43
	Kenya [721]	Gitaru	37.68	-0.81	225
		Kiambere	37.91	-0.64	165
		Turkwel	35.34	1.91	106
		Kamburu	37.69	-0.81	93
		Kindaruma	37.81	-0.81	72
		Sondu Miru	34.85	-0.34	60
	Sudan [1,665]	Merowe	31.99	18.72	1,250
		Roseires	34.39	11.80	415
	Tanzania [528]	Kidatu	36.91	-7.64	200
		Kinhansi/Lower Kinhansi	36.35	-8.40	180
		Mtera	35.99	-7.14	80
		Pangani Falls	38.65	-5.35	68
	Uganda [620]	Bujagali	33.13	0.49	250
		Kiira/Kiyira	33.18	0.45	200
		Nalubaale (Owen falls)	33.18	0.44	180
SAPP [7,744]	Angola [1,100]	Capanda	15.46	-9.79	520
		Gove	15.87	-13.45	320
		Cambambe	14.48	-9.75	260
	Lesotho [72]	'Muela	28.45	-28.78	72
	Malawi [374]	Nkula Falls/Nkula	34.82	-15.51	135
		Kapichira	34.75	-15.89	128
		Tedzani	34.78	-15.55	111
	Mozambique [2,293]	Cahora Bassa (HCB South Bank)	32.71	-15.59	2,075
		Corumana	32.13	-25.22	166

	Mavuzi	33.49	-19.52	52
Namibia [347]	Ruacana	14.22	-17.38	347
South Africa [600]	Gariep	25.50	-30.62	360
	Van der Kloof	24.73	-29.99	240
Zambia [2,208]	Kariba Dam North	28.76	-16.52	1,080
	Kafue Gorge Upper	28.42	-15.81	900
	Itehzi - Tehzi	26.02	-15.76	120
	Victoria Falls	25.86	-17.93	108
Zimbabwe [750]	Lake Kariba/Kariba Dam	28.76	-16.52	750

Supplementary Table B-2 – Interannual variability of usable capacity by country and power pool, measured as the coefficient of variation in usable capacity under RCP4.5. We aggregate (sum) the individual usable hydropower capacity time series of each power plant to calculate country-level usable capacity. Columns present the historical reference variability (1970 – 2005) and the projected variability for RCP 4.5 (2010 – 2039, 2040 – 2069, and 2070 – 2099). The higher the interannual variability (closer to 1), the more variable the supply across years. The direction of changes column represents increases (purple arrow) and decreases (orange arrow) by the end of the century. The darker the shading in the "Historical" column, the highest the variability.

Country [MW]	Historical	RCP 4.5			Direction of Changes
	1970 – 2005	2010 – 2039	2040 – 2069	2070 – 2099	
Egypt [2,842]	0.06	0.04*	0.04*	0.08	↑
Morocco [902]	0.26	0.24***	0.24***	0.32	↑
COMELEC [3,744]	**0.05**	**0.04*** **	**0.04*** **	**0.08**	↑
Cote d'Ivoire [824]	0.05	0.05	0.05	0.05	↑
Ghana [1,100]	0.05	0.05*	0.05***	0.05*	↓
Guinea [315]	0.09	0.11	0.11	0.11	↑
Liberia [88]	0.09	0.09	0.10	0.11	↑
Mali [262]	0.02	0.02	0.02	0.03*	↑
Nigeria [1,920]	0.10	0.09***	0.10***	0.12	↑
Senegal [120]	0.02	0.02	0.02	0.03*	↑
Togo [66]	0.02	0.02*	0.03	0.03	↑
WAPP [4,695]	**0.05**	**0.05*** **	**0.05*** **	**0.06**	↑
Cameroon [750]	0.12	0.11	0.12	0.13	↑
Democratic Republic of the Congo [2,756]	0.13	0.13	0.14*	0.14	↑
Equatorial Guinea [120]	0.17	0.17	0.20	0.20	↑
Gabon [286]	0.13	0.13	0.15	0.16	↑
CAPP [3,912]	**0.11**	**0.10**	**0.12***	**0.12**	↑
Ethiopia [10,164]	0.16	0.15***	0.16***	0.18	↑
Kenya [721]	0.12	0.11	0.13*	0.13	↑
Sudan [1,665]	0.15	0.14*	0.13	0.14	↓
Tanzania [528]	0.03	0.03	0.04	0.05	↑

Uganda [630]	0.1	0.10	0.11	0.10**	-
EAPP [13,708]	**0.12**	**0.11*** **	**0.12*** **	**0.13**	↑
Angola [1,100]	0.03	0.04	0.04	0.04*	↑
Lesotho [72]	0.24	0.25	0.26	0.27	↑
Malawi [374]	0.10	0.10	0.11	0.13	↑
Mozambique [2,293]	0.01	0.01	0.01	0.02***	↑
Namibia [347]	0.02	0.02	0.02	0.03*	↑
South Africa [600]	0.26	0.25***	0.27***	0.31	↑
Zambia [2,208]	0.02	0.03	0.03	0.03	↑
Zimbabwe [750]	0.00	0.00	0.00	0.00	↑
SAPP [7,744]	**0.01**	**0.02****	**0.02****	**0.02**	↑

Statistical significance for the interannual variability compared to the historical reference: '***' 0.001 '**' 0.01 '*' 0.05

Supplementary Table B-3 – Seasonal variability of usable capacity by country and power pool, measured as the coefficient of variation in usable capacity under RCP4.5. We aggregate (sum) the individual hydropower usable capacity time series of each power plant to calculate country-level usable capacity. Columns present the historical reference variability (1970 – 2005) and the projected variability for RCP 4.5 (2010 – 2039, 2040 – 2069, and 2070 – 2099). The higher the seasonal variability (closer to 1), the more variable the supply within a year. The direction of changes column represents increases (purple arrow) and decreases (orange arrow) by the end of the century. The darker the shading in the "Historical" column, the highest the variability.

Country [MW]	Historical	RCP 4.5			Direction of Changes
	1970 – 2005	2010 – 2039	2040 – 2069	2070 – 2099	
Egypt [2,842]	0.08	0.07	0.08	0.08	↓
Morocco [902]	0.42	0.44	0.42*	0.39	↓
COMELEC [3,744]	**0.06**	**0.06**	**0.06**	**0.07**	↑
Cote d'Ivoire [824]	0.31	0.31	0.31	0.31	↓
Ghana [1,100]	0.09	0.09	0.09	0.09	↓
Guinea [315]	0.39	0.41	0.42	0.42	↑
Liberia [88]	0.54	0.54	0.56	0.54	-
Mali [262]	0.08	0.08	0.08	0.08	↑
Nigeria [1,920]	0.69	0.69	0.69	0.68	↓

Senegal [120]	0.08	0.08	0.08	0.08	↑
Togo [66]	0.08	0.08	0.08	0.08	↑
WAPP [4,695]	**0.34**	**0.34**	**0.34**	**0.34**	**-**
Cameroon [750]	0.70	0.68	0.68	0.67	↓
Democratic Republic of the Congo [2,756]	0.49	0.48	0.48	0.46	↓
Equatorial Guinea [120]	0.62	0.64	0.65	0.63	↑
Gabon [286]	0.57	0.58	0.59	0.59	↑
CAPP [3,912]	**0.33**	**0.33**	**0.33**	**0.32**	↓
Ethiopia [10,164]	0.53	0.52	0.51	0.47*	↓
Kenya [721]	0.27	0.27	0.27	0.26*	↓
Sudan [1,665]	0.45	0.44	0.41	0.40*	↓
Tanzania [528]	0.33	0.33	0.34	0.34	↑
Uganda [630]	0.3	0.30	0.30	0.29	↓
EAPP [13,708]	**0.37**	**0.36**	**0.35**	**0.33***	↓
Angola [1,100]	0.27	0.25	0.27	0.28	↑
Lesotho [72]	0.78	0.80	0.84	0.82	↑
Malawi [374]	0.81	0.82	0.83	0.82	↑
Mozambique [2,293]	0.03	0.03	0.03	0.03	↑
Namibia [347]	0.18	0.18	0.18	0.18	↓
South Africa [600]	0.53	0.62	0.66*	0.63*	↑
Zambia [2,208]	0.24	0.24	0.25	0.24	↑
Zimbabwe [750]	0.00	0.01	0.01	0.01	↑
SAPP [7,744]	**0.16**	**0.16**	**0.16**	**0.16**	**-**

Statistical significance for the seasonal variability compared to the historical reference: '***' 0.001 '**' 0.01 '*' 0.05

Supplementary Table B-4 – Highly complementary countries. We present a list of pairs of countries from the five power pools presented in the analysis, which display high complementarity (CI > 0.5). Complementarity index for the historical reference (1970 – 2005) compared to the end-of-the-century (2070 – 2099) under two emissions scenarios (RCP 4.5 and RCP 8.5). We present the pairs of countries in decreasing complementarity order. There are currently no existing interconnections between the countries. The darker the purple shading, the highest the complementarity between countries. The distance to interconnect represents the shortest distance for interconnection from the existing or planned power lines from one country to another.

Country 1 [MW]	Power Pool	Country 2 [MW]	Power Pool	Historical	RCP 4.5 2070-2099	RCP 8.5 2070-2099	Distance to Interconnect [km]
Angola [1,100]	SAPP	Nigeria [1,920]	WAPP	0.74	0.77	0.76	1,188
Angola [1,100]	SAPP	Sudan [1,665]	EAPP	0.74	0.73	0.71	2,413
Cameroon [750]	CAPP	Tanzania [528]	EAPP	0.70	0.68	0.69	1,980
Angola [1,100]	SAPP	Ghana [1,100]	WAPP	0.69	0.74	0.76	1,746
Cameroon [750]	CAPP	Namibia [347]	SAPP	0.66	0.63	0.62	2,206
Egypt [2,842]	COMELEC	Mozambique [2,293]	SAPP	0.65	0.72	0.71	3,990
Angola [1,100]	SAPP	Cote d'Ivoire [824]	WAPP	0.62	0.65	0.68	2,025
Cameroon [750]	CAPP	Malawi [374]	SAPP	0.60	0.62	0.60	2,630
Nigeria [1,920]	WAPP	Zambia [2,208]	SAPP	0.59	0.61	0.61	2,714
Sudan [1,665]	EAPP	Zambia [2,208]	SAPP	0.56	0.57	0.60	2,155
DRC [2,756]	CAPP	Sudan [1,665]	EAPP	0.56	0.56	0.57	2,130
Angola [1,100]	SAPP	Cameroon [750]	CAPP	0.56	0.59	0.59	1,002
DRC [2,756]	CAPP	Nigeria [1,920]	WAPP	0.54	0.55	0.55	1,269
Cameroon [750]	CAPP	South Africa [600]	SAPP	0.53	0.55	0.55	3,352
Sudan [1,665]	EAPP	Tanzania [528]	EAPP	0.53	0.58	0.55	1,299

Guinea [315]	WAPP	Malawi [374]	SAPP	0.53	0.58	0.59	4,894
Cote d'Ivoire [824]	WAPP	Tanzania [528]	EAPP	0.50	0.53	0.56	3,812
Nigeria [1,920]	WAPP	Tanzania [528]	EAPP	0.50	0.55	0.56	2,335

Supplementary Table B-5 – Highly complementary power plants. We present the list of highly complementary power plants (CI > 0.5). Complementarity index for the historical reference (1970 – 2005) compared to the end-of-the-century (2070 – 2099) under two emissions scenarios (RCP 4.5 and RCP 8.5). We present the pairs of power plants in decreasing complementarity order. The shading denotes the highest complementary relationships: the darker the purple shade the higher the complementarity between power plants.

Power Plant 1 [MW]	Country 1 [Power Pool]	Power Plant 2 [MW]	Country 2 [Power Pool]	Historical	RCP 4.5 2070-2099	RCP 8.5 2070-2099
Ruacana [347]	Namibia [SAPP]	Shiroro [600]	Nigeria [WAPP]	0.94	0.95	0.97
Mavuzi [52]	Mozambique [SAPP]	Tis Abbay I and II [85]	Ethiopia [EAPP]	0.91	0.88	0.88
Kpong [160]	Ghana [WAPP]	Victoria Falls [108]	Zambia [SAPP]	0.90	0.88	0.86
Buyo [165]	Cote d'Ivoire [WAPP]	Nzilo [228]	DRC [CAPP]	0.90	0.89	0.89
Corumana [166]	Mozambique [SAPP]	Kpong [160]	Ghana [WAPP]	0.88	0.90	0.92
Buyo [165]	Cote d'Ivoire [WAPP]	Nseke [260]	DRC [CAPP]	0.87	0.86	0.86
Gilgel Gibe I [185]	Ethiopia [EAPP]	Victoria Falls [108]	Zambia [SAPP]	0.86	0.87	0.85
Aswan Dam 2 [270]	Egypt [COMELEC]	Kapichira [128]	Malawi [SAPP]	0.86	0.85	0.81
Kidatu [200]	Tanzania [EAPP]	Roseires [415]	Sudan [EAPP]	0.86	0.82	0.8
Aswan Dam 1 [322]	Egypt [COMELEC]	Kapichira [128]	Malawi [SAPP]	0.86	0.84	0.8
Kapichira [128]	Malawi [SAPP]	Kpong [160]	Ghana [WAPP]	0.85	0.88	0.88
Buyo [165]	Cote d'Ivoire [WAPP]	Van Der Kloof [240]	South Africa [SAPP]	0.84	0.81	0.85
Kinhansi Lower Kinhansi [180]	Tanzania [EAPP]	Roseires [415]	Sudan [EAPP]	0.84	0.83	0.8
Awash II [64]	Ethiopia [EAPP]	Mavuzi [52]	Mozambique [SAPP]	0.84	0.77	0.76
Aswan Dam 2 [270]	Egypt [COMELEC]	Nkula Falls Nkula [135.1]	Malawi [SAPP]	0.84	0.86	0.83

Aswan Dam 1 [322]	Egypt [COMELEC]	Nkula Falls Nkula [135.1]	Malawi [SAPP]	0.84	0.86	0.82
Kpong [160]	Ghana [WAPP]	Tedzani [110.7]	Malawi [SAPP]	0.84	0.83	0.81
Aswan Dam 2 [270]	Egypt [COMELEC]	Imboulou [120]	DRC [CAPP]	0.83	0.80	0.78
Aswan Dam 1 [322]	Egypt [COMELEC]	Imboulou [120]	DRC [CAPP]	0.83	0.80	0.78
Mount Coffee [88]	Liberia [WAPP]	Tedzani [110.7]	Malawi [SAPP]	0.83	0.87	0.88
Gilgel Gibe I [185]	Ethiopia [EAPP]	Mavuzi [52]	Mozambique [SAPP]	0.82	0.72	0.71
Imboulou [120]	DRC [CAPP]	Kpong [160]	Ghana [WAPP]	0.82	0.82	0.81
Kpong [160]	Ghana [WAPP]	Nkula Falls Nkula [135.1]	Malawi [SAPP]	0.82	0.85	0.88
Almassira [128]	Morocco [COMELEC]	Tis Abbay I and II [85]	Ethiopia [EAPP]	0.82	0.62	0.61
Kaleta [240]	Guinea [WAPP]	Mavuzi [52]	Mozambique [SAPP]	0.82	0.82	0.83
Edea [264]	Cameroon [CAPP]	Nseke [260]	DRC [CAPP]	0.81	0.81	0.81
Aswan Dam 2 [270]	Egypt [COMELEC]	Corumana [166]	Mozambique [SAPP]	0.81	0.81	0.79
Aswan Dam 1 [322]	Egypt [COMELEC]	Corumana [166]	Mozambique [SAPP]	0.81	0.81	0.78
Aswan Dam 2 [270]	Egypt [COMELEC]	Tedzani [110.7]	Malawi [SAPP]	0.80	0.77	0.73
Mount Coffee [88]	Liberia [WAPP]	Victoria Falls [108]	Zambia [SAPP]	0.80	0.81	0.82
Aswan Dam 1 [322]	Egypt [COMELEC]	Tedzani [110.7]	Malawi [SAPP]	0.80	0.76	0.73
Felou [62.3]	Mali [WAPP]	Ruzizi I [81]	DRC [CAPP]	0.80	0.75	0.77
Gilgel Gibe I [185]	Ethiopia [EAPP]	Poubara [160]	Gabon [CAPP]	0.80	0.73	0.72
Felou [62.3]	Mali [WAPP]	Moukoukoulou [74]	DRC [CAPP]	0.80	0.76	0.75
Mavuzi [52]	Mozambique [SAPP]	Melka Wakena [153]	Ethiopia [EAPP]	0.80	0.63	0.66
Tis Abbay I and II [85]	Ethiopia [EAPP]	Victoria Falls [108]	Zambia [SAPP]	0.80	0.81	0.83

Bujagali [250]	Uganda [EAPP]	Roseires [415]	Sudan [EAPP]	0.80	0.83	0.81
Aswan Dam 2 [270]	Egypt [COMELEC]	Victoria Falls [108]	Zambia [SAPP]	0.79	0.73	0.7
Manantali [200]	Mali [WAPP]	Nalubaale Owen Falls [180]	Uganda [EAPP]	0.79	0.76	0.78
Esna Isna [86]	Egypt [COMELEC]	Moukoukoulou [74]	DRC [CAPP]	0.79	0.80	0.79
Awash II [64]	Ethiopia [EAPP]	Victoria Falls [108]	Zambia [SAPP]	0.79	0.80	0.82
Aswan Dam 1 [322]	Egypt [COMELEC]	Victoria Falls [108]	Zambia [SAPP]	0.79	0.72	0.69
Gilgel Gibe I [185]	Ethiopia [EAPP]	Tedzani [110.7]	Malawi [SAPP]	0.79	0.89	0.86
Edea [264]	Cameroon [CAPP]	Nzilo [228]	DRC [CAPP]	0.79	0.78	0.77
Corumana [166]	Mozambique [SAPP]	Mount Coffee [88]	Liberia [WAPP]	0.79	0.80	0.81
Sambangalou [120]	Senegal [WAPP]	Tedzani [110.7]	Malawi [SAPP]	0.78	0.78	0.85
Buyo [165]	Cote d'Ivoire [WAPP]	Gove [320]	Angola [SAPP]	0.77	0.79	0.82
Tedzani [110.7]	Malawi [SAPP]	Tis Abbay I and II [85]	Ethiopia [EAPP]	0.77	0.82	0.83
Corumana [166]	Mozambique [SAPP]	Turkwel [106]	Kenya [EAPP]	0.77	0.69	0.75
Jebba [560]	Nigeria [WAPP]	Ruacana [347]	Namibia [SAPP]	0.77	0.78	0.80
Nangbeto [65.6]	Togo [WAPP]	Tedzani [110.7]	Malawi [SAPP]	0.77	0.79	0.80
Esna Isna [86]	Egypt [COMELEC]	Ruzizi I [81]	DRC [CAPP]	0.77	0.74	0.75
Buyo [165]	Cote d'Ivoire [WAPP]	Corumana [166]	Mozambique [SAPP]	0.77	0.76	0.78
Cahora Bassa Hcb South Bank [2075]	Mozambique [SAPP]	High Aswan Dam [2100]	Egypt [COMELEC]	0.76	0.73	0.86
Awash II [64]	Ethiopia [EAPP]	Poubara [160]	Gabon [CAPP]	0.76	0.76	0.77
Kainji [760]	Nigeria [WAPP]	Ruacana [347]	Namibia [SAPP]	0.76	0.77	0.76
Gove [320]	Angola [SAPP]	Kpong [160]	Ghana [WAPP]	0.76	0.75	0.74

Gilgel Gibe II [420]	Ethiopia [EAPP]	Ruacana [347]	Namibia [SAPP]	0.76	0.79	0.81
Ruacana [347]	Namibia [SAPP]	Song Loulou [406]	Cameroon [CAPP]	0.75	0.77	0.78
Almassira [128]	Morocco [COMELEC]	Awash II [64]	Ethiopia [EAPP]	0.75	0.53	0.52
Corumana [166]	Mozambique [SAPP]	Gilgel Gibe I [185]	Ethiopia [EAPP]	0.75	0.83	0.86
Kapichira [128]	Malawi [SAPP]	Mount Coffee [88]	Liberia [WAPP]	0.75	0.79	0.80
Allal Al Fassi [240]	Morocco [COMELEC]	Felou [62.3]	Mali [WAPP]	0.75	0.59	0.54
Almassira [128]	Morocco [COMELEC]	Gilgel Gibe I [185]	Ethiopia [EAPP]	0.74	0.50	0.48
Lagdo [80]	Cameroon [CAPP]	Moukoukoulou [74]	DRC [CAPP]	0.74	0.74	0.78
Allal Al Fassi [240]	Morocco [COMELEC]	Esna Isna [86]	Egypt [COMELEC]	0.74	0.56	0.50
Nseke [260]	DRC [CAPP]	Roseires [415]	Sudan [EAPP]	0.74	0.73	0.73
Almassira [128]	Morocco [COMELEC]	Kaleta [240]	Guinea [WAPP]	0.74	0.68	0.68
Poubara [160]	Gabon [CAPP]	Tis Abbay I and II [85]	Ethiopia [EAPP]	0.73	0.73	0.70
Mount Coffee [88]	Liberia [WAPP]	Nkula Falls Nkula [135.1]	Malawi [SAPP]	0.73	0.77	0.78
Nseke [260]	DRC [CAPP]	Taabo [210]	Cote d'Ivoire [WAPP]	0.73	0.73	0.75
Kinhansi Lower Kinhansi [180]	Tanzania [EAPP]	Kossou [174]	Cote d'Ivoire [WAPP]	0.73	0.73	0.74
Felou [62.3]	Mali [WAPP]	Zongo II [150]	DRC [CAPP]	0.73	0.69	0.67
KIIra Kiyira [200]	Uganda [EAPP]	Roseires [415]	Sudan [EAPP]	0.72	0.74	0.73
Mavuzi [52]	Mozambique [SAPP]	Sambangalou [120]	Senegal [WAPP]	0.72	0.71	0.76
Kpong [160]	Ghana [WAPP]	Poubara [160]	Gabon [CAPP]	0.72	0.74	0.73
Edea [264]	Cameroon [CAPP]	Kinhansi Lower Kinhansi [180]	Tanzania [EAPP]	0.72	0.70	0.69

Kpong [160]	Ghana [WAPP]	Mavuzi [52]	Mozambique [SAPP]	0.72	0.69	0.68
Gilgel Gibe I [185]	Ethiopia [EAPP]	Kapichira [128]	Malawi [SAPP]	0.72	0.84	0.87
Kpong [160]	Ghana [WAPP]	Nzilo [228]	DRC [CAPP]	0.72	0.73	0.74
Nzilo [228]	DRC [CAPP]	Roseires [415]	Sudan [EAPP]	0.72	0.71	0.70
Aswan Dam 2 [270]	Egypt [COMELEC]	Gove [320]	Angola [SAPP]	0.72	0.72	0.72
Edea [264]	Cameroon [CAPP]	Van Der Kloof [240]	South Africa [SAPP]	0.72	0.66	0.67
Aswan Dam 1 [322]	Egypt [COMELEC]	Gove [320]	Angola [SAPP]	0.72	0.72	0.72
Kaleta [240]	Guinea [WAPP]	Zongo II [150]	DRC [CAPP]	0.72	0.76	0.73
Capanda [520]	Angola [SAPP]	Shiroro [600]	Nigeria [WAPP]	0.72	0.73	0.75
Cambambe [260]	Angola [SAPP]	Shiroro [600]	Nigeria [WAPP]	0.72	0.71	0.71
Gilgel Gibe II [420]	Ethiopia [EAPP]	Kidatu [200]	Tanzania [EAPP]	0.71	0.67	0.65
Aswan Dam 2 [270]	Egypt [COMELEC]	Poubara [160]	Gabon [CAPP]	0.71	0.69	0.68
Esna Isna [86]	Egypt [COMELEC]	Zongo II [150]	DRC [CAPP]	0.71	0.72	0.71
Aswan Dam 1 [322]	Egypt [COMELEC]	Poubara [160]	Gabon [CAPP]	0.71	0.69	0.68
Kapichira [128]	Malawi [SAPP]	Nangbeto [65.6]	Togo [WAPP]	0.71	0.75	0.77
Allal Al Fassi [240]	Morocco [COMELEC]	Lagdo [80]	Cameroon [CAPP]	0.71	0.55	0.56
Kapichira [128]	Malawi [SAPP]	Sambangalou [120]	Senegal [WAPP]	0.71	0.71	0.77
Nzilo [228]	DRC [CAPP]	Taabo [210]	Cote d'Ivoire [WAPP]	0.70	0.70	0.72
Gilgel Gibe I [185]	Ethiopia [EAPP]	Imboulou [120]	DRC [CAPP]	0.70	0.75	0.75
Kaleta [240]	Guinea [WAPP]	Moukoukoulou [74]	DRC [CAPP]	0.70	0.73	0.71
Itehzi Tehzi [120]	Zambia [SAPP]	Kossou [174]	Cote d'Ivoire [WAPP]	0.70	0.71	0.71
Kaleta [240]	Guinea [WAPP]	Poubara [160]	Gabon [CAPP]	0.70	0.69	0.68

Gilgel Gibe I [185]	Ethiopia [EAPP]	Nkula Falls Nkula [135.1]	Malawi [SAPP]	0.70	0.82	0.85
Kapichira [128]	Malawi [SAPP]	Tis Abbay I and II [85]	Ethiopia [EAPP]	0.70	0.74	0.75
Kpong [160]	Ghana [WAPP]	Nseke [260]	DRC [CAPP]	0.70	0.70	0.71
Nangbeto [65.6]	Togo [WAPP]	Nkula Falls Nkula [135.1]	Malawi [SAPP]	0.69	0.73	0.75
Corumana [166]	Mozambique [SAPP]	Tis Abbay I and II [85]	Ethiopia [EAPP]	0.69	0.70	0.72
Lagdo [80]	Cameroon [CAPP]	Zongo II [150]	DRC [CAPP]	0.69	0.68	0.71
Buyo [165]	Cote d'Ivoire [WAPP]	Nkula Falls Nkula [135.1]	Malawi [SAPP]	0.69	0.69	0.70
Nkula Falls Nkula [135.1]	Malawi [SAPP]	Sambangalou [120]	Senegal [WAPP]	0.69	0.69	0.75
Gilgel Gibe II [420]	Ethiopia [EAPP]	Kinhansi Lower Kinhansi [180]	Tanzania [EAPP]	0.68	0.66	0.65
A El Hansali [92]	Morocco [COMELEC]	Kaleta [240]	Guinea [WAPP]	0.68	0.54	0.61
Mavuzi [52]	Mozambique [SAPP]	Mount Coffee [88]	Liberia [WAPP]	0.68	0.70	0.71
Buyo [165]	Cote d'Ivoire [WAPP]	Kinhansi Lower Kinhansi [180]	Tanzania [EAPP]	0.68	0.70	0.72
Gilgel Gibe II [420]	Ethiopia [EAPP]	Nseke [260]	DRC [CAPP]	0.68	0.66	0.66
Nkula Falls Nkula [135.1]	Malawi [SAPP]	Tis Abbay I and II [85]	Ethiopia [EAPP]	0.68	0.71	0.73
Kpong [160]	Ghana [WAPP]	Van Der Kloof [240]	South Africa [SAPP]	0.68	0.75	0.80
Awash II [64]	Ethiopia [EAPP]	Corumana [166]	Mozambique [SAPP]	0.67	0.68	0.69
Cambambe [260]	Angola [SAPP]	Gilgel Gibe II [420]	Ethiopia [EAPP]	0.67	0.68	0.69

Buyo [165]	Cote d'Ivoire [WAPP]	Kapichira [128]	Malawi [SAPP]	0.67	0.67	0.68
Melka Wakena [153]	Ethiopia [EAPP]	Victoria Falls [108]	Zambia [SAPP]	0.67	0.66	0.73
Roseires [415]	Sudan [EAPP]	Ruacana [347]	Namibia [SAPP]	0.67	0.69	0.71
Gilgel Gibe II [420]	Ethiopia [EAPP]	Nzilo [228]	DRC [CAPP]	0.66	0.63	0.64
Aswan Dam 2 [270]	Egypt [COMELEC]	Nzilo [228]	DRC [CAPP]	0.66	0.68	0.69
Roseires [415]	Sudan [EAPP]	Van Der Kloof [240]	South Africa [SAPP]	0.66	0.61	0.62
Aswan Dam 1 [322]	Egypt [COMELEC]	Nzilo [228]	DRC [CAPP]	0.66	0.68	0.69
Aswan Dam 2 [270]	Egypt [COMELEC]	Mavuzi [52]	Mozambique [SAPP]	0.66	0.60	0.57
Aswan Dam 1 [322]	Egypt [COMELEC]	Mavuzi [52]	Mozambique [SAPP]	0.66	0.59	0.57
Edea [264]	Cameroon [CAPP]	Gove [320]	Angola [SAPP]	0.66	0.66	0.66
Gove [320]	Angola [SAPP]	Mount Coffee [88]	Liberia [WAPP]	0.65	0.64	0.63
Taabo [210]	Cote d'Ivoire [WAPP]	Van Der Kloof [240]	South Africa [SAPP]	0.65	0.60	0.64
A El Hansali [92]	Morocco [COMELEC]	Esna Isna [86]	Egypt [COMELEC]	0.65	0.61	0.73
Gove [320]	Angola [SAPP]	Roseires [415]	Sudan [EAPP]	0.65	0.64	0.64
Gariep [360]	South Africa [SAPP]	Kpong [160]	Ghana [WAPP]	0.65	0.68	0.8
Kaleta [240]	Guinea [WAPP]	Tedzani [110.7]	Malawi [SAPP]	0.65	0.66	0.68
Almassira [128]	Morocco [COMELEC]	Kpong [160]	Ghana [WAPP]	0.64	0.47	0.45
Esna Isna [86]	Egypt [COMELEC]	Mwadingusha [68]	DRC [CAPP]	0.64	0.62	0.62
Mount Coffee [88]	Liberia [WAPP]	Nzilo [228]	DRC [CAPP]	0.64	0.63	0.62
Awash II [64]	Ethiopia [EAPP]	Imboulou [120]	DRC [CAPP]	0.64	0.64	0.65
Aswan Dam 2 [270]	Egypt [COMELEC]	Nseke [260]	DRC [CAPP]	0.64	0.65	0.66
Aswan Dam 1 [322]	Egypt [COMELEC]	Nseke [260]	DRC [CAPP]	0.64	0.65	0.66
Gilgel Gibe I [185]	Ethiopia [EAPP]	Gove [320]	Angola [SAPP]	0.63	0.68	0.69

Cambambe [260]	Angola [SAPP]	Roseires [415]	Sudan [EAPP]	0.62	0.63	0.64
Aswan Dam 2 [270]	Egypt [COMELEC]	Van Der Kloof [240]	South Africa [SAPP]	0.62	0.70	0.75
Aswan Dam 1 [322]	Egypt [COMELEC]	Van Der Kloof [240]	South Africa [SAPP]	0.62	0.70	0.74
Mount Coffee [88]	Liberia [WAPP]	Nseke [260]	DRC [CAPP]	0.62	0.61	0.60
Aswan Dam 2 [270]	Egypt [COMELEC]	Kidatu [200]	Tanzania [EAPP]	0.62	0.66	0.68
Aswan Dam 1 [322]	Egypt [COMELEC]	Kidatu [200]	Tanzania [EAPP]	0.62	0.66	0.68
Lagdo [80]	Cameroon [CAPP]	Mwadingusha [68]	DRC [CAPP]	0.62	0.63	0.71
Esna Isna [86]	Egypt [COMELEC]	Mavuzi [52]	Mozambique [SAPP]	0.62	0.65	0.66
Nseke [260]	DRC [CAPP]	Song Loulou [406]	Cameroon [CAPP]	0.61	0.61	0.61
Mount Coffee [88]	Liberia [WAPP]	Van Der Kloof [240]	South Africa [SAPP]	0.61	0.65	0.67
Nalubaale Owen Falls [180]	Uganda [EAPP]	Tekeze Tk5 [300]	Ethiopia [EAPP]	0.61	0.66	0.65
Corumana [166]	Mozambique [SAPP]	Melka Wakena [153]	Ethiopia [EAPP]	0.61	0.65	0.7
Aswan Dam 2 [270]	Egypt [COMELEC]	Kinhansi Lower Kinhansi [180]	Tanzania [EAPP]	0.61	0.66	0.68
Gove [320]	Angola [SAPP]	Nangbeto [65.6]	Togo [WAPP]	0.61	0.61	0.63
Aswan Dam 1 [322]	Egypt [COMELEC]	Kinhansi Lower Kinhansi [180]	Tanzania [EAPP]	0.61	0.66	0.68
Gilgel Gibe II [420]	Ethiopia [EAPP]	Van Der Kloof [240]	South Africa [SAPP]	0.61	0.54	0.56
Buyo [165]	Cote d'Ivoire [WAPP]	Tedzani [110.7]	Malawi [SAPP]	0.61	0.61	0.61
Imboulou [120]	DRC [CAPP]	Tis Abbay I and II [85]	Ethiopia [EAPP]	0.60	0.61	0.6
Almassira [128]	Morocco [COMELEC]	Aswan Dam 2 [270]	Egypt [COMELEC]	0.60	0.42	0.40
Corumana [166]	Mozambique [SAPP]	Edea [264]	Cameroon [CAPP]	0.60	0.58	0.58

Almassira [128]	Morocco [COMELEC]	Aswan Dam 1 [322]	Egypt [COMELEC]	0.60	0.41	0.40
A El Hansali [92]	Morocco [COMELEC]	Tis Abbay I and II [85]	Ethiopia [EAPP]	0.60	0.46	0.52
Nzilo [228]	DRC [CAPP]	Turkwel [106]	Kenya [EAPP]	0.60	0.56	0.59
Kaleta [240]	Guinea [WAPP]	Victoria Falls [108]	Zambia [SAPP]	0.60	0.60	0.62
Buyo [165]	Cote d'Ivoire [WAPP]	Victoria Falls [108]	Zambia [SAPP]	0.59	0.60	0.60
Gove [320]	Angola [SAPP]	Tis Abbay I and II [85]	Ethiopia [EAPP]	0.59	0.59	0.58
Corumana [166]	Mozambique [SAPP]	Sambangalou [120]	Senegal [WAPP]	0.59	0.59	0.65
Nzilo [228]	DRC [CAPP]	Song Loulou [406]	Cameroon [CAPP]	0.59	0.58	0.58
Nkula Falls Nkula [135.1]	Malawi [SAPP]	Roseires [415]	Sudan [EAPP]	0.59	0.57	0.55
Gilgel Gibe I [185]	Ethiopia [EAPP]	Nzilo [228]	DRC [CAPP]	0.59	0.66	0.68
Kaleta [240]	Guinea [WAPP]	Kapichira [128]	Malawi [SAPP]	0.58	0.60	0.62
Kidatu [200]	Tanzania [EAPP]	Kpong [160]	Ghana [WAPP]	0.58	0.60	0.62
Kinhansi Lower Kinhansi [180]	Tanzania [EAPP]	Kpong [160]	Ghana [WAPP]	0.58	0.60	0.62
Nseke [260]	DRC [CAPP]	Turkwel [106]	Kenya [EAPP]	0.58	0.54	0.57
Edea [264]	Cameroon [CAPP]	Ruacana [347]	Namibia [SAPP]	0.58	0.59	0.6
Kidatu [200]	Tanzania [EAPP]	Shiroro [600]	Nigeria [WAPP]	0.58	0.57	0.57
Corumana [166]	Mozambique [SAPP]	Taabo [210]	Cote d'Ivoire [WAPP]	0.57	0.57	0.58
High Aswan Dam [2100]	Egypt [COMELEC]	Kariba Dam North [1080]	Zambia [SAPP]	0.57	0.58	0.62
Gilgel Gibe II [420]	Ethiopia [EAPP]	Gove [320]	Angola [SAPP]	0.57	0.55	0.56
Kapichira [128]	Malawi [SAPP]	Roseires [415]	Sudan [EAPP]	0.57	0.55	0.53

Kaleta [240]	Guinea [WAPP]	Ruzizi I [81]	DRC [CAPP]	0.57	0.58	0.59
Gariep [360]	South Africa [SAPP]	Roseires [415]	Sudan [EAPP]	0.57	0.52	0.57
Felou [62.3]	Mali [WAPP]	Mavuzi [52]	Mozambique [SAPP]	0.57	0.56	0.56
Kinhansi Lower Kinhansi [180]	Tanzania [EAPP]	Shiroro [600]	Nigeria [WAPP]	0.57	0.56	0.56
Gilgel Gibe I [185]	Ethiopia [EAPP]	Nseke [260]	DRC [CAPP]	0.56	0.63	0.65
Kaleta [240]	Guinea [WAPP]	Nkula Falls Nkula [135.1]	Malawi [SAPP]	0.56	0.58	0.6
Moukoukoulou [74]	DRC [CAPP]	Tis Abbay I and II [85]	Ethiopia [EAPP]	0.56	0.57	0.57
Capanda [520]	Angola [SAPP]	Gilgel Gibe II [420]	Ethiopia [EAPP]	0.56	0.59	0.60
Gilgel Gibe I [185]	Ethiopia [EAPP]	Van Der Kloof [240]	South Africa [SAPP]	0.56	0.68	0.73
Imboulou [120]	DRC [CAPP]	Kaleta [240]	Guinea [WAPP]	0.56	0.57	0.58
Corumana [166]	Mozambique [SAPP]	Roseires [415]	Sudan [EAPP]	0.56	0.53	0.52
Lagdo [80]	Cameroon [CAPP]	Mavuzi [52]	Mozambique [SAPP]	0.56	0.58	0.62
Gariep [360]	South Africa [SAPP]	Gilgel Gibe I [185]	Ethiopia [EAPP]	0.55	0.63	0.75
Tis Abbay I and II [85]	Ethiopia [EAPP]	Zongo II [150]	DRC [CAPP]	0.55	0.59	0.58
Bui [400]	Ghana [WAPP]	Lake Kariba Kariba Dam [750]	Zimbabwe [SAPP]	0.55	0.56	0.56
Grand Renaissance Dam [6450]	Ethiopia [EAPP]	Inga II [1775]	DRC [CAPP]	0.55	0.52	0.52
Nzilo [228]	DRC [CAPP]	Tis Abbay I and II [85]	Ethiopia [EAPP]	0.55	0.55	0.56
Kinhansi Lower Kinhansi [180]	Tanzania [EAPP]	Song Loulou [406]	Cameroon [CAPP]	0.55	0.53	0.52
Nangbeto [65.6]	Togo [WAPP]	Nzilo [228]	DRC [CAPP]	0.55	0.55	0.57

Kafue Gorge Upper [900]	Zambia [SAPP]	Shiroro [600]	Nigeria [WAPP]	0.55	0.57	0.59
Edea [264]	Cameroon [CAPP]	Nkula Falls Nkula [135.1]	Malawi [SAPP]	0.55	0.52	0.51
Almassira [128]	Morocco [COMELEC]	Esna Isna [86]	Egypt [COMELEC]	0.55	0.60	0.72
Awash II [64]	Ethiopia [EAPP]	Moukoukoulou [74]	DRC [CAPP]	0.54	0.54	0.57
Nseke [260]	DRC [CAPP]	Shiroro [600]	Nigeria [WAPP]	0.54	0.55	0.55
Song Loulou [406]	Cameroon [CAPP]	Van Der Kloof [240]	South Africa [SAPP]	0.54	0.49	0.49
Aswan Dam 2 [270]	Egypt [COMELEC]	KIIra Kiyira [200]	Uganda [EAPP]	0.53	0.56	0.6
Aswan Dam 1 [322]	Egypt [COMELEC]	KIIra Kiyira [200]	Uganda [EAPP]	0.53	0.56	0.6
A El Hansali [92]	Morocco [COMELEC]	Gilgel Gibe I [185]	Ethiopia [EAPP]	0.53	0.37	0.4
Nangbeto [65.6]	Togo [WAPP]	Nseke [260]	DRC [CAPP]	0.53	0.53	0.54
Fincha [134]	Ethiopia [EAPP]	Muela [72]	Lesotho [SAPP]	0.53	0.49	0.47
Nseke [260]	DRC [CAPP]	Tis Abbay I and II [85]	Ethiopia [EAPP]	0.53	0.53	0.53
Allal Al Fassi [240]	Morocco [COMELEC]	Kaleta [240]	Guinea [WAPP]	0.53	0.41	0.36
Edea [264]	Cameroon [CAPP]	Kapichira [128]	Malawi [SAPP]	0.53	0.50	0.49
Tis Abbay I and II [85]	Ethiopia [EAPP]	Van Der Kloof [240]	South Africa [SAPP]	0.53	0.58	0.61
Awash II [64]	Ethiopia [EAPP]	Gove [320]	Angola [SAPP]	0.53	0.50	0.50
Manantali [200]	Mali [WAPP]	Mtera [80]	Tanzania [EAPP]	0.52	0.52	0.52
Nzilo [228]	DRC [CAPP]	Shiroro [600]	Nigeria [WAPP]	0.52	0.53	0.53
Kossou [174]	Cote d'Ivoire [WAPP]	Mtera [80]	Tanzania [EAPP]	0.52	0.53	0.53
Corumana [166]	Mozambique [SAPP]	Gilgel Gibe II [420]	Ethiopia [EAPP]	0.52	0.48	0.47
Gilgel Gibe I [185]	Ethiopia [EAPP]	Moukoukoulou [74]	DRC [CAPP]	0.52	0.47	0.47

Awash II [64]	Ethiopia [EAPP]	Nzilo [228]	DRC [CAPP]	0.52	0.52	0.52
Imboulou [120]	DRC [CAPP]	Roseires [415]	Sudan [EAPP]	0.52	0.48	0.47
Kossou [174]	Cote d'Ivoire [WAPP]	Nkula Falls Nkula [135.1]	Malawi [SAPP]	0.51	0.51	0.51
Gariep [360]	South Africa [SAPP]	Tis Abbay I and II [85]	Ethiopia [EAPP]	0.51	0.55	0.64
Almassira [128]	Morocco [COMELEC]	Felou [62.3]	Mali [WAPP]	0.51	0.51	0.62
Gariep [360]	South Africa [SAPP]	Gilgel Gibe II [420]	Ethiopia [EAPP]	0.51	0.45	0.50
Gilgel Gibe I [185]	Ethiopia [EAPP]	Zongo II [150]	DRC [CAPP]	0.51	0.47	0.46
Roseires [415]	Sudan [EAPP]	Tedzani [110.7]	Malawi [SAPP]	0.50	0.49	0.47

Supplementary Table B-6 – Interconnection scenarios based on complementarity assessment. We determine six interconnection scenarios based on the complementarity assessment described in Supplementary Notes B.3.1 and B.3.2. The "Most attractive CI" column summarizes the country level complementarities used to determine the six interconnection scenarios. We add a seventh interconnection scenario (not in the table), which combines all five power pools.

Scenario	Power Pools Interconnected [GW]	Individual Power Pools [MW]	Most Attractive CI
1	CAPP & SAPP [11.7]	CAPP [3,912] SAPP [7,744]	Namibia – Cameroon (CI = 0.66), Malawi – Cameroon (CI = 0.60), Angola – Cameroon (CI = 0.56), South Africa – Cameroon (CI = 0.53)
2	CAPP & EAPP [17.6]	CAPP [3,912] EAPP [13,708]	Tanzania – Cameroon (CI = 0.70), Sudan – DRC (CI = 0.56)
3	WAPP & CAPP [8.6]	WAPP [4,695] CAPP [3912]	DRC – Nigeria (CI = 0.54)
4	EAPP & SAPP [21.5]	EAPP [13,708] SAPP [7,744]	Angola – Sudan (CI = 0.74), Zambia – Sudan (CI = 0.56)
5	WAPP, CAPP, & SAPP [16.4]	WAPP [4,695] CAPP [3912] SAPP [7,744]	Angola – Nigeria (CI = 0.74), Angola – Ghana (CI = 0.69), Namibia – Cameroon (CI = 0.66), Angola – Cote d'Ivoire (CI = 0.62), Malawi – Cameroon (CI = 0.60), Nigeria – Zambia (CI = 0.59), Angola – Cameroon (CI = 0.56), DRC – Nigeria (CI = 0.54), South Africa – Cameroon (CI = 0.53), Guinea – Malawi (CI = 0.53)
6	WAPP, CAPP, & EAPP [22.3]	WAPP [4,695] CAPP [3912] EAPP [13,708]	DRC – Nigeria (CI = 0.54), Tanzania – Nigeria (CI = 0.50), Tanzania – Cote d'Ivoire (CI = 0.50)

Supplementary Table B-7 – Interannual variability of usable capacity by power pool interconnection scenario, measured as the coefficient of variation in usable capacity for RCP 4.5. We aggregate (sum) the usable hydropower capacity of each country to calculate the power pool level usable capacity and coefficients of variation—the closer to 0 the interannual variability metric, the less variable the hydropower supply across years. The darker the shading in the historical column, the highest the variability. The direction of changes column represents increases (purple arrow) and decreases (orange arrow) by the end of the century. The combinations presented are not exhaustive but are meant to represent a sample of possible power pool connections.

Interconnection Scenarios [GW]	Historical	RCP 4.5			Direction of Changes
	1970-2005	2010 – 2039	2040 – 2069	2070 – 2099	
COMELEC [3.7]	0.05	0.04***	0.04***	0.08	↑
WAPP [4.7]	0.05	0.05***	0.05***	0.06	↑
CAPP [3.9]	0.11	0.10	0.12*	0.12	↑
EAPP [13.7]	0.12	0.11***	0.12***	0.12	-
SAPP [7.7]	0.01	0.02**	0.02**	0.02	↑
CAPP & SAPP [11.7]	0.03	0.03	0.03*	0.04	↑
CAPP & EAPP [17.6]	0.10	0.10***	0.09***	0.10	-
WAPP & CAPP [8.6]	0.06	0.06**	0.06***	0.06	-
EAPP & SAPP [21.5]	0.07	0.07***	0.06***	0.07	-
WAPP, CAPP, & SAPP [16.4]	0.03	0.03**	0.03***	0.03	-
WAPP, CAPP, & EAPP [22.3]	0.08	0.08***	0.07***	0.08	-
All Power Pools [33.8]	0.05	0.05***	0.05***	0.05	-

Statistical significance for the seasonal variability of individual power pools compared to the historical reference: '***' 0.001 '**' 0.01 '*' 0.05

Supplementary Table B-8 – Seasonal variability of usable capacity by power pool interconnection scenario, measured as the coefficient of variation in usable capacity for RCP 4.5. We aggregate (sum) the usable hydropower capacity of each country to calculate the power pool level usable capacity and coefficients of variation—the closer to 0 the seasonal variability metric, the less variable the hydropower supply within a year. The darker the shading in the historical column, the highest the variability. The direction of changes column represents increases (purple arrow) and decreases (orange arrow) by the end of the century. The combinations presented are not exhaustive but are meant to represent a sample of possible power pool connections.

Interconnection Scenarios [GW]	Historical	RCP 4.5			Direction of Changes
	1970-2005	2010 – 2039	2040 – 2069	2070 – 2099	
COMELEC [3.7]	0.06	0.06	0.06	0.07	↑
WAPP [4.7]	0.34	0.34	0.34	0.34	-
CAPP [3.9]	0.33	0.33	0.33	0.32	↓
EAPP [13.7]	0.37	0.36	0.35	0.33*	↓
SAPP [7.7]	0.16	0.16	0.16	0.16	-
CAPP & SAPP [11.7]	0.19	0.19	0.18	0.19	-
CAPP & EAPP [17.6]	0.24	0.24	0.24	0.24*	-
WAPP & CAPP [8.6]	0.19	0.19	0.19	0.19	-
EAPP & SAPP [21.5]	0.13	0.13	0.13	0.13*	-
WAPP, CAPP, & SAPP [16.4]	0.09	0.09	0.09	0.09	-
WAPP, CAPP, & EAPP [22.3]	0.27	0.27	0.26	0.26	↓
All Power Pools [33.8]	0.12	0.12	0.12	0.12	-

Statistical significance for the seasonal variability of individual power pools compared to the historical reference: '***' 0.001 '**' 0.01 '*' 0.05

Supplementary Table B-9 – Remotely sensed, global gridded, and georeferenced datasets for the power pool analysis.

Model Component	*Details*	*Temporal Resolution*	*Spatial Resolution*	*Period*	*Data Source*
Power Plant Locations	Latitude and Longitude	Static	Coordinates	Static	West African Renewable Power Database[220], Global Reservoir and Dam Database (GRanD)[221], Conway et al., 2017[222]
Digital Elevation Model	Elevation (m)	Static	1 arc degree	Static	Shuttle Radar Topography Mission (SRTM) [122]
Soil Information	Soil moisture capacity (mm/m) Effective soil depth (cm)	Static	Polygon outlines with information (GIS)	Statics	FAO's Digital Soil Map [123]
Flow Characteristics	Flow accumulation and drainage direction raster files	Static	15 arc-second	Static	Shuttle Elevation Derivatives at multiple Scales (HydroSHEDS) dataset [124]
Control Climate Experiments	Precipitation ($kg/m^2/s$) Temperature (K)	Daily	0.25 degrees	1950 – 2005*	NASA Earth Exchange Global Daily Downscaled Projections (NEX-GDDP) [55]
Future Climate Experiments	Precipitation ($kg/m^2/s$) Temperature (K)	Daily	0.25 degrees	2006 – 2099*	
Glacier Information	Area (km^2) Median elevation (meters above sea level) and glacier area (km^2)	Collected at different times	Polygon outlines with information (GIS)	Static	Randolph Glacier Inventory (RGI) [95]
Runoff	Streamflow at different outlet locations	Monthly	Text files with coordinates	Collected at different times	GRDC[223]

	Runoff (mm)	Monthly	0.5 degrees	1902 – 2014	GRUN[137]
Transmission	Existing and Planned Transmission Lines	Static	Lines with information (GIS)	Static	World Bank Data Catalog224

Supplementary Table B-10 – General circulation models (GCMs) list from NASA's NEX-GDDP dataset used in the analysis. We use a multi-model ensemble of all 21 GCMs for the analyses presented in the main paper.

General Circulation Models
INCM4.0
BCC-CSM1-1
NorESM1-M
MRI-CGCM3
MPI-ESM-MR
MPI-ESM-LR
MIROC5
MIROC-ESM
MIROC-ESM-CHEM
IPSL-CM5A-MR
IPSL-CM5A-LR
GFDL-ESM2M
GFDL-ESM2G
GFDL-CM3
CanESM2
CSIRO-Mk3-6-0
CNRM-CM5
CESM1-BGC
CCSM4
BNU-ESM
ACCESS1-0

B.3 Supplementary Notes

Supplementary Note B-1 Complementarity of power plants under climate change

We perform an exploratory analysis of potential complementarities between power plants, countries, and power pools in Africa to generate attractive interconnection scenarios. The region's existing infrastructure does not yet enable the electricity transfers that we propose here[261]. Therefore, our analysis provides an initial recommendation of the most appealing linkages between countries in a power pool and across power pools based on hydropower resources and their future under different climate change scenarios. The complementarity analysis serves as the basis for creating power pool interconnection scenarios (see Supplementary Note B.3.2).

The complementarity index includes three features using the formulation described in the methods section. Temporal correlations (Pearson correlation – r) parameters capture the strength of the association between the usable capacity time series of two systems. These parameters do not capture the size of the system, just how temporally correlated the systems are. Then, the usable capacity complementarity index (UCI) captures how similar the two systems' usable capacity level is. We combine these two metrics to identify the best pairs of systems. For example, we can determine which countries or power plants can balance their dry/rainy months with similar production levels and what interconnections of power pools would be required to allow these electricity flows. The closer the complementarity index (CI) is to +1, the higher the complementarity between the pair. We consider pairs as highly complementary when the CI is greater than +0.5. We present the two partial complementarity metrics and the combined CI at the country level in Supplementary Figure B-15.

When looking solely at the Pearson correlations (r), we observe the highest complementarities in the EAPP (Panel A. Supplementary Figure B-15, and Supplementary Figure B-14 for power plant level results). Sudan and Ethiopia are both negative temporally correlated with Tanzania and Uganda ($r < -0.75$), suggesting their interconnection would reduce temporal variability. Additionally, the only other power pool where pairs of countries have high negative correlations is the CAPP. The Democratic Republic of Congo (DRC) and Cameroon have a high negative temporal correlation ($r < -0.5$). For the other three power pools, their hydropower systems do not have strong negative temporal correlations ($r > -0.5$). When looking

at the temporal complementarity across power pools, we can see that countries in different power pools could also complement each other. For example, the Pearson correlation coefficient between Tanzania and Cameroon is -0.71. However, these countries are in two different power pools, and they are distant from each other.

When looking at the UCI, the heterogeneity of the usable hydropower capacity of the countries within a power pool becomes apparent. For example, in the EAPP, Ethiopia and Tanzania's UCI's suggests interconnection is less attractive because the systems' sizes are so different (UCI = 0.2). Ethiopia's installed capacity is almost 20 times greater than Tanzania's. Furthermore, there are some attractive UCI values across power pools. Still, as previously mentioned, this would require the interconnection of power pools to allow electricity transfer between countries in different power pools.

When combining the two previous indexes, we can get a clearer picture of potential interconnections within and across the power pools. For example, the high temporal complementarities in the EAPP become less attractive due to the difference in the country-level UCIs. Additionally, the highest values of the CI (> 0.5) require building transmission between power pools. We find that to allow for these complementarities, the interconnection of the WAPP and the SAPP, the CAPP and the EAPP, and the EAPP and the SAPP would need to be completed (see Supplementary Tables B-4 and B-5, for highly complementary power plant and country pairs).

Finally, before looking at the most attractive interconnection scenarios using the previous analysis (Supplementary Note B.3.2), we look at the potential effects of climate change on these metrics. Supplementary Figure B-16 shows the change in the CI when considering the effects of climate change. Panels B. and C. show the difference in the CI of the multi-model ensemble for RCP 4.5 and 8.5, respectively. We can observe a mix of increases and decreases in complementarities depending on the power pools. Within power pools under both emission scenarios, the complementarities remain the same or mostly decrease. On the other hand, there is an increase in the CI (higher under RCP 8.5) across some power pools, which strengthens the case for the interconnection of the African power pools.

Supplementary Note B-2 Scenario generation for interconnection of power pools

Using the results from the complementarity analysis in Supplementary Note B.3.1, we construct seven interconnection scenarios between power pools. We recognize that the infrastructure required to allow these electricity flows across countries is limited, and most of it is non-existent. We provide these interconnection scenarios as a baseline to serve as a guideline for the future interconnection of African countries and power pools. These interconnection scenarios utilize the potential complementarities of hydropower resources across the five African power pools.

Using the results from Supplementary Table B-4 and Supplementary Figures B-15, B-16, and B-17, we construct seven interconnection scenarios for the power pools. Supplementary Figure B-17 shows the filtered CI for high complementarities (matching Supplementary Table B-4). With these results, we generate six interconnection scenarios. Additionally, we include a seventh interconnection scenario that represents the combination of all five power pools interconnected. These scenarios would require building the transmission capabilities within each power pool and across the power pools for each specific scenario. As previously mentioned, the current interconnection of the power pools in the continent is limited, and most of these electricity flows are not possible now. We present the list of the seven interconnection scenarios with the most attractive pairs of complementarities summarized in Supplementary Table B-6. The seven scenarios are the following: 1 Central Africa power pool and Southern African power pool interconnection, 2 Central African power pool (CAPP) and Eastern Africa power pool (EAPP) interconnection, 3 West African Power Pool (WAPP), Central African power pool (CAPP), and Southern African power pool (SAPP) interconnection, 4 West African power pool (WAPP), Central African power pool (CAPP), and Eastern Africa power pool (EAPP), 5 West African power pool (WAPP) and Central African power pool (CAPP), 6 Eastern Africa power pool (EAPP) and Southern African power pool (SAPP), and 7 all power pools interconnected. The interconnection of the Maghreb Electricity Committee (COMELEC) and the Southern African power pool (SAPP) to allow for electricity trade between Egypt and Malawi was deemed to require full interconnection of the five power pools.

Supplementary Note B-3 Statistical Significance of the Coefficient of Variation

We explored the annual usable capacity distributions to provide more insight as to why the statistical significance of the COVs varies even if some changes seem larger than others. The distribution of the COVs drives the statistical significance of the differences between the COVs. There are two key elements at play, the mean changes in the values, and the changes in the standard deviations. Using the example of the COMELEC, the changes in the COV might seem small, but if we inspect the standard deviation of the distribution of the annual values, we observe that the distribution narrows, which leads to the statistical significance of the COV. For other power pools, larger changes are not statistically significant as much, because the distribution is much wider to begin with (e.g., the CAPP), so even with similar changes do not reflect statistical significance. Another factor that is driving the significance of the COVs, especially when looking at the end of the century column (2070 – 2099) in both Table 3-5 in the main manuscript and Supplementary Table B-7 in Appendix B, is the climate model spread. By the end of the century, climate models tend to diverge more on their results. For all these power pools (except the COMELEC under RCP 8.5), the standard deviation increases by the end of the century. This increase in the divergence between climate models affects the statistical significance and therefore, by the end of the century for all the power pools (except the SAPP under RCP 8.5) there is no statistically significant difference between the COVs.

Appendix C – Climate change and hydropower generation in Rwanda: an assessment of current and future power plants

The analysis and results presented in this appendix have been partially published in the "Rwanda: Least Cost Power Development Plan (LCPDP) 2020 – 2040" report written and edited by Rebecca Mutesi Bisangwa[250].

C.1 Introduction

Currently more than half a billion people in Sub-Saharan Africa (SSA) lack access to modern electricity services[6]. Rwanda is the most densely populated country in SSA, with a total population in 2019 of 12.6 million[125]. The country's electricity matrix is composed of 98 MW of hydropower capacity, 103 MW of thermal capacity, and 12 MW of solar capacity[262]. Current electricity access varies significantly between urban and rural communities: 12% and 72% respectively; but the country aims to achieve 100% electrification by 2024[262]. Hydropower can help achieve the electrification goals while minimizing greenhouse emissions. Additionally, hydropower can help balance intermittent renewables (e.g., solar and wind) to meet the country's growing electricity needs. Unfortunately, climate change can threaten the viability of future hydropower development and operations. Given the limited research on climate-induced risks to hydropower plants in SSA, this work aims at increasing the knowledge and understanding about the potential effects that climate change is likely to pose on hydropower in Rwanda. A flexible data requirement climate risk and vulnerability framework for hydropower assessment under climate change is applied to Rwanda.

The initial analysis for Rwanda includes seven cascading hydropower plants. Table C-1 presents the list of the power plants and their main characteristics (information provided by the Rwanda Energy Group - REG). These power plants include the Rusumo Regional Hydropower Project (90 MW), which is planned to begin operations in 2022 (potentially earlier), and the Nyundo Hydropower Plant (3.9 MW) which is currently in the planning stage. Figure C-1 presents

a map with the seven power plants and their corresponding sub-basins which have been calculated using ArcGIS and its hydrology tools.

Table C-1 – Power Plant Characteristics.

Power Plant	*Type*	*Installed Capacity (MW)*	*Effective Height (m)*	*Live Storage Capacity (MCM)*	*Design Flow (m3/s)*	*Status*	*Construction*
Nyabarongo I	Impoundment	28	44.5	13.37	54	Operating	2014
Ntaruka	Impoundment	11.25	169	201	12	Operating	1957
Mukungwa I	Impoundment	12	65	89.6	14	Operating	1988
Rwaza	Run-of-river	2.6	-	-	12	Operating	2018
Mukungwa II	Run-of-river	3.6	6	0.9	13.6	Operating	2013
Nyundo	Run-of-river	3.9	-	-	13	Planned	Unclear
Rusumo Regional HPP	Impoundment Run-of-river	90	15.3	184.5	116.9	Planned	2022

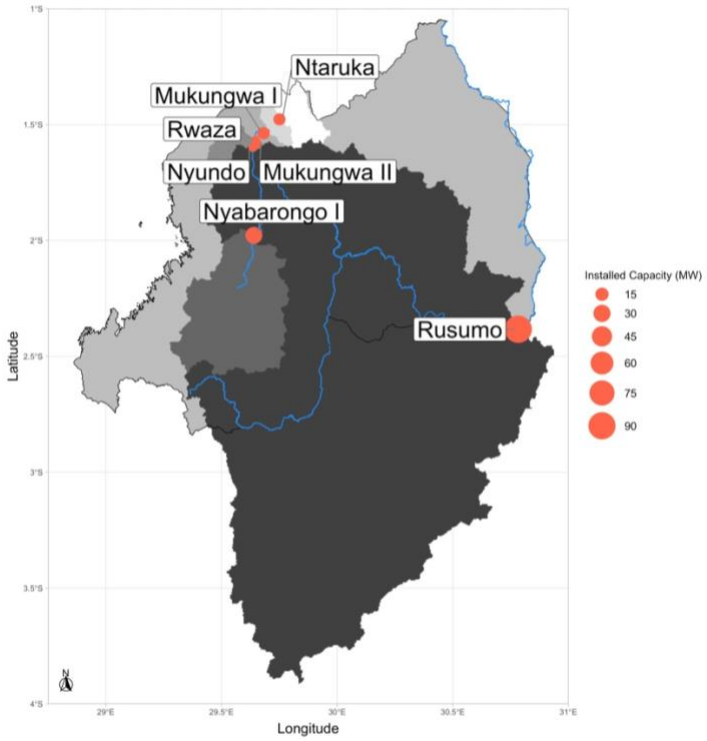

Figure C-1 – Hydropower plants in Rwanda that will be analyzed under different climate models and climate scenarios.

For all power plants climate projections and historical experiments have been obtained from the Nasa's Earth Exchange Global Daily Downscaled Projections Dataset (NEX-GDDP). The initial analysis was performed using the inputs from 21 general circulation models (GCMs) under two different emission scenarios. Table C-2 presents the list with the names of the 21 GCMs used. The emission scenarios analyzed include representative concentration pathways (RCP) 4.5 and 8.5. RCP 4.5 represents a mid-emissions scenario, in which greenhouse gas concentrations in the atmosphere peak around 2040 and decline after that. On the other hand, RCP 8.5 presents a business-as-usual scenario, in which greenhouse gas atmospheric concentrations continue to increase throughout the century. The calibration of the model was performed using the GRUN dataset[137], which provides a reconstruction of global runoff from 1902 to 2014.

Table C-2 – Global Climate Models (GCM) obtained from NASA's NEX-GDDP dataset and used for streamflow simulations

Global Climate Models
INCM4.0
BCC-CSM1-1
NorESM1-M
MRI-CGCM3
MPI-ESM-MR
MPI-ESM-LR
MIROC5
MIROC-ESM
MIROC-ESM-CHEM
IPSL-CM5A-MR
IPSL-CM5A-LR
GFDL-ESM2M
GFDL-ESM2G
GFDL-CM3
CanESM2
CSIRO-Mk3-6-0
CNRM-CM5

CESM1-BGC
CCSM4
BNU-ESM
ACCESS1-0

To generate projections of future streamflow and hydropower usable capacity under different climate models and climate scenarios, a water balance model was used. The model's main appeal is that it does not require using computationally intensive hydrological models with high data requirements and could therefore be applied to regions of the world with limited data, like Rwanda. The model consists of a water balance hydrological model paired with a hydropower operations model. The water balance equation in the model is based on the following:

$$Q_t = S_{t-1} + P_t - AET_t - S_t \ldots \text{(C.1)}$$

Where, Q_t is the runoff generated at month t, S_{t-1} is the previous month's soil moisture storage component, P_t is the precipitation at month t, AET_t is the actual evapotranspiration at month t, and S_t is that month's soil moisture storage component. The water balance model is calibrated using the shuffled complex evolution (SCE) algorithm, which is widely used in hydrological applications[103,104].

Additionally, the model has been coupled with a reservoir operations model[106] for hydropower plants with large storage capabilities. In the case of Rwanda, the two power plants with storage capabilities larger than one-month worth of supply were analyzed as reservoir power plants. These power plants were Mukungwa I and Ntaruka. The reservoir adjacent to the Mukungwa I power plant (lake Ruhondo) would be able to supply 2.5 times the monthly design flow of the power plant if no inflows were reported. Likewise, the adjacent reservoir to the Ntaruka power plant (a combination of Lake Ruhondo and Lake Burera) could supply 6.5 times the monthly design flow with no inflows.

C.2 Rwanda's Climate

Using the climate variables obtained from the NEX-GDDP dataset we were able to characterize future climate for the six sub-basins corresponding to the seven hydropower plants in the analysis (precipitation, maximum temperature, minimum temperature, and potential evapotranspiration). Figures C-2 through C-7 show the average monthly precipitation for each of the sub-basins. The Rwaza Muko and Mukungwa II power plants are close to each other so for the analysis they are considered as one sub-basin. The average monthly precipitation for the historical period ranges from 1130 mm in the Rusumo basin to 1290 mm for Nyundo and the Rwza Muko/Mukungwa II basins. Throughout the century the multi-model mean of precipitation increases for all basins. By the end of the century precipitation increases on average between 7.8%-8.9% for RCP 4.5, and 17.8%-22.2% for RCP 8.5.

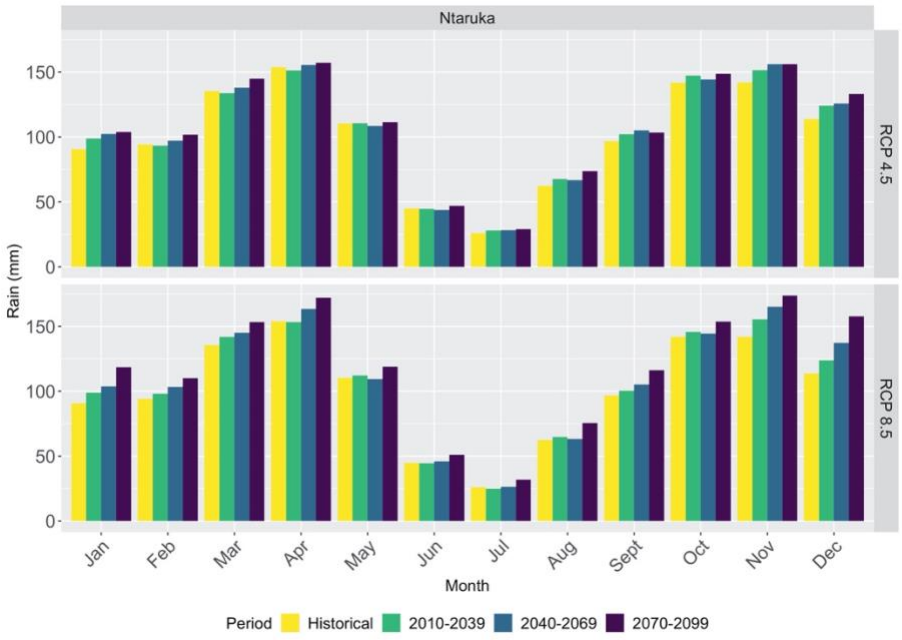

Figure C-2 – Average Multi-Model Precipitation (mm) for the Ntaruka Sub-basin. The historical annual precipitation for the basin was 1210 mm. By the end of the century precipitation increases to 1310 mm for RCP 4.5 and 1430 mm for RCP 8.5.

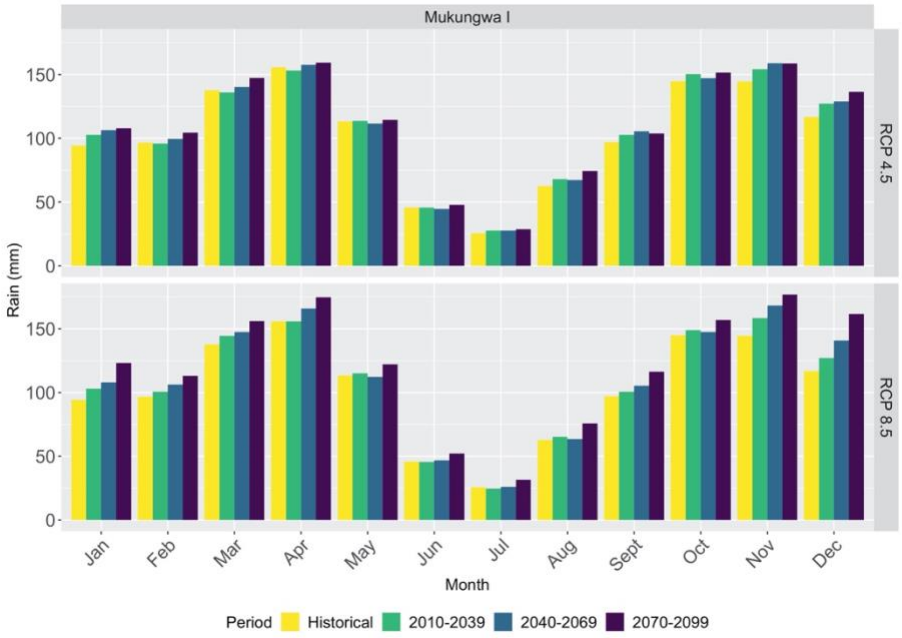

Figure C-3 – Average Multi-Model Precipitation (mm) for the Mukungwa I Sub-basin. The historical annual precipitation for the basin was 1230 mm. By the end of the century precipitation increases to 1340 mm for RCP 4.5 and 1460 mm for RCP 8.5.

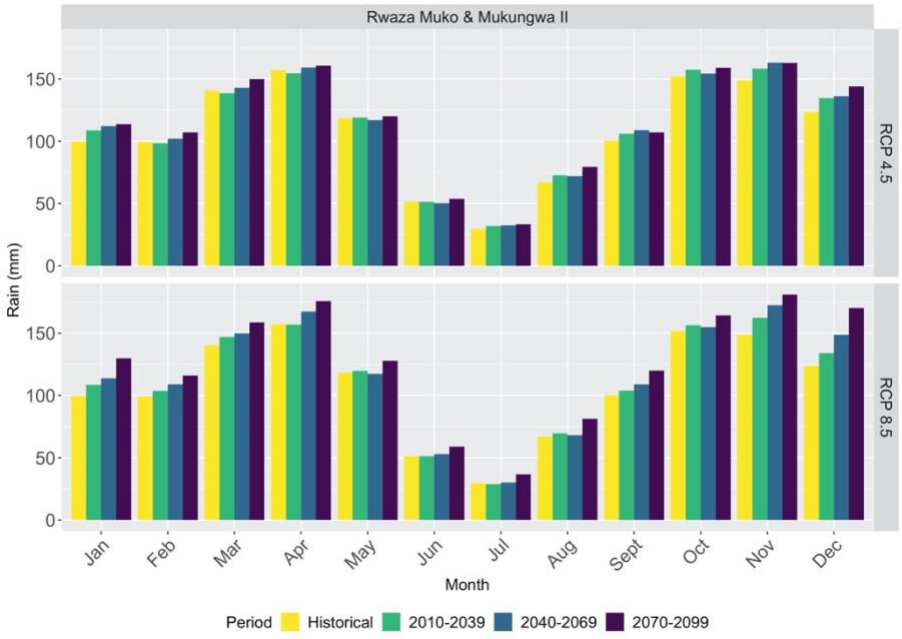

Figure C-4 – Average Multi-Model Precipitation (mm) for the Rwaza Muko/Mukungwa II Sub-basin. The historical annual precipitation for the basin was 1290 mm. By the end of the century precipitation increases to 1390 mm for RCP 4.5 and 1520 mm for RCP 8.5.

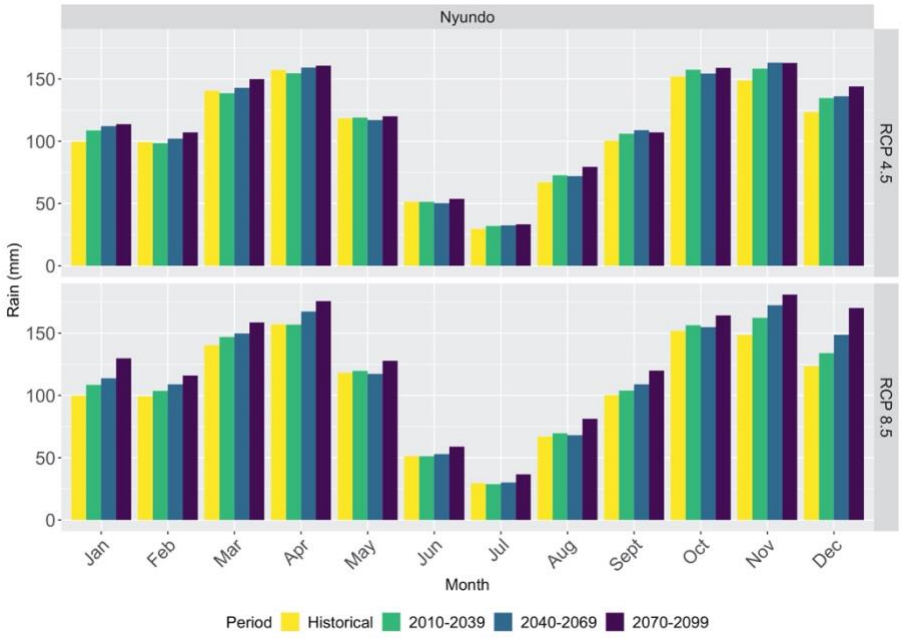

Figure C-5 – Average Multi-Model Precipitation (mm) for the Nyundo Sub-basin. The historical annual precipitation for the basin was 1290 mm. By the end of the century precipitation increases to 1390 mm for RCP 4.5 and 1520 mm for RCP 8.5.

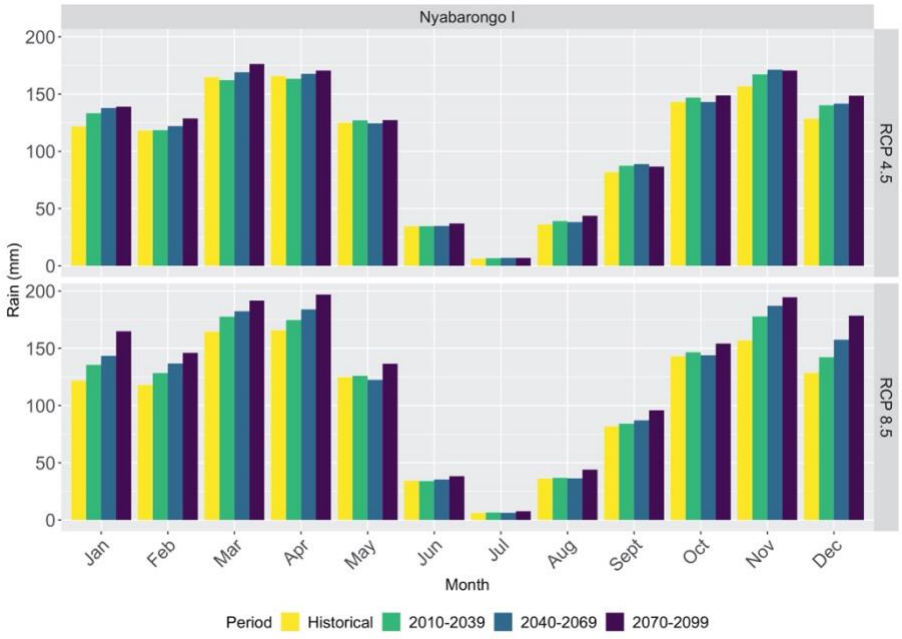

Figure C-6 – Average Multi-Model Precipitation (mm) for the Nyabarongo I Sub-basin. The historical annual precipitation for the basin was 1280 mm. By the end of the century precipitation increases to 1380 mm for RCP 4.5 and 1550 mm for RCP 8.5.

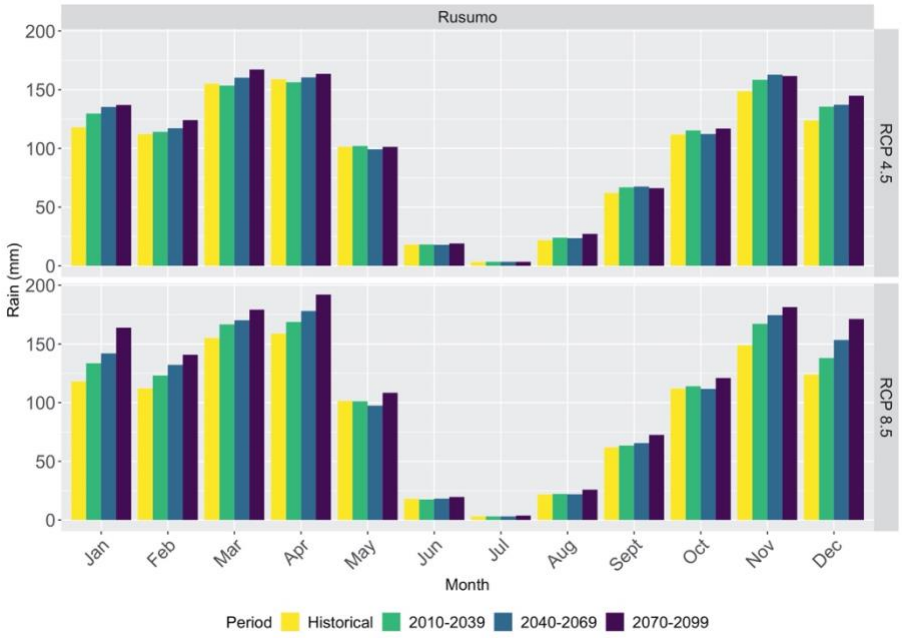

Figure C-7 – Average Multi-Model Precipitation (mm) for the Rusumo Sub-basin. The historical annual precipitation for the basin was 1130 mm. By the end of the century precipitation increases to 1230 mm for RCP 4.5 and 1380 mm for RCP 8.5.

After looking at the precipitation changes the next figures (Figure C-8 through C-13) present the changes in Minimum and Maximum temperature for each sub-basin. Overall temperature increases are observed for all sub-basins, with more noticeable increases under RCP 8.5 than RCP 4.5. The average minimum annual temperature increase by the end of the century is 2.2 °C under RCP 4.5 and 4.2 °C under RCP 8.5. The average maximum annual temperature increase by the end of the century was 2°C under RCP 4.5 and 3.8°C under RCP 8.5. The power plant in the hottest basin is the Rusumo power plant with an annual minimum historical temperature in the basin around 14.3°C, followed by the Nyabarongo I basin with an annual average minimum temperature historically of 12.5 °C.

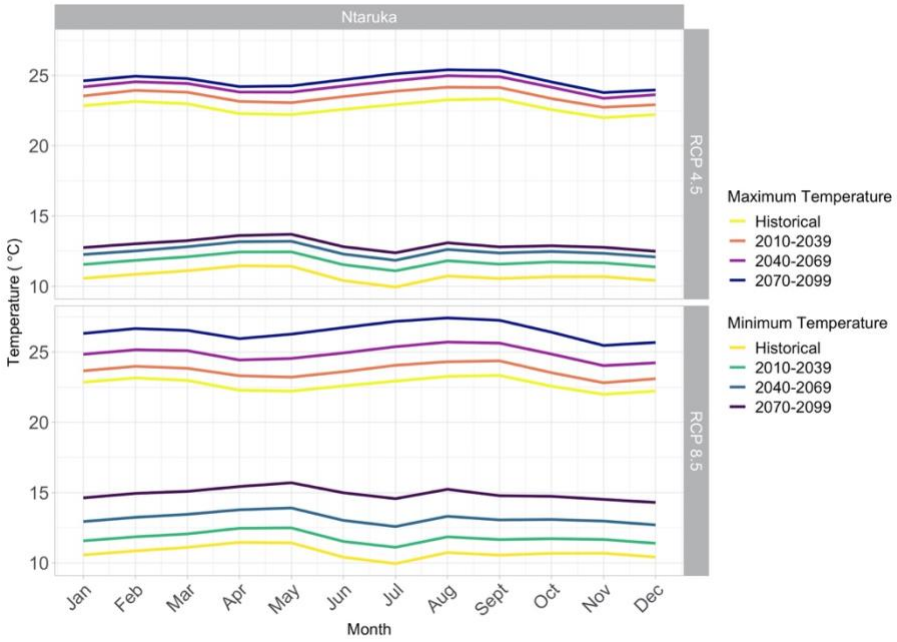

Figure C-8 – Changes in Minimum and Maximum Temperature (°C) for the Ntaruka Sub-basin. Average minimum temperature increases from 10.7 °C in the historical period to 13 °C under RCP 4.5 and 14.9 °C under RCP 8.5. Average maximum temperature increases from 22.7 °C in the historical period to 24.6 °C under RCP 4.5 and 26.5 °C under RCP 8.5.

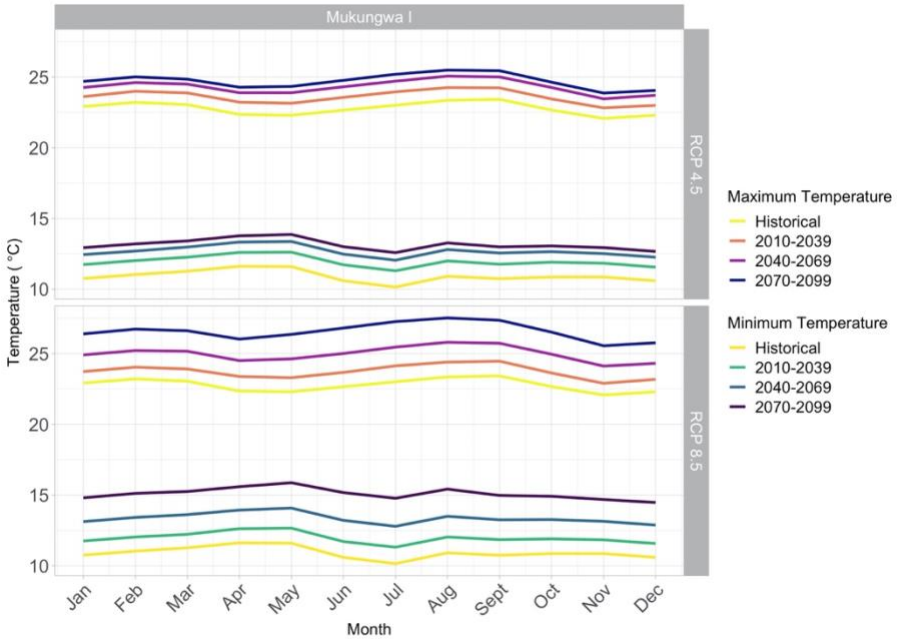

Figure C-9 – Changes in Minimum and Maximum Temperature (°C) for the Mukungwa I Sub-basin. Average minimum temperature increases from 10.9 °C in the historical period to 13.1 °C under RCP 4.5 and 15.1 °C under

RCP 8.5. Average maximum temperature increases from 22.8 °C in the historical period to 24.7 °C under RCP 4.5 and 26.6 °C under RCP 8.5.

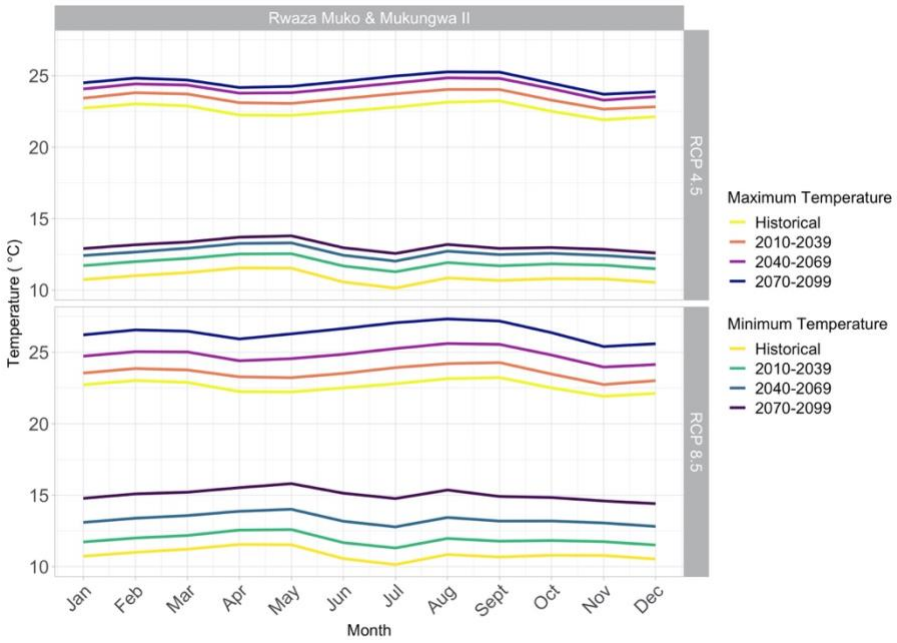

Figure C-10 – Changes in Minimum and Maximum Temperature (°C) for the Rwaza Muko/Mukungwa II Sub-basin. Average minimum temperature increases from 10.9 °C in the historical period to 13.1 °C under RCP 4.5 and 15.0 °C under RCP 8.5. Average maximum temperature increases from 22.6 °C in the historical period to 24.6 °C under RCP 4.5 and 26.4 °C under RCP 8.5.

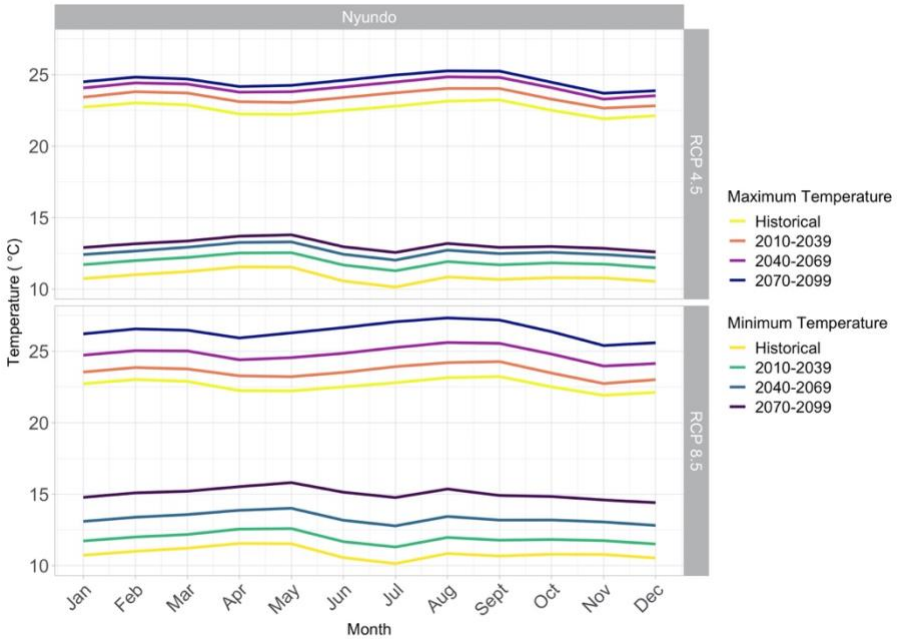

Figure C-11 – Changes in Minimum and Maximum Temperature (°C) for the Nyundo Sub-basin. Average minimum temperature increases from 10.9 °C in the historical period to 13.1 °C under RCP 4.5 and 15.0 °C under RCP 8.5. Average maximum temperature increases from 22.6 °C in the historical period to 24.6 °C under RCP 4.5 and 26.4 °C under RCP 8.5.

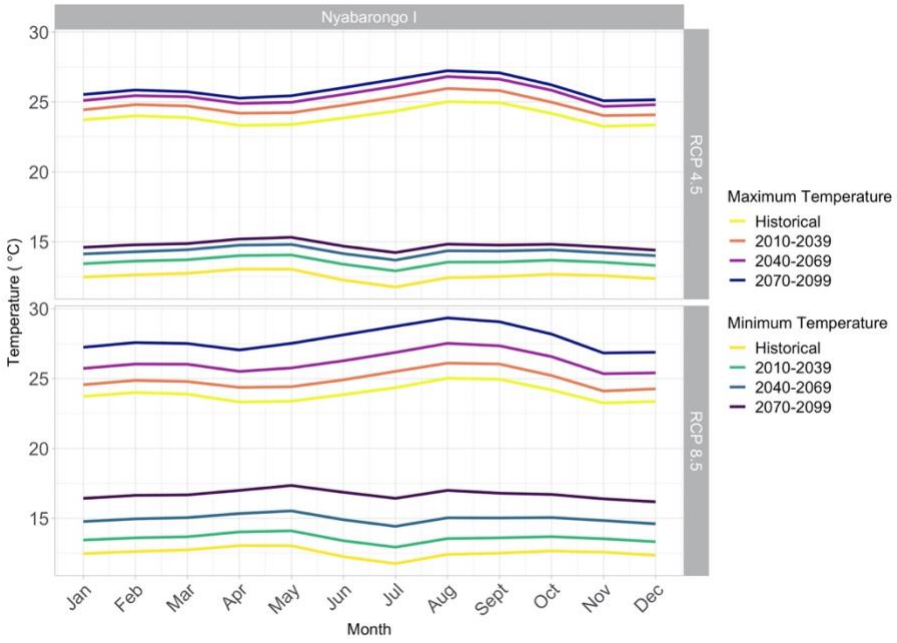

Figure C-12 – Changes in Minimum and Maximum Temperature (°C) for the Nyabarongo I Sub-basin. Average minimum temperature increases from 12.5 °C in the historical period to 14.8 °C under RCP 4.5 and 16.7 °C under RCP 8.5. Average maximum temperature increases from 23.9 °C in the historical period to 25.9 °C under RCP 4.5 and 27.8 °C under RCP 8.5.

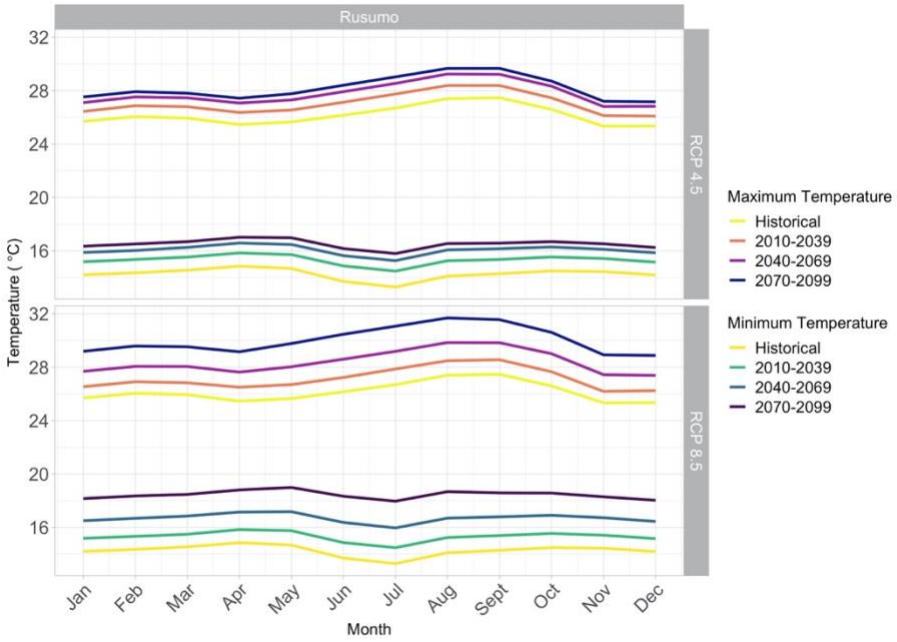

Figure C-13 – Changes in Minimum and Maximum Temperature (°C) for the Rusumo Sub-basin. Average minimum temperature increases from 14.3 °C in the historical period to 16.5 °C under RCP 4.5 and 18.4 °C under RCP 8.5. Average maximum temperature increases from 26.1 °C in the historical period to 28.2 °C under RCP 4.5 and 30 °C under RCP 8.5.

Finally, Figure C-14 presents the changes in Potential Evapotranspiration (PET) for all basins. The values calculated with the Hargreaves method increase from 1470 mm annually to 1540 mm by the end of the century under RCP 4.5 and 1620 mm under RCP 8.5.

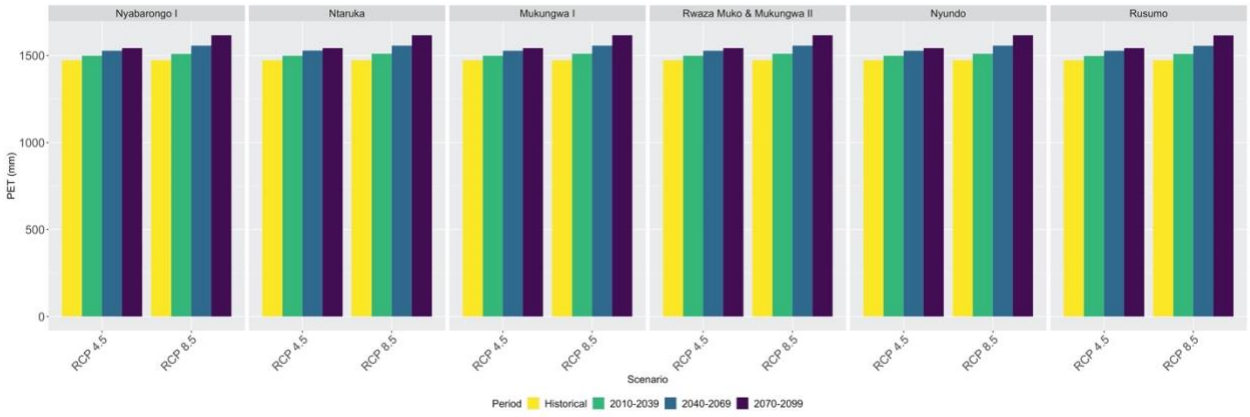

Figure C-14 – Changes in Potential Evapotranspiration (Hargreaves Method). Historical PET was on average 1470 mm for all sub-basins and it increases by the end of the century to 1540 mm under RCP 4.5 and 1620 under RCP 8.5.

Overall, all basins are becoming hotter and wetter as the century progresses under both climate scenarios and the multi-model ensemble.

C.3 Streamflow and Usable Capacity Results

Projections for future power plant usable capacity (available MW of hydropower considering electricity maximization) were run under the two emission scenarios and the 21 GCMs. Each future run was divided into three time frames for the purpose of the analysis. The near future (2010-2039), the mid-century (2040-2069), and the end of the century (2070-2099). Even though the end of the century projections might not be as relevant for present-day planning decisions, it is important to include them and to understand the potential shifts in trends. Additionally, infrastructure typically outlasts its planned life and therefore power plants and reservoirs built nowadays might still be operating by the end of the century with the proper retrofits. To be able to understand the trends under the two different scenarios of climate change, projections are compared to a historical experiment run. The historical experiment (1970-2005) is conducted using the outputs for the retrospective run of the GCMs. This comparison is performed using this historical experiment to keep the biases of the GCMs constant and to be able to understand the trends of climate change into the century. All sub-basins are compared, even if the power plants have not been constructed yet. The ability to compare changes between what could have been generated in the past and the future allows us to understand the impact of climate change on hydropower in Rwanda.

The results section is divided into three parts. A streamflow analysis which includes monthly average naturalized streamflow and an analysis of the 10^{th} percentile (low flow), the 50^{th} percentile (median flow), and the 90^{th} percentile (high flow) streamflow. A second analysis of simulated normalized usable capacity considering power plants operate with all available streamflow as run-of-river or reservoir every month of the analysis period. Three seasons were analyzed: Rainy Season 1 (January through May), Dry Season (June through September), and Rainy Season 2 (October through November). Finally, a third analysis shows the full spread of the 21 GCMs results for usable hydropower capacity for each power plant as boxplots.

C.3.1 Streamflow Analysis

The following section presents the results obtained for streamflow under the two scenarios, and three different time frames: near future (2010-2039), mid-future (2040-2069) and end-of-century (2070-2099). Figures C-15 through C-20 present the average monthly results from the multi-model ensemble. Overall, there are increases in streamflow for all sub-basins which can be seen in greater detail in Tables C-3, C-4 and C-5. These tables presents results for the low streamflow (10^{th} percentile), median streamflow (50^{th} percentile), and high streamflow (90^{th} percentile). The changes in projected flow encompass all the results from the 21 GCMs. Tables C-3, C-4 and C-5 present the results for the three cases respectively: low flow, median flow and high flow. The results present naturalized streamflow without considering water demand within the basin.

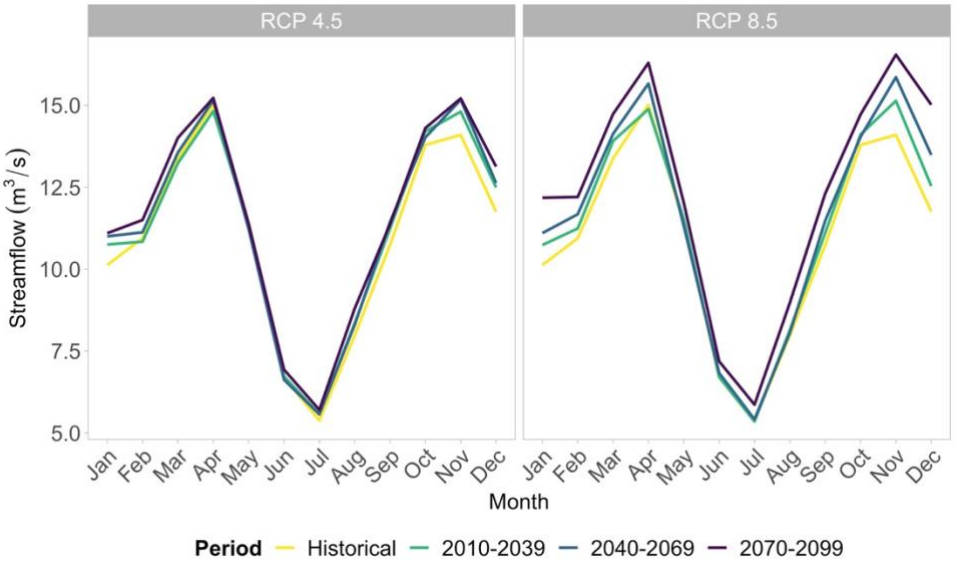

Figure C-15 – Average monthly streamflow from the multi-model ensemble for the Ntaruka sub-basin.

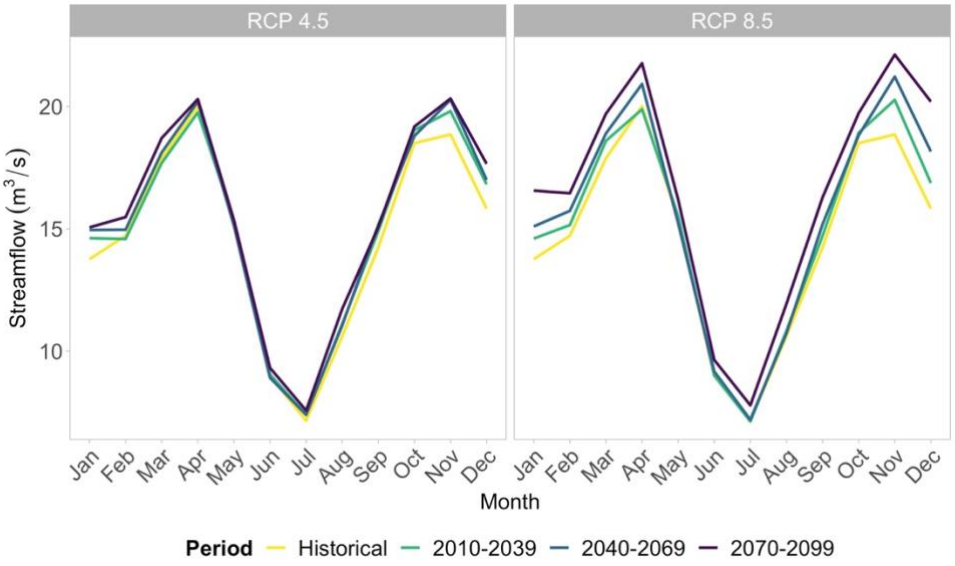

Figure C-16 – Average monthly streamflow from the multi-model ensemble for the Mukungwa I sub-basin.

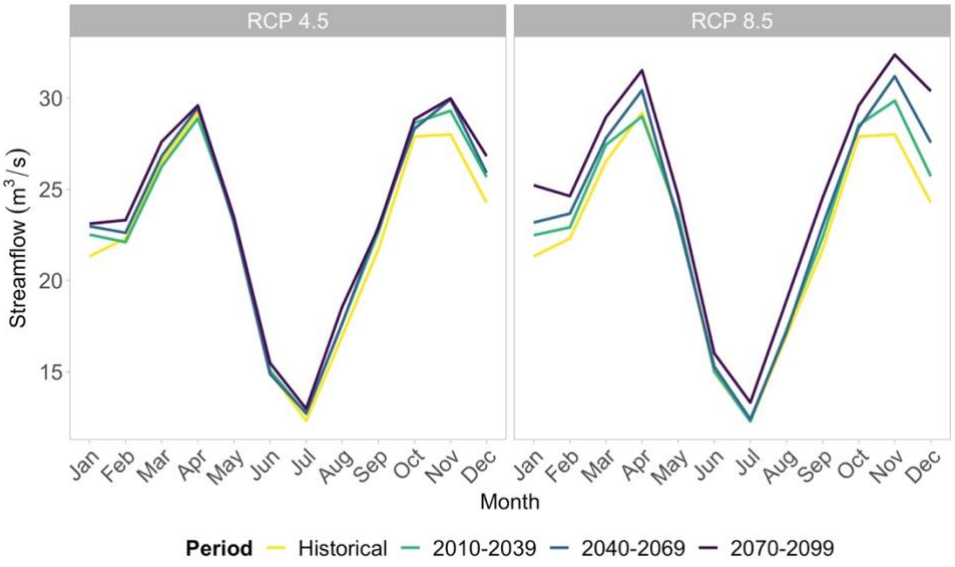

Figure C-17 – Average monthly streamflow from the multi-model ensemble for the Rwaza Muko/Mukungwa II sub-basin.

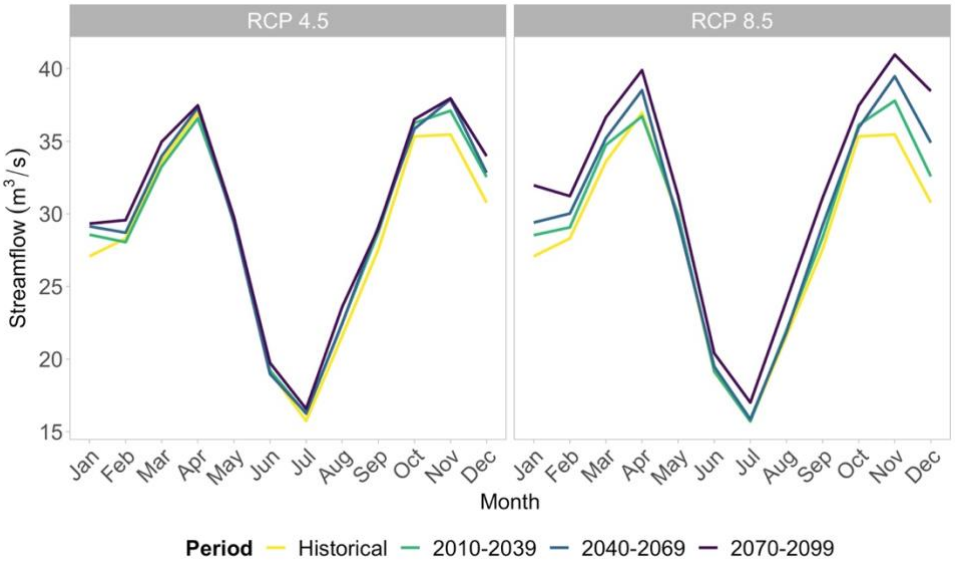

Figure C-18 – Average monthly streamflow from the multi-model ensemble for the Nyundo sub-basin.

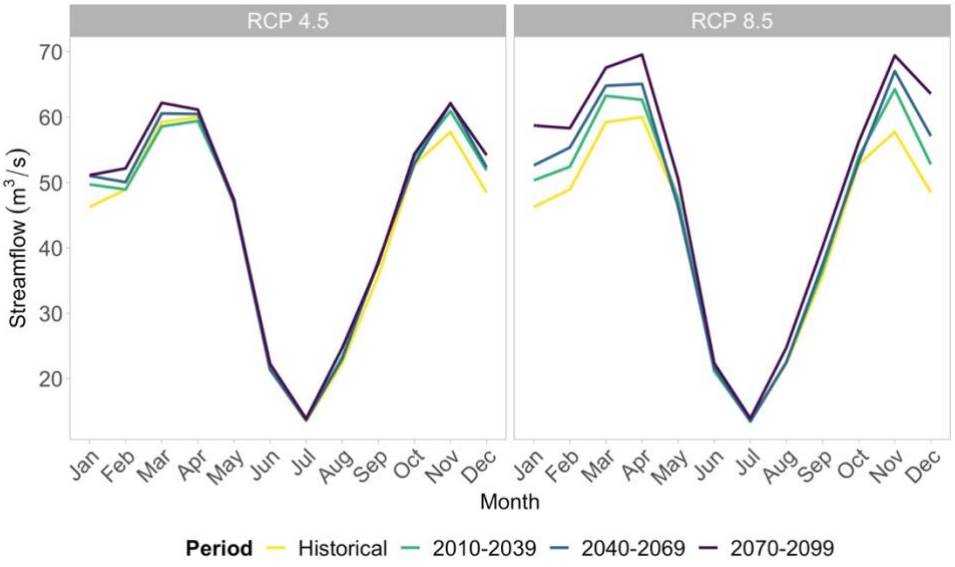

Figure C-19 – Average monthly streamflow from the multi-model ensemble for the Nyabarongo I sub-basin.

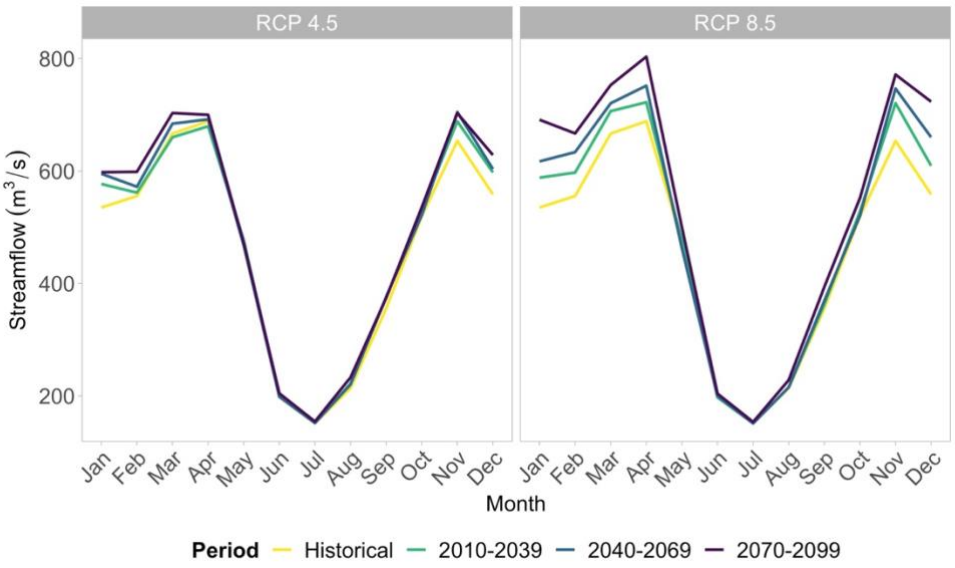

Figure C-20 – Average monthly streamflow from the multi-model ensemble for the Rusumo sub-basin.

Table C-3 – Projected Changes in 10th Percentile Naturalized Streamflow.

	Change in Projected 10th Percentile Flows					
Sub-basin	**RCP 4.5**			**RCP 8.5**		
	2010-2039	**2040-2069**	**2070-2099**	**2010-2039**	**2040-2069**	**2070-2099**
Nyabarongo I	1.5%	-7.1%	-1.4%	-4.3%	-8.1%	1.9%
Ntaruka	0.3%	-4.0%	-0.8%	-7.4%	-7.5%	7.4%
Mukungwa I	-1.2%	-5.0%	-1.5%	-8.8%	-8.6%	7.0%
Rwaza & Mukungwa II	-0.8%	-5.5%	-1.3%	-8.9%	-8.9%	5.3%
Nyundo	-0.7%	-5.3%	-1.2%	-8.8%	-8.8%	5.4%
Rusumo Regional HPP	2.4%	-4.2%	-0.4%	-2.6%	-7.0%	2.7%

Table C-4 – Projected Changes in Median (50th Percentile) Naturalized Streamflow.

	Change in Projected 10th Percentile Flows					
Sub-basin	**RCP 4.5**			**RCP 8.5**		
	2010-2039	**2040-2069**	**2070-2099**	**2010-2039**	**2040-2069**	**2070-2099**
Nyabarongo I	3.8%	3.9%	6.2%	4.4%	6.7%	14.8%

Ntaruka	3.1%	5.1%	7.1%	3.4%	7.1%	15.7%
Mukungwa I	3.1%	5.1%	7.0%	3.9%	6.9%	14.9%
Rwaza & Mukungwa II	3.3%	4.9%	7.0%	3.8%	7.1%	15.6%
Nyundo	3.3%	4.8%	7.1%	3.8%	7.1%	15.5%
Rusumo Regional HPP	3.5%	4.6%	6.3%	4.5%	6.5%	14.5%

Table C-5 – Projected Changes in 90th Percentile Naturalized Streamflow.

	Change in Projected 90th Percentile Flows					
Sub-basin	**RCP 4.5**			**RCP 8.5**		
	2010-2039	**2040-2069**	**2070-2099**	**2010-2039**	**2040-2069**	**2070-2099**
Nyabarongo I	4.7%	8.6%	12.0%	12.3%	20.9%	31.0%
Ntaruka	5.2%	8.3%	10.8%	7.4%	13.9%	24.8%
Mukungwa I	5.1%	8.5%	11.1%	7.5%	14.6%	24.8%
Rwaza & Mukungwa II	5.1%	8.5%	11.5%	7.2%	13.6%	24.2%
Nyundo	5.1%	8.5%	11.5%	7.2%	13.6%	24.2%
Rusumo Regional HPP	4.6%	7.5%	11.5%	9.1%	15.7%	27.4%

The results show a trend of increasing streamflow for the median and the high flow. The increases vary depending on the period analyzed but consistently progressing as we go further into the century. The highest increases are projected for the high flows under RCP 8.5 (24.2%-31.0%). These increases will potentially translate to increased generation constrained to the power plant design characteristics.

On the other hand, the 10th percentile flows show a mix of both decreases and increases. Decreases are mostly projected for the near-future and the mid-century. These decreases are larger under RCP 8.5. The effect of these decreases in usable capacity will be discussed in the following sections. These decreases might not necessarily affect generation overall. Additionally, adjacent reservoirs might help buffer some of the effects of decreased streamflow.

C.3.2 Normalized Usable Capacity

Figures C-21 and C-22 show the projected changes in normalized usable capacity. Additionally, Table C-6 presents the mean usable capacity for each power plant under both climate scenarios for the multi-model ensemble. We define usable capacity as the maximum monthly capacity in MW, constrained by the power plant's installed capacity, the simulated streamflow can maintain for a specific time frame. We analyze the changes in usable capacity (MW) for each month of the system considered between the projection runs and the control run. Three different seasons are portrayed: rainy season 1, dry season, and rainy season 2.

Table C-6 – Average Monthly Usable Capacity under 21 GCM Multi-model Ensemble.

Power Plant	Mean Monthly Usable Capacity (MW)						
	Historical	RCP 4.5			RCP 8.5		
		2010-2039	2040-2069	2070-2099	2010-2039	2040-2069	2070-2099
Ntaruka	10.6	10.6	10.6	10.6	10.5	10.5	10.6
Mukungwa I	8.2	8.3	8.4	8.5	8.3	8.4	8.7
Mukungwa II	1.2	1.2	1.2	1.2	1.2	1.3	1.3
Rwaza Muko	2.6	2.6	2.6	2.6	2.6	2.6	2.6
Nyundo	3.9	3.9	3.9	3.9	3.9	3.9	3.9
Nyabarongo I	16.5	16.9	17.0	17.2	16.9	17.2	18.0
Rusumo	59.5	60.5	60.6	61.2	60.5	61.0	62.6

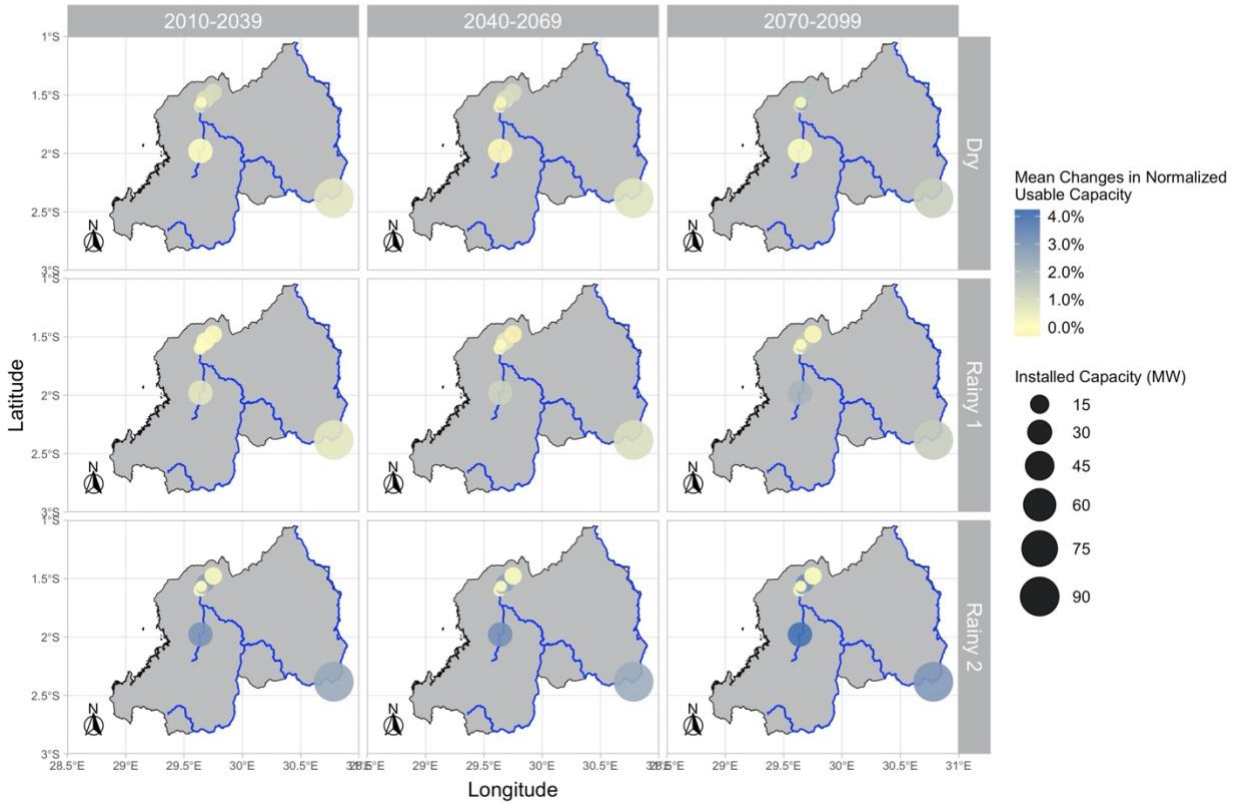

Figure C-21 – Rwanda's mean relative changes in normalized usable capacity for RCP 4.5 between the historical reference (1970-2005), the near future (2010-2039), the mid-century (2040-2069), and the end-of-the-century (2070-2099). The top panel presents the dry season (Jun-Sep) the middle panel the first rainy season (Jan-May), and the bottom panel the second rainy season (Oct-Dec).

There is a trend for increasing normalized usable capacity which is most noticeable by the end of the century and under RCP 8.5 throughout the three seasons. The potential decreases in streamflow are not reflected in the overall usable capacity with almost no change in the dry season's normalized usable capacity under both emission scenarios for the near-future and mid-century time frames (Figure C-21 and C-22). The Rusumo Hydropower Project, which is currently under construction, would seem to experience increases in capacity factor by throughout the century under all scenarios, especially during the rainy seasons (both) and the end of the century.

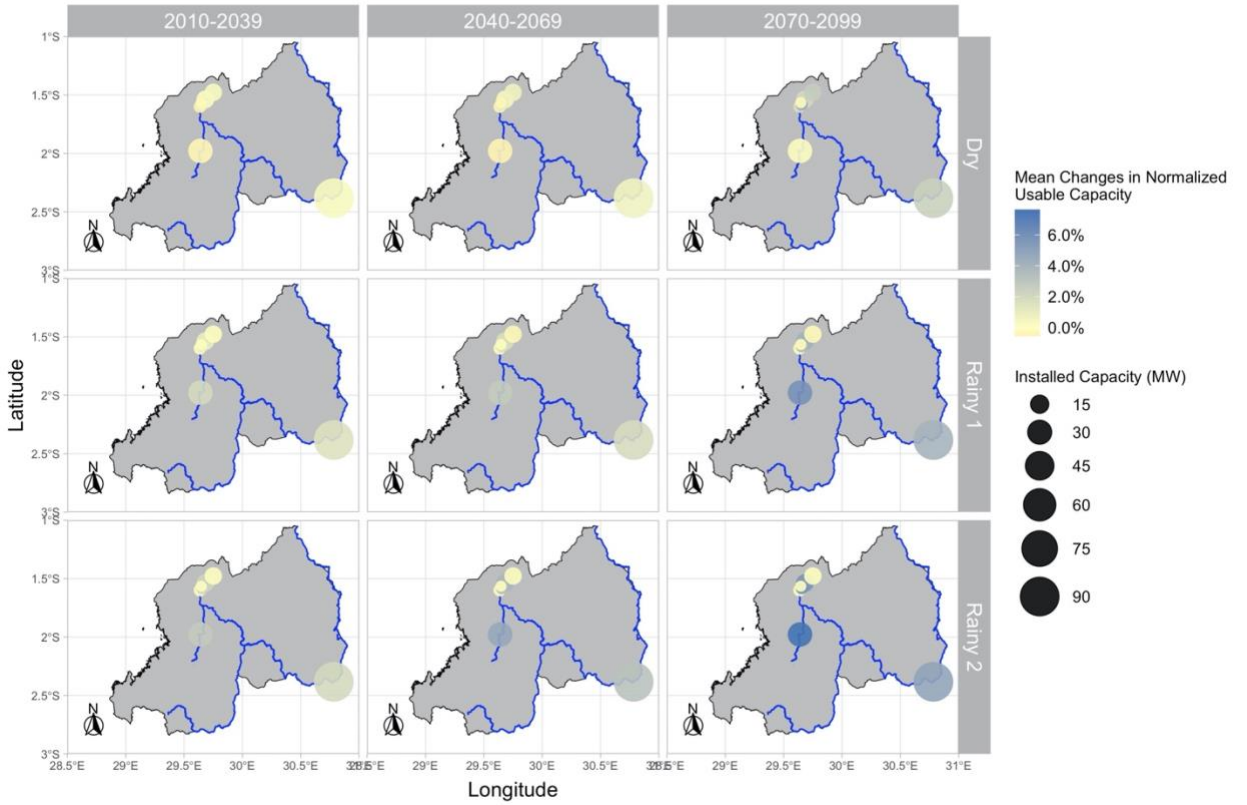

Figure C-22 – Rwanda's mean relative changes in normalized usable capacity for RCP 8.5 between the historical reference (1970-2005), the near future (2010-2039), the mid-century (2040-2069), and the end-of-the-century (2070-2099). The top panel presents the dry season (Jun-Sep) the middle panel the first rainy season (Jan-May), and the bottom panel the second rainy season (Oct-Dec).

C.3.3 Usable Capacity Boxplots

In this section the results for the full spread of the multi-model usable capacity for each power plant is presented. This section presents the boxplots including the monthly usable capacity of each power plant under both RCPs (Figures C-23 through C-29). The objective of these plots is to understand the shifts in the distributions (tails). These plots were built using the full simulations of the 21 GCMs.

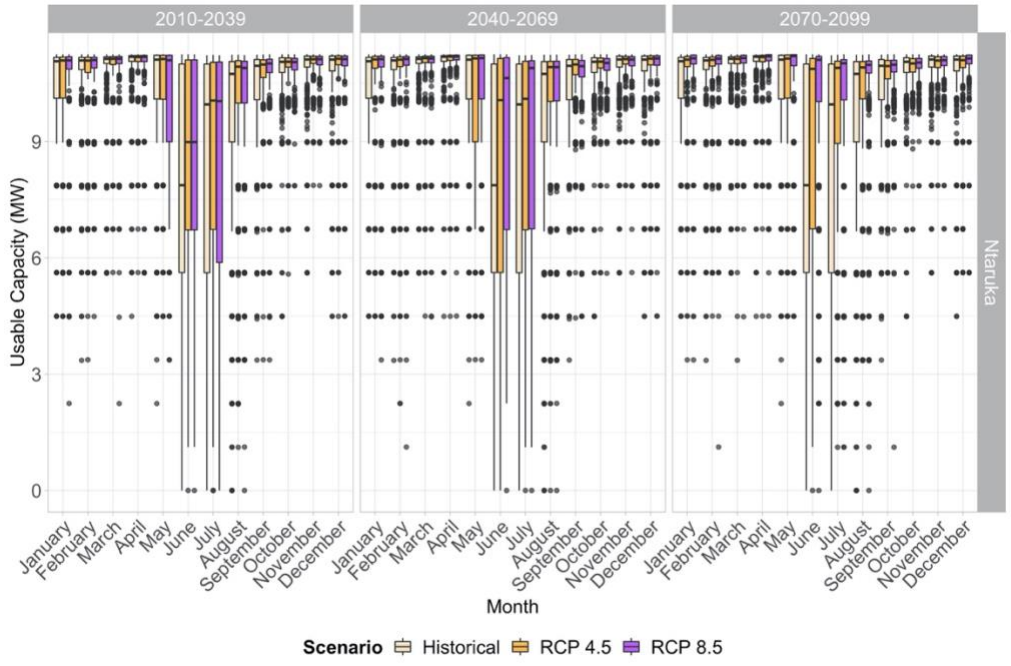

Figure C-23 – Usable capacity (MW) for the Ntaruka power plant as an impoundment power plant. The boxplots present the full spread of the 21 GCM experiments for the historical period (wheat), RCP 4.5 (orange), and RCP 8.5 (purple). Each column shows one of the analysis time frames.

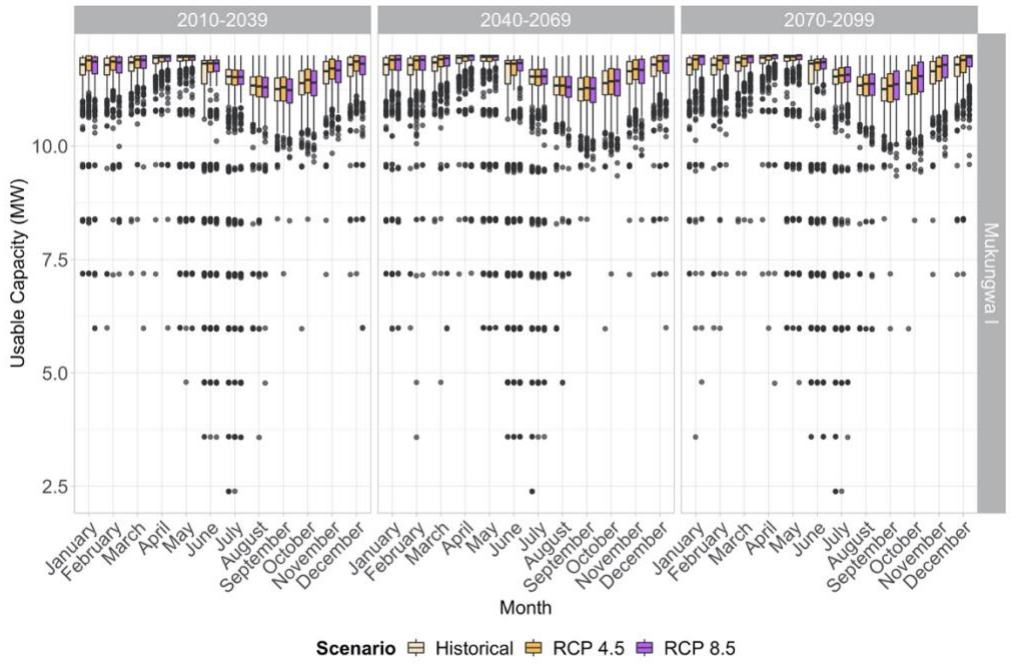

Figure C-24 – Usable capacity (MW) for the Mukungwa I power plant as an impoundment power plant. The boxplots present the full spread of the 21 GCM experiments for the historical period (wheat), RCP 4.5 (orange), and RCP 8.5 (purple). Each column shows one of the analysis time frames.

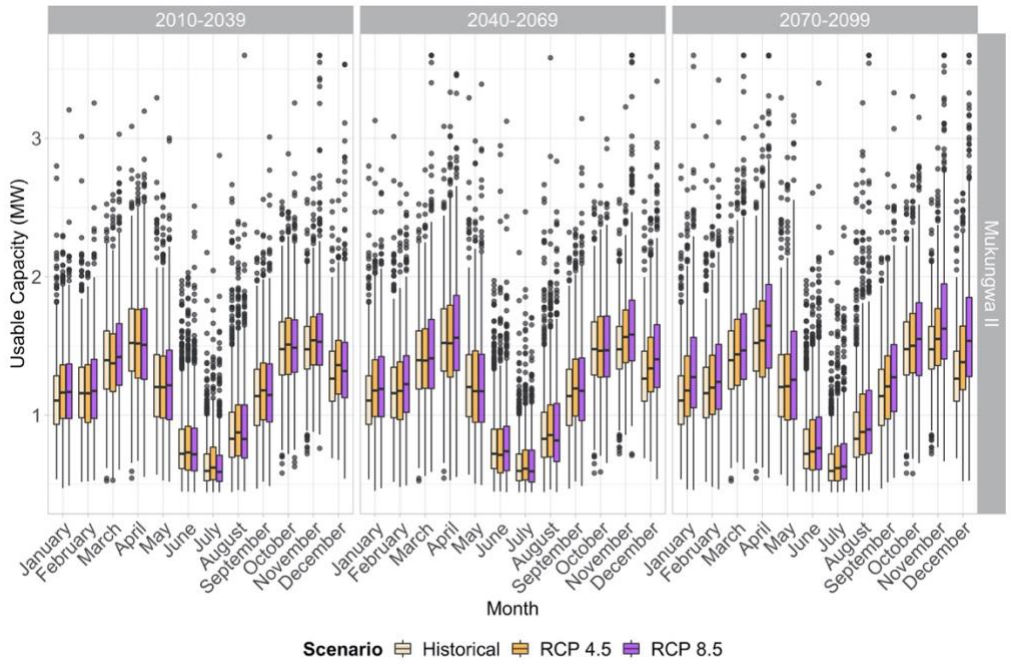

Figure C-25 – Usable capacity (MW) for the Mukungwa II power plant. The boxplots present the full spread of the 21 GCM experiments for the historical period (wheat), RCP 4.5 (orange), and RCP 8.5 (purple). Each column shows one of the analysis time frames.

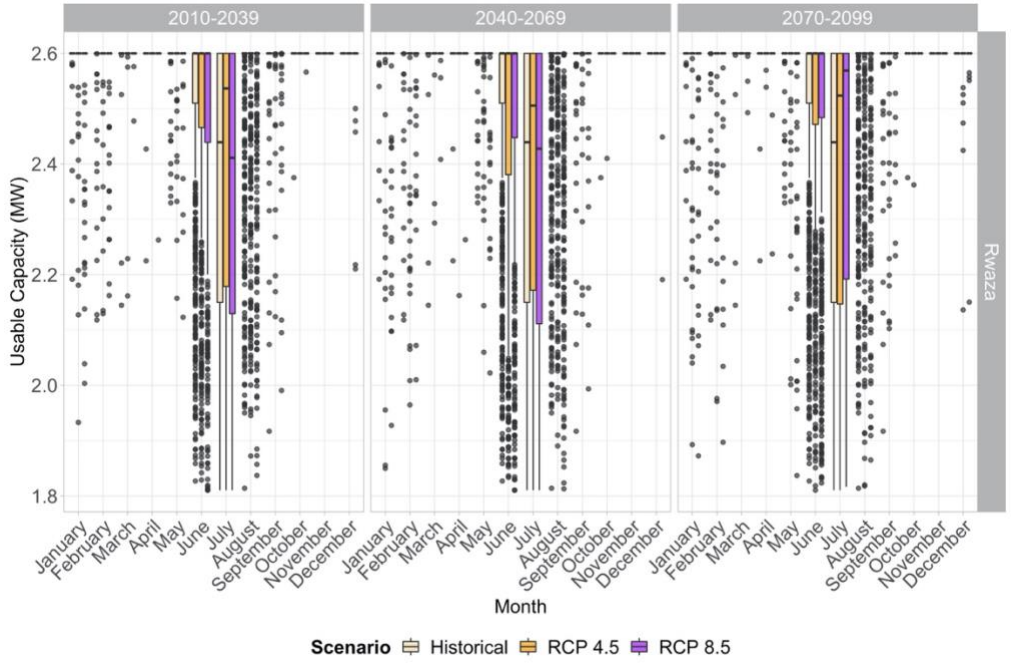

Figure C-26 – Usable capacity (MW) for the Rwaza Muko power plant. The boxplots present the full spread of the 21 GCM experiments for the historical period (wheat), RCP 4.5 (orange), and RCP 8.5 (purple). Each column shows one of the analysis time frames.

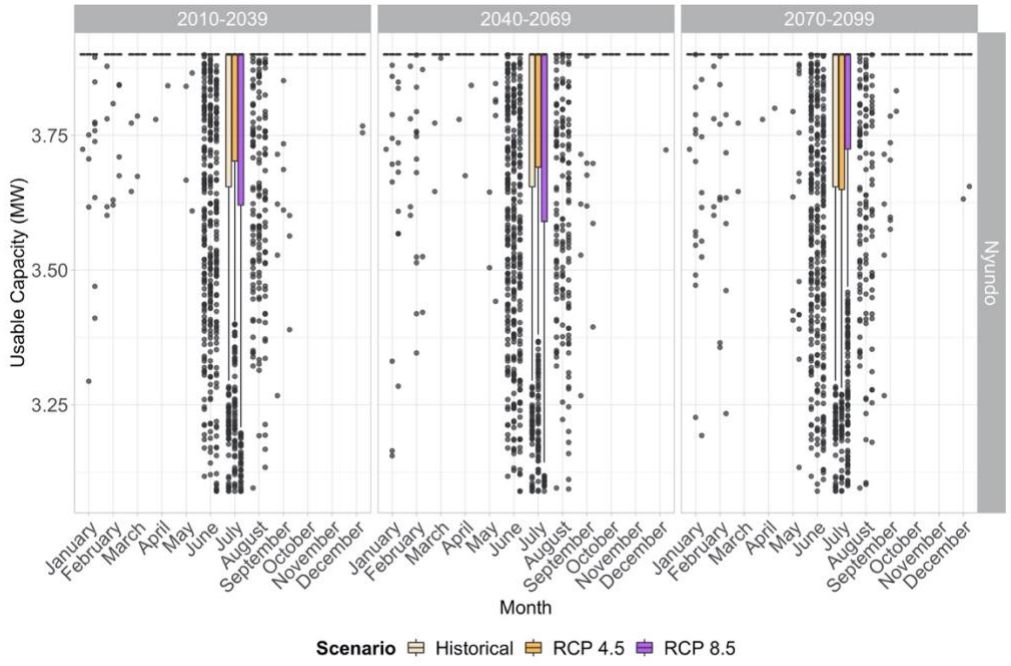

Figure C-27 – Usable capacity (MW) for the Nyundo power plant. The boxplots present the full spread of the 21 GCM experiments for the historical period (wheat), RCP 4.5 (orange), and RCP 8.5 (purple). Each column shows one of the analysis time frames.

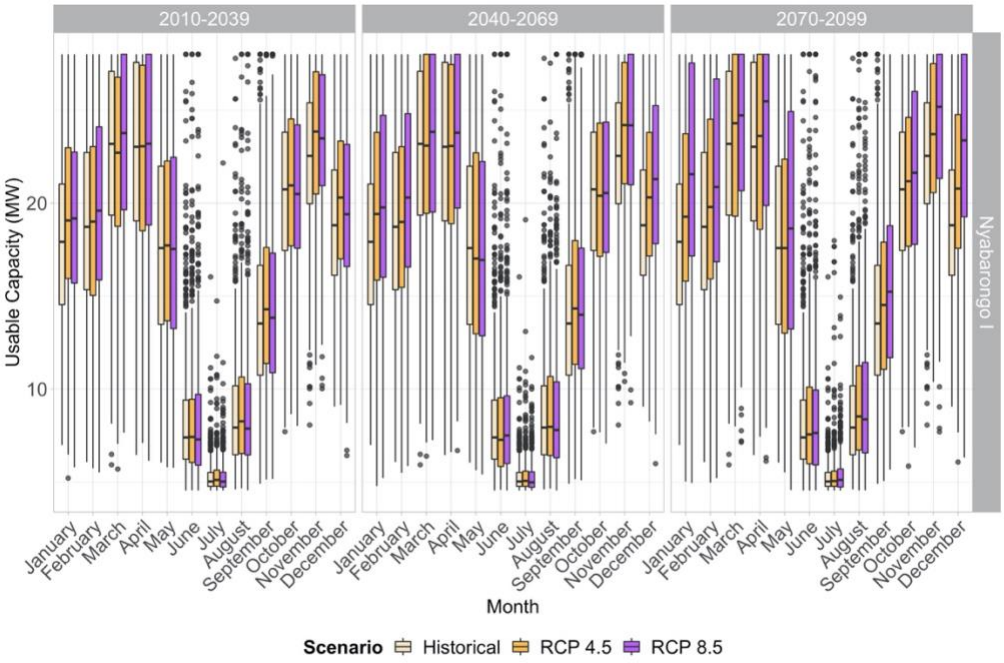

Figure C-28 – Usable capacity (MW) for the Nyabarongo I power plant. The boxplots present the full spread of the 21 GCM experiments for the historical period (wheat), RCP 4.5 (orange), and RCP 8.5 (purple). Each column shows one of the analysis time frames.

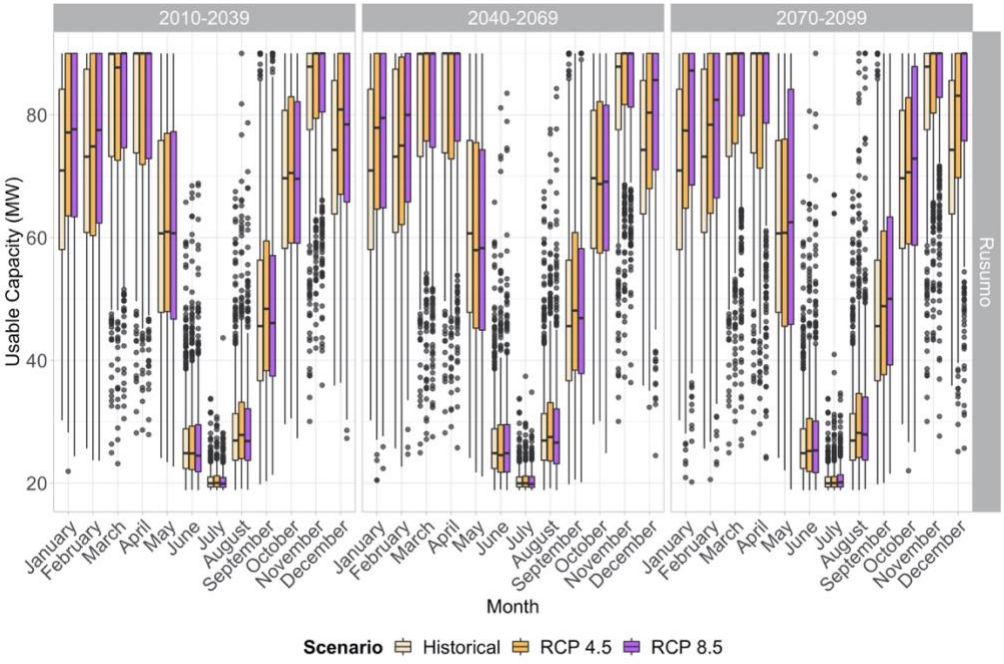

Figure C-29 – Usable capacity (MW) for the Rusumo power plant. The boxplots present the full spread of the 21 GCM experiments for the historical period (wheat), RCP 4.5 (orange), and RCP 8.5 (purple). Each column shows one of the analysis time frames.

Smaller power plants like the Nyundo (3.9 MW) and Rwaza (2.6 MW) have less variability during the year of usable capacity. These power plants should be able to operate at full capacity during the rainy seasons (both) given their lower design flow. During the drier months both power plants experience in increase in variability. Given the size of the power plants this should not be problematic for the operations of the system. Other power plants exhibit increases in monthly usable capacities. This would be beneficial, given that all increases in streamflow can be utilized for power output and would not seem to pose danger to the structures.

C.4 Conclusions

An increase in streamflow and usable capacity is projected for the seven Rwandan hydropower plants analyzed through the 21st century. These changes would vary in magnitude depending on the power plant. Dry season usable capacity for run-of-river power plants has the greatest potential for increases, with shifts seen in all power plants.

Appendix D – Supporting Information Chapter 4

D1. Supplementary Tables

Supplementary Table D-1 – Countries included in the Hydropower Plant Database. We present the list of the five regions and the corresponding countries included in RICCH. For each of the countries we present the total number of power plants and the total installed capacity for these power plants. We use the key attributes of these power plants to run the water balance and hydropower operations model to obtain the climate impacts on usable capacity.

Region	Countries	Number of Power Plants	Installed Capacity Included (MW)
Mexico and Central America	Costa Rica	8	1070 MW
	Dominican Republic	2	178 MW
	El Salvador	3	450 MW
	Guatemala	6	697 MW
	Honduras	2	380 MW
	Mexico	27	11,895 MW
	Nicaragua	1	54 MW
South America	Argentina	23	11,129 MW
	Bolivia	3	199 MW
	Brazil	149	100,994 MW
	Chile	26	5,582 MW
	Colombia	19	9,000 MW
	Ecuador	4	3,152 MW
	Paraguay	2	1,760 MW
	Peru	18	4,200 MW
	Venezuela	8	17,641 MW
Africa	Angola	3	1,100 MW
	Cameroon	3	750 MW
	Cote d'Ivoire	4	824 MW

	Democratic Republic of the Congo	9	2,831 MW
	Egypt	5	2,842 MW
	Equatorial Guinea	1	120 MW
	Ethiopia	10	3,714 MW
	Gabon	3	286 MW
	Ghana	3	1,100 MW
	Guinee-Conakry	2	315 MW
	Kenya	6	721 MW
	Lesotho	1	72 MW
	Liberia	1	88 MW
	Malawi	3	374 MW
	Mali	2	262 MW
	Morocco	6	902 MW
	Mozambique	3	2,293 MW
	Namibia	1	347 MW
	Nigeria	3	1,920 MW
	Senegal	1	120 MW
	South Africa	2	600 MW
	Sudan	2	1,665 MW
	Tanzania	4	528 MW
	Togo	1	66 MW
	Uganda	3	630 MW
	Zambia	4	2,208 MW
	Zimbabwe	1	750 MW
Middle East	Iran	13	9,679 MW
	Iraq	6	2,497 MW
	Syrian Arab Republic	3	1,505 MW
	Cambodia	4	897 MW

Southeast Asia and the Pacific	Indonesia	18	4,241 MW
	Laos	9	2,928 MW
	Malaysia	8	1,941 MW
	Myanmar	12	2,537 MW
	Papua New Guinea	2	132 MW
	Philippines	14	3,342 MW
	Thailand	8	3,712 MW
	Vietnam	57	15,047 MW

Supplementary Table D-2 – Overview of the key attributes of the Hydropower Plant Database. We present the names of the hydropower plants, their locations, key characteristics, and the source used to obtain the information. For every attribute we provide the units when appropriate and an example.

Key attributes	Description	Units	Example
country	The full name of the country where the power plant is located.	-	Costa Rica
region	The name of the region as defined in the Supplementary Table 1.	-	Latin America & Caribbean
hydrosheds_region	The regions as defined by Hydrosheds[124] used for basin delineation.	-	north_america
name	The full name of the hydropower plant.	-	Angostura Hydroelectric Power Station Costa Rica
name_shp	The abbreviated name of the hydropower plant used as a reference for shapefile documents.	-	angostura_costa_rica
power_mw	The installed capacity of the hydropower plant in MW.	MW	210
longitude	The longitude location of the power plant.	°	-83.64
latiitude	The longitude location of the power plant.	°	9.92
calculated_design_flow	The design flow of the hydropower plant in meters cube per second. This value is either calculated with the hydraulic head or provided as a design parameter.	m^3/s	38
head_m	Maximum hydraulic head of the power plant in meters (m).	m	577
max_vol_m3	Maximum volume of the adjacent reservoir if present in Million Meters Cube.	MMC	-
reservoir_operations	A		
Source	Original source used to determine the characteristics of the power plant.	-	GEODB
URL	URL of the source used.	-	http://globalenergyobservatory.org

D.2 Supplementary Figures

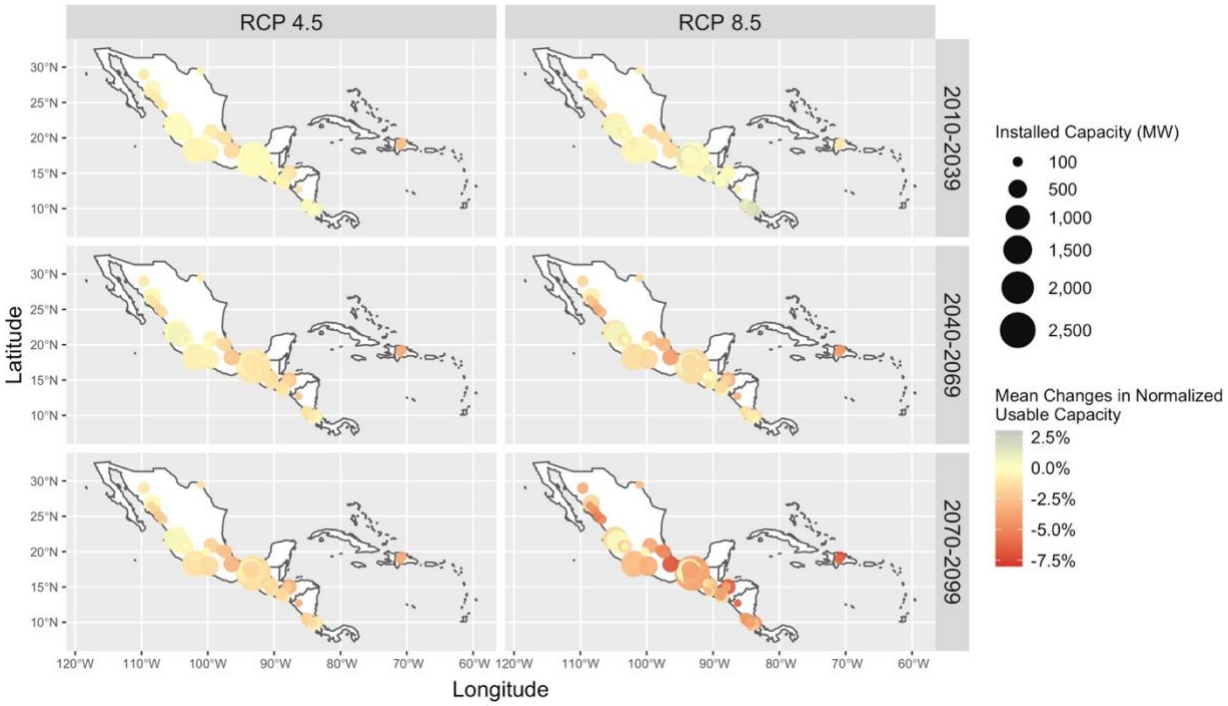

Supplementary Figure D-1 – Mean relative changes in annual normalized usable capacity for RCP 4.5 and RCP 8.5 for Central America and Mexico. Panels show the differences in percentage points for each power plant in the region between the historical reference (1970 – 2005) and the near future (2010 – 2039), the mid-century (2040 2069), and the end-of-the-century (2070 – 2099). The intensity of the color shows the direction of the change (blue increases and red decreases). The size of the circle represents the installed capacity of the power plant in MW.

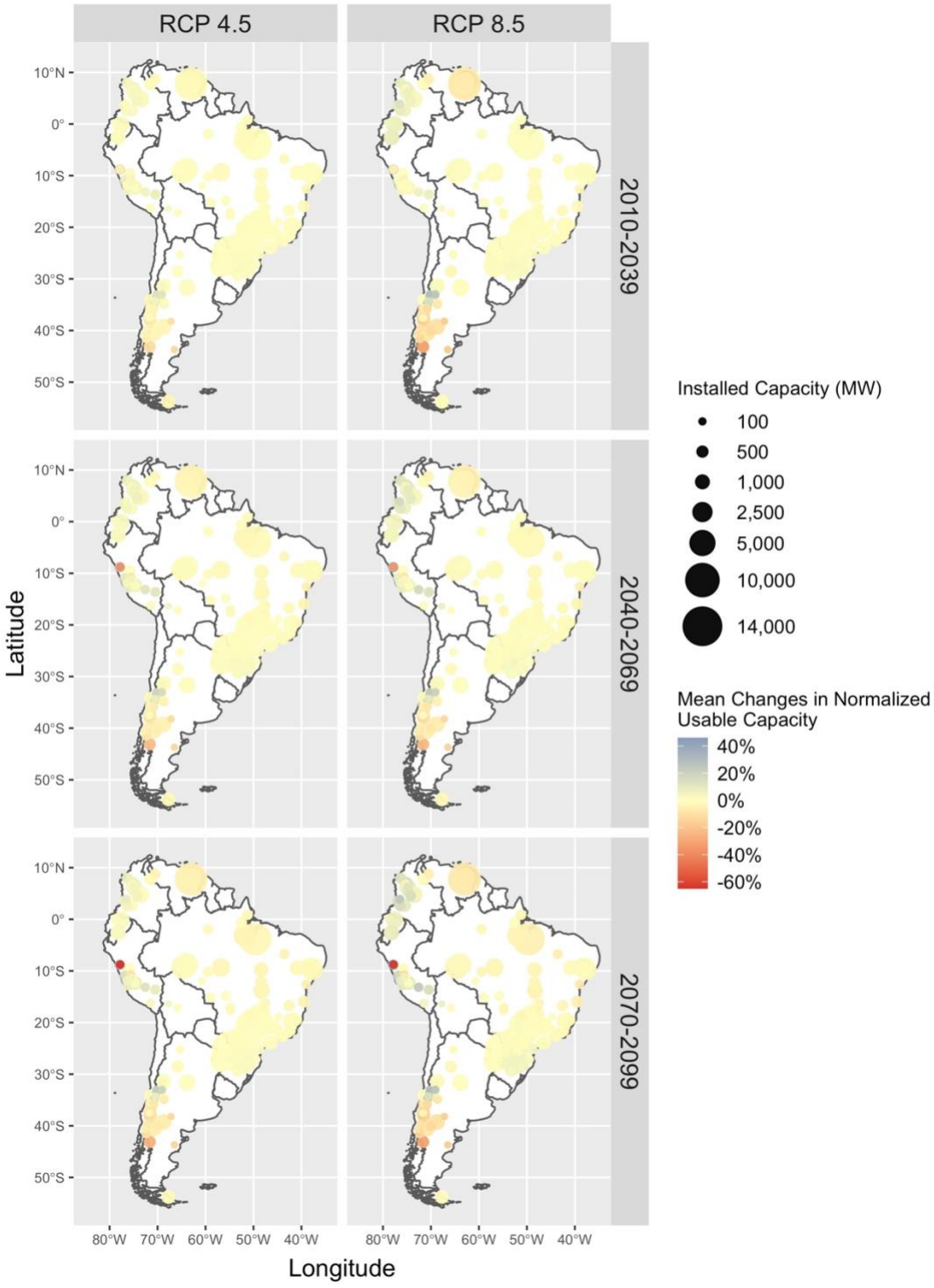

Supplementary Figure D-2 – Mean relative changes in annual normalized usable capacity for RCP 4.5 and RCP 8.5 for South America. Panels show the differences in percentage points for each power plant in the region between the historical reference (1970 – 2005) and the near future (2010 – 2039), the mid-century (2040 – 2069), and the end-of-the-century (2070 – 2099). The intensity of the color shows the direction of the change (blue increases and red decreases). The size of the circle represents the installed capacity of the power plant in MW.

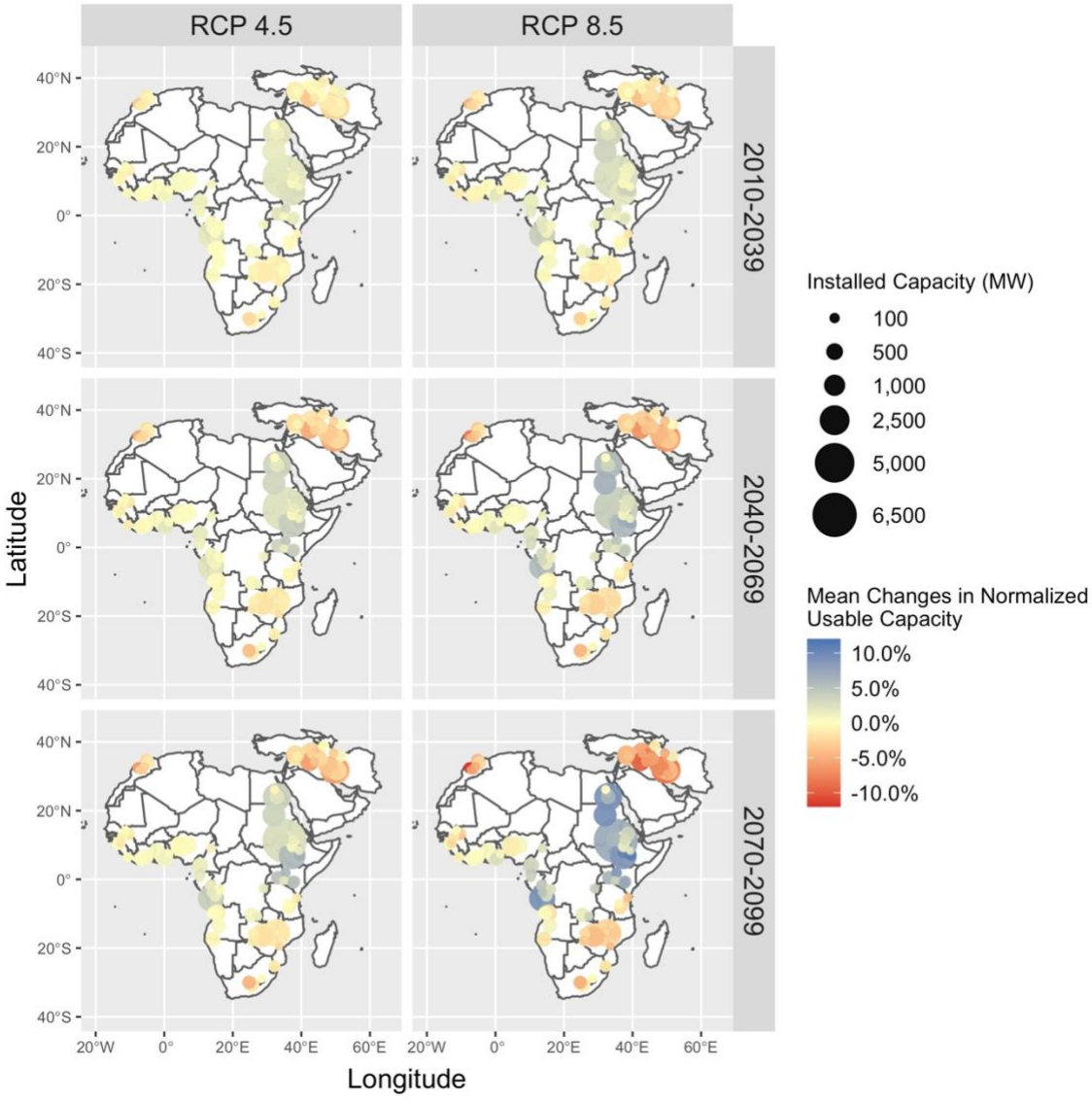

Supplementary Figure D-3 – Mean relative changes in annual normalized usable capacity for RCP 4.5 and RCP 8.5 for Africa. Panels show the differences in percentage points for each power plant in the region between the historical reference (1970 – 2005) and the near future (2010 – 2039), the mid-century (2040 – 2069), and the end-of-the-century (2070 – 2099). The intensity of the color shows the direction of the change (blue increases and red decreases). The size of the circle represents the installed capacity of the power plant in MW.

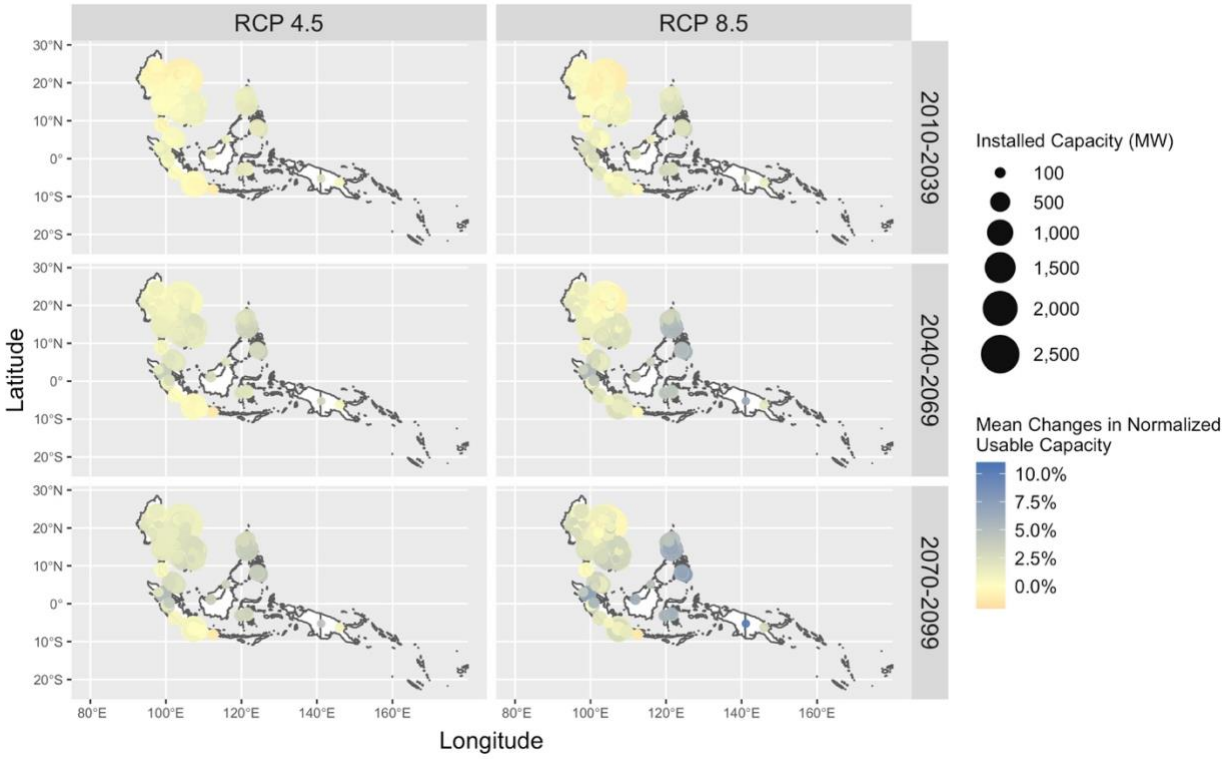

Supplementary Figure D-4 – Mean relative changes in annual normalized usable capacity for RCP 4.5 and RCP 8.5 for Southeast Asia and the Pacific. Panels show the differences in percentage points for each power plant in the region between the historical reference (1970 – 2005) and the near future (2010 – 2039), the mid-century (2040 – 2069), and the end-of-the-century (2070 – 2099). The intensity of the color shows the direction of the change (blue increases and red decreases). The size of the circle represents the installed capacity of the power plant in MW.